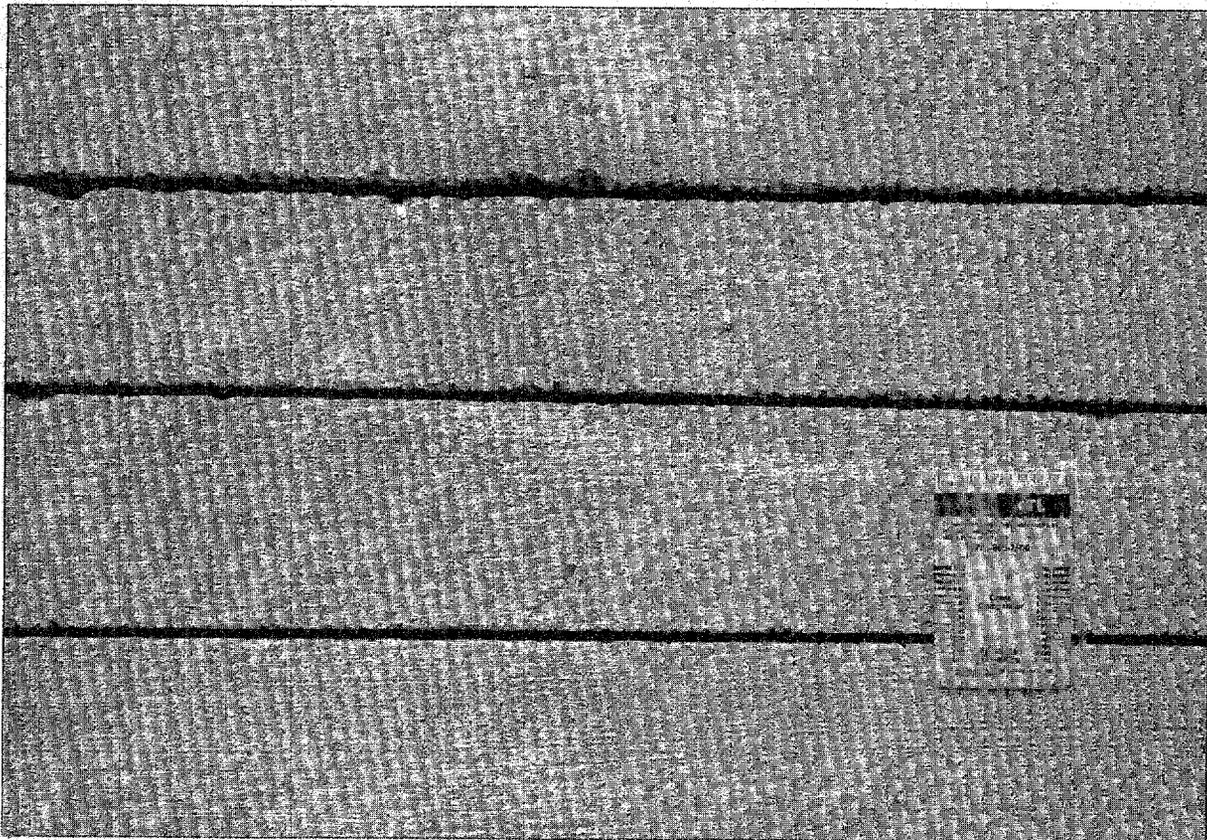# Guidelines for Timing Contraction Joint Sawing and Earliest Loading for Concrete Pavements, Volume I: Final Report

# FOREWORD

This report is one of a two-volume set documenting early age (4 to 24 hours) and early loading (1 to 28 days) tests to determine properties of highway concretes. Analyses are made for timing of sawcutting concrete pavement contraction joints and determining the earliest concrete pavement loadings. Correlations are developed for nondestructive tests versus concrete strength properties. Guidelines are developed for earliest "near" sawing time determinable from concrete strength properties and latest "far" sawing needed to avert uncontrolled pavement cracking. Guidelines are presented for earliest loading of new pavements with construction equipment.

Volume I consists of text and test results pertinent to developing correlations between early age concrete strength properties and nondestructive test results. Information, test data, and analysis leading to development of guidelines are provided. Volume II contains listings of test results not included within Volume I, and also includes a review of the state of the art.

This report will be of interest to those involved in the design and construction of jointed concrete pavements. Sufficient copies are being distributed to provide two copies to each FHWA Region, and three copies to each FHWA Division and State highway agency. Direct distribution is being made to the FHWA Division Offices. Additional copies may be purchased from the National Technical Information Service (NTIS), 5285 Port Royal Road, Springfield, Virginia 22161.

Charles J. Nemmers, P.E.
Director, Office of Engineering and Highway
Operations Research and Development

## NOTICE

| 1. Report No.<br>FHWA-RD-91-079 | 2. Government Accession No. | 3. Recipient's Catalog No. |
|---|---|---|

| 4. Title and Subtitle<br><br>Guidelines for Timing Contraction Joint Sawing and Earliest Loading for Concrete Pavements<br>Volume I - Final Report | 5. Report Date<br>February 1994 |
|---|---|
| | 6. Performing Organization Code |
| 7. Author(s)   P. A. Okamoto, P. J. Nussbaum, K. D. Smith,<br>M. I. Darter, T. P. Wilson, C. L. Wu, S. D. Tayabji | 8. Performing Organization Report No. |

| 9. Performing Organization Name and Address<br><br>Construction Technology Laboratories, Inc.<br>5420 Old Orchard Road<br>Skokie, Illinois  60077 | 10. Work Unit No. (TRAIS)<br>NCP 2E2C1042 |
|---|---|
| | 11. Contract or Grant No.<br>DTFH61-88-C-00062 |
| 12. Sponsoring Agency Name and Address<br>Office of Engineering and Highway Operations R&D<br>Federal Highway Administration<br>6300 Georgetown Pike<br>McLean, VA  22101-2296 | 13. Type of Report and Period Covered<br>Final Report<br>July 1988 - April 1991 |
| | 14. Sponsoring Agency Code |

15. Supplementary Notes
FHWA Contract Manager (COTR)
Dr. Stephen Forster, HNR-20

16. Abstract

A study with the objectives of providing guidelines for timing of contraction joint sawcutting to avert uncontrolled pavement cracking and providing guidelines for early loading of pavements by construction traffic has been conducted. A laboratory study of early age (4 to 24 hours) and early pavement loading (1 to 28 days) concrete strength properties for a range of highway concrete mixes was made. Sawcutting tests were made to determine earliest contraction joint sawcutting. Earliest sawcut timing was correlated on basis of sawcut ratings to concrete strength properties and non-destructive test results that can be used for determining earliest sawcutting time. Concrete pavement placement and joint sawcutting were observed at three highway construction sites to verify test results. Latest sawcutting time was targeted on basis of buildup of restraint stresses attributable to slab cooling. Guidelines for sawcut timing are presented to facilitate construction site decision making based on non-destructive test methods.

Early loading by construction traffic was analyzed using ILLI-SLAB finite element models. Load tests were made at two pavement sites to verify that analytical model results are applicable to new pavements. Guidelines are presented to facilitate construction site decision making for early trafficking of new pavements based on nondestructive test methods.

This is the first of two volumes. The second volume is FHWA-RD-91-080, Guidelines for Timing Construction Joint Sawing and Earliest Loading for Concrete Pavements - Volume II - Appendix.

| 17. Key Words<br><br>Concrete, concrete strength properties, concrete pavements, contraction joints, sawcutting, restraint stresses, traffic loading, concrete pavement construction, sawcutting guidelines. | 18. Distribution Statement<br><br>No restrictions. This document is available through the National Technical Information Service, Springfield, Virginia  22161 |
|---|---|

| 19. Security Classif. (of this report)<br>Unclassified | 20. Security Classif. (of this page)<br>Unclassified | 21. No. of Pages<br>292 | 22. Price |
|---|---|---|---|

Form DOT F 1700.7     (8-72)          Reproduction of completed page authorized

# SI* (MODERN METRIC) CONVERSION FACTORS

## APPROXIMATE CONVERSIONS TO SI UNITS

| Symbol | When You Know | Multiply By | To Find | Symbol |
|---|---|---|---|---|
| | | **LENGTH** | | |
| in | inches | 25.4 | millimeters | mm |
| ft | feet | 0.305 | meters | m |
| yd | yards | 0.914 | meters | m |
| mi | miles | 1.61 | kilometers | km |
| | | **AREA** | | |
| in² | square inches | 645.2 | square millimeters | mm² |
| ft² | square feet | 0.093 | square meters | m² |
| yd² | square yards | 0.836 | square meters | m² |
| ac | acres | 0.405 | hectares | ha |
| mi² | square miles | 2.59 | square kilometers | km² |
| | | **VOLUME** | | |
| fl oz | fluid ounces | 29.57 | milliliters | mL |
| gal | gallons | 3.785 | liters | L |
| ft³ | cubic feet | 0.028 | cubic meters | m³ |
| yd³ | cubic yards | 0.765 | cubic meters | m³ |

NOTE: Volumes greater than 1000 l shall be shown in m³.

| Symbol | When You Know | Multiply By | To Find | Symbol |
|---|---|---|---|---|
| | | **MASS** | | |
| oz | ounces | 28.35 | grams | g |
| lb | pounds | 0.454 | kilograms | kg |
| T | short tons (2000 lb) | 0.907 | megagrams (or "metric ton") | Mg (or "t") |
| | | **TEMPERATURE (exact)** | | |
| °F | Fahrenheit temperature | 5(F-32)/9 or (F-32)/1.8 | Celcius temperature | °C |
| | | **ILLUMINATION** | | |
| fc | foot-candles | 10.76 | lux | lx |
| fl | foot-Lamberts | 3.426 | candela/m² | cd/m² |
| | | **FORCE and PRESSURE or STRESS** | | |
| lbf | poundforce | 4.45 | newtons | N |
| lbf/in² | poundforce per square inch | 6.89 | kilopascals | kPa |

## APPROXIMATE CONVERSIONS FROM SI UNITS

| Symbol | When You Know | Multiply By | To Find | Symbol |
|---|---|---|---|---|
| | | **LENGTH** | | |
| mm | millimeters | 0.039 | inches | in |
| m | meters | 3.28 | feet | ft |
| m | meters | 1.09 | yards | yd |
| km | kilometers | 0.621 | miles | mi |
| | | **AREA** | | |
| mm² | square millimeters | 0.0016 | square inches | in² |
| m² | square meters | 10.764 | square feet | ft² |
| m² | square meters | 1.195 | square yards | yd² |
| ha | hectares | 2.47 | acres | ac |
| km² | square kilometers | 0.386 | square miles | mi² |
| | | **VOLUME** | | |
| mL | milliliters | 0.034 | fluid ounces | fl oz |
| L | liters | 0.264 | gallons | gal |
| m³ | cubic meters | 35.71 | cubic feet | ft³ |
| m³ | cubic meters | 1.307 | cubic yards | yd³ |

| Symbol | When You Know | Multiply By | To Find | Symbol |
|---|---|---|---|---|
| | | **MASS** | | |
| g | grams | 0.035 | ounces | oz |
| kg | kilograms | 2.202 | pounds | lb |
| Mg (or "t") | megagrams (or "metric ton") | 1.103 | short tons (2000 lb) | T |
| | | **TEMPERATURE (exact)** | | |
| °C | Celcius temperature | 1.8C + 32 | Fahrenheit temperature | °F |
| | | **ILLUMINATION** | | |
| lx | lux | 0.0929 | foot-candles | fc |
| cd/m² | candela/m² | 0.2919 | foot-Lamberts | fl |
| | | **FORCE and PRESSURE or STRESS** | | |
| N | newtons | 0.225 | poundforce | lbf |
| kPa | kilopascals | 0.145 | poundforce per square inch | lbf/in² |

* SI is the symbol for the International System of Units. Appropriate rounding should be made to comply with Section 4 of ASTM E380.

(Revised September 1993)

# TABLE OF CONTENTS - VOLUME I

# TABLE OF CONTENTS - VOLUME I (continued)

# TABLE OF CONTENTS - VOLUME II

# LIST OF FIGURES - VOLUME I

# LIST OF FIGURES - VOLUME II

# LIST OF TABLES - VOLUME I

# LIST OF TABLES - VOLUME II

# LIST OF TABLES - VOLUME II (continued)

LIST OF TABLES - VOLUME II (continued)

# CHAPTER 1. INTRODUCTION

Contraction (control) and warping joints are installed in plain and conventionally reinforced portland cement concrete pavements to control random slab cracking due to stresses resulting from restraints to temperature and moisture associated concrete dimensional changes. For highway pavements these joints are commonly sawcut to create a vertical weakened plane, aligning cracks with predetermined joint locations. Joints reduce spalling, facilitate pavement maintenance and sealing, and, with proper spacing and/or mechanical devices, provide slab to slab load transfer.

Sawcuts to create the weakened plane contraction and warping joints must be made in monolithic concrete pavements within the window of opportunity. Limits for the window of opportunity are:

- As soon as the concrete has hardened sufficiently to permit sawing without excessive ravelling.

- Before random slab cracking can occur.

For most projects, single-blade sawcutting machines are used to create the joint. However, on some wide pavements installed using full width slipform pavers, multiple gang-mounted saw blade spansaws are used.

Early loading of highway pavements by construction traffic is generally restricted until concrete strengths, as monitored by cylinder and/or beam test specimens, have attained design compressive and flexural strengths. With the advent of heavier sawing equipment, faster paving rates, and with right-of-way access limitations on rehabilitation and reconstruction projects, concerns about effects of earliest pavement use with heavy sawing equipment and early applications of construction traffic loadings to facilitate paving operations have been raised.

The objectives of this project were to provide recommendations and guidelines that will resolve:

- The concerns about the time limits of the joint sawcutting window of opportunity based on considerations of acceptable joint edge ravelling, random pavement cracking, and saw equipment loading.

- To determine magnitudes and earliest use of pavements by construction traffic.

The project work plan consisted of 7 major elements:

- Performing a state-of-the-art literature review. The review provided information on: early age concrete strength development, nondestructive testing equipment suitable for monitoring concrete strength characteristics, sawcutting equipment characteristics, and effects of early loading of pavements. It helped identify items with sufficient information to meet project objectives. The state-of-the-art review is presented in a separate appendix.

- Acquisition of data on early age (4 to 24 hrs) concrete properties such as compressive strength, flexural strength, split tensile strength, and modulus of elasticity of concrete mixes used for highway pavement construction. Concurrently concrete characteristics such as ultrasonic pulse velocity, concrete maturity,

1

and impact strength were determined by nondestructive testing methods. Concrete properties such as compressive strength, flexural strength, and modulus of elasticity of mixes used for highway pavement construction were also obtained for ages ranging from 1 day through 28 days. Ultrasonic pulse velocity and concrete maturity were evaluated for use in monitoring strength development to allow for earliest pavement opening to construction equipment.

- Making full-scale sawing tests on slabs. Sawing was done at time intervals dependent on rate of concrete hardening. Concrete strength properties and characteristics determined from destructive and nondestructive tests were determined concurrently with sawcutting.

- Making observations of joint sawcutting operations at construction sites in Utah, Wisconsin, and Iowa. Full-scale load tests with a loaded truck were made at the Iowa and Utah sites for a range of pavement ages (2 through 8 days). Companion strength development and nondestructive tests were made for pavement segments where joint observations were made.

- Comparing results from calculations for pavement stresses using finite element techniques and laboratory elastic moduli data with measured stress values obtained from full-scale highway pavement load tests.

- Preparing recommendations and guidelines pertaining to the limits of the joint sawing window of opportunity. Joint acceptability criteria with respect to joint edge ravelling was established. The acceptability criteria were correlated to concrete strength characteristics and nondestructive concrete parameters. Effects of pavement stresses due to sawing equipment loads were considered in establishing guidelines for sawcutting limits. The far sawcutting window of opportunity boundary was set ahead of significant potential for initial incidence of random longitudinal or transverse slab cracking. This is determined from considerations of insitu concrete temperature during slab finishing and curing and potential friction between pavement and subbase.

- Preparing recommendations and guidelines pertaining to criteria for allowing construction traffic on recently placed highway concrete pavements. Stresses due to axle loads at various pavement locations were compared to flexural and compressive strengths for a range of concrete maturity conditions. Fatigue considerations are provided by setting allowable stresses at a minimum percentage of flexural strength to limit early pavement loading fatigue damage. In the case of dowel bearing pressures, allowable pressures are set at an adequate safety factor from compressive strength.

2

# CHAPTER 2. STATE-OF-THE-ART REVIEW

A summary of the literature review of jointing practices, sawcut depth, and evaluation of early age concrete properties is presented. The summary includes review of nondestructive test (NDT) methods that could be considered for characterization of insitu (pavement) concrete properties of early age concrete. Other areas covered in the review such as early age concrete strength development, pavement to subbase friction, concrete sawcutting blades, and early loading of concrete are summarized in volume II - appendix F.

## JOINTS AND SAWCUT DEPTH

The purpose of forming or sawing joints in fresh concrete is to create a point of weakness which will induce cracking at a desired location. A joint may be thought of as a "notch" in the pavement's surface. The notch toughness of fresh concrete is fairly low compared to other materials (such as steel, aggregates, and hardened concrete). Notch toughness for early age pavements is controlled by the strength of the weakest component of the fresh concrete, the cement paste. This is supported by field observations. Cores taken through successfully formed contraction joints typically show the concrete cracks through the paste, i.e., very rarely will aggregates split across the crack. Cores taken through fatigue cracks that occur well after the concrete hardens, however, typically show the cracks fracture both paste and aggregate.

## Joint Forming and Sawing Practices

The practice of forming joints dates back to the earliest days of concrete paving. Sawing joints has only been popular in the United States in the last 50 or fewer years. Kansas was the first State to make widespread use of sawed joints and to develop standard specifications. Most States initially followed the lead of Kansas in continuing to form control joints at 80- to 100-ft (24-to 31-m) intervals to prevent shrinkage cracking and sawing intermediate joints later. Minnesota demonstrated that formed control joints could be eliminated if all joints were sawed early enough. To ensure prevention of uncontrolled cracking, Minnesota preferred to saw on the early side of the window of feasible sawing time, i.e., when the concrete was still young enough that sawing created slight spalling and erosion at the joint edges.

To achieve maximum production rates, it is desirable to saw joints to the minimum permissible depth that will successfully cause a controlled crack. In the past 10 to 15 years, recommended sawcut depths have remained fairly constant for transverse contraction joints, but have increased somewhat for longitudinal joints as a result of experiences with uncontrolled longitudinal cracking. Table 1 shows the results of a survey of design and construction practices in the United States in 1977, which found that the practice in most States was to saw or form both transverse and longitudinal joints to a depth equal to or less than 1/4 of the slab thickness, or D/4.[1] A survey of construction practices in European countries conducted at about the same time found a wide range of sawcut depths, from D/5 to D/2 for transverse joints and from as little as D/4 to D/3 for longitudinal joints, as shown in table 2.[2]

A more recent survey of U.S. joint construction practices conducted by the FHWA shows that in 1987 most States were still sawing transverse joints to a depth of D/4 where D is the pavement depth, as shown in table 3.[3] The majority of these States have short-jointed concrete pavements without reinforcement. Sawcut depths of D/4 are reported for

# Table 1. 1977 survey of joint construction practices by State.[1]

| | Longitudinal Joints | | | | Transverse Joints | | | |
| | Centerline | | | | Contraction Joints | | | |
| | Type | | | Dimensions | Type | | | Dimensions |
| State | Sawed | Formed | Insert | Depth (in) | Sawed | Formed | Insert | Depth (in) |
|---|---|---|---|---|---|---|---|---|
| AL | * | | | D/4 | * | | | D/4 |
| AZ | * | | | 2 | * | * | | 2 |
| AR | * | | * | | * | | | 2 |
| CA | * | | * | 2 | * | | * | 2 |
| CO | * | | * | 1¼, 2 | * | | * | 1¼, 2 |
| CT | * | | * | | * | | | |
| DE | * | | | D/4+¼ | * | | | 2½ |
| DC | * | * | | D/5, D/4 | * | * | | D/5, D/4 |
| FL | * | | * | D/4–D/5 | * | | | D/4 |
| GA | * | | * | D/4 | * | | | D/3.6 |
| HI | | | * | 2 | * | | | 2½ |
| ID | * | | * | 2 | * | | | D/4, 2¼ |
| IL | * | | * | D/4 | * | | | 2 3/4 |
| IN | * | * | | D/4, D/4½ | * | | | D/4 |
| IA | * | | | D/4 | * | | | D/4 |
| KS | * | | | 2½ | * | | | |
| KY | * | | * | D/4+¼ | * | | | 2 |
| LA | | * | * | 3 | | | | 3 |
| ME | * | * | | D/4+½, 1 | * | | | D/4 |
| MD | * | | * | 2¼ | * | | | 2 |
| MA | * | | | 2½ | * | | | 2¼ |

1 in = 2.54 cm

Table 1. 1977 survey of joint construction practices by State (continued).

| | Longitudinal Joints Centerline | | | | Transverse Joints Contraction Joints | | | |
| | Type | | | Dimensions | Type | | | Dimensions |
| State | Sawed | Formed | Insert | Depth (in) | Sawed | Formed | Insert | Depth (in) |
|---|---|---|---|---|---|---|---|---|
| MI | * | | | 2½ | * | | | 2½ |
| MN | * | | | | * | | | |
| MS | | | * | 2 | | | | |
| MO | * | | | D/4 | * | | | D/4 |
| MT | * | | * | 2 | * | | | D/4 |
| NE | * | | | | * | | | D/4 |
| NV | * | | | 2 | * | | | 2 |
| NJ | * | * | | 2 3/4, 7/8 | | | | |
| NM | * | | | 2 | * | | | D/4 |
| NY | * | * | | 2 | * | * | | 2 |
| NC | * | * | | | * | | | 2 3/4 |
| ND | * | | * | 2½, 3 | * | * | * | |
| OH | * | | | D/3 | * | | | |
| OK | * | | | D/4 | * | | | D/4 |
| OR | * | | | 2 | | | | |
| PA | * | | | D/4+¼ | * | | | D/4 |
| SC | * | | * | D/4 | * | * | * | D/4 |
| SD | * | | | | * | | | D/4 |
| TN | * | | * | D/4 | | | | D/4 |
| TX | * | | | D/4 | * | * | | D/4 |
| UT | * | | | 2¼ | * | | | 2¼ |
| VA | * | | * | D/3, 2½ | * | | | D/4+¼ |

1 in = 2.54 cm

# Table 1. 1977 survey of joint construction practices by State (continued).

| State | Longitudinal Joints Centerline | | | | Transverse Joints Contraction Joints | | | |
| | Type | | | Dimensions | Type | | | Dimensions |
| | Sawed | Formed | Insert | Depth (in) | Sawed | Formed | Insert | Depth (in) |
|---|---|---|---|---|---|---|---|---|
| WA | * | | | D/4+½ | * | * | | 2 |
| WV | * | | * | D/4, 2½ | * | | | D/4 |
| WI | * | | | 1½ | * | | | 2 |
| WY | | * | * | D/4, D/4, 2 | | * | * | D/4,2 |

D = Depth of portland cement concrete slab.

1 in = 2.54 cm

# Table 2. 1977 survey of joint construction practices in European countries.[2]

| | Joints — Transverse contraction | | Joints — Longitudinal | |
|---|---|---|---|---|
| | Reduction of Section % | Crack Inducer Details | Sawn Depth (mm) | Other types Depth (mm) |
| Austria | R 50 | X | R 50 | R 20 |
| Belgium | R > 30 | R Bottom: asbestos cement Top: sawn | R 60-70 | |
| Czechoslovakia | R 20-25 | | 50 | |
| Denmark | R 50 | Top inducer 50 mm deep | | 50 |
| France | A 20 | | R 1/5 of slab thickness | R 50-60 |
| Great Britian | 25-33 | Timber, steel, or synthetic fillet | P 1/8-1/3 of slab thickness | A 1/8-1/3 of slab thickness |
| Netherlands | 50-70 | N | 60 or 1/3 of slab thickness | |
| Italy | R 20-25 | | 60 | 60 |
| Spain | R Min. 22 | R None | R Min. 22% of slab thickness | R Min. 22% of slab thickness |
| Sweden | .20 | Not used | 20 | |
| Switzerland | 30 | Top: Sawn or asbestos plastic strip | 30 | |
| West Germany | R 25% of thickness at top | R N for bottom inducer | R 25% of slab thickness | R 1.5 times width |

R = Required by specifications or regulations.
N = Not required by specifications.
A = As shown on plans.
X = Specifically prohibited.
P = Permitted by specification under certain conditions or requirements.

10 mm = 0.4 in

## Table 3. 1987 survey of joint construction practices by State.[3]

| State | Longitudinal Joints Centerline Type | | | Transverse Joints Contraction Joints Type | | |
|---|---|---|---|---|---|---|
| | Sawed Depth (in) | Formed Depth (in) | Insert Thickness (mils) | Sawed Depth (in) | Insert Depth (in) | Formed Depth (in) |
| Alabama | 3/4 | | | d/4 | | |
| Alaska | | | | | | |
| Arizona | 3/4 | | | | | |
| Arkansas | d/3 | | | d/3 | | |
| California | d/4 | | 0.013 | d/4 | d/4 | |
| Colorado | 2-2 1/2 | | 20 | 2-2 1/2 | | |
| Connecticut | d/3 | | | d/3 | | |
| Delaware | d/4+1/4 | | | d/4+1/4 | | |
| DC | | | | | | |
| Florida | d/3 | d/3 | | d/3 | d/3 | d/3 |
| Georgia | d/4 | | | d/4 | | |
| Hawaii | d/4 | | | d/4 | d/4 | d/4 |
| Idaho | d/3 | | | d/3 | | |
| Illinois | d/3 | | | d/4 | | |
| Indiana | d/3 | d/2 | 12 | d/4 | | d/3 |
| Iowa | d/4 | | | d/4 | | |
| Kansas | 2.5 | | 20 | d/4 | | |
| Kentucky | 1 | 1 1/2 | | d/4 | | |
| Louisiana | d/3 | | 12-30 | d/4 | d/4 | d/4 |
| Maine | | | | | | |
| Maryland | d/4 | | | d/4 | 2 | |
| Massachusetts | | | | | | |

d = Portland Cement Concrete Thickness.

1 in = 2.54 cm

# Table 3. 1987 survey of joint construction practices by State (continued).

| State | Longitudinal Joints Centerline Type | | | Transverse Joints Contraction Joints Type | | |
|---|---|---|---|---|---|---|
| | Sawed Depth (in) | Formed Depth (in) | Insert Thickness (mils) | Sawed Depth (in) | Insert Depth (in) | Formed Depth (in) |
| Michigan | 1 | | | 2.5 | | |
| Minnesota | 2-3 | 2-3 | | 1 5/8-2 | full | 1/4 |
| Mississippi | d/3 | d/3 | | d/4 | | |
| Missouri | d/4 | | | d/4 | | |
| Montana | | | | 3 | | |
| Nebraska | d/4 | | | d/4 | | |
| Nevada | | | | | | |
| New Hampshire | | | | | | |
| New Jersey | 2.5-2.75 | | | | | |
| New Mexico | d/3 | | | d/4 | | |
| New York | d/4 | | | d/3 | | |
| North Carolina | | | | | | |
| North Dakota | d/3 | | | d/3 | | |
| Ohio | d/3 | 1 | | d/4 | | |
| Oklahoma | d/4 | | | d/3 | | |
| Oregon | d/3 | | | d/3 | | |
| Pennsylvania | d/3 | | | d/4 | | |
| Puerto Rico | 1 3/8 | | | | | |
| Rhode Island | | | | | | |
| South Carolina | 1 1/2 | | | 5/8 | | |
| South Dakota | d/3 | | | d/4 | | |
| Tennessee | 1 1/4 | | | 3 | | |
| Texas | d/4 | | | d/4 | | |

1 in = 2.54 cm

**Table 3. 1987 survey of joint construction practices by State (continued).**

| | Longitudinal Joints<br>Centerline<br>Type | | | Transverse Joints<br>Contraction Joints<br>Type | | |
|---|---|---|---|---|---|---|
| State | Sawed<br>Depth (in) | Formed<br>Depth (in) | Insert<br>Thickness (mils) | Sawed<br>Depth (in) | Insert<br>Depth (in) | Formed<br>Depth (in) |
| Utah | d/3 | | | d/3 | | 3/4 |
| Vermont | | | | | | |
| Virginia | | | 20 | d/4 | | |
| Washington | d/4 | | 20 | d/4 | | |
| West Virginia | | | | | | |
| Wisconsin | | | 20 | d/4 | | |
| Wyoming | 1 1/4 | | | 1 1/4 | | |

10 in = 25 cm

reinforced concrete pavements with joint spacings of 40 ft (12.2 m) in several States, 58.5 ft (17.8 m) in Louisiana, 60 ft (18.3 m) in Texas, and 62.5 ft (19.1 m) in Missouri. Transverse sawcut depths of D/3 are used in a few States.

Longitudinal joint depths, however, have increased from the previous typical value of D/4 or less to D/4 or more, with D/3 being the most often reported value, as shown in table 3. The results of a recent survey of European joint construction practices shown in table 4 show transverse joint depths more consistently D/4 to D/3 now than in the past and longitudinal joint depths greater than in the past (at least D/4 and as much as D/2) in some countries.[4]

## European Practice of Inducing Cracks at Bottom of Slab

An interesting possibility for enhancing the likelihood of controlled cracking, and perhaps reducing required sawcut depth, exists for concrete slabs placed on cement-treated bases. West Germany has found that making transverse and longitudinal notches in the cement-treated base with a triangular crack inducer effectively forces cracks in the concrete directly above at the desired joint locations in the concrete slab. The required sawcut depth may be reduced so the combined depth of sawcut and height of the crack inducer at the slab bottom equals the previously required depth of sawcut, as illustrated in figure 1. West Germany has used this technique successfully to construct concrete pavements on high-strength cement-treated bases without using any bondbreaker.

## Effect of Subbase Type on Cracking

Friction between the underlying base and the concrete slab also has a very significant effect on required sawing depth. The greater the friction, the greater the tensile stresses that will build up in the slab, and the more critical timing of sawing becomes. For example, test sections constructed at Rothsay, MN in 1970 possessed different subbase types. The sections with granular subbases showed almost no uncontrolled longitudinal cracking, whereas those sections with asphalt or cement-treated subbases showed extensive longitudinal cracking, as shown in table 5. The plastic tape that was used to form the longitudinal joints in these pavements was placed at the same depth for all sections, which illustrated that for high-friction bases, the sawcut may need to be deeper. The trend toward greater sawcut depths may be due to the trend toward use of treated subbases (asphalt, cement). Relatively little research has been done on this topic.

Factors contributing to the success of controlling longitudinal cracking by sawing have been investigated, which may apply to some degree to transverse contraction joints as well.[7] The success of the operation was related to the standard deviation of the concrete strength. Improving quality control and reducing variability in concrete strength was proposed as a means for reducing required sawcut depth. This topic, too, requires further research.

The practice of sawing joints in stabilized subbases, bonding the concrete slab, and sawing matching joints in the slab has been used in Germany to control cracking.[8] This practice is significantly different from current U.S. practice and shows potential in reducing uncontrolled cracking potential when stabilized bases are used.

**Table 4.  1986 survey of joint construction practices in European countries.[4]**

| Country | Joints — Transverse Contraction — Reduction of Section % | Joints — Transverse Contraction — Crack Inducer Details | Joints — Longitudinal — Sawn Depth (mm) | Joints — Longitudinal — Other types Depth (mm) |
|---|---|---|---|---|
| Austria | R<br>$\geq$ 50 mm<br>(0.20-0.25xthickness) | X | R<br>0.25-0.30<br>slab thickness | R<br>20 |
| Belgium | R<br>33 | R<br>Top:  sawn | 33% of slab<br>thickness | |
| Czech. | R<br>20-25 | | 50 | |
| Denmark | R<br>25 | Top inducer 50 mm deep | 40-50 | 50 |
| Finland | 25 | Not used | 30% of slab<br>thickness | |
| France | A<br>20-25 | Not used | R<br>1/5-1/3<br>of slab thickness | R<br>50-60 |
| Germany<br>(Dem. Rep.) | 25-30 at top | Not used | 25-30% of slab<br>thickness<br>20-25 mm | 50-70 |
| Germany<br>(Fed. Rep.) | R<br>25-30% of thickness<br>at top | R<br>N for bottom inducer | R<br>30-40% of<br>slab thickness<br>if more than<br>two anchored lane<br>40-45% | R<br>1.5 times<br>width |
| Great Britian | 25-33 | Timber or synthetic<br>fillet | R<br>¼-1/3<br>of slab<br>thickness | R<br>¼-1/3<br>of slab<br>thickness |
| Italy | R<br>20-25 | | 60 | 60 |
| Netherlands | 33 | X | 30-40%<br>of slab thickness | R |
| Norway | 33 | Not used | 1/3 of slab<br>thickness | R |

R = Required by specifications or regulations.   A = As shown on plans.
X = Specifically prohibited.   N = Not included in specifications.

10 mm = 0.4 in

## Table 4. 1986 survey of joint construction practices in European countries (continued).

| | Joints | | Joints | |
|---|---|---|---|---|
| | Transverse Contraction | | Longitudinal | |
| Country | Reduction of Section % | Crack Inducer Details | Sawn Depth (mm) | Other types Depth (mm) |
| Spain | R<br>Min. 22 | R<br>None | R<br>Min. 22%<br>of slab<br>thickness | R<br>Min. 22%<br>of slab<br>thickness |
| Sweden | 30 | Not used | 50 | |
| Switzerland | 33 | Top: sawn | | |

10 mm = 0.4 in

reinforcement (if used)
terminated 300 ± 50 mm
from center of joint

seal

compressible caulking
material where required

dowel bars 400 mm long
at 300 mm centers

plastic sheath over
at least 2/3 length

bottom crack inducer

reinforcement (if used)
terminated 60 ± 20 mm
from center of joint

seal

compressible caulking
material where required

bottom crack inducer
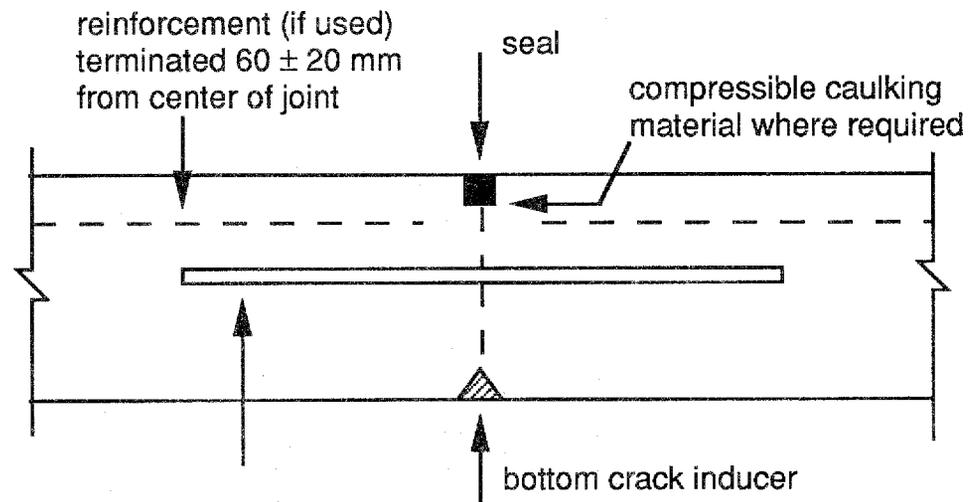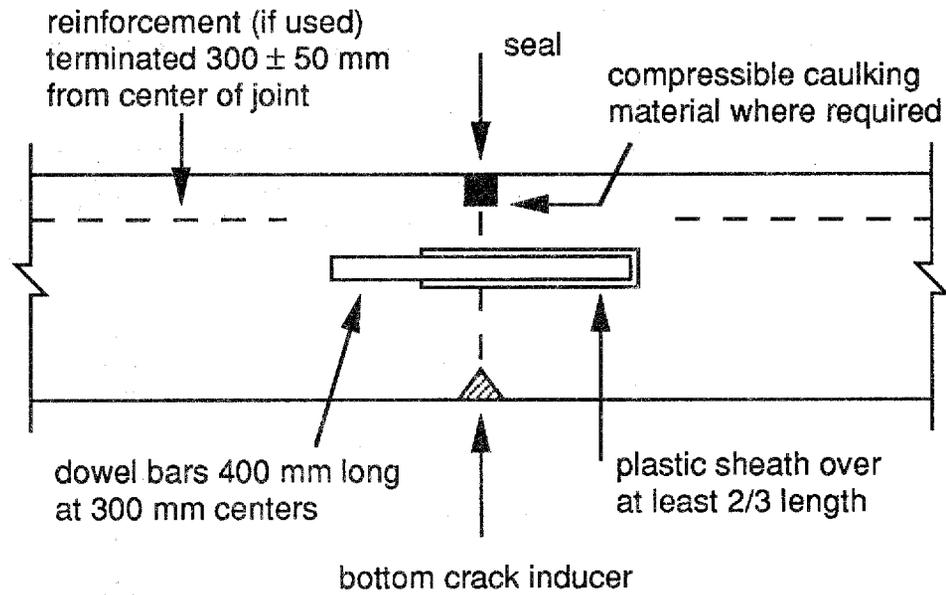
tie bars at 600 mm centers
12 mm mild steel 1000 mm long or
12 mm HY deformed steel 750 mm long

NOTE: Combined depth of top groove and bottom crack inducer
should be between 1/3 and 1/4 slab depth.

Source: reference 5

100 mm = 3.9 in

Figure 1. Use of bottom crack inducer to reduce transverse
and longitudinal sawcut depths.

# Table 5. Effect of base type on longitudinal cracking.[6]

| SECTION | AGE | BASE | JOINT FORMING | JOINT DEPTH, IN | DEPTH/ THICK, IN | LONG. CRACKS, FT/MILE |
|---------|-----|------|---------------|-----------------|------------------|-----------------------|
| OH 2 | 13 | NONE | SAW | 3.75 | 0.25 | 258 |
| ONT 1-1 | 5 | NONE | SAW | 3.00 | 0.25 | 0 |
| AZ 1-2,3 | 10 | NONE | SAW | 3.25 | 0.25 | 0 |
| | | | | | | NO BASE MEAN = 86 |
| MN 5 | 18 | AGG | INSERT | 2.75 | 0.30 | 1261 |
| MN 2 | 10 | AGG | SAW | 2.75 | 0.32 | 224 |
| NY 2 | 12 | AGG | SAW | 2.25 | 0.25 | 194 |
| NY 1 | 22 | AGG | SAW | 2.00 | 0.22 | 132 |
| MI 4 | 15 | AGG | SAW | 2.75 | 0.30 | 91 |
| MN 1 | 17 | AGG | INSERT | 2.75 | 0.32 | 75 |
| NC 1 1,4,7,8 | 20 | AGG | SAW | 2.75 | 0.30 | 74 |
| OH 1 | 14 | AGG | SAW | 2.25 | 0.25 | 0 |
| MI 1 | 12 | AGG | SAW | 2.75 | 0.30 | 0 |
| | | | | | | AGG BASE MEAN = 228 |
| CA 1-5 | 16 | LCB | INSERT | 2.00 | 0.24 | 230 |
| AZ 1-6,7 | 5 | LCB | SAW | 2.25 | 0.25 | 0 |
| CA 6 | 7 | LCB | INSET | 2.00 | 0.24 | 0 |
| | | | | | | LCB MEAN = 77 |
| NC 1-2,3 | 20 | SC | SAW | 2.75 | 0.30 | 2260 |
| CA 7 | 7 | CTB | SAW | 3.00 | 0.29 | 2060 |
| MN 1 | 17 | CTB | INSERT | 2.75 | 0.32 | 1320 |
| CA 1-1,3,9 | 16 | CTB | INSERT | 2.00 | 0.24 | 500 |
| AZ 1-1 | 15 | CTB | SAW | 2.25 | 0.25 | 233 |
| NC 1-5 | 20 | CTB | SAW | 2.75 | 0.30 | 179 |
| CA 3 | 12 | CTB | INSERT | 2.00 | 0.22 | 11 |
| CA 1-5 | 16 | CTB | INSERT | 2.00 | 0.26 | 0 |
| CA 2-3 | 7 | CTB | SAW | 2.00 | 0.24 | 0 |
| | | | | | | CTB MEAN = 729 |
| MN 1 | 17 | ATB | INSERT | 2.75 | 0.32 | 3550 |
| CA 8 | 7 | AC | SAW | 3.00 | 0.29 | 1026 |
| NY 1 | 22 | ATB | SAW | 2.00 | 0.22 | 73 |
| OH 1 | 14 | ATB | SAW | 2.25 | 0 | |
| NC 1-6 | 20 | ATB | SAW | 2.75 | 0.25 | 0 |
| CA 2-2 | 7 | AC/PCTB | SAW | 2.00 | 0.24 | 0 |
| ONT 1-2 | 5 | PATB | SAW | 2.20 | 0.27 | 0 |
| | | | | | | ATB MEAN = 664 |

1000 ft/mi = 189 m/km        1 in = 25 mm

15

## Pavement Restraint Stresses Causing Cracking

Restraint stresses in pavements are due to prevention of deformations in a manner similar to those of fixed end beams where contraction, expansion, and rotations are prevented. For pavements, the restraint conditions analogous to the fixed end beam occur at some distance inward from pavement free edges and ends. At edges and ends, deformations occur and restraint stresses reduce to zero as distances from slab edges or ends inward towards slab middle are decreased.

Deformation restraints of interest in considerations of early age concrete pavement cracking consist of restraints to uniform axial contraction and restraints to bending deformations occurring after initial concrete set. At slab ends where no restraints, that is zero stress conditions occur, the uniform axial deformations are recognized as slab end contraction movements. Bending deformations due to thermal gradients are known as curling.

Pavement axial contraction in the absence of external forces such as prestressing can be attributed to either or both uniform through slab cross-section reductions of concrete temperature and concrete drying. Upward bending can be attributed to nonuniform concrete temperature and/or nonuniform concrete drying attributable to immediately below concrete slab surface temperature and/or moisture content less than those near slab bottom. Axial and curling deformations and restraint stresses due to drying are not considered significant for early age plain concrete pavements' nonloading-associated cracking, because curing compounds used to assure moist curing are applied immediately following surface texturing. The curing compounds prevent drying from the top pavement surface. Prevention of top surface drying during early pavement life performs two functions significant to restraint stress development:

- Maintain a uniform moisture content throughout the pavement cross-section thus providing a zero moisture gradient that could otherwise cause warping restraint stresses or slab edge and corner warping.

- Prevent surface moisture evaporation that otherwise could contribute to slab top surface cooling.

## Axial Restraint Stresses

Axial contraction restraint stresses are due to friction resistance between slab bottoms and subbase or subgrade surfaces. The stresses increase from zero at slab ends to a maximum value at slab midlength or when the restraint stresses due to friction resistance build up to the full restraint stress attributable to uniform slab cross-section temperature change.

Stress due to friction resistance, $p_f$, can be calculated according to equation 1 shown in figure 2. Restraint stress, $p_r$, at distances from slab ends greater than the slab length participating in uniform temperature associated movement is shown in equation 2 of figure 2. Slab end lengths, $L_m/2$, participating in slab end movement can be determined by setting $p_f = p_r$ and solving for $L_m/2$, as shown in equation 3 of figure 2. The distance from slab end that full axial restraint stress is attained is about 3168 in (264 ft, 80.5 m) when equation 3 is solved for the following conditions:

$$w = 0.0868 \text{ lb/in}^3 \ (2400 \text{ kg/m}^3)$$
$$E = 3 \times 10^6 \text{ psi} \ (20,700 \text{ MPa})$$

16
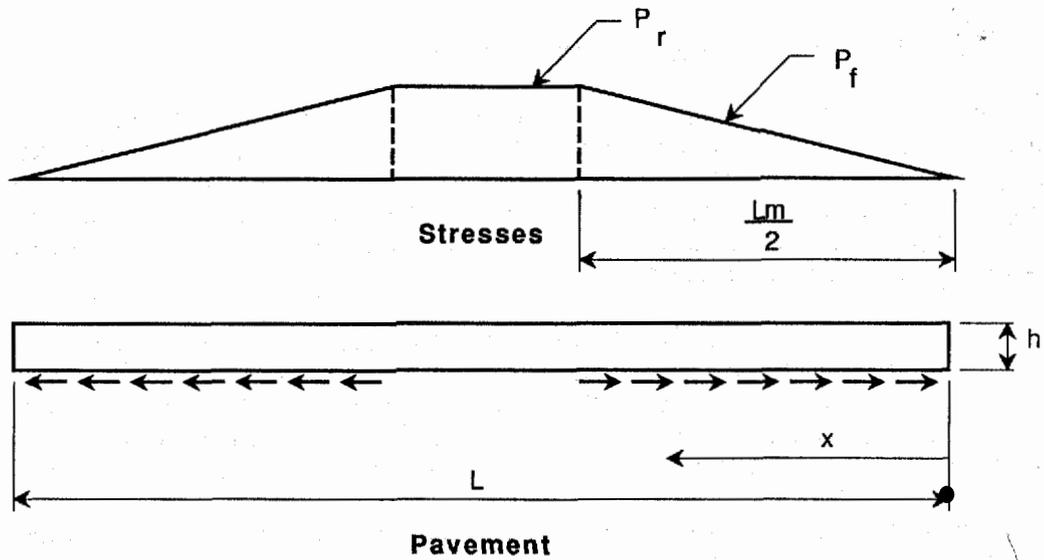
$$p_f = \frac{(wh)\,\mu\,x}{h} \quad \dots \dots \dots \dots \dots \dots \dots \dots \dots \dots \dots \dots \dots \dots (1)$$

where : $p_f$ = axial stress due to friction restraint,

$w$ = density of concrete,   lb/in³

$h$ = slab thickness, in

$(wh)$ = slab weight,   lb/in²

$\mu$ = coefficient of subgrade friction, (no dimension)

$x$ = distance from slab end, in

$$p_r = E\,\alpha\,\Delta T1 \quad \dots \dots \dots \dots \dots \dots \dots \dots \dots \dots \dots \dots \dots \dots (2)$$

where : $p_r$ = axial stress due to full restraint of movement

$E$ = modulus of elasticity, psi

$\alpha$ = coefficient of thermal expansion, in/in/°F

$\Delta T1$ = change in uniform temperature, °F

$$\frac{Lm}{2} = \frac{E\,\alpha\,\Delta T1\,h}{(wh)\,\mu} \quad \dots \dots \dots \dots \dots \dots \dots \dots \dots \dots \dots \dots (3)$$

where : $Lm/2$ = x, in  (slab end length participating in end movement)

| | |
|---|---|
| 1000 psi = 6.9 MPa | 1000 lb/in³ = 271 MPa/m |
| 1 in/in/°F = 1.8 mm/mm/°C | 10 in = 25 cm |
| °C = 5/9 (°F-32) | |

Figure 2.  Pavement axial restraint stresses.

$$\alpha = 5.5 \times 10^{-6} \text{ in/in } °F \ (9.9 \times 10^{-6} \text{ mm/mm } °C)$$
$$\Delta T_1 = 25 °F \ (-4 °C)$$
$$h = 10 \text{ in } (25 \text{ cm})$$
$$\mu = 1.5$$

The 264 ft (80.5 m) distance is reduced to about 40 ft (12.2 m) when a subgrade friction factor, $\mu$, of 10 is used in place of 1.5. Subgrade friction factors of 1.5 to 2.0 have been determined for slabs over granular subbases, whereas subgrade friction values of about 5 and greater have been determined for pavements supported by stabilized subbases or lean concrete subbases. Heavy applications of wax based curing compounds ahead of paving can significantly reduce magnitudes of friction values.

For the fully restrained axial stress, $p_r$, that is at distances greater than $L_m/2$ from slab ends, the uniform axial restrained stress is 412 psi (2.84 MPa) when equation 2 is used for the above stated for E, $\alpha$, and $\Delta T_1$ values. Restraint stresses are about 198 psi (1.37 MPa) when an E of $2 \times 10^6$ psi (13,790 MPa) and $\Delta T_1$ of 18 °F (-8 °C) are used in place of the higher values.

## Bending Restraint Stresses

Full bending restraint stresses are due to differences between slab surface and slab bottom temperatures when the stress can not be relieved by curling deformations, that is at greater than critical distances, $x_c/2$, inward from slab edges. At distances less than one-half the critical distances, $x_c$, the curling restraint stress can be expressed by equation 4, after Bradbury as shown in figure 3.[9] At distances greater than one-half the critical distance, $x_c$, the fully restrained curling stress is expressed by equation 5. It should be noted that the coefficient C, as shown in figure 4 reaches a maximum value of 1.084 corresponding to a B/L ratio of 8.5.[9] For B/L ratio values greater than 12, the coefficient C reaches a value of 1.043. The error for disregarding C values greater than 1.0 is about 8 percent or less.

The critical distance, $x_c$, can be calculated by setting B = 6.7 L, as shown in figure 4 for C = 1.0. Using equation 6 in figure 3, the critical distance $x_c$ is 222 in (18.5 ft, 5.6 m) for a 10-in (25 cm) thick early age concrete pavement with E at $2 \times 10^6$ psi (13,790 MPa), $\alpha = 5.5 \times 10^{-6}$ in/in/°F ($9.9 \times 10^{-6}$ mm/mm/°C), and k = 140 lb/in$^3$ (38 MPa/m). Eisenmann provides the following more user friendly method for calculating the critical distance, $x_c$ for slabs with curling due to top slab surface cooling:[10]

$$x_c = 5.09 \ h \ (\alpha \ \Delta T \ E)^{1/2} \ * \ \dots \dots \dots \dots \dots \dots \dots \dots \dots \dots (7)$$

where

$h$ = slab thickness, in

$\alpha$ = coefficient of thermal expansion, in/in/°F

$\Delta T$ = temperature gradient, °F/in

$E$ = modulus of elasticity, psi

---

* Equation 7 constant 5.09 is back calculated to accommodate English units. Eisenmann shows a constant of 25.9 in the equation for metric units.

18

**Stresses**

$$\frac{Lm}{2}$$
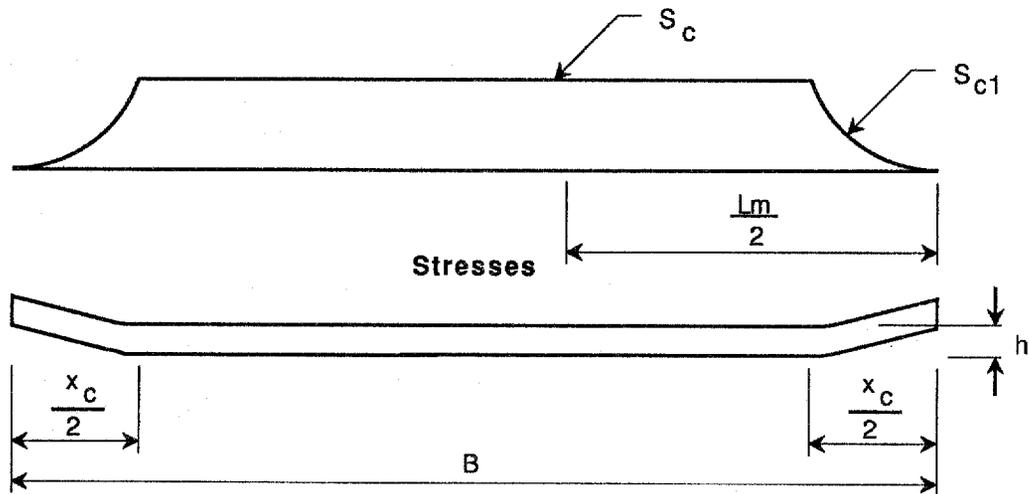
**Pavement**

$$S_{c1} = \frac{C\,E\,\alpha\,\Delta T2}{2} \quad \dots\dots\dots\dots\dots\dots\dots\dots\dots\dots\dots\dots\dots\dots\dots\dots\dots\dots \text{(4)}$$

where : $S_{c1}$ = curling restraint stress for $x < 0.5x_c$ , psi

$E$ = modulus of elasticity, psi

$\alpha$ = coefficient of thermal expansion, in/in/°F

$\Delta T2$ = temperature difference between slab surface and bottom, °F

$C$ = curling stress coefficient (figure 4)

$$S_c = \frac{1.04\,E\,\alpha\,\Delta T2}{2} \quad \dots\dots\dots\dots\dots\dots\dots\dots\dots\dots\dots\dots\dots\dots\dots\dots\dots\dots \text{(5)}$$

where : $S_c$ = fully restrained curling stress for $x \geq 0.5x_c$ , psi

$B$ = slab width or length, in

$$x_c = B = 6.7\ell \quad \text{for} \quad C = 1.0 \quad \dots\dots\dots\dots\dots\dots\dots\dots\dots\dots\dots\dots\dots\dots\dots\dots \text{(6)}$$

where : $\ell = \left[\dfrac{Eh^3}{12(1-\mu_1^2)\,k}\right]^{1/4}$   in; radius of relative stiffness

$h$ = slab thickness, in

$k$ = modulus of subgrade reaction, lb/in$^3$

$\mu_1$ = Poissons Ratio

1000 psi = 6.9 MPa          1000 lb/in$^3$ = 271 MPa/m

1 in/in/°F = 1.8 mm/mm/°C          10 in = 25 cm

°C = 5/9 (°F-32)

**Figure 3.   Pavement bending restraint stress.**
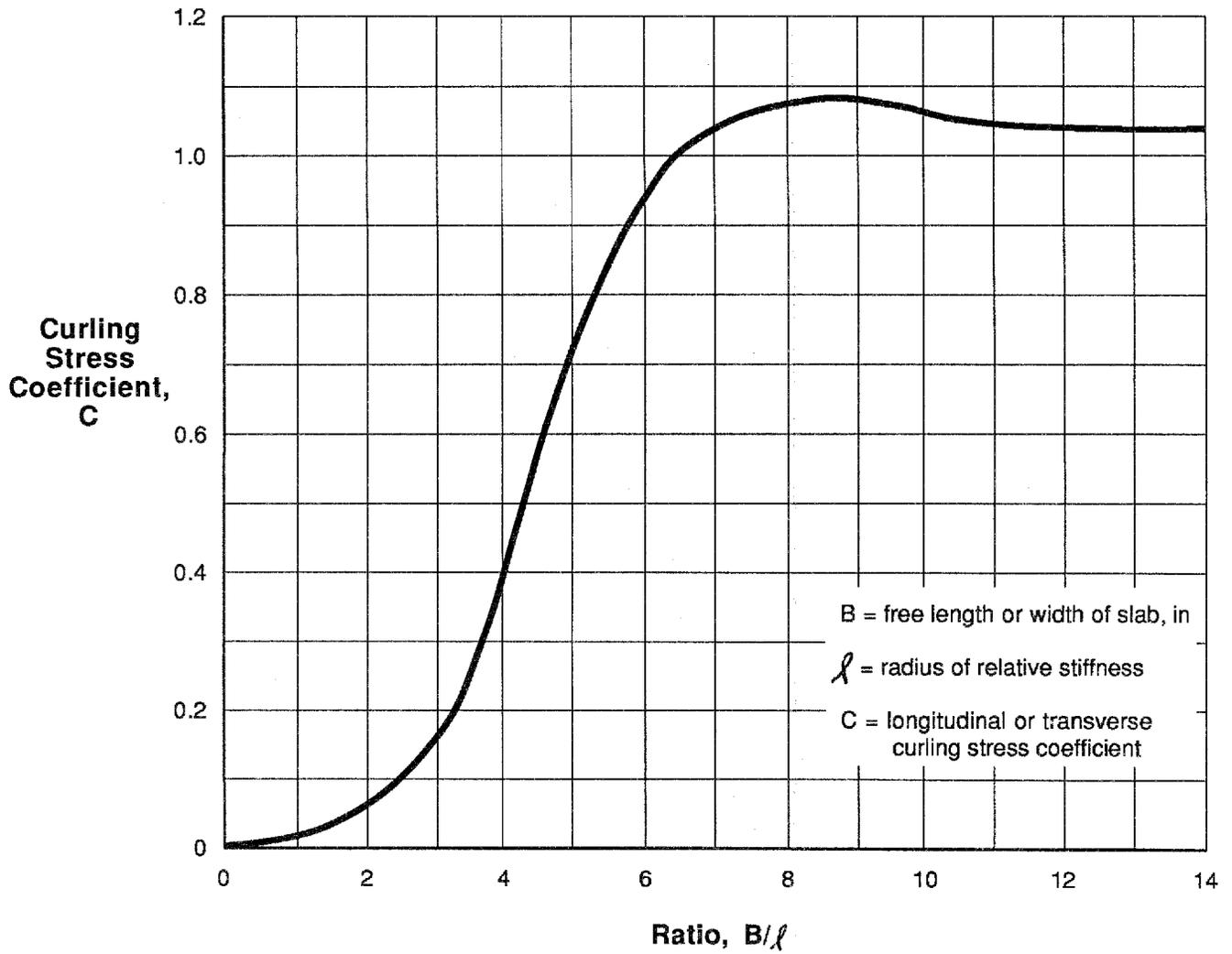
Figure 4.   Curling stress coefficient. (9)

It is noted that equation 7 does not consider the modulus of subgrade reaction, k, in calculating critical distances. Using equation 7, and a temperature gradient of 2 °F/in (0.4 °C/cm) the calculated critical distance is 238 in (19.8 ft, 6.0 m). Variance from the previously calculated $x_c$ value of 222 in (5.6 m) is about 7 percent. If a subgrade modulus of 100 lb/in$^3$ (27.1 MPa/m) had been used in place of 140 lb/in$^3$ (38 MPa/m), variance would have been less than 2 percent.

The approximately 18.5 ft (5.6 m) critical distance, $x_c$, indicates that the $x_c/2$ distance from slab edge is about 9.3 ft (2.8 m). For a two-lane wide road with shoulders, all placed at one pass, the paving width is about 38 ft (11.6 m). Thus at distances of about 9.3 ft (2.8 m) from both edges, a mid-portion pavement width of about 19.5 ft (5.9 m) will experience full curling restraint stresses. For the above cited concrete properties, the full curling restraint stress, $S_c$, using equation 5, is about 114 psi (789 kPa).

## Superposition of Axial and Bending Restraint Stresses

The sum of axial and bending restraint stresses of mid-width of a 38 ft (11.6m) wide pavement placed full width before longitudinal joint sawing is done can be calculated using equation 1 from figure 2 and equation 5 from figure 3. For a 10 in (25 cm) thick pavement with early age properties of E = 2x10$^6$ psi (13,790 MPa), $\alpha$ = 5.5x10$^{-6}$ in/in/°F (9.9x10$^{-6}$ mm/mm/°C), $\Delta T_2$ (curling) = 2 °F/in (0.44 °C/cm), $\Delta T_1$ = 30 °F (-1 °C), $\mu$ = 1.5, x = 228 in (5.8 m), and (wh) = 0.868 lb/in$^2$ (6 kPa), the axial restraint stress due to sub-grade friction is $p_f$ = 30 psi (207 kPa) and the bending restraint stress is $S_c$ = 114 psi (787 kPa). The sum of axial and bending restraint stresses before joint sawing is about 144 psi (994 kPa).

Restraint stresses in the longitudinal direction prior to transverse control joint sawing can be calculated for the same pavement using equation 2 from figure 2 and equation 5 from figure 3. For portions of the pavement at distances greater than about 210 ft (64.1 m) calculated using equation 3 for the above properties and conditions, restraint stresses can be calculated using equation 2 from figure 2 and equation 5 from figure 3. The full axial restraint stress is $p_r$ = 330 psi (2275 kPa) and the bending stress is $S_c$ = 114 psi (787 kPa). The combined restraint stress is 444 psi (3.1 MPa). It is noted that the fully restrained axial stress of 330 psi (2.2 MPa) signals that concrete control joint sawcutting should be done ahead of significant temperature drops that can contribute to restraint stresses.

## Early Age Concrete Temperature Reductions and Cracking

Observations of random slab cracking of highway pavements during the first cooling period after pavement placement have prompted studies to determine magnitudes of concrete temperature reductions that can cause cracking. For pavements, the random cracking consists primarily of transverse and longitudinal cracks. Under controlled laboratory conditions, approximately 4-by 4-in (10-by 10-cm) beams in cross-section fully restrained at ends, were exposed after a range of uniform temperature cooling rates.[11]

Concrete temperature and restraint stress histories, respectively, are graphically presented in figure 5.[11] Five stages are noted in the temperature and restraint stress histories:
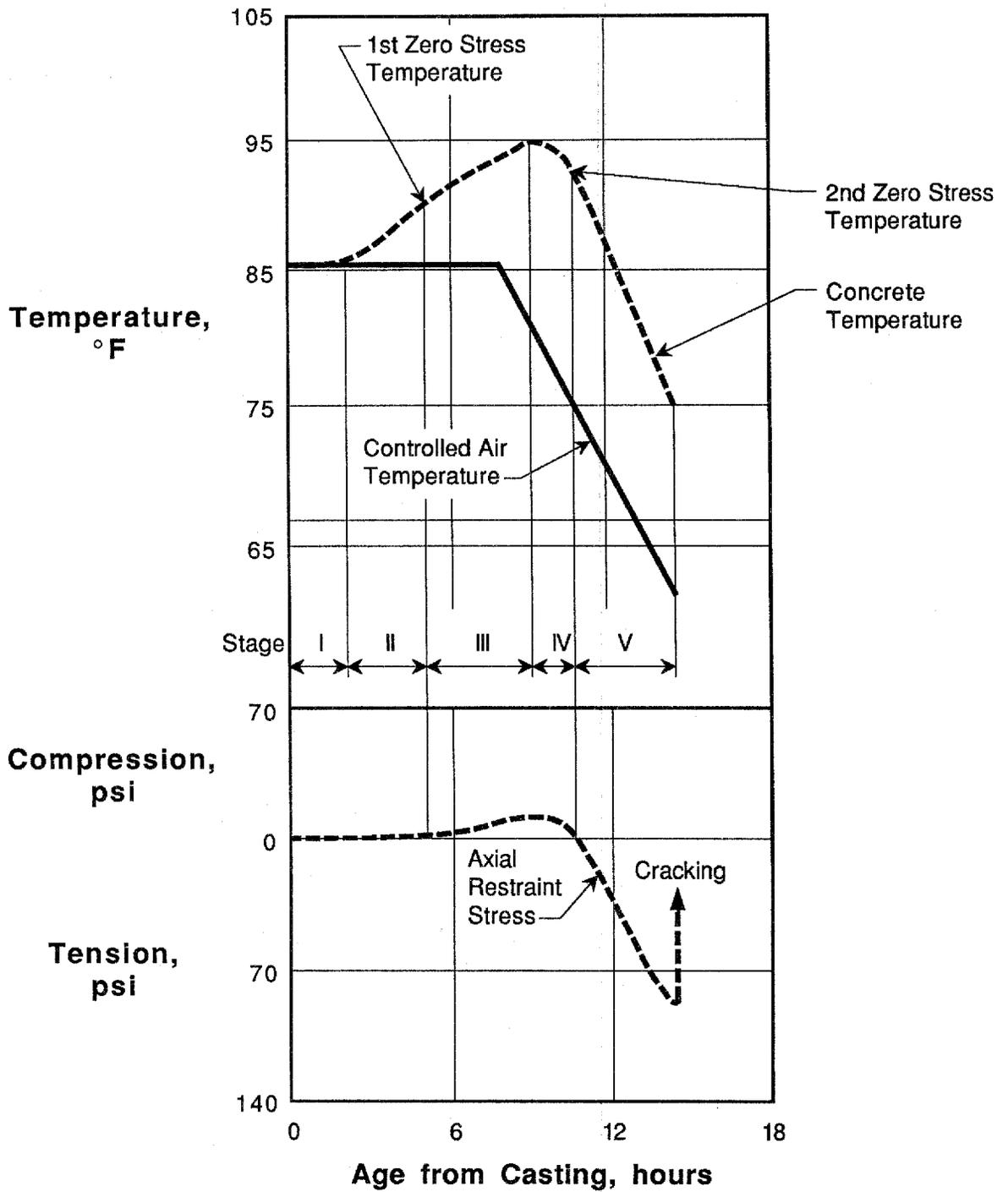
$°C = 5/9 (°F - 32)$

$100 \text{ psi} = 0.7 \text{ MPa}$

(11)

Figure 5.  Cracking tendency test results.

22

Stage 1 -  concrete starts to harden without temperature gain

Stage II -  concrete temperature rises with no concurrent compressive stress

Stage III -  concrete temperature rises with concurrent compressive stress gain

Stage IV -  concrete starts to cool with end of this stage coinciding with the 2nd zero stress temperature

Stage V -  concrete continues to cool concurrent with tensile stress gain, this stage ending with concrete cracking

Results from tests summarized in table 6 indicate that concrete cracking is due to temperature differences ranging from about 16 to 29 °F (9 to 16 °C) for 2nd zero stress temperature cracking. The 2nd zero temperature condition corresponds to the temperature of the concrete when there is a transition from concrete compression to tension during initial concrete cooling, as illustrated in figure 5.

Temperature histories and cracking observations were obtained for approximately 36-ft (11-m) long, 5-ft (1.5-m) wide and 8.7-in (220-mm) thick experimental pavement segments constructed at an exterior location near Munich, Germany.[8] Data, as shown in figure 6, indicate that cracking occurred in a slab placed on top of a cement stabilized base when the pavement top surface cooled by about 21 °F (12 °C) from the maximum near surface temperature. The slab was installed at about 11:00 hours. The crack occurred about 9 hours after concrete placement at about 19:00 to 21:00 hours. At that time, near top surface slab temperature was about equal to slab bottom. However, the top slab surface was about 7 °F (4 °C) cooler than slab mid-depth.

Combined restraint stresses were calculated from temperature data shown in figure 6.[8] Split tensile strength data for corresponding hours of the restraint stress history are shown in the top portion of figure 7. The concrete split tensile strength was exceeded by combined stresses data calculated for the near to surface temperature conditions for about the same time period when cracking was reported.

## Placement Scheduling to Prevent Random Slab Cracking

Observations of cracking occurring in slabs installed at exterior locations and in beams under controlled laboratory conditions indicate that cracking occurs when cooling from maximum concrete temperature during early hydration exceeds about 15 °F (8 °C). To minimize potential for cracking, surface temperature cooling in excess of 7 to 10 °F (4 to 6 °C) should be avoided. For concrete placed during morning hours, hydration and solar radiation effects are most favorable for concrete warming. Fast cooling rates can occur within 8 hours as the sun looses its radiation heating effectiveness in early afternoon. In areas experiencing hot days and cool nights, consideration should be given to placing concrete at night. Thus concrete hydration warming along with ambient and solar heating will not be superimposed and the window of sawing opportunity will be widened. Effective coverage with curing compound will minimize top concrete surface cooling due to evaporation.

23

**Table 6. Concrete cracking due to cooling.**

| Temperature Conditions, °F | Start of Ambient Cooling at 3.6 °F/h, Hours After Concrete Placement | | | | | |
|---|---|---|---|---|---|---|
| | 2 | 4 | 6 | 8 | 24 | 48 |
| Maximum 2nd Zero Stress Crack ΔT (Non Air Entrained Concrete) | 87 | 91 | 92 | 95 | 98 | 90 |
| | 78 | 89 | 91 | 92 | 94 | 94 |
| | 57 | 64 | 73 | 76 | 70 | 66 |
| | 21 | 25 | 18 | 16 | 24 | 28 |
| Maximum 2nd Zero Stress Crack ΔT (Air Entrained Concrete) | 87 | 90 | 91 | 95 | 96 | - |
| | 81 | 88 | 91 | 92 | 94 | - |
| | 53 | 59 | 66 | 74 | 67 | - |
| | 28 | 29 | 25 | 18 | 27 | - |

3.6 °F/h = 2 °C/h

°C = 5/9 (°F-32)
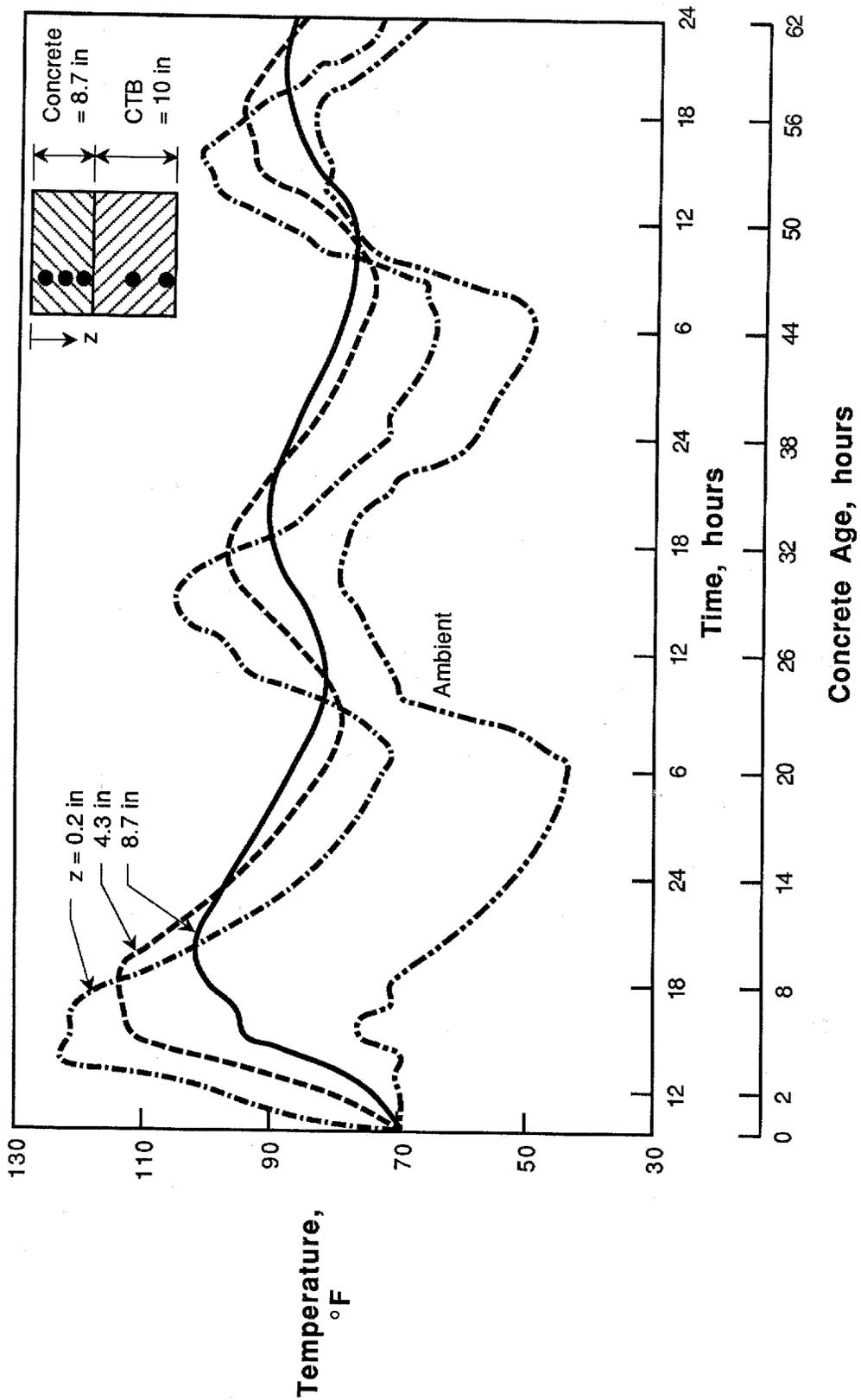
Figure 6. Temperature history in concrete slab placed on sunny day with cool night.[8]
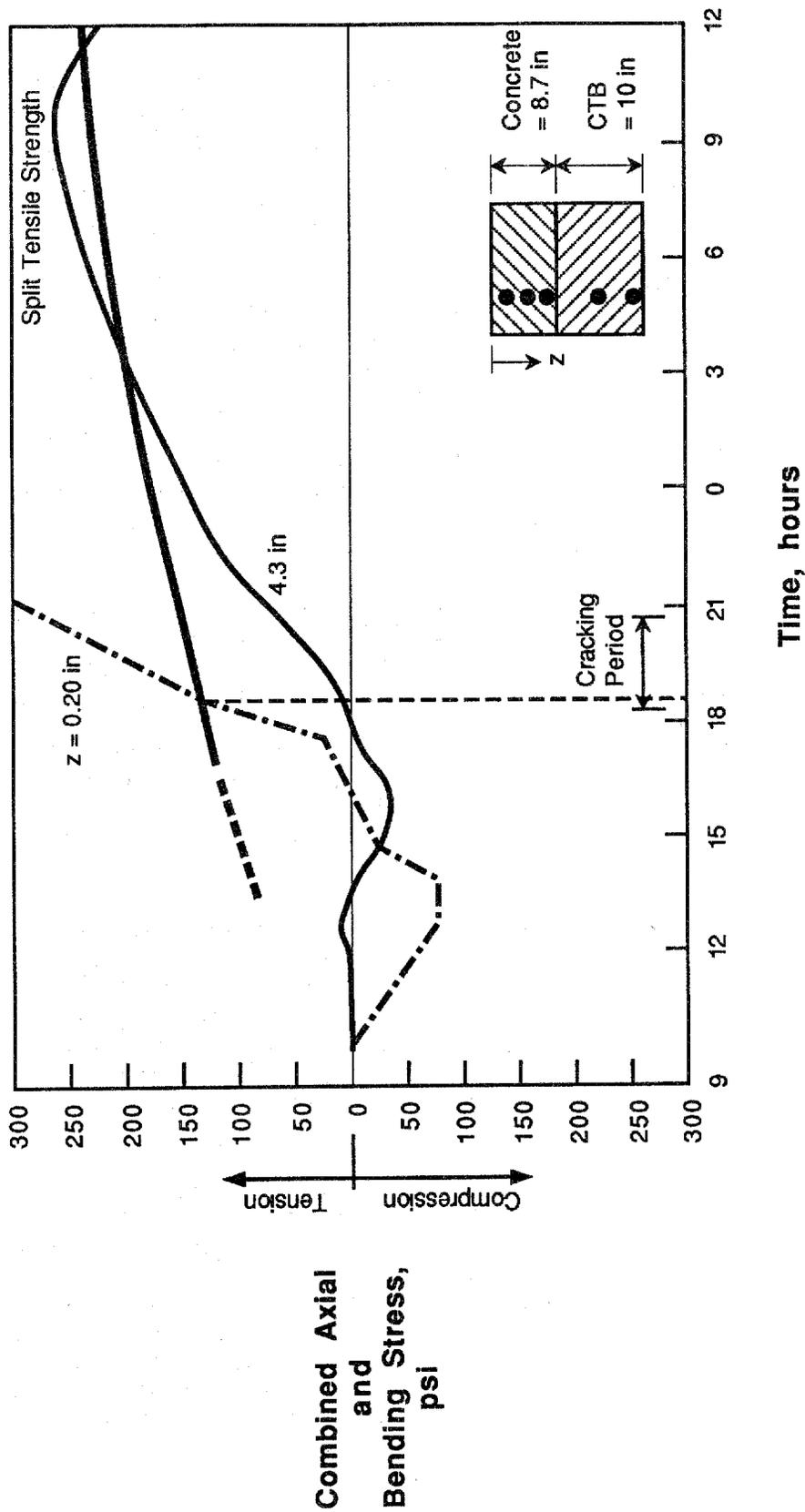
Figure 7. Combined restraint stresses.[8]

100 psi = 0.7 MPa

1 in = 2.5 cm

26

## Depth of Joint Sawcuts

The required depth of joint sawing/forming to control crack location is a complex issue. Current accepted practice is one-quarter or one-third of the slab depth for transverse joints and one-third of the slab depth for longitudinal joints, with the overriding belief being that uncontrolled longitudinal cracking may be more catastrophic from a maintenance and rehabilitation viewpoint than uncontrolled transverse cracking. However, little research has been performed to verify the effectiveness of these current guidelines.

Under an FHWA contract, a comprehensive data base was compiled which contained detailed design, construction, and performance data for 95 jointed concrete pavement sections, including depth of sawing/forming for the longitudinal and transverse joints and also field-measured transverse and longitudinal cracking.[6] For the purposes of the joint sawing study, this information was evaluated in an effort to learn of the relative effects of various sawcut depths on the development of slab cracking. For each section, the ratio of the sawcut (forming) depth (D) to the slab thickness (T) was computed for both transverse and longitudinal joints and plotted against the amount of transverse and longitudinal cracking, respectively. The expected result would be that as the D/T ratio increased, less construction-induced slab cracking would occur.

The results of this investigation are illustrated in figures 8 and 9. Figure 8 depicts the amount of transverse cracking as a function of the D/T ratio for the transverse joints. It is observed that no clear trend emerges concerning the effect of the D/T ratio on transverse cracking. This is believed due to the fact that other parameters are influencing the development of cracking. While the depth of joint sawing/forming is definitely an important factor, other factors also influence the initiation and propagation of uncontrolled cracking. These factors include, among others, time of sawing, pavement design (thickness, base type, slab length, slab width), curing conditions, and joint sawing/forming technique. It is believed that most of the transverse slab cracking can be attributed to load- or temperature-induced stresses.

Figure 9 shows the amount of longitudinal cracking as a function of the D/T ratio for the longitudinal joint. Again, no clear trend emerges concerning the effect of deeper sawcuts. Obviously, many of the same factors that were cited for contributing to the development of transverse cracking are also influencing the development of longitudinal cracking. For example, all sections showing greater than 1000 linear ft (305 m) of longitudinal cracking per mile (1.6 km) are from a State which used plastic tape inserts to form the longitudinal joint. Studies by the State agency revealed that the plastic tape did not adequately form the joint.

It is interesting to note from both figures 8 and 9 the range of points that fall vertically for a given D/T ratio. These points represent groups of experimental projects whose designs vary slightly from one another in terms of such items as base type, slab thickness, slab length, and load transfer devices. With the exception of these changes, all other design and construction factors were the same. Thus, the increase in cracking can be attributed to the addition/inclusion of certain design factors. For the most part, longer slab lengths (which would induce large thermal curling stresses) contributed to the development of increased transverse slab cracking and the use of stabilized bases (which produce higher amounts of friction between the slab and base material) contributed to the development of longitudinal slab cracking.

27

Transverse Cracking (cracks/mile)

D = sawcut depth
T = slab thickness

D/T
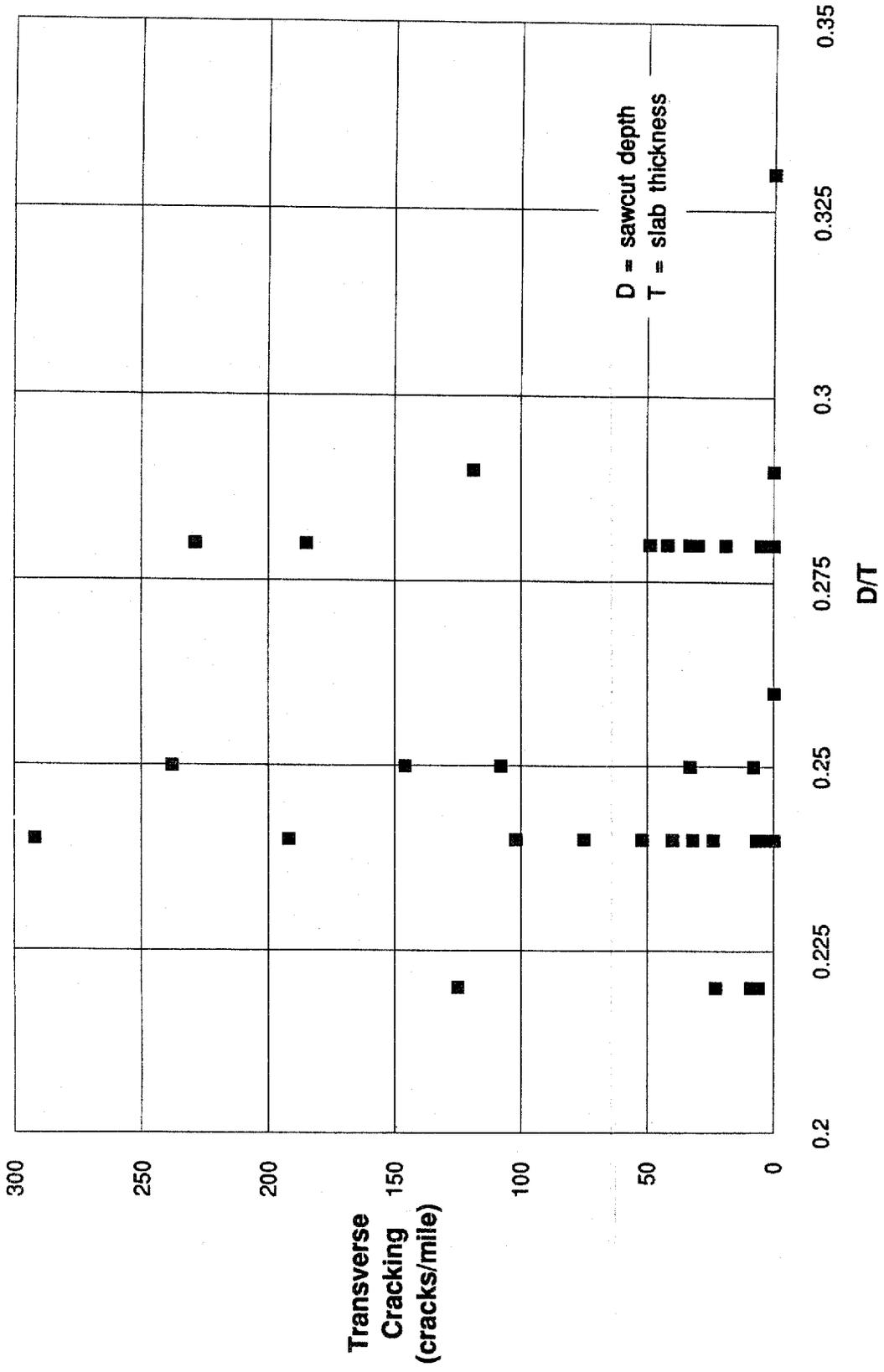
1 mile = 1.6 km

Figure 8. Amount of transverse cracking as a function of sawcut depth.
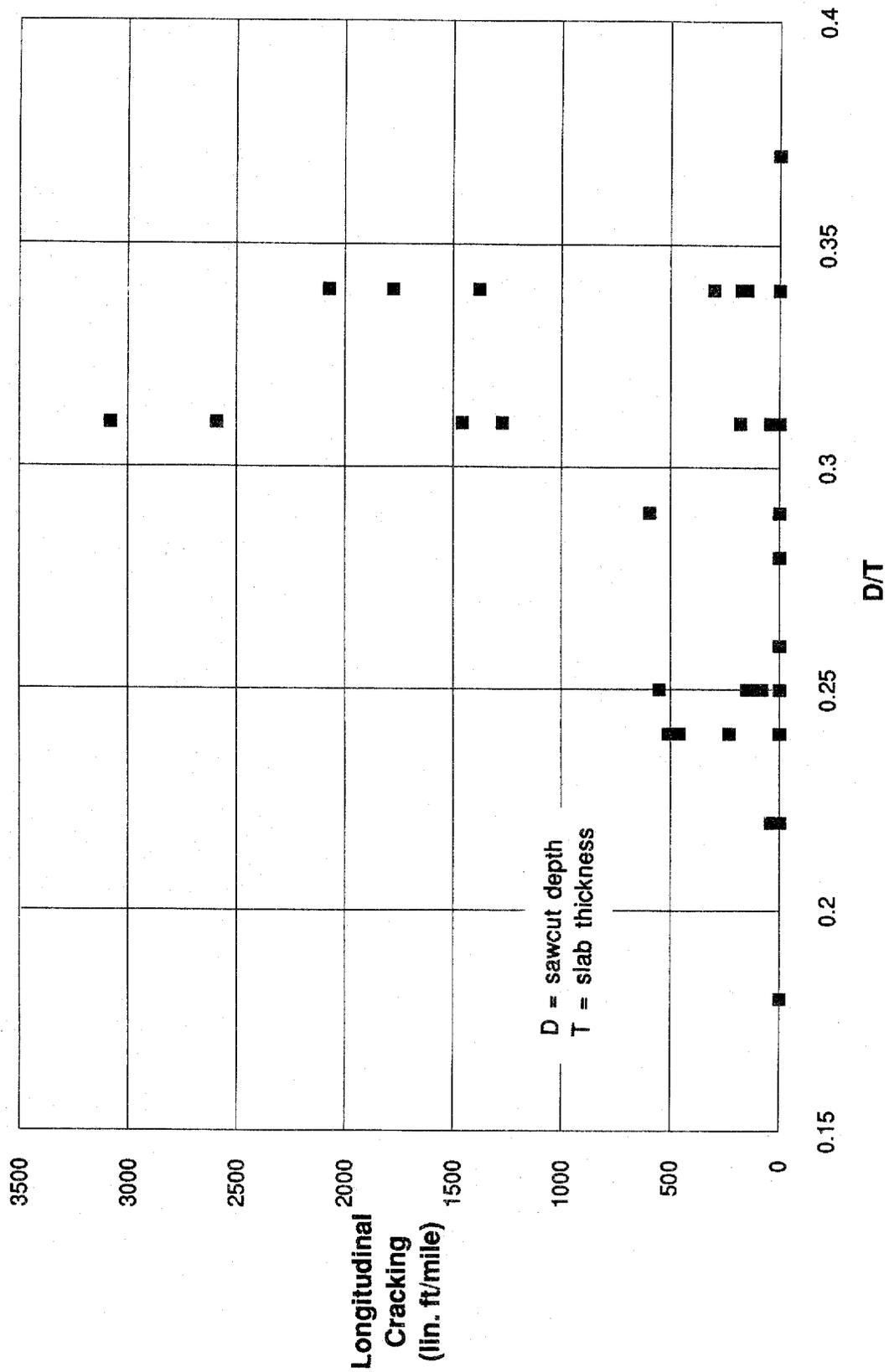
1 mile = 1.6 km

Figure 9. Amount of longitudinal cracking as a function of sawcut depth.

Thus, from the available field data, no evidence is available to support the available guidelines on the required depth of joint sawing/forming. There are simply too many other factors that influence the development of slab cracking. On the other hand, there is no evidence to refute the available guidelines on the required depth of joint sawing/forming either, which would suggest that the available guidelines continue to be used in practice until further research is able to establish the appropriate joint sawing depth.

Required depth of joint sawcuts was studied using statistical methods.[8] The potential that cracking due to axial restraint stresses and the potential that bending restraint stresses occur below sawcuts is graphically presented in figure 10. The plotted data indicate that sawcut depth (notch) should be about 30 percent of slab thickness for cracks to occur below sawcuts with a probability of 88 percent for the case of axial restraint stresses and a 98 percent probability for bending restraint stresses. The sawcut depth of about 30 percent of slab thickness is in general agreement with joint cutting and/or forming practices in many regions of the continental U.S.

The plotted data in figure 10 indicates that for equal cracking potential below the sawcut, the transverse joint should have a deeper sawcut to relieve axial restraint stresses than the longitudinal joint to relieve bending restraint stresses. Due to dowel bars and benefits of aggregate interlock to transfer load at transverse joints it is not feasible to increase the depth of transverse joint sawcuts. The curve in figure 10 for bending restraint stresses may also change when paving full width. Longitudinal joints may not be located in critical stress areas when two 12-ft (3.7-m) lanes, a 4-ft (1.2-m) inside lane shoulder, and a 10-ft (30.5-m) outside lane shoulder are simultaneously placed. This construction situation may require earlier and deeper sawing to control crack location.

## EVALUATING EARLY AGE CONCRETE PROPERTIES

Test methods to estimate early age strength properties of concrete can be broadly classified into two categories. The first category includes test methods which measure strength properties that are correlated with compressive or flexural strength. Test methods in this category include cylinder compressive, beam flexural, core compressive, pull-out, pull-off, and break-off test methods. The second test method category includes measurements of such as surface hardness, penetration resistance, time of set, pulse velocity, maturity , and electrical resistance. With the exception of core compressive strength testing, commonly used methods to evaluate early age concrete strength are nondestructive or semi-destructive tests.

For normal concrete, determination of early age concrete strength properties has been generally for concrete 1 to 3 days or older. Very little strength-related work has been done on concrete less than 1 day old. Most of the published data on strength and nondestructive testing addresses evaluation of concrete properties of an existing structure. Literature on early age strength testing is generally in reference to monitoring strength development during new construction at ages for 1 day or more for formwork removal purposes. Descriptions of test methods used to evaluate strength properties are found in tables 7 through 15. Other methods such as the impact-echo method are not discussed since equipment is not readily available or the procedures are still in the experimental phase. The advantages and disadvantages listed are listed in reference to the project objectives of characterizing concrete for proper sawing time and early loading.

The two most common methods of nondestructively evaluating early age concrete properties are the maturity method and the ultrasonic pulse velocity method. Other test

30
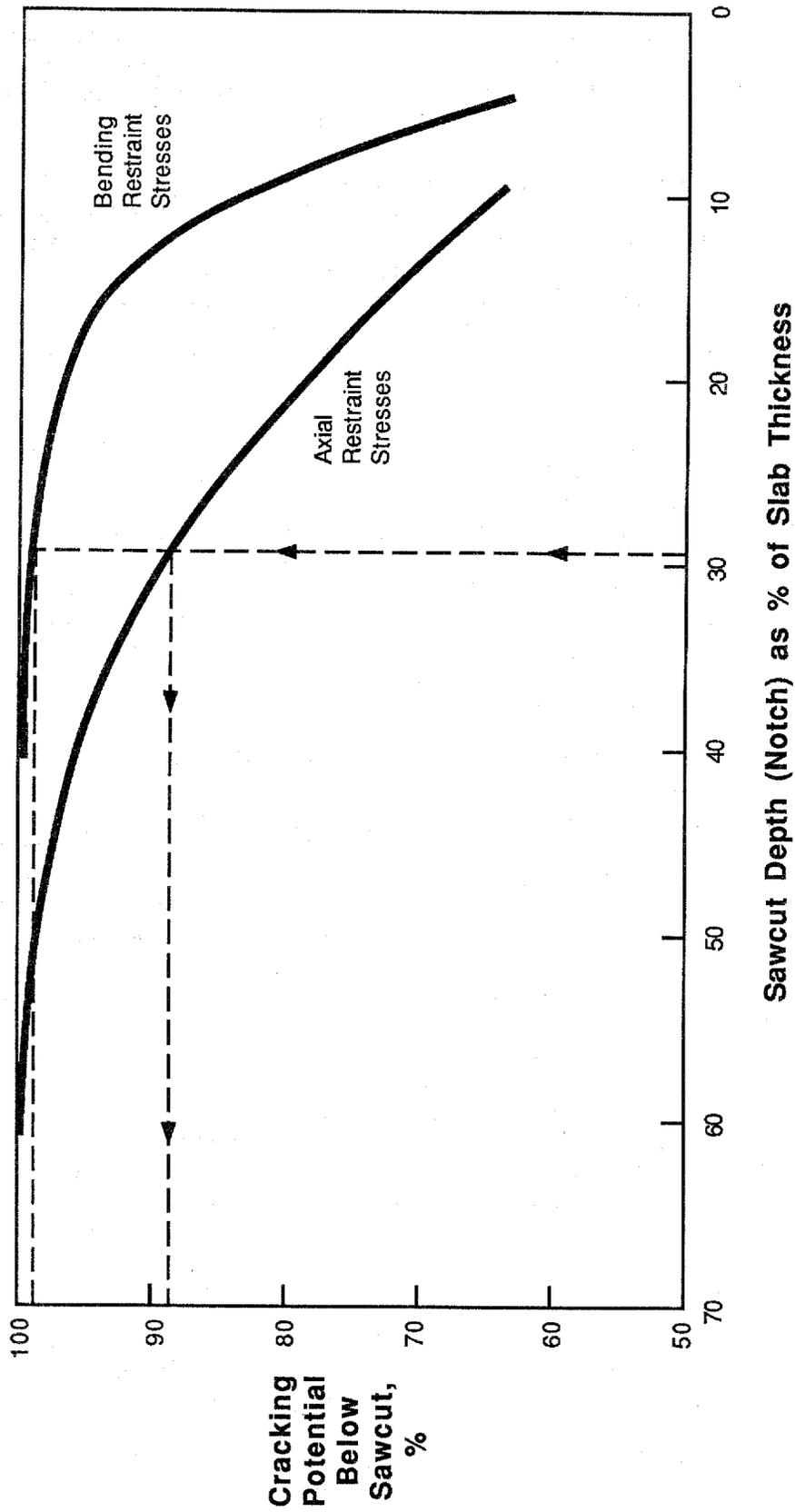
**Figure 10. Probability that a crack will occur below sawcut.[8]**

**Table 7. Cylinder compressive strength test method.**

| | |
|---|---|
| **Description** | Compressive strength data of cylinders fabricated during paving and cured under the same conditions as the pavement is compared to previously obtained core data. In situ compressive strength is estimated using previously established correlation between core and cylinder compressive strengths for subsequent construction. |
| **Standards and Specifications** | ASTM C31-87a Standard Practice for Making and Curing Concrete Test Specimens in the Field. |
| **Equipment** | Cylinder molds.<br><br>Compression testing machine. |
| **Advantages** | Easy test method.<br><br>Commonly used to estimate 28-day compressive strength.<br><br>Relatively cheap test.<br><br>Good correlation between cylinder and core in situ compressive strength at ages up to 3 days (correlation coefficient as high as 0.90).<br><br>Can correlate compressive strength with other properties such as modulus of elasticity, flexural strength, and split tensile strength. |
| **Disadvantages** | Need to properly cure, transport specimens to testing lab, and cap cylinders. Improper handling, storage, and test procedures can affect strength.<br><br>Cylinder strength can be significantly different than in situ strength since bleeding, compaction, and curing conditions are not duplicated. Have to correlate in situ and cylinder strength prior to construction.<br><br>Accuracy in estimating strength is a function of correlation between cylinder and in situ strength. Correlation reflects material, curing, construction, and testing variability.<br><br>Distribution of cylinder strength (variability) may differ from in situ strength. Good cylinder test quality control procedures result in a symmetrical bell-shaped distribution while poor construction quality control results in skewed strength distribution.<br><br>Cylinder strength may not be indicative of slab strength at saw cut elevation. |

**Table 8.  Core compressive strength test method.**

| | |
|---|---|
| **Description** | Obtaining concrete cores in pavement and directly determining in situ compressive strength. |
| **Standards and Specifications** | ASTM C42-84a Standard Method of Obtaining and Testing Drilled Cores and Sawed Beams of Concrete. |
| **Equipment** | Core rig, barrel, water tank/supply, and generator. |
| | Concrete saw to trim ends. |
| | Capping table. |
| | Compression testing machine. |
| **Advantages** | Relatively easy test. |
| | Directly provides estimate of in situ compressive (or modulus of elasticity, split tensile) strength. |
| **Disadvantages** | Relatively expensive and time consuming to obtain, prepare, and test cores. |
| | Have to correct compressive strength for height-diameter ratio. |
| | Distribution of strength may be skewed if poor quality control is maintained.  This may not be reflected if small sample size is selected. |
| | Have to patch core holes. |
| | Core ends require sawing and capping. |
| | Large core diameter may be required depending on maximum size aggregate. |
| | Difficult to obtain cores at ages less than 24 hours. |
| | Compressive strength may not be indicative of strength near surface. |

**Table 9. Impact/rebound test method.**

| | |
|---|---|
| **Description** | Impacting the concrete surface in a standard procedure with a given mass and standard activation energy and measuring rebound. |
| **Standards and Specifications** | ASTM C805-85 Standard Test Method for Rebound Number of Hardened Concrete. |
| **Equipment** | Schmidt Hammer (Swiss Hammer). |
| **Advantages** | Quick and easy test method. |
| | True nondestructive testing technique. |
| | Relatively cheap and commercially available equipment. |
| | Evaluating only near-surface concrete that is representative of concrete strength at sawing elevation where ravelling is of concern. |
| **Disadvantages** | No theoretical relationship between concrete hardness (resilience) and compressive strength. |
| | Have to correlate rebound number with compressive strength for individual concrete mixes. |
| | Lower correlation with compressive strength reported than other NDT methods. |
| | Rebound number is a function of surface texture, moisture conditions, conditions, type of coarse aggregate, and concrete age. |
| | Higher accuracy in estimating in situ strength if correlation done with cores rather than cylinders or manufacturer provided correlation. |
| | Only assessing concrete in immediate vicinity of plunger that is a function of local conditions. |
| | Have to grind a smooth surface if tining texture (troweled surface may result in a higher rebound number). |
| | Limited research with compressive strength less than 2000 psi. |

**Table 10. Ultrasonic pulse velocity test method.**

| | |
|---|---|
| **Description** | Electronically measuring the time of travel of an ultrasonic wave passing through the concrete. Pulse velocity is calculated by dividing the measured path length between the two transducers by the travel time. Velocity can then be correlated with strength/stiffness properties. |
| **Standards and Specifications** | ASTM C597-83 Standard Test Method for Pulse Velocity Through Concrete. |
| **Equipment** | Pulse velocity meter. |
| **Advantages** | Quick and easy test method with commercially available equipment.<br><br>True nondestructive test method.<br><br>Increases in compressive strength highly correlated with significant increases in pulse velocity especially at early ages (correlation coefficients reported as high as 0.92).<br><br>Has been used to monitor changes in quality of paste with time.<br><br>Can be correlated with the modulus of elasticity.<br><br>Testing near surface may be indicative of strength and aggregate to paste bond at saw cut elevation. |
| **Disadvantages** | Equipment is relatively expensive and requires calibration.<br><br>Have to correlate pulse velocity with compressive strength cylinders or cores. Best correlation is obtained by correlating with beam samples.<br><br>Surface irregularities can distort contact and influence travel time. Have to maintain good acoustic coupling between tranducer and concrete surface.<br><br>Velocity may be sensitive to presence of moisture, steel reinforcement, cracks, and voids.<br><br>Velocity may be sensitive to w/c ratio, coarse aggregate size/type/content, curing conditions, cement type, and admixtures.<br><br>Have to propagate pulse using surface transmission (indirect) or semi-direct transmission (surface to edge) unless boxouts are used. |

**Table 11. Maturity test method.**

| | |
|---|---|
| **Description** | Method of accounting for combined effects of time and concrete temperature on strength development. Concrete strength is expressed as a function of maturity which accounts for thermal history of concrete (time and temperature effects). |
| **Standards and Specifications** | ASTM C1074-87 Standard Practice for Estimating Concrete Strength by the Maturity Method. <br><br> ACI 306R-78 Cold Weather Concreting. |
| **Equipment** | Thermocouples or maturity meter. <br><br> Time-temperature recorder. |
| **Advantages** | Easy to calculate maturity value. <br><br> Commercially available equipment to measure maturity value. <br><br> Does not depend upon curing conditions. <br><br> High correlations reported between maturity and concrete strength. <br><br> Has been used to determine when to post-tension and strip formwork. |
| **Disadvantages** | Have to assume rate of strength development is either a linear (Nurse-Saul function) or exponential (Arrhenius) function. <br><br> Have to develop maturity-strength correlation. <br><br> Compressive strength used in estimating maturity often based on cylinder strength that may not be representative of in situ strength. <br><br> For maximum accuracy, a laboratory program is needed to determine the datum temperature (or activation energy) used in calculating maturity. <br><br> Maturity meters assume a strength gain-temperature relationship that may not be representative of specific concrete mixes. <br><br> Strength maturity relationship may be a function of curing temperature, aggregate type, cement type, admixtures, and water-cement ratio. <br><br> Maturity meters are relatively expensive. |

**Table 12. Penetration resistance test method.**

| | |
|---|---|
| **Description** | Drive hardened steel rod into concrete using a special gun and powder charge. The compressive strength is estimated using correlation developed between strength and probe penetration. |
| **Standards and Specifications** | ASTM C803-82 Standard Test Method for Penetration Resistance of Hardened Concrete. |
| **Equipment** | Windsor Probe. |
| **Advantages** | Quick and easy test method. |
| | Probe depth is a function of near surface concrete properties corresponding to depth of saw cut. |
| | Has been used to determine early age strength gain (to determine formwork stripping time). |
| **Disadvantages** | Requires special equipment. |
| | Probe distance is not only a function of mortar matrix strength but of aggregate hardness and type. |
| | Have to correlate probe penetration depth with cylinder or core compressive strength for maximum reliability. |
| | Higher accuracy in estimating in situ strength if correlated to core strengths. Troweled cylinder sufaces increase surface layer hardness resulting in lower probe penetration and excessive scatter in data. |
| | Probe does not cause concrete to fail in same manner as compression failure. |
| | Semi-destructive test. |
| | Gun barrel cleanliness and orientation to surface can affect velocity and consequently estimates of compressive strength. |

**Table 13. Pullout strength test method.**

| | |
|---|---|
| **Description** | Embedding a metal insert with an enlarged head in the fresh concrete surface. Measure ultimate load required to pull cone-shaped fragment. |
| **Standards and Specifications** | ASTM C900-87 Standard Practice for Pullout Strength of Hardened Concrete. |
| **Equipment** | Portable hydraulic jack. |
| | Load cell and load indicator readout box. |
| | Metal inserts. |
| **Advantages** | Pullout force is a function of near surface concrete properties corresponding to depth of saw cut. |
| | Failure is initiated at insert head. Ultimate force is possibly a function of compressive strength, fracture toughness of matrix, and/or aggregate-paste bond failure. |
| | Other test methods available, including the Building Research Establishment (BRE) method of drilling a hole and inserting wedge anchor (BRE internal fracture test). |
| | Has potential for being used to determine early age strength gain. Correlation coefficient as high as 0.95 reported between cylinder/core compressive strength and pullout force. |
| **Disadvantages** | Have correlate pullout force with strength. |
| | Have to locate testing locations prior to paving. |
| | Localized areas of concrete evaluated. |
| | Higher within-batch coefficient of variation than standard cylinder compression tests reported. |
| | Semi-destructive test. |

38

**Table 14. Pull-off strength test method.**

| | |
|---|---|
| **Description** | Pulling a partially pre-cored concrete section by a metallic disc attached with resin adhesive to concrete surface. Can also test without pre-coring. |
| **Standards and Specifications** | None. |
| **Equipment** | Metallic discs. |
| | Portable hydraulic jack. |
| | Load cell and load indicator readout box. |
| **Advantages** | May measure bond between paste and aggregate. |
| | Pull-off test measures near surface concrete properties corresponding to saw cut elevations. |
| | Directly measures a mechanical concrete property (tensile strength). |
| | No pre-planning locations necessary. |
| **Disadvantages** | Relatively high within-batch coefficient of variation reported. |
| | Function of aggregate type. |
| | Costs increase when partial coring done. |
| | Have to establish good bond between disc and surface with fast-setting epoxy resin that is insensitive to moisture. |
| | Surface finishing may influence pull-off strength. |
| | Semi-destructive test. |

**Table 15. Break-off test method.**

| | |
|---|---|
| **Description** | Tubular disposable forms inserted into fresh concrete. Insert removed (or concrete is partially cored if no insert) and force is applied perpendicular to insert. Flexural strength is directly measured. |
| **Standards and Specifications** | European specifications. |
| **Equipment** | Load cell and load indicator readout box.<br><br>Portable hydraulic jack. |
| **Advantages** | Simple and quick test.<br><br>Commercially available equipment.<br><br>Directly measures a mechanical property of concrete (flexural strength).<br><br>Measures near-surface properties corresponding to saw-cut elevation. |
| **Disadvantages** | Have to pre-plan location if concrete is not partially cored.<br><br>Hard to insert tubes into slipform low slump concrete.<br><br>Insert diameter is a function of maximum-size aggregate.<br><br>Semi-destructive test. |

methods have been used to estimate strength properties but often combined with the maturity or pulse velocity methods. Newer test methods proposed have not been standardized or extensively verified.

For determining strength of concrete at latter ages such as 7 and 28 days for construction specification compliance, field cured cylinders and beams are commonly tested. Cylinders and beams are tested in compression and flexure, respectively. Specimens may also be cored or sawed from the pavement to directly determine insitu compressive strength. Due to difficulties in obtaining, preparing, and testing specimens at ages less than 3 days, these test methods may not be applicable for joint sawing operations. Since concrete has very little early age tensile strength and it is commonly assumed that other properties such as tensile, split-tensile strengths, modulus of elasticity, etc. are related to compressive or flexural strength, other strength tests are not commonly required.

The most common nondestructive test to estimate compressive strength is the impact rebound hardness test using a Schmidt (Swiss) hammer. Rebound of a spring loaded mass and standard activation energy impacting the concrete is measured. The rebound number measured has to be correlated with strength properties of the concrete since no theoretical relationship exists. The absorbed energy is related to the strength and stiffness of the concrete. The higher the rebound (lower absorbed energy) the higher the compressive strengths. Because there bound hammer test evaluates near-surface concrete, it is representative of strength where sawing occurs. Because strength is estimated near the surface this may not be a suitable test for early loading analysis.

A comprehensive laboratory investigation correlating several nondestructive testing techniques with each other as well as with cores and cylinders was done on early age strength evaluation by the Canada Center for Mineral and Energy Technology (CANMET) in 1976.[12] For four mixes with varying cement contents, tested at ages of 1, 2, and 3 days, maximum error in estimating core compressive strength from rebound hammer tests was approximately 650 psi (4.48 MPa). Compressive strength ranged from approximately 1500 to 3500 psi (10.3 to 24.1 MPa).

Recently, the use of the Clegg Impact Hammer and the Proceq Type PT hammer was demonstrated to determine surface hardness of cement-treated bases.[13] The Clegg tester uses an accelerometer fastened to a 10-lb (4.5-kg) hammer to measure impact acceleration. The Proceq hammer is a rebound pendulum type impact tester. Six soil materials were selected to evaluate impact hammer responses. Different amounts of cement were used to develop a range of compressive strength. Responses at ages ranging from 1 to 17 days were correlated with companion compressive strength cylinders. For both test methods the correlation between strength and rebound number was high. The conditional standard deviation for strengths up to 1000 psi (6.9 MPa) was less than 100 psi (690 kPa) for both hammers.

It may be possible to use a rebound value using one of the impact hammer devices to determine sawability of concrete. In addition to compressive strength, the Schmidt hammer may also be correlated with abrasion resistance. One study done at Aston University, United Kingdom, indicated that at 28 days the rebound number is highly correlated with abrasion resistance.[14]

Ultrasonic pulse velocity studies indicate this test method may be used to estimate compressive strength and other material concrete properties such as setting characteristics and modulus of elasticity. The travel time of short duration compressional waves passing through the concrete are electronically measured. Pulse velocity is calculated by dividing

the measured path length between the pulse transmitting and receiving transducers by the travel time. Velocity can then be correlated with strength properties. No standard correlations exist between strength and pulse velocity. The method is based on the relationship that the velocity of sound is proportional in the square root of the elastic modulus divided by density. Since density and concrete strength can be correlated, pulse velocity can be used to estimate strength properties. If the elastic modulus is proportional to the square root of compressive strength then velocity is proportional to the fourth root of compressive strength. This suggests that significant percentage increases in pulse velocity occur at lower compressive strengths (early age).

Many studies have been done to estimate early age compressive strength using the pulse velocity method.[15-18] Better correlations of pulse velocity and compressive strength at early ages than at higher strength levels have been reported. Correlation coefficient as high as 0.91 have been reported for core compressive strength and pulse velocity data at strengths less than 3500 psi (24.1 MPa).[12] Studies show that pulse velocity increases very rapidly during the first few hours while strength development is more gradual. At later ages increases in strength development are significantly larger than increases in pulse velocity.[15,16] The initial increase in velocity may be attributed to early silicate hydrate formation growth from cement particles providing a path link with aggregates. Strength gains show no significant increases until final set is achieved. Although tests follow the stiffening processes there is dependency between speed of setting and strength gain.

Although studies indicate the pulse velocity method is applicable in estimating early strength properties, it does have disadvantages. Due to the non-homogenity of concrete mixes there exists a high signal attenuation in plastic concrete. Pulse travel time may only be measured once the concrete undergoes initial set and is in a semi-viscous state. Even in this state the travel distance may have to be significantly reduced. Maximum travel distances of 3 to 4 in (76 to 102 mm) have been reported in plastic concrete.[17] Ideally access to two sides of the concrete is needed for the transmitting and receiving transducers. At early ages pulse velocity testing may have to be done on cylinders or with transducers on the slab edge and surface. Maximum testing distances on matured concrete of up to 50 ft (15.3 m) have been reported.

The maturity method has been used to estimate compressive strength of concrete at early ages for formwork removal. The method accounts for the combined effects of temperature and time on strength development. Increases in curing temperature can speed up the hydration process and increase strength development. Maturity is a function of the product of curing time and temperature. It is then assumed that a given mix will have the same strength at equal maturities independent of curing time and temperature histories. Time and temperature of insitu concrete can be monitored with thermistors, thermocouples, or commercially available maturity meters.

Two types of maturity functions are commonly used to combine the effects of time and temperature on strength development. The Nurse-Saul function assumes the rate of strength development is a linear function of temperature above a datum temperature (below which no concrete strength gain occurs with time). ASTM recommends use of a 0 °C (32 °F) datum temperature for a curing temperature range of 0 to 40 °C (32 to 104 °F), Type I cement, and no admixtures unless it is experimentally determined. The second maturity function assumes the rate of strength gain varies exponentially with curing temperature. This function, often called the Arrhenius function, requires the activation energy be estimated or experimentally determined.

42

Studies on early strength development indicate the maturity method concept is a simple and useful means of monitoring strength gain as a function of both time and temperature.[18] Strength gain as a function of maturity may be dependent on cement type, aggregate type, water-cement ratio, etc. Maturity models are generally dependent on individual concrete mix designs. The maturity models using the linear Nurse-Saul function can be improved by changing the datum temperature if not previously determined experimentally.

The probe penetration test has been used for measuring strength development of concrete at early ages to determine minimum formwork stripping times. A commercially available system known as the Windsor Probe is commonly used. A powder charge drives a hardened metal probe into the concrete. The exposed probe length is used as a measure of penetration resistance. Depth of penetration is inversely proportional to both the mortar and coarse aggregate properties. The correlation between probe penetration and compressive strength is therefore affected by the hardness of the aggregate. At early ages mortar strength has a larger effect on compressive strength. Significant errors in estimating compressive strengths are possible using calibration relationships supplied by the manufacturer. Correlations should be established for individual mixes.

The CANMET investigation of early age compressive strength indicates that for four different mixes (single aggregate source) the correlation coefficient between core compressive strength and exposed probe length was 0.73. This suggests that for compressive strengths of less than 4000 psi (27.6 MPa) the probe penetration method may be used to estimate compressive strengths. Predicted strengths were generally less than 750 psi (5.2 MPa). Other studies of compressive strength and probe penetration have indicated possible uses at strengths of greater than 2000 psi (13.8 MPa).

Pullout tests may also be used to monitor strength development of concrete at early age. The test measures the ultimate load required to pull an embedded steel insert with an enlarged head located near the concrete surface. The failure mechanism of the concrete around the insert is complex. Circumferential cracking begins at the enlarged head and propagates upward toward the reaction ring at the surface. Ultimate load may be a function of a combination of compressive strength, fracture toughness, aggregate paste bond, indirect tension, or shear. Studies on early strength development indicate that the pullout test is a feasible method in monitoring strength gain.[12,19] At compressive strengths of less than 3500 psi (24.1 MPa) the correlation coefficient in two studies between pullout load and core strength ranged from 0.74 up to 0.95.

Other test methods including the pull-off, break-off, and pulse echo test methods may have potential to estimate early age strength properties. Because equipment and/or procedures are still under development, not commonly used, or are still in the research and verification stage they were not investigated as part of the joint sawing study.

# CHAPTER 3. EARLY AGE CONCRETE PROPERTIES FROM LABORATORY TESTS

The state-of-the-art review process revealed that there was a significant dearth of data regarding early age strength characteristics and concrete property responses to nondestructive testing. This was particularly noted for concrete strength characteristics and concrete nondestructive test responses for the first 24 hours after placement. For defining the limits for sawcutting window of opportunity and earliest pavement loading, respectively, two time increments are of interest:

- The first 24 hours starting with concrete placement.
- The 2-day to 10-day increment after concrete placement.

It is recognized that these time increments are most representative for highway construction occurring during summer and early fall in eastern, central plains, western mountain, and costal areas of the continental United States. For cooler or hotter concrete placement conditions, adjustments can be made for more rapid or slower curing effects by consideration of maturity effects on early concrete strength gains. Concrete maturity accounts for both curing time and temperature effects on strength development. Maturity effects on concrete strength properties and nondestructive test response properties, as part of the test program, are available to accommodate specific site curing condition variables.

Concrete characteristics that were identified in the state-of-the-art review to have a significant influence on concrete sawability at early ages included strength, paste to aggregate bond, and type of concrete coarse aggregate. Methods of tests to evaluate sawability characteristics included compressive strength, flexural strength, splitting tensile strength, setting time for mortar, pulse velocity, maturity measurements, and Clegg Impact Hammer tests.

## SELECTION OF TEST VARIABLES

Test variables were selected to cover a range of highway concrete mix constituents and to cover, as far as practicable in a controlled laboratory environment, the range of early pavement exposure conditions. Concrete mix constituent variables included type, shape, and hardness of coarse aggregate and amount of cement used. A fixed amount of fly ash was used in all the concrete mixes. The fly ash was not used as a portland cement concrete replacement. Test variables pertaining to environmental and curing conditions included three curing temperatures and two levels of curing relative humidity (RH). One of the curing conditions, 72 °F (22 °C) and 100 percent RH, is prescribed by American Society for Testing and Materials (ASTM) methods. The laboratory test program, as it pertains to a given concrete mix, was divided into two time segments. This was done because of size of laboratory technician testing crew, quality control of laboratory mix batching with reproducibility of mixes, and requirements of conditioning mix constituents at initial concrete temperatures which could be realistically expected at the respective curing temperatures. The first time segment consisted of specimens made for testing at ages ranging from a 4 to 24 hours. The second time segment consisted of specimens made for testing between 1

44

and 28 days. Test variables are listed in table 16 for laboratory tests made in the 4-to 24-hour period and in table 17 for the tests for the 1-to 28-day period. Test specimen quantities and dimensions are listed in table 18.

Three concrete coarse aggregates were used:
- Crushed limestone from Illinois (CS = crushed soft aggregate).
- Crushed rose quartzite from South Dakota (CH = crushed hard aggregate).
- Rounded silaceous river gravel from Ohio (RH = rounded hard aggregate).

All three aggregates (CS, CH, and RH) were used for making the 4- to 24-hour period test specimens and the sawing slabs. The CS and CH aggregate types were used for making the 1- through 28-day laboratory test specimens. Aggregate gradations are listed in table 19 and aggregate properties are listed in table 20.

The crushed Illinois dolomitic limestone aggregate, obtained from the McCook pit located in Northern Illinois, is a source approved by Illinois DOT for highway concrete pavement construction. The dolomitic limestone used was composed of both magnesium carbonate and calcium carbonate with a Moh's minimal hardness rating of approximately 3.5. Approximately five tons (4500 kg) of this material were delivered to the laboratory facility. A sufficient amount of the same crushed limestone production run was stored at a ready mix batching plant for subsequent sawing strip slab construction. The sawing strip slabs are described in Chapter 4. Investigation of Earliest Joint Sawcutting in this report.

The hard crushed rose quartzite aggregate was obtained from Sioux Falls, South Dakota from a source approved by the South Dakota DOT for highway concrete pavement construction. The quartzite aggregate was composed of quartz minerals with a hardness rating of about 7.5. Approximately 20 tons (18,100 kg) were trucked from South Dakota to the laboratory facilities and 15 tons (13,600 kg) were delivered to the ready mix plant scheduled to batch sawing strip slab concrete mixes.

The hard rounded river gravel was obtained from Dilles Bottom, Ohio from a source approved by the Ohio DOT for highway concrete pavement construction. The gravel was mixture containing mainly limestone, dolomite, quartzite, and chert. The predominant minerals in the rock were quartz, calcite, and feldspar with hardness ratings ranging from 4 to 6. Approximately 15 tons (13,600 kg) of the Ohio material was trucked to Northern Illinois and distributed in 5-ton (4500-kg) and 10-ton (9100-kg) proportions to the laboratory and the local ready mix producer for use in sawing slabs.

Concrete mix fine aggregate constituent was the same for all mixes. The natural quartz sand used for the laboratory test specimens and the sawing slabs obtained from Algonquin, Illinois, meets Illinois DOT requirements. Fine aggregate gradation is listed in table 19.

Cementitious materials used for making laboratory test specimens and sawing slabs were Type I portland cement and a Class F fly ash. Two levels of cement amounts, 500 and 650 lb/yd$^3$ (297 and 386 kg/m$^3$) of concrete, were used. The amount of fly ash was a constant 100 lb/yd$^3$ (59 kg/m$^3$) for all mixes.

**Table 16. Scope of early age concrete properties tests - 4 to 24 hours.**

| Test | Test Method | Cement Content, lb/yd³ | Coarse Aggregate Type[1] | Number of Specimens Tested at Each Age Curing Temperature at 50% RH | | | Number at T=50, 72, and 100 °F Testing Age, hours | | | | Total Number of Specimens |
|---|---|---|---|---|---|---|---|---|---|---|---|
| | | | | 50 °F | 72 °F | 100 °F | 4 | 6 | 9 | 24 | |
| Compressive Strength  f'c | ASTM C39-86 | 500 | CS | 3 | 3 | 3 | 9 | 9 | 9 | 9 | 216 |
| | | | CH | 3 | 3 | 3 | 9 | 9 | 9 | 9 | |
| | | | RH | 3 | 3 | 3 | 9 | 9 | 9 | 9 | |
| | | 650 | CS | 3 | 3 | 3 | 9 | 9 | 9 | 9 | |
| | | | CH | 3 | 3 | 3 | 9 | 9 | 9 | 9 | |
| | | | RH | 3 | 3 | 3 | 9 | 9 | 9 | 9 | |
| Flexural Strength  (modulus of rupture, MR) | ASTM C78-84 | 500 | CS | 2 | 2 | 2 | 6 | 6 | 6 | 6 | 144 |
| | | | CH | 2 | 2 | 2 | 6 | 6 | 6 | 6 | |
| | | | RH | 2 | 2 | 2 | 6 | 6 | 6 | 6 | |
| | | 650 | CS | 2 | 2 | 2 | 6 | 6 | 6 | 6 | |
| | | | CH | 2 | 2 | 2 | 6 | 6 | 6 | 6 | |
| | | | RH | 2 | 2 | 2 | 6 | 6 | 6 | 6 | |
| Splitting Tensile Strength  ST | ASTM C496-86 | 500 | CS | 3 | 3 | 3 | 9 | 9 | 9 | 9 | 216 |
| | | | CH | 3 | 3 | 3 | 9 | 9 | 9 | 9 | |
| | | | RH | 3 | 3 | 3 | 9 | 9 | 9 | 9 | |
| | | 650 | CS | 3 | 3 | 3 | 9 | 9 | 9 | 9 | |
| | | | CH | 3 | 3 | 3 | 9 | 9 | 9 | 9 | |
| | | | RH | 3 | 3 | 3 | 9 | 9 | 9 | 9 | |

[1] NOTE: CS = Crushed Soft (Limestone aggregate - Illinois)  500 lb/yd³ = 297 kg/m³, 650 lb/yd³ = 386 kg/m³
CH = Crushed Hard (Quartzite aggregate - South Dakota)  50 °F = 10 °C, 72 °F = 22 °C, 100 °F = 38 °C
RH = Rounded Hard (River gravel aggregate - Ohio)

46

**Table 16. Scope of early age concrete properties tests - 4 to 24 hours (continued).**

| Test | Test Method | Cement Content, lb/yd$^3$ | Coarse Aggregate Type[1] | Number of Specimens Tested at Each Age Curing Temperature at 50% RH | | | Number at T=50, 72, and 100 °F | | | | Total Number of Specimens |
|------|------|------|------|------|------|------|------|------|------|------|------|
| | | | | | | | Testing Age, hours | | | | |
| | | | | 50 °F | 72 °F | 100 °F | 4 | 6 | 9 | 24 | |
| Pulse Velocity | ASTM C597-83 | 500 | CS | 3 | 3 | 3 | 3 | 3 | 3 | 3 | 72 |
| | | | CH | 3 | 3 | 3 | 3 | 3 | 3 | 3 | |
| | | | RH | 3 | 3 | 3 | 3 | 3 | 3 | 3 | |
| PV | | 650 | CS | 3 | 3 | 3 | 3 | 3 | 3 | 3 | |
| | | | CH | 3 | 3 | 3 | 3 | 3 | 3 | 3 | |
| | | | RH | 3 | 3 | 3 | 3 | 3 | 3 | 3 | |
| Maturity | ASTM C1074-87 | 500 | CS | 1 | 1 | 1 | 1 | 1 | 1 | 1 | 24 |
| | | | CH | 1 | 1 | 1 | 1 | 1 | 1 | 1 | |
| MAT | | | RH | 1 | 1 | 1 | 1 | 1 | 1 | 1 | |
| | | 650 | CS | 1 | 1 | 1 | 1 | 1 | 1 | 1 | |
| | | | CH | 1 | 1 | 1 | 1 | 1 | 1 | 1 | |
| | | | RH | 1 | 1 | 1 | 1 | 1 | 1 | 1 | |
| Modulus of Elasticity | ASTM C469-87a | 500 | CS | - | 2 | - | 2 | 2 | 2 | 2 | 16 |
| Ec | | 650 | CS | - | 2 | - | 2 | 2 | 2 | 2 | |

[1] NOTE: CS = Crushed Soft (Limestone aggregate - Illinois)
CH = Crushed Hard (Quartzite aggregate - South Dakota)
RH = Rounded Hard (River gravel aggregate - Ohio)

500 lb/yd$^3$ = 297 kg/m$^3$, 650 lb/yd$^3$ = 386 kg/m$^3$
50 °F = 10 °C, 72 °F = 22 °C, 100 °F = 38 °C

47

Table 16. Scope of early age concrete properties tests - 4 to 24 hours (continued).

| Test | Test Method | Cement Content, lb/yd³ | Coarse Aggregate Type¹ | Number of Specimens — Curing Temperature at 50% RH | 72 °F (nominal) | Number at T=72 °F — Testing Age, hours (varied with rate of concrete hardening) | Total Number of Tests |
|---|---|---|---|---|---|---|---|
| Sawability | -- | 500 | CS | - | - | 4 (diamond blade) | 46 |
| | | | CH | - | 1 | 8 (diamond blade) | |
| | | | RH | - | 1 | 5 (diamond blade) | |
| | | 650 | CS | - | 1 | 17 (diamond and abrasive blade) | |
| | | | CH | - | 1 | 6 (diamond blade) | |
| | | | RH | - | 1 | 6 (diamond blade) | |
| Setting Time for Mortar | ASTM C403-88 | 500 | CS | - | 1 | 2 | 12 |
| | | | CH | - | 1 | 2 | |
| | | | RH | - | 1 | 2 | |
| | | 650 | CS | - | 1 | 2 | |
| | | | CH | - | 1 | 2 | |
| | | | RH | - | 1 | 2 | |
| Coefficient of Thermal Expansion | -- | 500 | CS | - | 2 | 2 at 8 hours    2 at 16 hours | 24 |
| | | | CH | - | 2 | 2 at 8 hours    2 at 16 hours | |
| | | | RH | - | 2 | 2 at 8 hours    2 at 16 hours | |
| | | 650 | CS | - | 2 | 2 at 8 hours    2 at 16 hours | |
| | | | CH | - | 2 | 2 at 8 hours    2 at 16 hours | |
| | | | RH | - | 2 | 2 at 8 hours    2 at 16 hours | |

¹ NOTE: CS = Crushed Soft (Limestone aggregate - Illinois)
CH = Crushed Hard (Quartzite aggregate - South Dakota)
RH = Rounded Hard (River gravel aggregate - Ohio)

500 lb/yd³ = 297 kg/m³, 650 lb/yd³ = 386 kg/m³
50 °F = 10 °C, 72 °F = 22 °C, 100 °F = 38 °C

**Table 16. Scope of early age concrete properties tests - 4 to 24 hours (continued).**

| Test | Test Method | Cement Content, lb/yd$^3$ | Coarse Aggregate Type[1] | Number of Specimens Tested at Each Age Curing Temperature at 50% RH | | | Number at T=72 °F<br><br>Testing Age, hours<br>(varied with rate of concrete hardening) | Total Number of Tests |
|------|-------------|-----------|-----------|------|------|------|------|------|
| | | | | 50 °F | 72 °F | 100 °F | | |
| Clegg Impact Hammer | --- | 500 | CS | 3 | 3 | 3 | 6 | 33 |
| | | | CH | 3 | 3 | 3 | 5 | |
| | | | RH | 3 | 3 | 3 | 6 | |
| | | 650 | CS | 3 | 3 | 3 | 7 | |
| | | | CH | 3 | 3 | 3 | 5 | |
| | | | RH | 3 | 3 | 3 | 4 | |
| Petrographic Examination of Hardened Concrete | ASTM C856-83 | 500 | CS | - | - | - | - | 3 |
| | | | CH | - | 1 | - | 1 | |
| | | | RH | - | 1 | - | 1 | |
| | | 650 | CS | - | 1 | - | 1 | |
| | | | CH | - | - | - | - | |
| | | | RH | - | - | - | - | |
| Cube Compressive Strength | ASTM C109-88 | 500 | CS | - | 2 | - | 10 | 56 |
| | | | CH | - | 2 | - | 10 | |
| | | | RH | - | 2 | - | 10 | |
| | | 650 | CS | - | 2 | - | 10 | |
| | | | CH | - | 2 | - | 10 | |
| | | | RH | - | 2 | - | 6 | |

[1] NOTE: CS = Crushed Soft (Limestone aggregate - Illinois)
CH = Crushed Hard (Quartzite aggregate - South Dakota)
RH = Rounded Hard (River gravel aggregate - Ohio)

500 lb/yd$^3$ = 297 kg/m$^3$, 650 lb/yd$^3$ = 386 kg/m$^3$
50 °F = 10 °C, 72 °F = 22 °C, 100 °F = 38 °C

Table 17. Scope of concrete property tests - 1 to 28 days.

| Test | Test Method | Cement Content, lb/yd³ | Coarse Aggregate Type[1] | Number of Specimens Tested at Each Age | | | | Specimen Subtotal — Testing Age, days | | | | | Total Number of Specimens |
|---|---|---|---|---|---|---|---|---|---|---|---|---|---|
| | | | | 100% RH 72 °F | 50% RH 50 °F | 50% RH 72 °F | 50% RH 100 °F | 1 | 3 | 7 | 14 | 28 | |
| Compressive Strength f'c | ASTM C39-86 | 500 | CS | 3 | 3 | 3 | 3 | 12 | 12 | 12 | 12 | 12 | 240 |
| | | | CH | 3 | 3 | 3 | 3 | 12 | 12 | 12 | 12 | 12 | |
| | | 650 | CS | 3 | 3 | 3 | 3 | 12 | 12 | 12 | 12 | 12 | |
| | | | CH | 3 | 3 | 3 | 3 | 12 | 12 | 12 | 12 | 12 | |
| Flexural Strength (modulus of rupture, MR) | ASTM C78-84 | 500 | CS | 2 | 2 | 2 | 2 | 8 | 8 | 8 | 8 | 8 | 160 |
| | | | CH | 2 | 2 | 2 | 2 | 8 | 8 | 8 | 8 | 8 | |
| | | 650 | CS | 2 | 2 | 2 | 2 | 8 | 8 | 8 | 8 | 8 | |
| | | | CH | 2 | 2 | 2 | 2 | 8 | 8 | 8 | 8 | 8 | |
| Modulus of Elasticity Ec | ASTM C469-87 | 500 | CS | 3 | 3 | 3 | 3 | 12 | 12 | 12 | 12 | 12 | 240 |
| | | | CH | 3 | 3 | 3 | 3 | 12 | 12 | 12 | 12 | 12 | |
| | | 650 | CS | 3 | 3 | 3 | 3 | 12 | 12 | 12 | 12 | 12 | |
| | | | CH | 3 | 3 | 3 | 3 | 12 | 12 | 12 | 12 | 12 | |

[1] NOTE: CS = Crushed Soft (Limestone aggregate - Illinois)
CH = Crushed Hard (Quartzite aggregate - South Dakota)

500 lb/yd³ = 297 kg/m³, 650 lb/yd³ = 386 kg/m³
50 °F = 10 °C, 72 °F = 22 °C, 100 °F = 38 °C

**Table 17. Scope of concrete property tests - 1 to 28 days (continued).**

| Test | Test Method | Cement Content, lb/yd$^3$ | Coarse Aggregate Type[1] | Number of Specimens Tested at Each Age | | | | Specimen Subtotal Testing Age, days | | | | | Total Number of Specimens |
|---|---|---|---|---|---|---|---|---|---|---|---|---|---|
| | | | | 100% RH 72 °F | 50% RH 50 °F | 50% RH 72 °F | 50% RH 100 °F | 1 | 3 | 7 | 14 | 28 | |
| Pulse Velocity | ASTM C597-83 | 500 | CS | 3 | 3 | 3 | 3 | 3 | 3 | 3 | 3 | 3 | 60 |
| | | | CH | 3 | 3 | 3 | 3 | 3 | 3 | 3 | 3 | 3 | |
| | | 650 | CS | 3 | 3 | 3 | 3 | 3 | 3 | 3 | 3 | 3 | |
| PV | | | CH | 3 | 3 | 3 | 3 | 3 | 3 | 3 | 3 | 3 | |
| Maturity | ASTM C1074-87 | 500 | CS | 1 | 1 | 1 | 1 | 1 | 1 | 1 | 1 | 1 | 20 |
| | | | CH | 1 | 1 | 1 | 1 | 1 | 1 | 1 | 1 | 1 | |
| MAT | | 650 | CS | 1 | 1 | 1 | 1 | 1 | 1 | 1 | 1 | 1 | |
| | | | CH | 1 | 1 | 1 | 1 | 1 | 1 | 1 | 1 | 1 | |

[1] NOTE: CS = Crushed Soft (Limestone aggregate - Illinois)
    CH = Crushed Hard (Quartzite aggregate - South Dakota)

500 lb/yd$^3$ = 297 kg/m$^3$, 650 lb/yd$^3$ = 386 kg/m$^3$
50 °F = 10 °C, 72 °F = 22 °C, 100 °F = 38 °C

**Table 18. Test specimen summary.**

| Test | Specimen Dimension, in | Number of Specimens | Replicate Specimens |
|---|---|---|---|
| Compressive Strength | 6 x 12 cylinder | 456 | 3 |
| Flexural Strength | 6 x 6 x 21 beam | 304 | 2 |
| Splitting Tensile Strength | 6 x 12 cylinder | 216 | 3 |
| Mortar Strength | 2 x 2 x 2 cube | 56 | 2 |
| Pulse Velocity | 6 x 12 cylinder | 132 | 3 |
| Concrete Maturity | cylinder and sawing strip | 44 | 1 |
| Coefficient of Thermal Expansion | 3 x 3 x 11.25 beam | 24 | 2 |
| Modulus of Elasticity | 6 x 12 cylinder | 256 | 3 |
| Sawability | 10 x 48 x 240 sawing strip | 6 | 1 |
| Clegg Impact Hammer | 10 x 24 x 24 block | 3 | 1 |
| Setting Time for Mortar | 8 x 12 cylinder | 12 | 2 |
| Petrographic Examination | 4 x 10 core | 3 | 1 |

NOTE: For laboratory tests summarized in tables 16 and 17.

1 in = 2.54 cm

**Table 19. Aggregate gradations.**

| Coarse Aggregate | Percentage Passing | | | | | |
|---|---|---|---|---|---|---|
| | 1-1/2 in | 1 in | 3/4 in | 1/2 in | 3/8 in | #4 |
| Crushed Limestone | 100 | 100 | 76 | 35 | 19 | 4 |
| Crushed Quartzite | 100 | 100 | 93 | 41 | 15 | 2 |
| Round River Gravel | 100 | 99 | 90 | 50 | 11 | 0 |

| Fine Aggregate | #4 | #8 | #16 | #30 | #50 | #100 | #200 |
|---|---|---|---|---|---|---|---|
| Fineness Modulus 2.64 | 100 | 92 | 73 | 49 | 17 | 4 | 1 |

1 in = 25.4 mm

**Table 20.  Aggregate properties.**

| Type | Source | Bulk Specific Gravity (OD) | Absorption, percent |
|---|---|---|---|
| Crushed Limestone | McCook, IL | 2.68 | 1.80 |
| Crushed Quartzite | Sioux Falls, SD | 2.62 | 0.20 |
| Rounded River Gravel | Dilles Bottom, OH | 2.49 | 2.04 |
| Fine Aggregate | Algonquin, IL | 2.66 | 1.20 |

Three curing exposure conditions were used for specimens molded for the 4- to 24-hour test period and four curing conditions were used for specimens tested in the 1- to 28-day period. The curing conditions were:

- 100 °F (38 °C) at 50 percent RH

- 72 °F (22 °C) at 50 percent RH

- 50 °F (10 °C) at 50 percent RH

- 72 °F (22 °C) at 100 percent RH

The 72 °F (22 C °) at 100 percent RH curing condition was not used for the 4- to 24-hour tests since specimens could not be extracted from molds and cured long enough for the humidity level to be a significant factor on early age strength gain. The 72 °F (22 °C) at 100 percent RH condition was included for the 1-day through 28-day period not because it is a representative construction condition, but because it is a standard ASTM requirement for quality control testing methods. The ASTM standard is 73 °F (23 °C) plus or minus 3 °F (1.7 °C).

Time intervals for testing were 4 hr, 6 hr, 9 hr, 1 day, 3 days, 7 days, 14 days, and 28 days. Scope of laboratory tests are shown in tables 16 and 17.

**Concrete Mix Design**

Constituents of the concrete mixes used for the laboratory test specimens and sawing slabs were proportioned to be representative of mixes used for highway concrete pavement construction. Six different concrete mixes were used for making laboratory specimens and sawing slabs. The 6 mixes were made using the CS, CH, and RH coarse aggregate types. Mixes were made using either a 500 or 650 lb/yd$^3$ (297 kg/m$^3$ or 386 kg/m$^3$) amount of cement with each coarse aggregate type. The following mixes were produced:

- Crushed soft limestone coarse aggregate with 500 lb cement per cubic yard (297 kg/m$^3$), CS-500.

- Crushed soft limestone coarse aggregate with 650 lb cement per cubic yard (386 kg/m$^3$), CS-650.

- Crushed hard quartzite coarse aggregate with 500 lb cement per cubic yard (297 kg/m$^3$), CH-500.

- Crushed hard quartzite coarse aggregate with 650 lb cement per cubic yard (386 kg/m$^3$), CH-650.

- Rounded hard river gravel coarse aggregate with 500 lb cement per cubic yard (297 kg/m$^3$), RH-500.

- Crushed hard river gravel coarse aggregate with 650 lb cement per cubic yard (386 kg/m$^3$), RH-650.

Details of mix proportions are listed in table 21. Coarse to fine aggregate proportions were about 1.35. Amount of Class F fly ash was 100 lb/yd$^3$ (59 kg/m$^3$) for each mix. Water-cement ratio by weight ranged from 0.38 to 0.52. Air content of fresh concrete ranged from 5 to 6.5 percent. To produce entrained air, 300 ml of vinsol resin /100 lb (45 kg) cement were used. The mixes were selected to give a slump of approximately 1.5 to 2.0 in (3.8 to 5.1 cm). This slump range is commonly measured in concrete pavement slipform construction. Slump ranged from 1.6 to 1.9 in (4.1 to 4.8 cm) for the 6 mixes.

## Aggregate Conditioning and Curing Conditions

Ahead of concrete mixing for making laboratory test specimens, concrete coarse and fine aggregate, water, cement, and fly ash were stored in regulated temperature rooms for at least 48 hours. The cement and fly ash were stored in airtight containers at 72 °F (22 °C). Mix water was also maintained at 72 °F (22 °C). Temperature conditioned coarse and fine aggregates matched the planned curing condition. By combining the temperature conditioned coarse aggregates with the other 72 °F (22 °C) mix constituents a range of initial mix temperatures was achieved. The initial mix temperatures for the 50, 72, and 100 °F (10, 22, and 38 °C) curing condition temperatures after mixing and specimen molding averaged 72, 79, and 86 °F (22, 26, and 30 °C), respectively. Initial mix temperatures are further summarized in this report when maturity test methods are described. Monitoring of mix constitutents at 48 hours indicated that constituent temperatures had attained those of conditioning exposures. Curing exposure conditions are listed in tables 16 and 17.

## Molding Test Specimens

Cylindrical 6-in (15 cm) diameter and 12-in (31 cm) long (6 by 12) test specimens were molded for making compressive strength, modulus of elasticity, and split tensile strength tests and were also molded for monitoring nondestructive pulse velocity and maturity measurements. Cylindrical test specimens for laboratory tests were consolidated using a vibrating table with a frequency of 3600 c/m and amplitude of 0.047 in (1.2 mm). For testing ages greater than 9 hours, cylindrical specimens were molded using plastic molds. Split cylindrical steel molds were used for specimens tested at ages of 9 hours or less to avoid damage during demolding at low strengths.

After mixing, molded concrete test specimens were transported into the curing chambers prior to specimens attaining initial set. Specimen surfaces were finished in control rooms and covered to minimize rapid loss of free water. Curing was maintained until approximately 20 minutes ahead of testing. Plastic cylinder molds were capped with plastic lids to retain specimen moisture. Steel cylinder molds were capped with steel plates until demolded. Molds were stripped immediately before testing when curing exposure was 24 hours or less. For tests after 1 day, cylindrical specimens were demolded after about 1 day curing exposure. Curing was done at three or four conditions, depending on specimen testing age, as listed in tables 16 and 17.

Beam test specimens for making flexural strength tests were molded in 6- by 6- by 21- in (15- by 15- by 53-cm) steel molds. Concrete was consolidated using a vibrating table. Molds were transported into curing chambers ahead of concrete attaining initial set. Specimen surfaces were finished in control rooms and were cured in the molds under

**Table 21. Concrete mix designs.**

| Mix Designation<br>Aggregate-Type<br>Cement Content, lb/yd$^3$ | CS500<br>Limestone<br>500 | CS650<br>Limestone<br>650 | CH500<br>Quartzite<br>500 | CH650<br>Quartzite<br>650 | RH500<br>Gravel<br>500 | RH650<br>Gravel<br>650 |
|---|---|---|---|---|---|---|
| Coarse Aggregate, lb/yd$^3$ (SSD) | 1790 | 1750 | 1790 | 1750 | 1730 | 1700 |
| Fine Aggregate, lb/yd$^3$ (SSD) | 1360 | 1210 | 1380 | 1220 | 1350 | 1180 |
| Cement, lb/yd$^3$ | 500 | 640 | 510 | 640 | 510 | 650 |
| Fly Ash, lb/yd$^3$ | 100 | 100 | 100 | 100 | 100 | 100 |
| Water, lb/yd$^3$ (SSD) | 260 | 270 | 230 | 260 | 240 | 250 |
| W/C by weight | 0.52 | 0.42 | 0.45 | 0.41 | 0.47 | 0.38 |
| W/(C+F) by weight | 0.43 | 0.36 | 0.38 | 0.35 | 0.39 | 0.33 |
| 28 day moist cured f'c (72 °F) | 4650 | 5800 | 4820 | 5560 | 4330 | 5370 |
| Slump, in | 1.8 | 1.7 | 1.8 | 1.8 | 1.6 | 1.9 |
| Air Content, percent | 5.4 | 5.0 | 5.7 | 5.5 | 6.5 | 4.8 |

NOTE: Mix Designation                     72 °F = 22 °C, 1 in = 25.4 mm

C = crushed aggregate geometry
R = rounded aggregate geometry
H = hard aggregate
S = soft aggregate
500 = nominal 500 lb/yd$^3$ (297 kg/m$^3$) cement content
650 = nominal 650 lb/yd$^3$ (386 kg/m$^3$) cement content

polyethylene to minimize rapid loss of water for tests conducted at 4 to 24 hours. Beams were demolded immediately ahead of testing for the 4-through 24-hour test condition and all others were demolded after about 1 day curing.

Concrete blocks for Clegg Impact Hammer test with 24- by 24-in (61- by 61-cm) plan dimension and 10-in (25.4 -cm) thickness were cast using each of the six concrete mixes delivered by ready mix truck as part of casting sawing strip slabs. Three blocks per mix were each cured at 50, 72, and 100 °F (10, 22, and 38 °C), respectively, as listed in table 16.

Concrete for molding cylindrical and beam specimens was batched in a pan mixer with 1-3/4 ft $^3$ (0.05 m$^3$) rated capacity. Five batches were made for each curing condition to produce 28 cylinders and 8 beams for the 4- to 24-hour test period and 19 cylinders and 10 beams for the 1 day through 28 day period. Cylinders used for modulus of elasticity tests were also used for compressive strength tests. Laboratory specimen test quantities are listed in table 18.

## TEST METHODS

Destructive test methods used to monitor early age strength development were:

- Cylinder compressive strength according to ASTM Designation: C 39-86.

- Modulus of Elasticity according to ASTM Designation: C 469-87a.

- Flexural strength (third-point loading) third point loading according to ASTM Designation: C 78-84.

- Splitting Tensile Strength according to ASTM Designation: C 496-84.

- Coefficient of Thermal Expansion - Small beams 11-1/4 in (28.6 cm) long and 3- by 3-in (7.6-cm by 7.6-cm) cross-section, were molded in steel molds using each of the six concrete mixes. Beams were fitted with reference pins at beam ends. Beams were cured at about 72 °F (22 °C) for 6 hours at 100 percent RH and demolded. They were immersed in a water bath maintained at 72 °F (22 °C) until either 8 or 16 hours. The beam length was measured with a one-ten thousandth in (0.0025 mm) comparator after 72 °F (22 °C) water bath exposure. Beams were then placed in a 120 °F (49 °C) water bath and length was measured when beam temperature monitored internally with a thermocouple reached water bath temperature. Subsequently beams were placed in a 50 °F (10 °C) bath and the measurements were repeated. Beams were tested within a 1 hour period to minimize effects of continuing cement hydration.

- Setting Time for Mortar according to ASTM Designation: C 403-88.

- Cube Compressive Strength according to ASTM Designation: C 109-88.

Nondestructive test methods used to monitor early age concrete properties that can be used as indicators of concrete strength development were:

58

- Concrete maturity according to ASTM Designation: C 1074-87.

- Pulse velocity according to ASTM Designation: C 597-83.

- Clegg Impact Hammer test (CIH).

For tests made according to ASTM procedures, variations from cited test methods only occurred when test sample demolding and curing period and conditions, because of early age time of test variables, were other than stated in the procedures. Compressive strength specimens tested at ages of 4, 6, and 9 hours were not capped with sulfur mortar in accordance with ASTM Designation: C 617. To avoid thermal shock and handling damage, neoprene cushioned steel cylinder caps were used instead of the recommended hot poured capping mortar. Tests on concrete cylinders at ages of 10 hours to 3 days on selected trial mixes indicated that no significant or consistent difference in either compressive strength or modulus of elasticity is introduced with the use of neoprene caps.

## Concrete Maturity

Concrete maturity is a nondestructive test (NDT) for estimating concrete strength. Maturity is a function of both curing temperature and time. Maturity concepts have been proposed and used since the 1950's to monitor and estimate strength gain. Once a relationship for a given mix is established between strength gain and the accumulated time-temperature effects, concrete strength gain during construction can be monitored. Several studies have demonstrated that maturity can be used to effectively monitor strength gain.[20-28] Two methods of expressing maturity are proposed in ASTM Designation: C 1074-87. Maturity can be expressed in terms of a time-temperature factor or in terms of equivalent age at a specified temperature. Maturity in terms of a time-temperature factor is computed from the temperature history as follows:

$$M = \Sigma(T-T_0) \Delta t \dots\dots\dots (8)$$

where

$M$ = maturity at age t, in degree-hours or degree-days
$T$ = average concrete temperature during time interval
$T_0$ = datum temperature
$\Delta t$ = time interval in days or hours

Equation 8 is commonly called the Nurse-Saul maturity or the time-temperature factor maturity function. The units used in ASTM C 1074-87 are °C-hours (or days). The Nurse-Saul maturity value in this report is stated in °F-hours or °F-days to be consistent with other temperature units referred to. The datum temperature is the temperature below which the concrete strength gain ceases. Datum temperatures which have been commonly used include 32 °F (0 °C) and 14 °F (-10° C). For concrete with Type I cement without admixtures and a curing range of 32 to 104 °F (0 to 40 °C) a datum temperature of 32 °F (0 °C) is recommended by ASTM. American Concrete Institute ACI 306R-78 "Cold Weather Concreting" uses 14 °F (-10 °C).[20] For the maturity values reported in this study a reference datum temperature of 32 °F (0 °C) was assumed. Details on selection of this datum temperature are later discussed with maturity methods for compressive strength

prediction at ages of 1 to 28 days. ASTM uses a formula to adjust Nurse-Saul maturity values to any datum temperatures. Procedures to experimentally determine the datum temperature of a specific mix are outlined in ASTM C 1074-87.

Based on investigations of mortar specimens it is recognized that hardening of concrete is not a linear function of curing temperature.[20]. The predicted strength of concrete using the linear Nurse-Saul function can deviate from actual strength for temperatures ranging less than 23 °F (-5 °C) and greater than 86 °F (30 °C). In the late 1970's the equivalent age maturity equation was proposed based upon the Arrhenius equation. The Arrhenius equation is used to quantify cement hydration as a nonlinear acceleration of chemical reactions with increases in temperature. The equivalent age Arrhenius equation is shown in equation 9.

$$t_e = \Sigma \, \Delta t \, \exp\,(-E/R \times T\,') \dotfill (9)$$

where

$t_e$ = equivalent age at a specified temperature, days or hours
$E$ = activation energy, J/mol
$R$ = universal gas constant, 8.3144 J/(mol-°K)
$T\,'$ = $[1/(273 + T) - 1/(273 + T_r)]$
$T$ = average concrete temperature during time interval
$T_r$ = reference temperature, °C
$\Delta t$ = time interval

The exponential equation is a function of the absolute temperature. The degree of nonlinearity is dependent on the activation energy, E, which is a function of temperature, type of cement, and admixture type and content. For concrete temperatures of 50, 72, and 100 °F (10, 22, and 38 °C), suggested values for the activation energy divided by the universal gas constant E/R are 5797, 4029, and 4029 °K, respectively.[25] For Type I cement without admixtures or additions, values of activation energy divided by gas constant can range from 4811 to 5412 °K. ASTM suggests that the activation energy divided by gas constant can be approximated as 5000 °K. Procedures are outlined in ASTM C 1074-87 to experimentally determine the activation energy, E, when maximum accuracy of strength prediction is desired. For the Arrhenius equivalent age reported in this report the activation energy divided by gas constant was assumed to be 5000 °K. Details on selection of this datum temperature are later discussed with maturity methods for compressive strength prediction at ages of 1 to 28 days. The reference temperature of 68 °F (20 °C) was selected since it is a commonly used maturity reference temperature. Therefore, for an equivalent age of 2.8 hours after 5.5 hours of curing at a given temperature indicates that the same concrete strength could have been reached at 2.8 hours cured at 68 °F (20 °C).

Maturity was calculated from temperatures recorded using a portable temperature logger. Air temperature and concrete cylinder temperature were automatically measured with thermocouples and printed every half hour. Monitoring was terminated when specimen temperatures stabilized at the isothermally controlled curing room temperature. By correlating maturity with corresponding strength for individual mixes, estimates of strength can be generated by simply recording the curing time and temperature histories.

## Pulse Velocity

The pulse velocity method consists of measuring the time of travel of a compression wave impulse through concrete. By assuming a direct travel path length, the velocity in ft/s can be computed. The test method described in ASTM C 597-83 is intended to be used to assess concrete uniformity and relative quality and cautions that the method should not be considered as a means of measuring strength or modulus of elasticity. However, ASTM notes that under certain circumstances a velocity-strength or velocity-elastic modulus may be established and serve as a basis of estimating strength or modulus of elasticity. The compressional wave velocity for a homogeneous, isotropic elastic medium is theoretically expressed as:

$$PV = sqrt\ [E/D*(1-\mu)/(1+\mu)/(1-2\mu)] \dots\dots\dots\dots\dots\dots\dots\dots\dots\dots (10)$$

where

$PV$ = compressional wave velocity, ft/s (1000 ft/s = 305 m/s)
$E$ = dynamic elastic modulus
$D$ = unit weight
$\mu$ = Poisson's ratio

Since the elastic modulus has been empirically correlated with concrete strength properties and modulus is related to pulse velocity, strength can be estimated directly from pulse velocity. Several studies have demonstrated that pulse velocity for a specific mix can be used to monitor strength gain.[15,17,29-35]

Compression waves are generated and transmitted through the concrete by a transducer held in contact with the surface. The pulses are received by a receiving transducer and the time taken by a pulse to travel through the concrete is accurately measured and digitally displayed in 0.1 microseconds. Commercially available pulse generators are battery powered and portable measuring approximately 7- by 4.5- by 6.5-in (17.8- by 11.4- by 16.5- cm). Electromechanical transducers are 1.97 in (5 cm) in diameter by 1.65 in (4.2 cm) long with resonant frequencies of 54,000 Hz. Transducer contact is enhanced by using a very thin couplant medium such as grease, oil, petroleum jelly, flexible sealant, or kaolin-glycerol paste.

Transducers are arranged on concrete surfaces in three basic configurations. The direct transmission is the preferred method of testing. The transducers are positioned so the pulse travels directly through the concrete. For cylinder testing the transducers were positioned on each end along the longitudinal axis. The semidirect method is used when access to geometrically parallel faces of the specimen is not possible. For pavement slab testing one transducer would be positioned on the surface and the other positioned on the slab side. The indirect method or surface transmission is the least satisfactory transducer arrangement because the pulse amplitude is only about 1 to 2 percent of that detected for the same path length when direct transmission is used. With the indirect transmission, the 2 transducers are placed on the same surface.

Pulse velocity is computed as the measured path length (ft) divided by the transit time (seconds). Manufacturer recommended accuracy in measuring path lengths and travel times is plus or minus 1 percent. By correlating strength to pulse velocity a relationship can be established to monitor strength gain with pulse velocity equipment.

## Clegg Impact Hammer

The Clegg Impact Hammer tester is commercially available and portable. The equipment is used to evaluate insitu soils and pavement bases and is suitable for materials ranging from soft clay to cement-stabilized base courses. The Clegg Impact Hammer can be correlated with California Bearing Ratio (CBR) values. The equipment for this method consists of a 10-lb (4.5-kg) hammer sliding in a guide tube for an 18-in (46-cm) free fall. An accelerometer fastened to the hammer provides a signal on impact. The signal is filtered and data is provided on a digital readout. A release button zeroes the meter prior to testing. Maximum deceleration is displayed in units of 10 gravities. After each test the equipment is moved laterally on the surface by approximately 3 in (76 cm). A minimum of 4 impact tests were recorded, averaged, and reported as one test value.

Although not intended to measure an index of concrete impact strength, one study showed good correlation of cement-stabilized soil compressive strength with Clegg Impact Hammer test values.[13] For several cement stabilized cohesionless soils good correlation was obtained for compressive strengths of less than 1000 psi (6.9 MPa).

The nondestructive pulse velocity, maturity and Clegg Impact Hammer tests were selected for evaluation of concrete early age properties because the equipment is mobile and easily used at construction sites. Each of the three methods can be used by inspectors with only a minimum amount of hands on training. Only the maturity meter requires installation of an instrumentation point, that is a thermocouple within pavement slabs. To monitor maturity for various increments of pavement placement (1 mi/1.6 km is not unusual) several maturity meters are required for monitoring. Pulse velocity and Clegg Hammer equipment is manually portable and increments of pavement placements can be tested at will. No surficial evidence remains after testing with maturity equipment or pulse velocity. Slight, approximately 2-in (5-cm) diameter surface impressions may remain in pavement surfaces at CIH test locations particularly if tests are done at very early ages.

## TEST RESULTS

Test results for 2 time increments are of interest:

1. For concrete sawcutting - strength for the first 24 hours after mixing and placing concrete.

2. For concrete pavement early loading by construction traffic - the 2 to 10 days after concrete placement.

Presentation of test results and discussion are presented separately for the 2 increments.

### Test Results - Sawing Time Period: 4 Hours to 24 Hours

Compressive, flexural (modulus of rupture), and splitting tensile strength testing was conducted at 4, 6, 9, and 24 hours. Nondestructive pulse velocity was also done at these ages. Concrete maturity at 4, 6, 9, and 24 hours was calculated from temperatures using both the temperature - time factor and equivalent age functions. The datum temperature used was 0 °C (32 °F) and activation energy divided by the gas constant used was 5000 °K.

Procedures to calculate concrete maturity are outlined in ASTM Designation: C 1074-87. Clegg Impact Hammer, sawability, mortar cube compressive strength, petrographic examination, and setting time for mortar tests were done in conjunction with large scale sawing strip construction further described in Chapter 4. Investigation of Earliest Joint Sawcutting.

Strength Versus Time. Results of the strength, pulse velocity, and maturity tests are listed in tables 1 and 2 of appendix A. Average strength values are reported for 3, 3, and 2 specimens for compressive, splitting tensile, and flexural strength, respectively. Strength tests as a function of curing age and temperature are summarized in figures 11 through 28. Compressive strengths for mixes with 500 lb/yd$^3$ (297 kg/m$^3$) cement contents cured at 72 °F (22 °C) for 24 hours ranged from 1860 to 2400 psi (12.8 to 16.5 MPa). For a cement quantity of 650 lb/yd$^3$ (386 kg/m$^3)$ the compressive strength ranged from 2560 to 3980 psi (17.7 to 27.4 MPa) when cured at 72 °F (22 °C) for 24 hours. Curing temperature at ages of less than 24 hours significantly affected compressive strength gain. As temperatures increased from 50 to 100 °F (10 to 38 °C), strength increased significantly. At 24 hours large increases in compressive strength were measured when temperatures increased from 50 to 72 °F (10 to 22 °C). No significant difference in compressive strength was measured between 72 and 100 °F (22 and 38 °C) curing for 24 hours. Largest incremental percentage increases in compressive strength with time were observed at the 50 °F (10 °C) curing condition.

Split tensile strengths for cement quantities of 500 lb/yd$^3$ (297 kg/m$^3)$ ranged from 220 to 290 psi (1.5 to 2.0 MPa) cured at 72 °F (22 °C) for 24 hours. For cement quantities of 650 lb/yd$^3$ (386 kg/m$^3$) 24 hour split tensile strengths ranged from 255 to 415 psi (1.8 to 2.9 MPa) cured at 72 °F (22 °C). Similar to the compressive strength data, curing temperatures at ages of less than 24 hours significantly affects split tensile strength. At 24 hours significant increases were noted only when curing temperatures increased from 50 to 72 °F (10 to 22 °C). When temperatures increased from 72 to 100 °F (22 to 38 °C) small increases or even decreases in split tensile strength were observed at 24 hours. Smaller increases in strength occurred with time as curing temperature increased.

The concrete modulus of rupture cured at 72 °F (22 °C) for 24 hours ranged from 315 to 475 psi (2.2 to 3.3 MPa) and from 355 to 575 psi (2.4 to 4.0 MPa) for cement quantities of 500 and 650 lb/yd$^3$ (297 and 386 kg/m$^3$), respectively. At less than 24 hours, as the curing temperatures increased, the modulus of rupture significantly increased. At 24 hours significant increases in modulus of rupture were generally observed only when curing temperatures increased from 50 to 72 °F (10 to 22 °C). Similar to split tensile data, when temperatures increased from 72 to 100 °F (22 to 38 °C) small increases or even decreases were observed in modulus of rupture at 24 hours.

Mix-Specific Inter-Strength Relationships. Relationship between compressive, splitting tensile, and flexural (modulus of rupture) strengths were evaluated for the 6 individual mixes (3 aggregate types and 2 cement contents). Least squares linear regression analyses as shown in tables 3, 4, and 5 of appendix A indicated that mix-specific relation-ships between strength types at early ages could be established. For the six mixes at ages of 24 hours and less, the modulus of rupture can be predicted from the square root of compressive strength. The modulus of rupture can also be expressed as a linear function of splitting tensile strength. Similar to the relationship between modulus of rupture and compressive strength, split tensile strength can be expressed as a function of the square root of compressive strength.

**Crushed Limestone**
**Cement = 500 pcy**

Legend:
- 50 deg. F
- 72 deg. F
- 100 deg. F

Compressive Strength, psi

Values:
- 4 hours: 10, 30, 140
- 6 hours: 30, 100, 480
- 9 hours: 80, 310, 1490
- 24 hours: 690, 2400, 2640

Curing Age, hours

500 lb/yd³ = 297 kg/m³
50 °F = 10 °C, 72 °F = 22 °C, 100 °F = 38 °C
1000 psi = 6.9 MPa
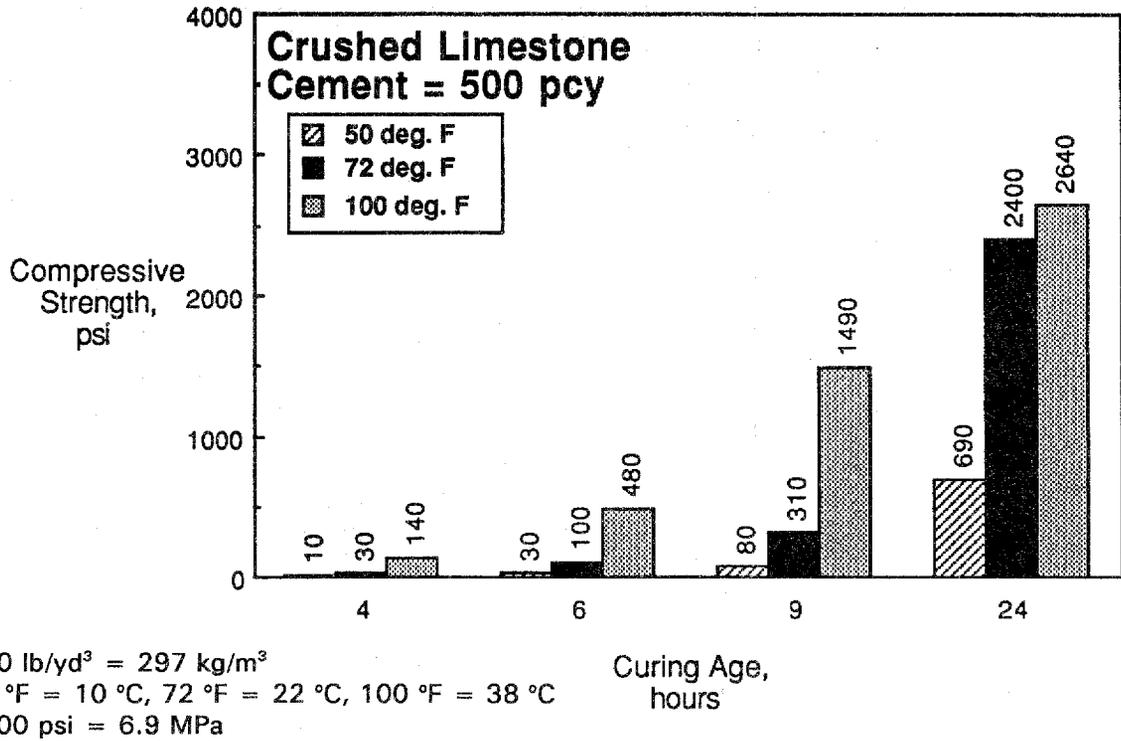
Figure 11.   Compressive strength for CS 500 at 4 to 24 hours.



**Crushed Limestone**
**Cement = 650 pcy**

Legend:
- 50 deg. F
- 72 deg. F
- 100 deg. F

Compressive Strength, psi

Values:
- 4 hours: 20, 60, 270
- 6 hours: 30, 280, 1200
- 9 hours: 100, 970, 2110
- 24 hours: 1340, 3980, 3420

Curing Age, hours

650 lb/yd³ = 386 kg/m³
50 °F = 10 °C, 72 °F = 22 °C, 100 °F = 38 °C
1000 psi = 6.9 MPa
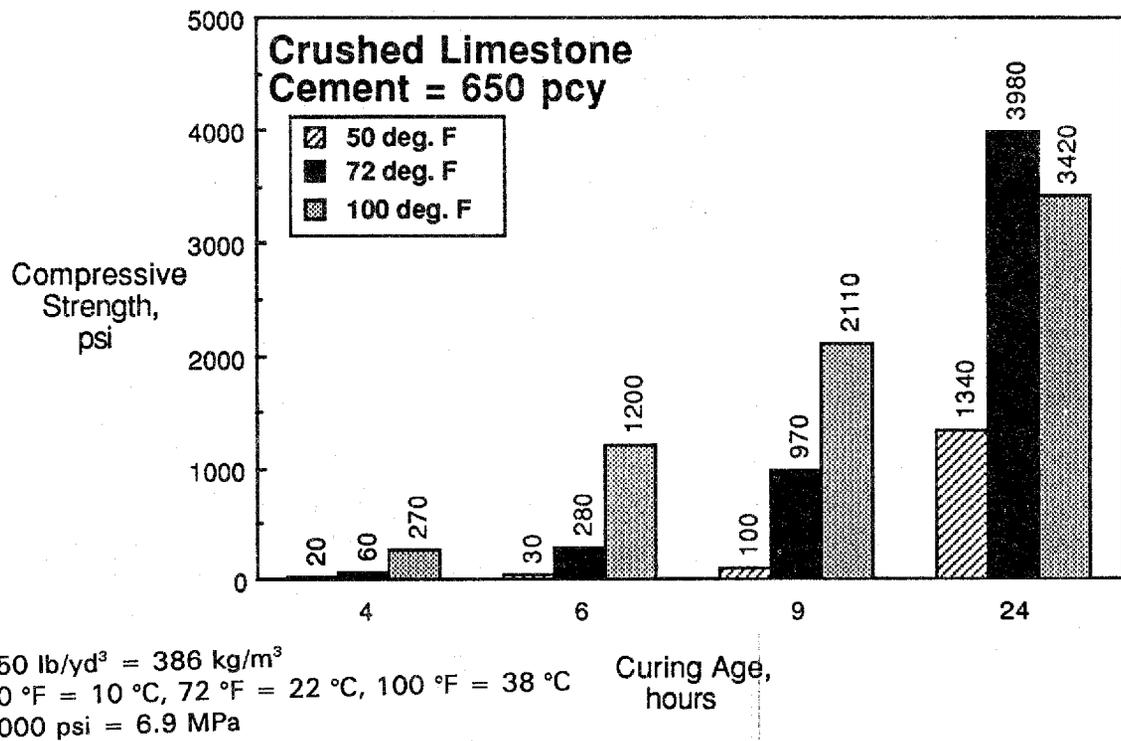
Figure 12.   Compressive strength for CS 650 at 4 to 24 hours.
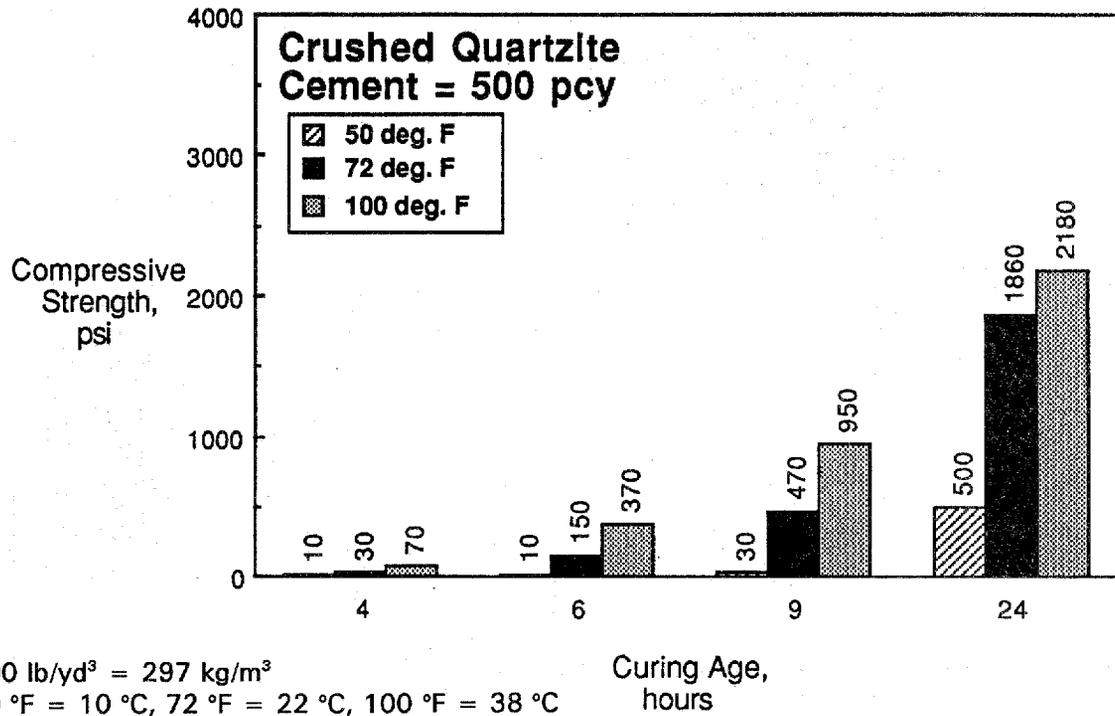
Figure 13. Compressive strength for CH 500 at 4 to 24 hours.
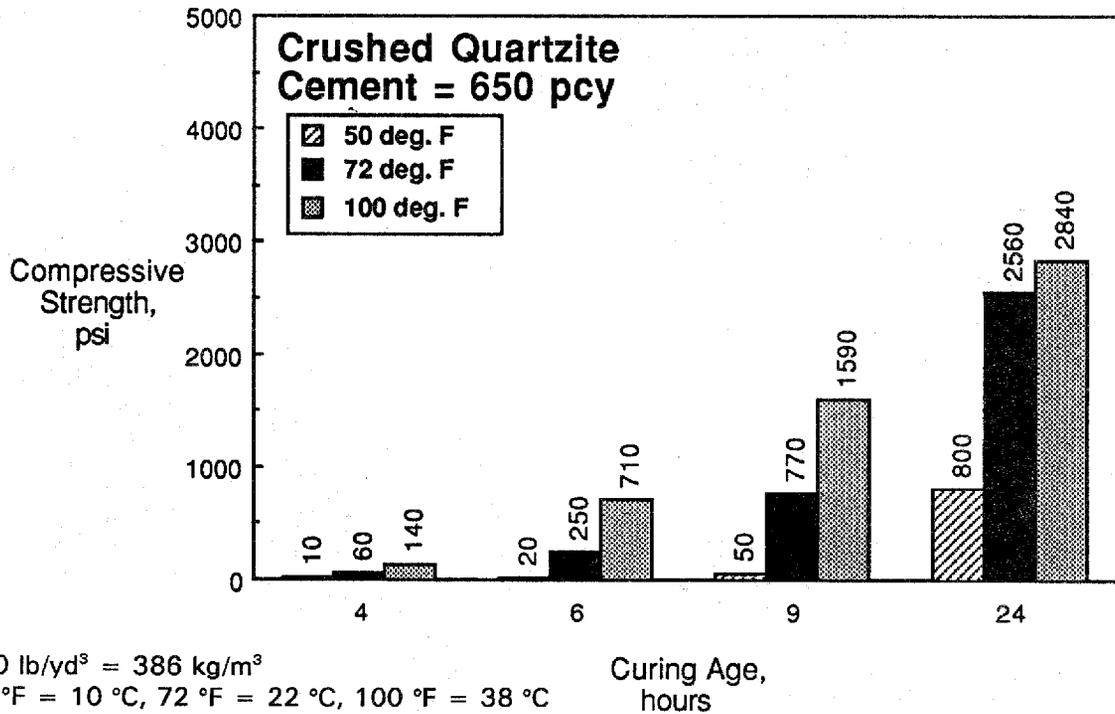
500 lb/yd³ = 297 kg/m³
50 °F = 10 °C, 72 °F = 22 °C, 100 °F = 38 °C
1000 psi = 6.9 MPa



Figure 14. Compressive strength for CH 650 at 4 to 24 hours.

650 lb/yd³ = 386 kg/m³
50 °F = 10 °C, 72 °F = 22 °C, 100 °F = 38 °C
1000 psi = 6.9 MPa
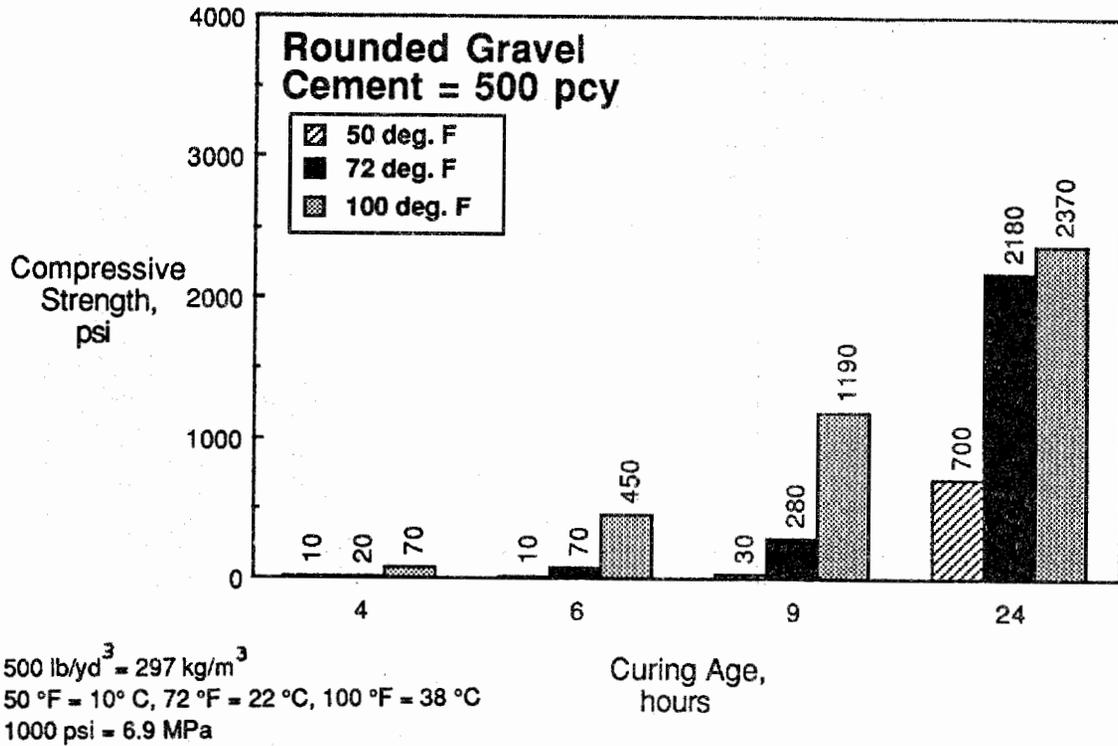
Figure 15.   Compressive strength for RH 500 at 4 to 24 hours.
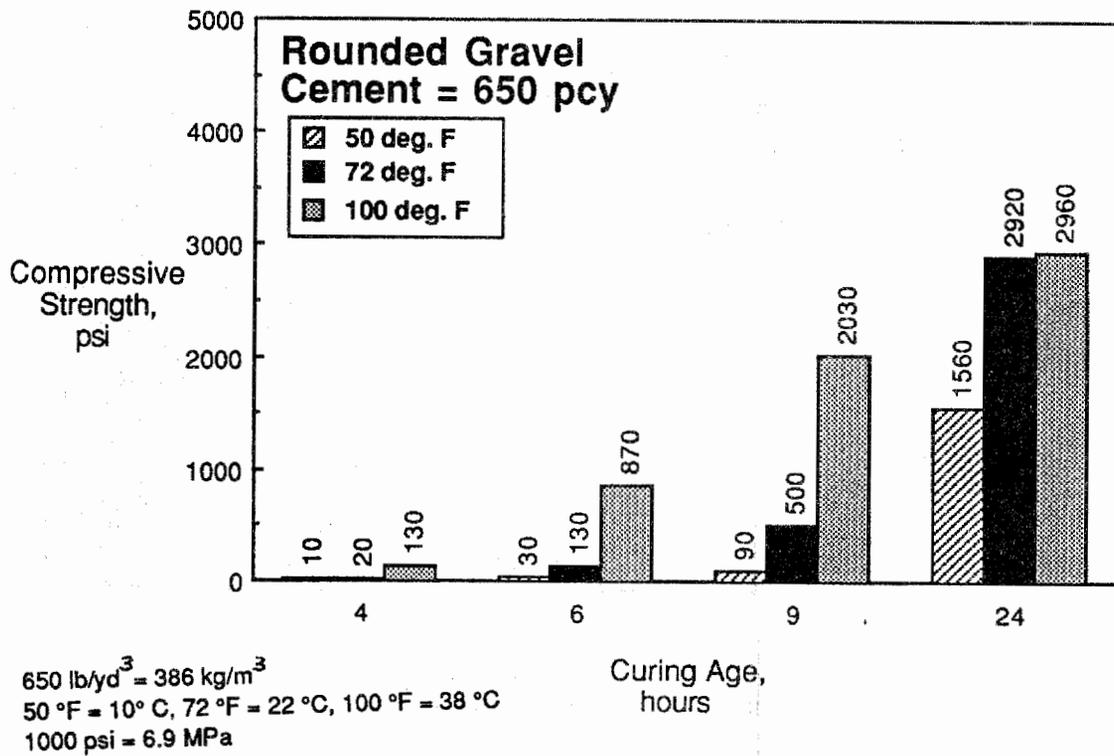


Figure 16.   Compressive strength for RH 650 at 4 to 24 hours.

66
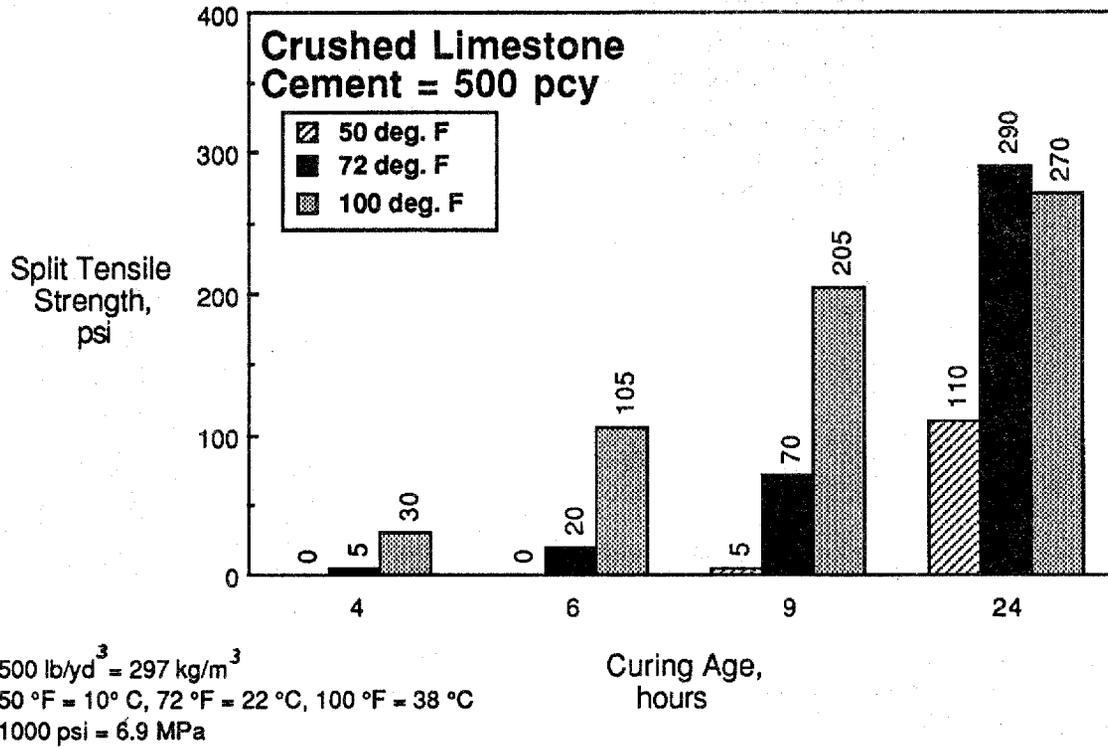
Figure 17. Split tensile strength for CS 500 at 4 to 24 hours.
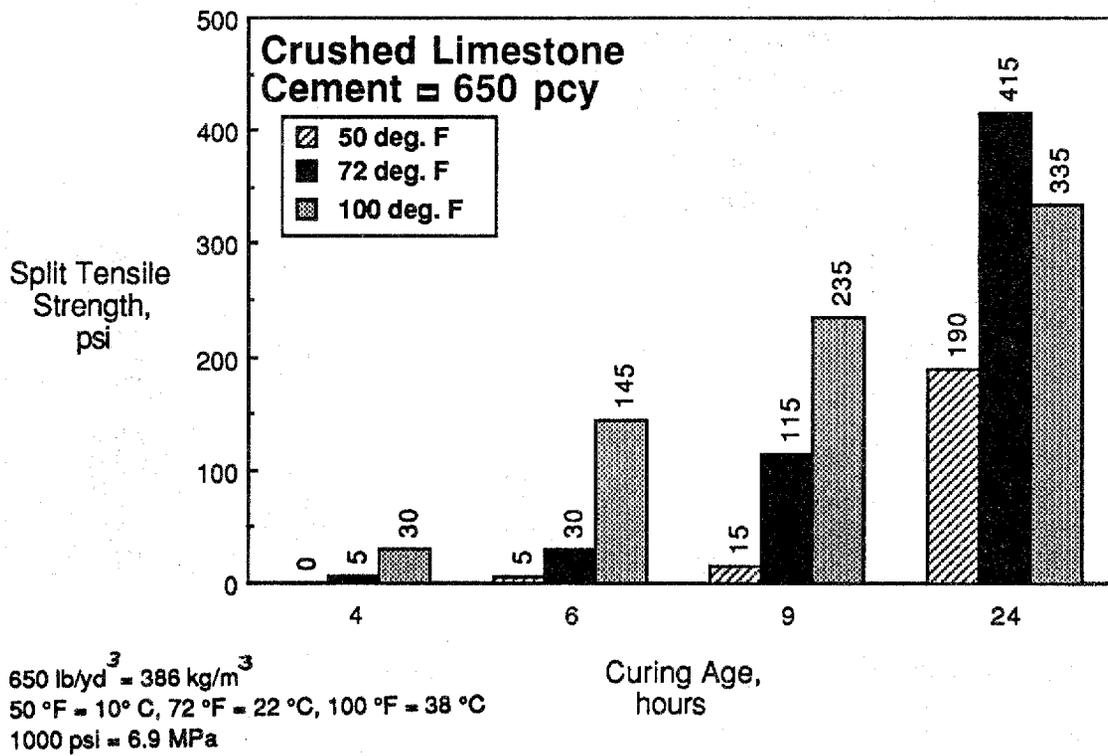


Figure 18. Split tensile strength for CS 650 at 4 to 24 hours.
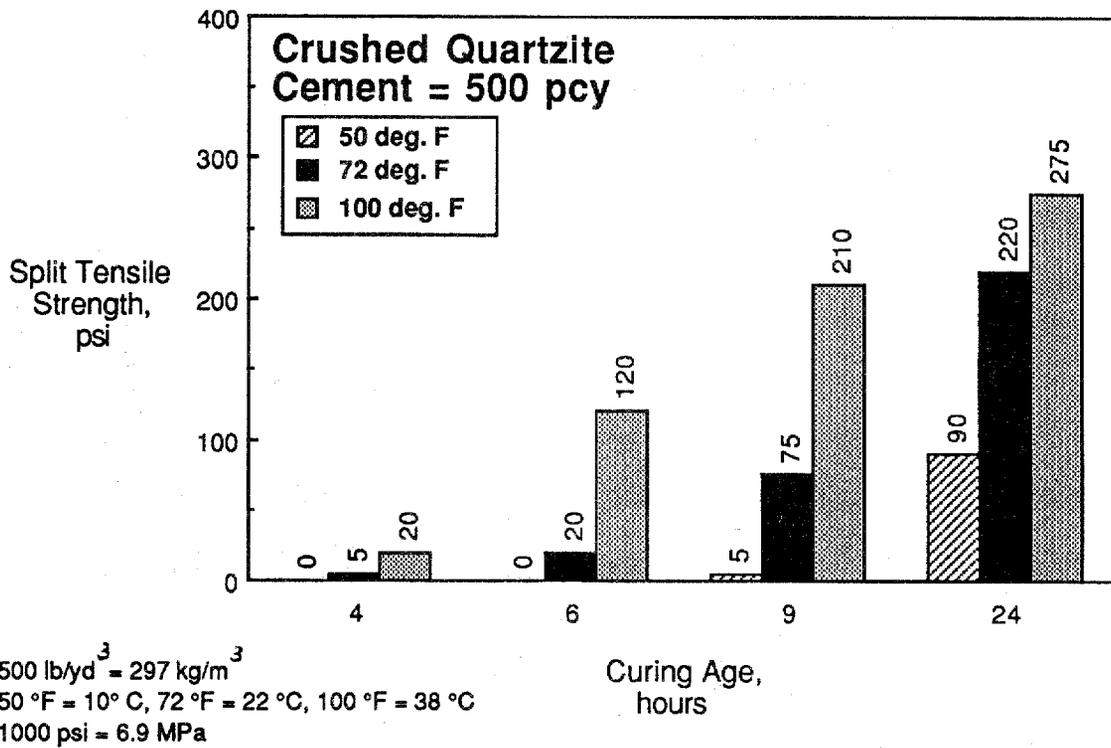
Figure 19.   Split tensile strength for CH 500 at 4 to 24 hours.
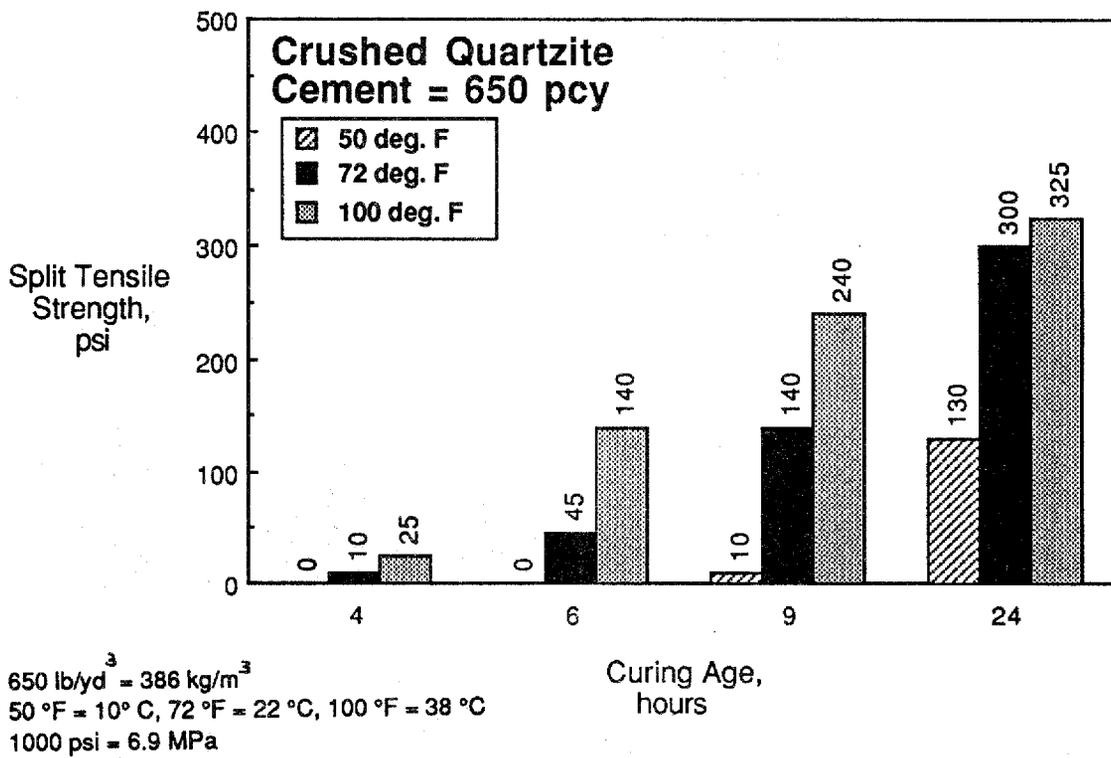


Figure 20.   Split tensile strength for CH 650 at 4 to 24 hours.
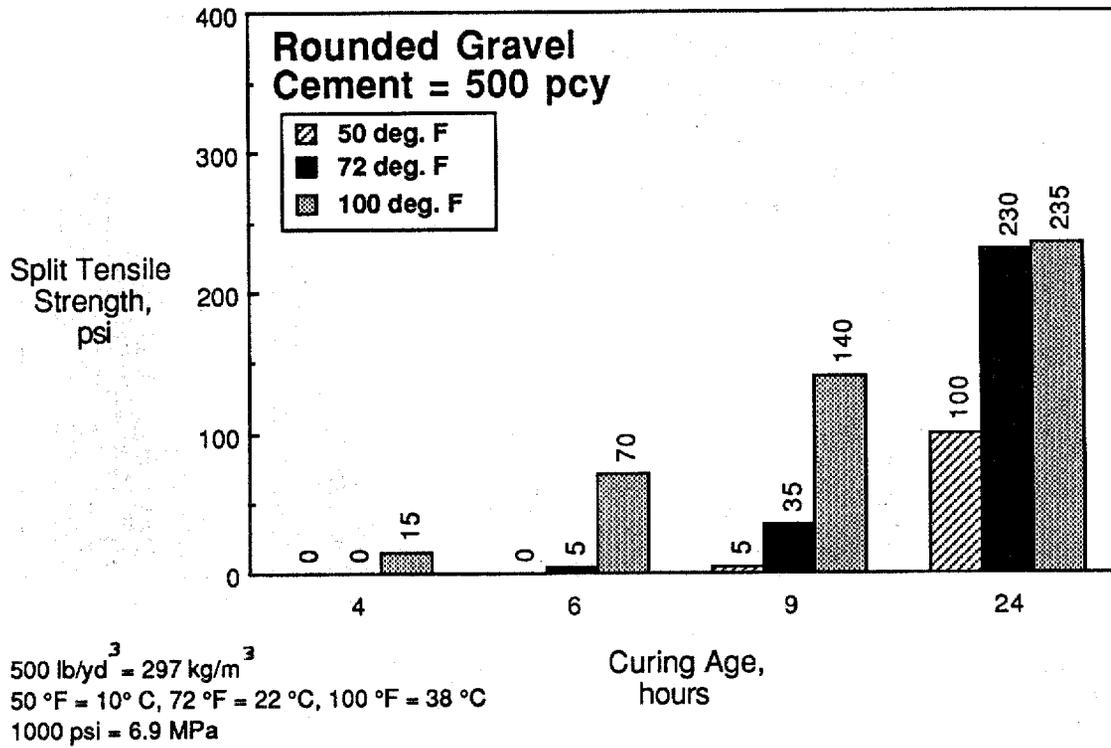
Figure 21.  Split tensile strength for RH 500 at 4 to 24 hours.
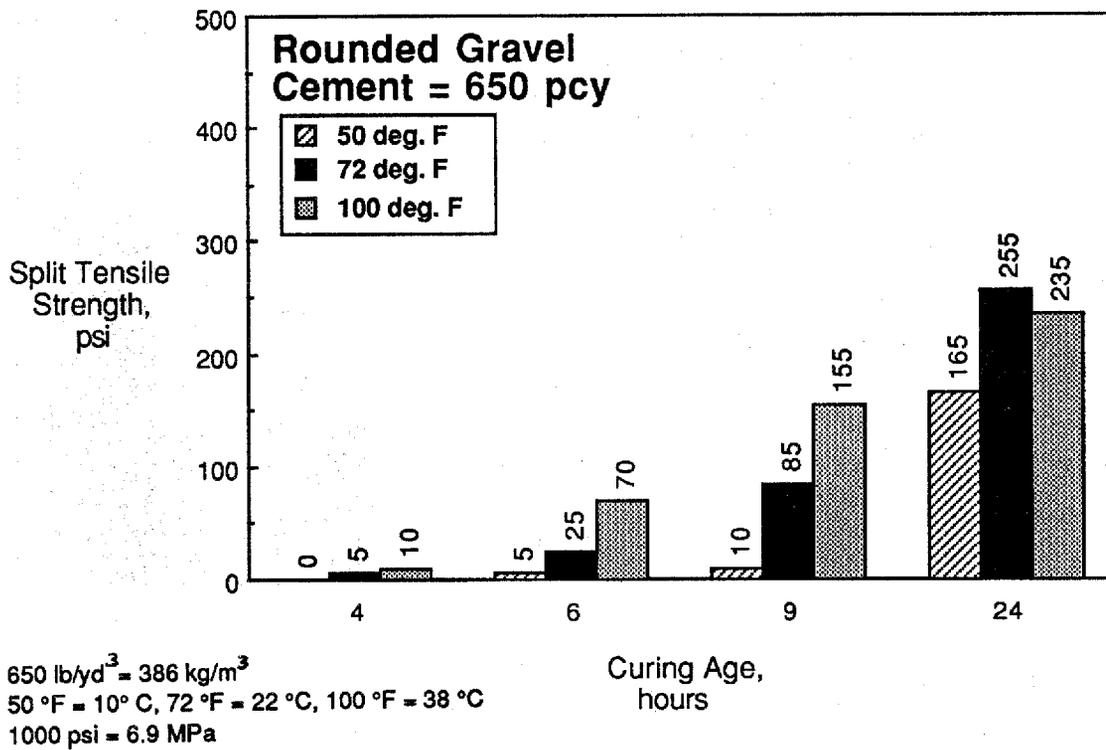


Figure 22.  Split tensile strength for RH 650 at 4 to 24 hours.
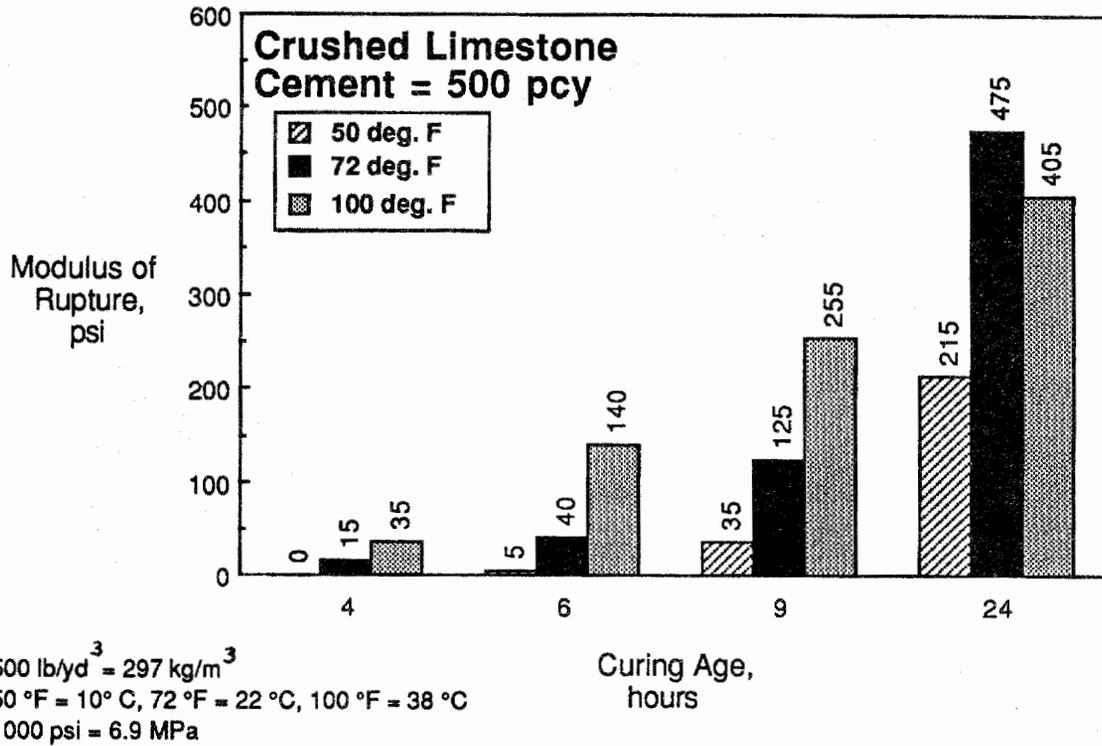
Figure 23. Flexural strength for CS 500 at 4 to 24 hours.
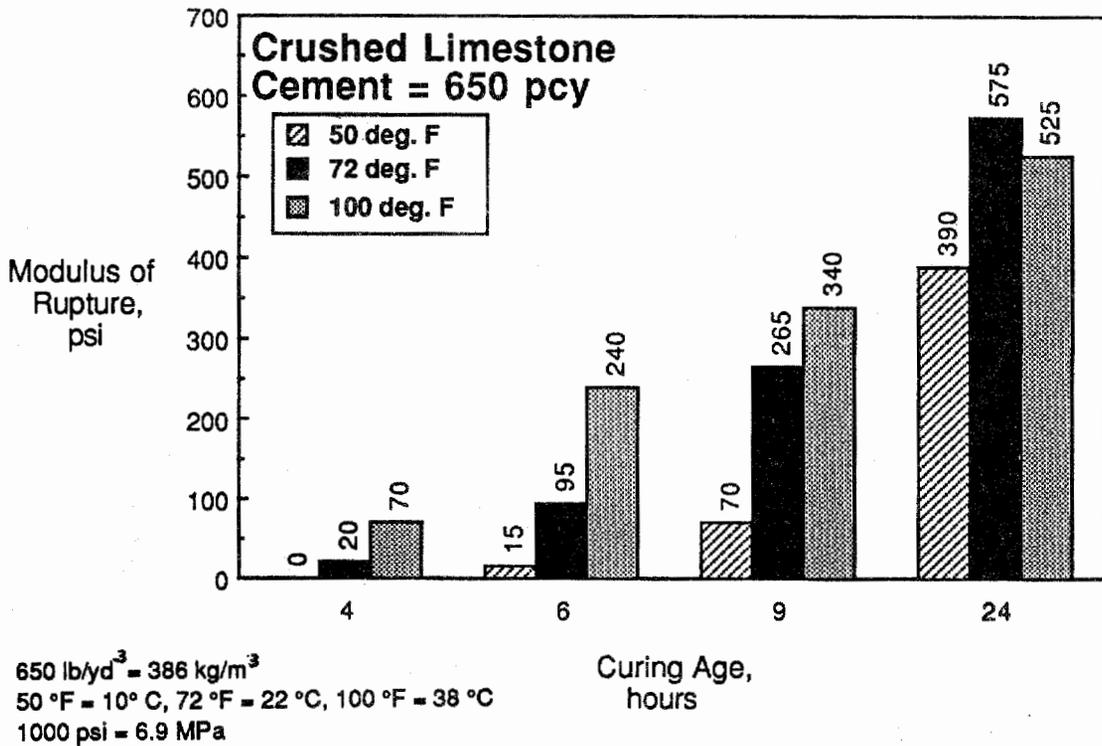


Figure 24. Flexural strength for CS 650 at 4 to 24 hours.
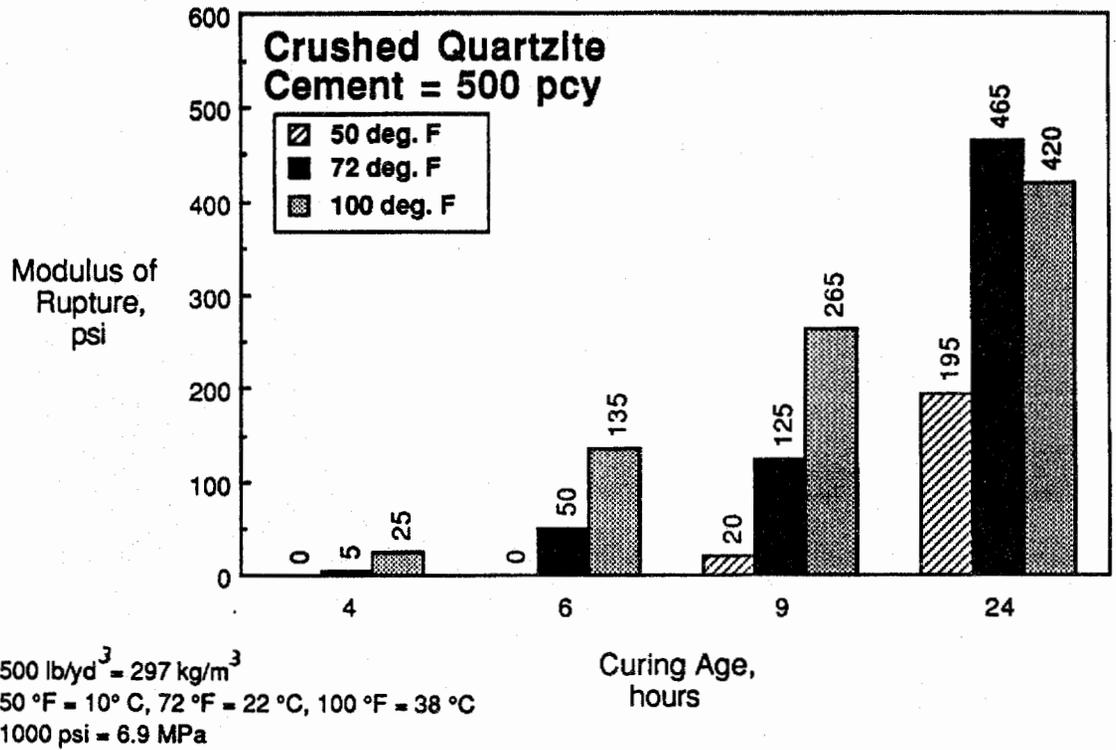
Figure 25.   Flexural strength for CH 500 at 4 to 24 hours.
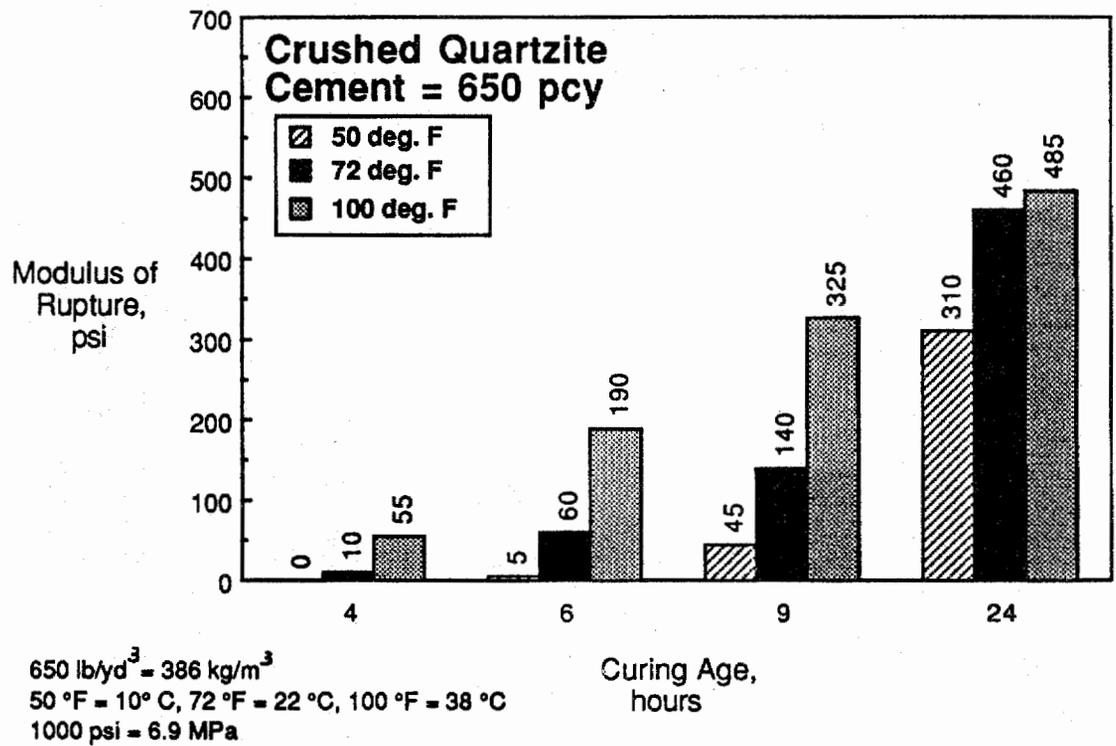


Figure 26.   Flexural strength for CH 650 at 4 to 24 hours.
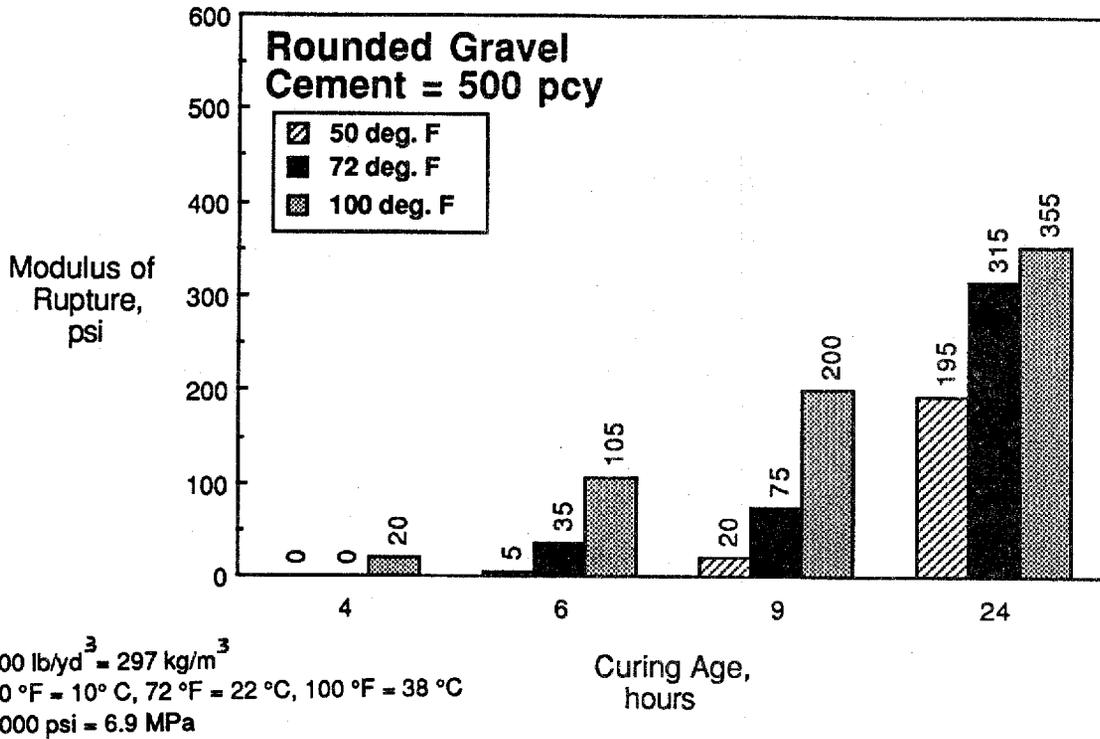
Figure 27. Flexural strength for RH 500 at 4 to 24 hours.

500 lb/yd$^3$ = 297 kg/m$^3$
50 °F = 10° C, 72 °F = 22 °C, 100 °F = 38 °C
1000 psi = 6.9 MPa
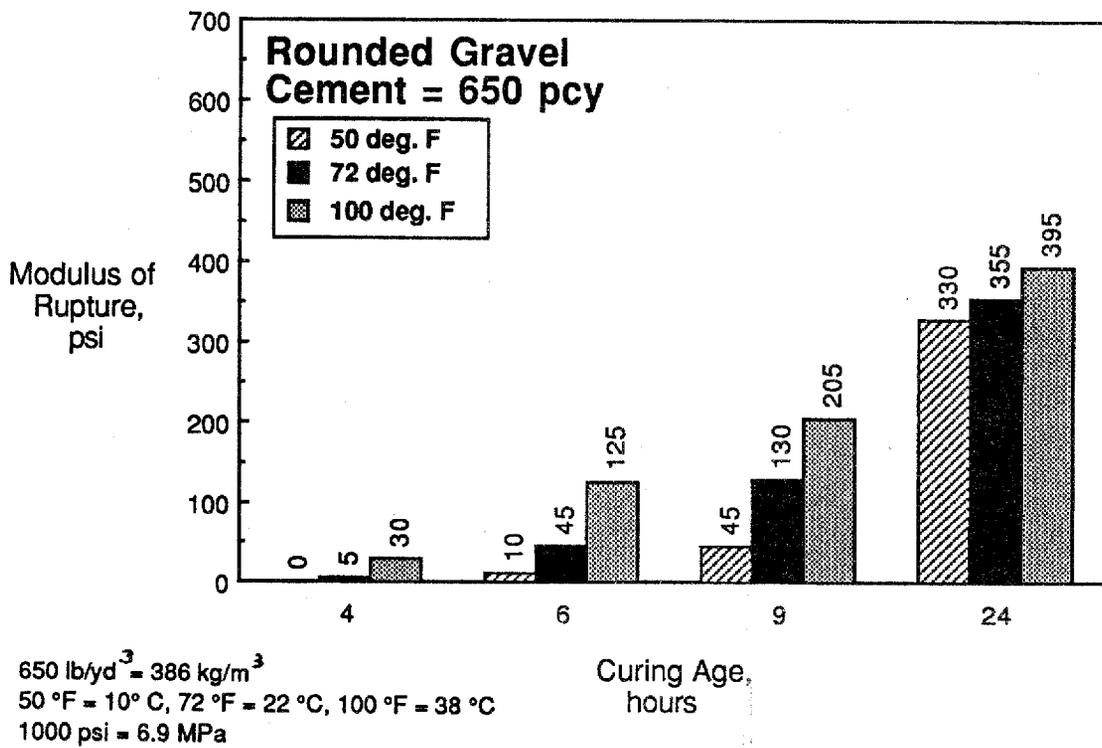


Figure 28. Flexural strength for RH 650 at 4 to 24 hours.

650 lb/yd$^3$ = 386 kg/m$^3$
50 °F = 10° C, 72 °F = 22 °C, 100 °F = 38 °C
1000 psi = 6.9 MPa

The coefficient of determination, R-squared, is a statistical measure of the reduction in the observed sample variance by considering a linear trend of the dependent variable as a function of the independent variable. The coefficient of determination ranges from zero to unity with unity indicating exact prediction of the dependent given the independent variable. For large sample sizes the square root of the coefficient of determination is approximately equal to the point estimate of the correlation coefficient, r.

The mix-specific interrelationships indicate that strength can be well predicted from other forms of strength. For the 3 interstrength relationships established for the 6 mixes the coefficient of determination, R-squared, ranged from 0.901 to 0.987 and averaged 0.960. The linear regression analysis for individual mixes is summarized in table 6 of appendix A. Average absolute error for prediction of modulus of rupture greater than 50 psi (0.35 MPa) from compressive strength ranged from 11 to 36 percent for the 6 individual mixes. Average prediction error for modulus of rupture greater than 50 psi (0.35 MPa) from split tensile strength ranged from 11 to 21 percent. Similarily, the average absolute error for prediction of split tensile strength greater than 50 psi (0.35 MPa) from compressive strength ranged from 5 to 21 percent for the 6 individual mixes. Errors for each mix are averages of the absolute value of predicted minus laboratory test value for the 4 test ages (4, 6, 9, and 24 hours) at the 3 curing conditions of 50, 72, and 100 °F (10, 22, and 38 °C).

General Inter-Strength Relationships. A general equation independent of aggregate type and cement content was derived for the relationship between the 3 different strength types using the combined data from all mixes. The development of a general mix independent equation was investigated since at ages of less than 24 hours the specimen fracture planes passed around the coarse aggregate rather than through the aggregate. Since the mortar content for all 6 mixes did not vary over a wide range, development of an aggregate and mix independent model could be expected. Similar to the mix-specific interstrength linear regression models, the modulus of rupture can be predicted as a square root function of compressive strength or linear function of split tensile strength. Splitting tensile strength can be predicted from the square root of compressive strength. A multiple linear regression analysis was conducted using independent variables of:

- Cement content - 500 and 650 lb/yd$^3$ (297 and 386 kg/m$^3$)

- Curing temperature - 50, 72, 100 °F (10, 22, 38 °C)

- Age - 4, 6, 9, 24 hours

- Aggregate geometry dummy variable - 0 = rounded, 1 = crushed

- Aggregate hardness dummy variable - 0 = soft, 1 = hard

- Aggregate dummy variable - 1 = crushed limestone, 2 = crushed quartzite, and 3 = rounded gravel

- Nurse-Saul concrete maturity

- Arrhenius concrete maturity

Various transformations to independent variables were also considered including square root, logarithmic, exponential, and inverse data transformations. The multiple linear regression analysis is summarized in table 22. For the combined data, two additional

73

**Table 22. Multiple linear regression analysis summary of early age strengths (4 to 24 hours).**

| Dependent Variable, Y | Independent Variable, X1 | Coef. [t-statistic] a | Independent Variable, X2 | Coef. [t-statistic] b | Independent Variable, X3 | Coef. [t-statistic] c | Independent Variable, X4 | Coef. [t-statistic] d | Constant | R - sq., adjusted |
|---|---|---|---|---|---|---|---|---|---|---|
| MR | sqrt(f'c) | 7.09 [20.2] | AGE | 5.13 [6.60] | GEOM | 38.13 [4.82] | **** | **** | -83.0 | 0.962 |
| MR | sqrt(f'c) | 7.16 [17.75] | AGE | 5.01 [5.61] | **** | **** | **** | **** | -57.8 | 0.950 |
| MR | sqrt(f'c) | 8.95 [30.37] | **** | **** | **** | **** | **** | **** | -43.6 | 0.929 |
| MR | ST | 1.16 [24.08] | AGE | 5.29 [8.23] | AGG | -9.47 [-2.48] | CEMENT | 0.10 [2.35] | -49.9 | 0.975 |
| MR | ST | 1.18 [24.23] | AGE | 5.05 [7.71] | AGG | -9.11 [-2.31] | **** | **** | 5.9 | 0.973 |
| MR | ST | 1.20 [24.44] | AGE | 4.82 [7.22] | **** | **** | **** | **** | -11.9 | 0.971 |
| MR | ST | 1.48 [36.86] | **** | **** | **** | **** | **** | **** | 13.3 | 0.950 |
| ST | sqrt(f'c) | 5.93 [36.62] | GEOM | 22.21 [3.71] | **** | **** | **** | **** | -50.5 | 0.950 |
| ST | sqrt(f'c) | 5.94 [33.77] | **** | **** | **** | **** | **** | **** | -36.1 | 0.941 |

NOTES: MR = modulus of rupture in psi, ST = Split tensile strength in psi, f'c = compressive strength in psi,
AGE = testing age in hours, GEOM = geometry of aggregate (0 = rounded, 1 = crushed),
AGG = type of aggregate (1 = limestone, 2 = quartzite, 3 = gravel), and CEMENT = cement content in pcy

General equation form Y = aX1+ bX2 + .... + constant

1000 lb/yd$^3$ = 593 kg/m$^3$
1000 psi = 6.9 MPa

74

independent variables were significant in predicting flexural strength from compressive strength (square root) data. The dummy variable for aggregate geometry (0 = rounded, 1 = crushed) and specimen age (hours) were statistically significant. Coefficients of determination only slightly decreased from 0.962 to 0.929 when the 2 additional variables were eliminated.

A multiple linear regression analysis for modulus of rupture on splitting tensile strength indicated that the cement content, curing age, and aggregate dummy variable were significant additional independent variables. As these additional variables were eliminated the coefficient of determination slightly decreased from 0.975 to 0.950. By including the three additional variables, 2-1/2 percent of the total variance in modulus of rupture could be further explained (difference in coefficient of determination).

The multiple regression analysis of splitting tensile on compressive strength (square root) indicated that aggregate geometry (crushed or rounded) was a significant variable. Without the aggregate geometry dummy variable the coefficient of determination dropped from 0.950 to 0.941.

As listed in table 22 for the general equations developed, the additional variables increase the coefficients of determination less than or equal to 0.033. This indicates that the variance explained by the additional independent variables is less than 3-1/2 percent. The models as a function of one independent variable can be used to simplify calculations without introducing any statistically significant prediction errors.

The single independent variable equations developed in the multiple regression analysis are independent of cement content and aggregate type for the early age laboratory data. The single variable general models are shown in figures 29 through 37. Average absolute error for prediction of modulus of rupture greater than 50 psi (0.35 MPa) from compressive and split tensile strength was 21 and 16 percent, respectively. Average error for split tensile strength greater than 50 psi (0.35 MPa) predicted from compressive strength was 17 percent.

The general single independent variable equations were compared to the mix-specific equations previously developed. Comparison was made by computing the difference in absolute value of the prediction errors using the general and mix-specific equations. Difference in prediction errors averaged 16, 7, and 10 psi (110, 48, 69 kPa) for the modulus of rupture and compressive, modulus of rupture and split tensile, and split tensile and compressive strength relationships, respectively. This indicates that the difference in the predicted values using the general form and mix-specific form (absolute errors) average 16 psi or less for the three interstrength equations. Average difference in percentage errors for prediction of modulus of rupture greater than 50 psi (0.35 MPa) from compressive and split tensile strength was 10 and 4 percent, respectively. Average difference in percentage errors for split tensile strength greater than 50 psi (0.35 MPa) predicted from compressive strength was 10 percent.

Prediction errors for the general and mix-specific equations are listed in tables 3 through 5 of appendix A for modulus of rupture and compressive, modulus of rupture and split tensile, and split tensile and compressive strength relationships, respectively. Based on the high coefficients of determination for the general equations and low error differences compared to mix-specific equations, the general equations (independent of aggregate type and cement content) appear to fit the early strength lab data well.
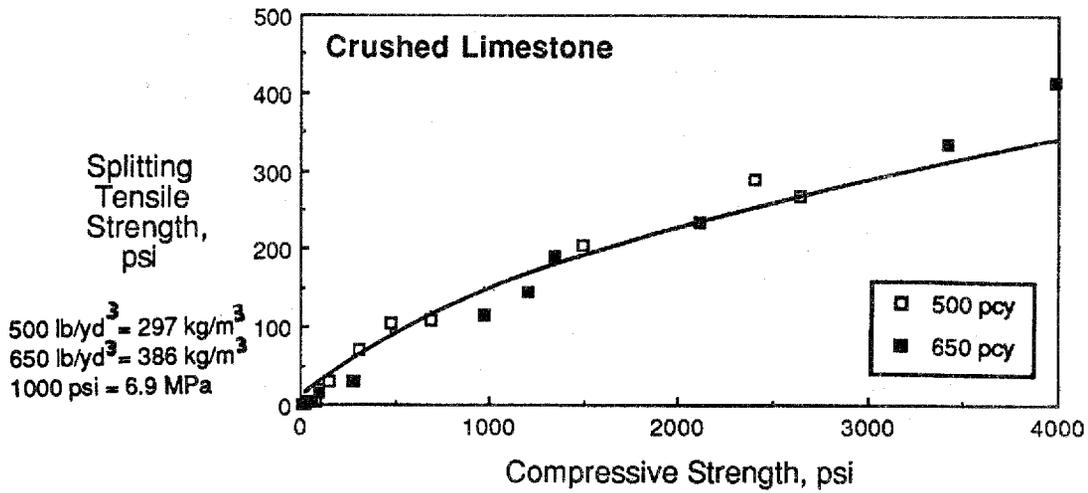
Figure 29.  Compressive vs. split tensile strength for CS.
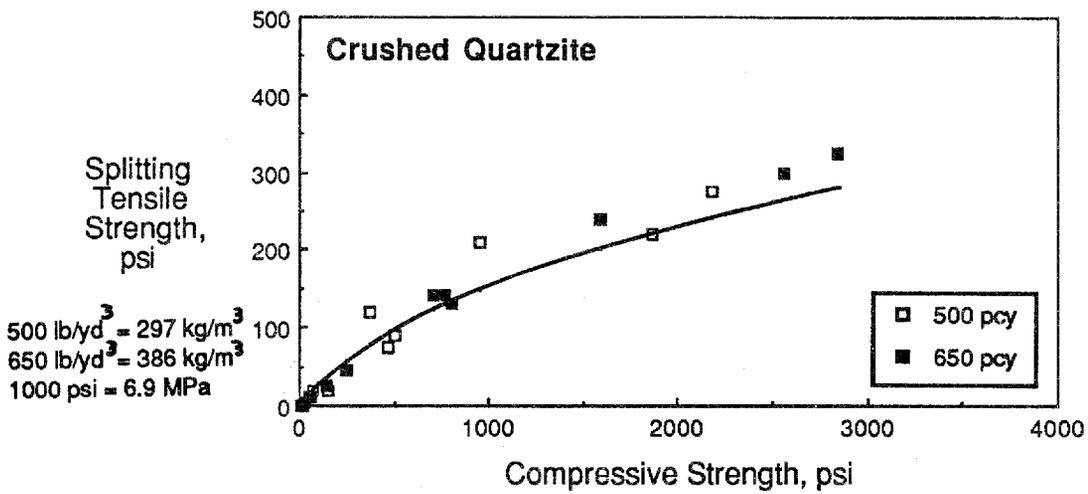


Figure 30.  Compressive vs. split tensile strength for CH.
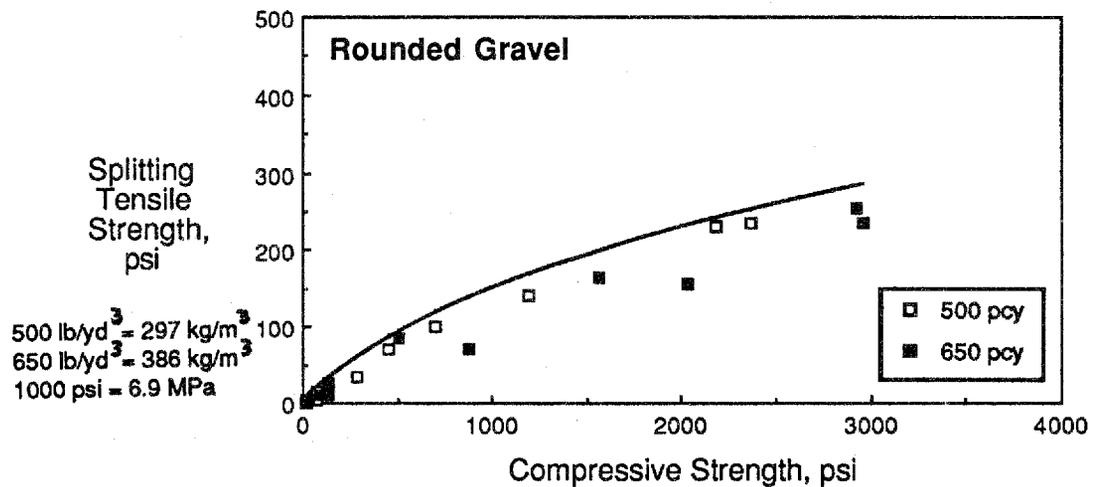


Figure 31.  Compressive vs. split tensile strength for RH.
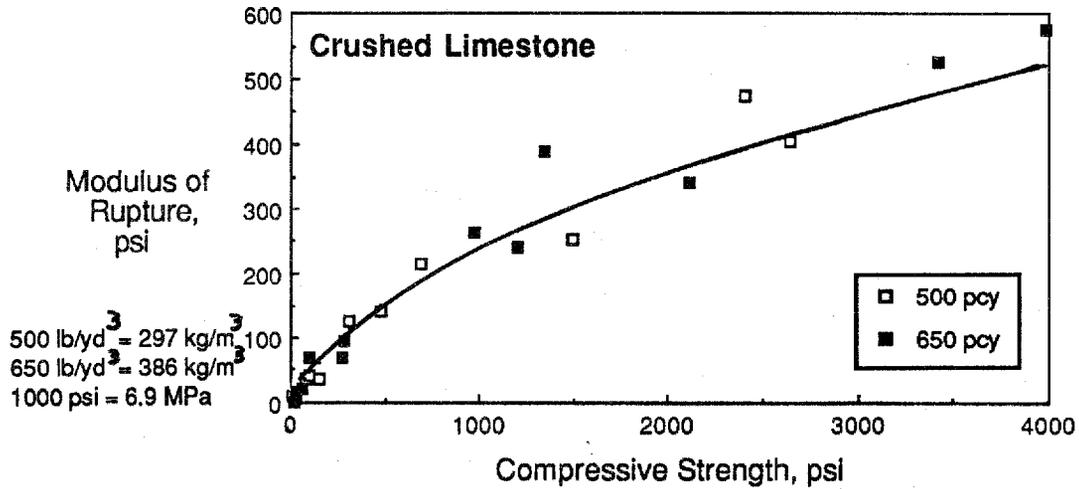
Figure 32. Compressive vs. flexural strength for CS.
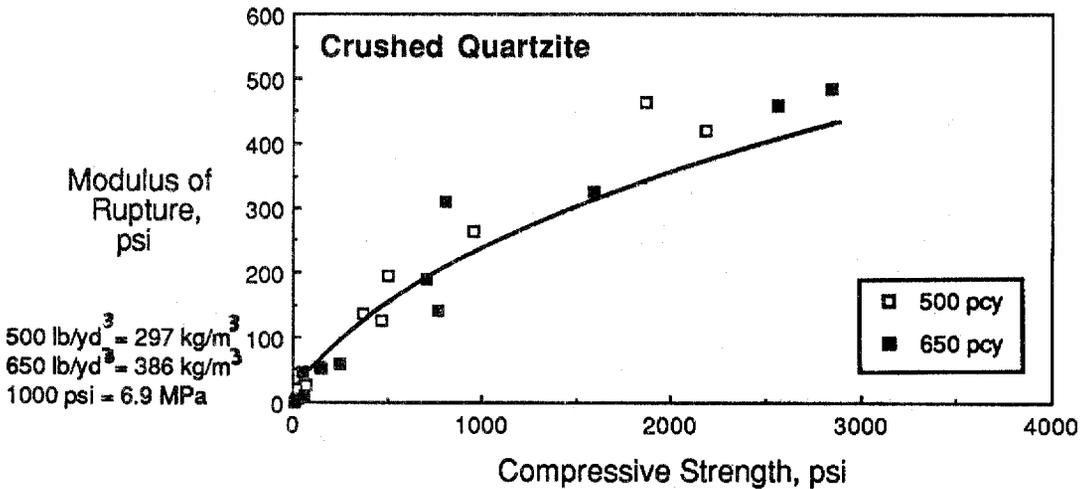
Figure 33. Compressive vs. flexural strength for CH.
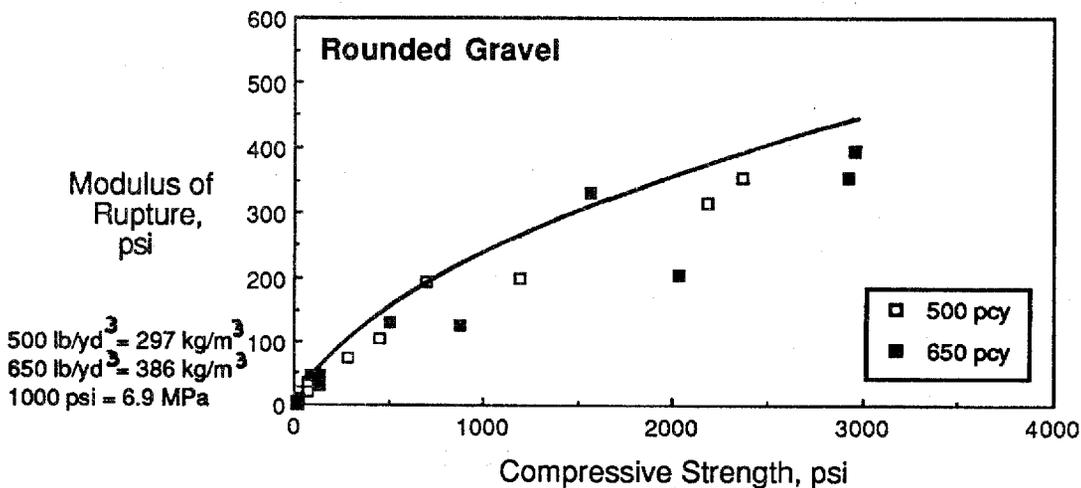
Figure 34. Compressive vs. flexural strength for RH.

77
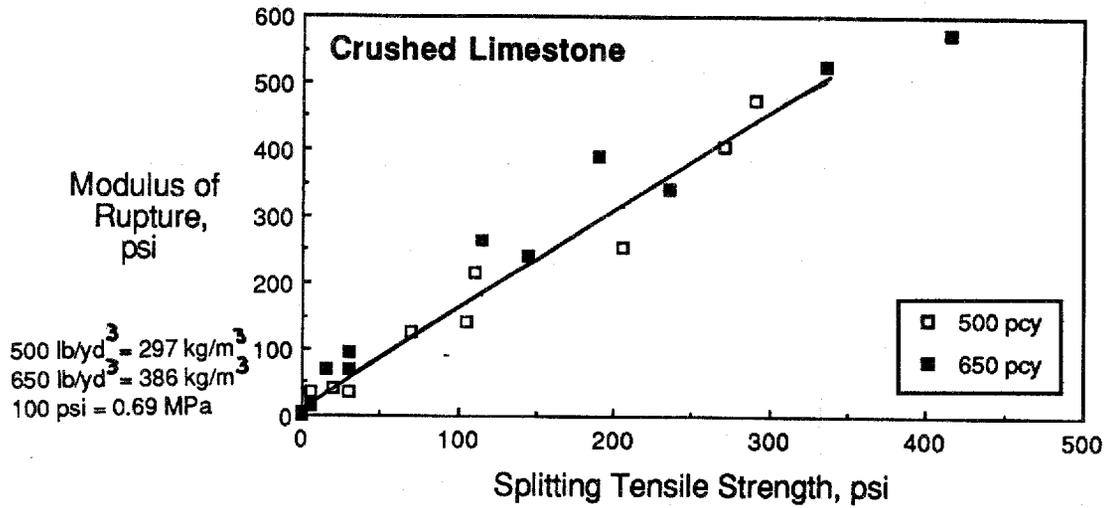
Figure 35.  Split tensile vs. flexural strength for CS.
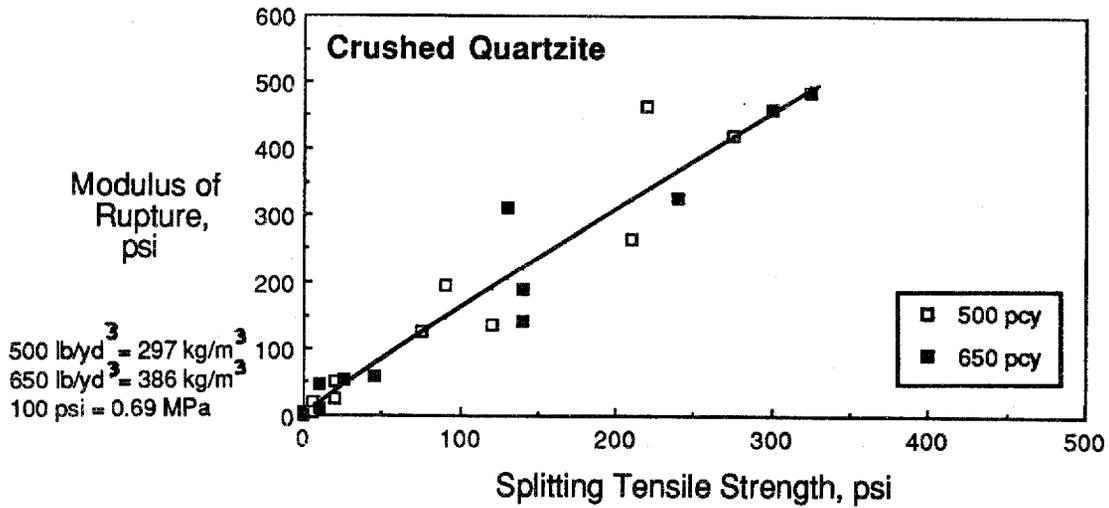


Figure 36.  Split tensile vs. flexural strength for CH.
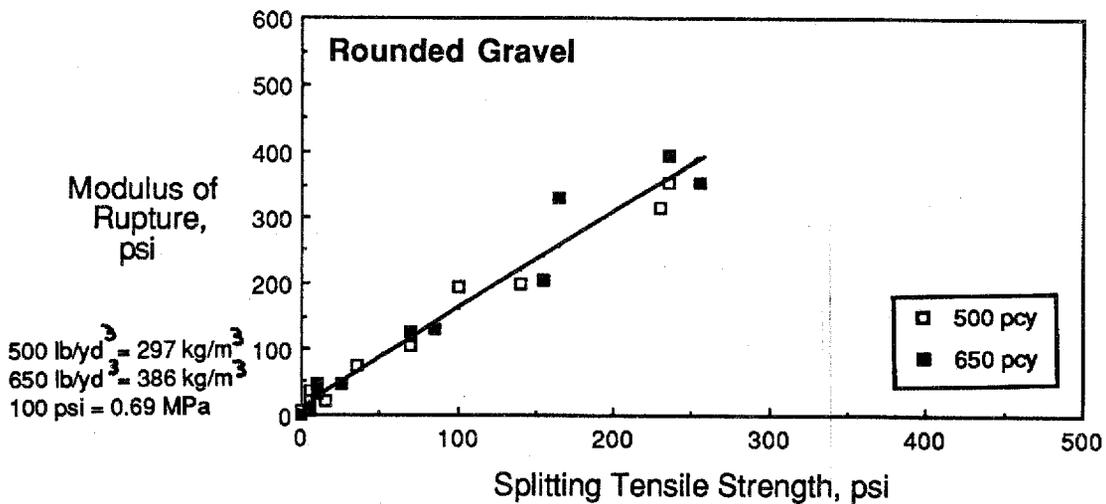


Figure 37.  Split tensile vs. flexural strength for RH.

<u>Mix-Specific Strength Versus NDT Relationships</u>. The early age concrete strengths were next correlated with nondestructive maturity and ultrasonic pulse velocity data. Compressive, split tensile, and flexural strengths were regressed on maturity or pulse velocity data using least squares linear regression techniques. The selected equation form for the lab data at ages of 1 through 24 hours was the log (base 10) of strength as a function of the inverse of maturity and log (base 10) of strength as a function of pulse velocity. Models were developed for each mix (3 aggregate types and 2 cement contents) relating strength (logarithmic) to maturity (inverse form) calculated at 4, 6, 9 and 24 hours for 50, 72, and 100 °F (10, 22, and 38 °C) curing temperatures. Similarly, models were developed relating the logarithmic strength form to pulse velocity for each mix. Models for strength (3 types) regressed on NDT data (Arrhenius maturity, Nurse-Saul maturity, and pulse velocity) are listed in tables 7 through 9 of appendix A.

Coefficients of determination listed in tables 7 through 9 of appendix A indicate very high degrees of correlation for individual mixes. For both nondestructive test methods, coefficients of determination, R-squared, ranged from 0.882 to 0.997. For the 3 NDT (2 maturity and 1 pulse velocity) models, the average coefficient of determination was 0.973, 0.953, and 0.957 for prediction of compressive strength, split tensile strength, and modulus of rupture, respectively. Overall, based on average statistical significance of predictability, the compressive strength models are slightly better than split tensile or modulus of rupture models.

<u>General Early Age Strength Versus NDT Relationships</u>. A multiple linear regression analysis of early age concrete strengths (4 to 24 hours) on maturity and pulse velocity was then done to develop general prediction models. Independent variables include:

- Cement content - 500 and 650 lb/yd$^3$ (297 and 386 kg/m$^3$)

- Curing temperature - 50, 72, 100 °F (10, 22, 38 °C)

- Curing age - 4, 6, 9, 24 hours

- Aggregate geometry dummy variable - 0 = rounded, 1 = crushed

- Aggregate hardness dummy variable - 0 = soft, 1 = hard

- Aggregate dummy variable - 1 = crushed limestone, 2 = crushed quartzite, 3 = rounded gravel

- Arrhenius concrete maturity - equivalent age, hours

- Nurse-Saul concrete maturity - °F-hours

- Pulse velocity - 1,000 ft /s (305 m/s)

- Initial mix temperature - °F

- Peak concrete temperature - °F

**Table 23. Early age (4 to 24 hours) cylinder temperature summary.**

| Mix | Cement Content, lb/yd$^3$ | Curing Temp., °F | Initial Temp., °F | Peak Temp., °F | Time to Peak, hours | Temp. Slope at 6 hours | Temperature, °F | | | | | |
|---|---|---|---|---|---|---|---|---|---|---|---|---|
| | | | | | | | 4 hours | 6 hours | 9 hours | 12 hours | 18 hours | 24 hours |
| Crushed Limestone | 500 | 50.0 | 73.8 | 73.8 | 0.0 | -2.8 | 57.2 | 56.8 | 55.1 | 56.1 | 55.9 | 56.0 |
| | | 72.0 | 79.8 | 92.2 | 10.5 | 1.2 | 82.2 | 86.7 | 91.6 | 91.6 | 86.8 | 84.1 |
| | | 100.0 | 87.6 | 116.0 | 6.5 | 4.6 | 106.0 | 115.0 | 112.0 | 107.0 | 103.0 | 102.0 |
| | 650 | 50.0 | 73.7 | 73.7 | 0.0 | -2.2 | 61.2 | 60.6 | 59.0 | 60.2 | 58.8 | 57.3 |
| | | 72.0 | 81.5 | 100.0 | 8.0 | 2.6 | 89.8 | 96.9 | 99.0 | 93.4 | 87.6 | 85.3 |
| | | 100.0 | 87.3 | 121.0 | 5.5 | 5.6 | 111.0 | 121.0 | 115.0 | 110.0 | 104.0 | 101.0 |
| Crushed Quartzite | 500 | 50.0 | 74.2 | 74.2 | 0.0 | -3.1 | 56.0 | 55.6 | 53.2 | 56.0 | 55.5 | 54.5 |
| | | 72.0 | 82.8 | 93.9 | 9.5 | 1.1 | 85.3 | 89.4 | 93.7 | 91.9 | 86.9 | 83.8 |
| | | 100.0 | 85.9 | 116.0 | 6.0 | 5.0 | 108.0 | 116.0 | 110.0 | 106.0 | 103.0 | 102.0 |
| | 650 | 50.0 | 75.5 | 75.5 | 0.0 | -3.3 | 56.4 | 55.9 | 54.8 | 53.0 | 55.7 | 55.6 |
| | | 72.0 | 83.1 | 93.3 | 9.5 | 0.8 | 83.1 | 87.8 | 93.0 | 91.1 | 86.2 | 83.3 |
| | | 100.0 | 85.8 | 120.0 | 5.5 | 5.7 | 112.0 | 120.0 | 111.0 | 107.0 | 103.0 | 101.0 |
| Rounded Gravel | 500 | 50.0 | 67.8 | 67.8 | 0.0 | -2.2 | 55.6 | 54.8 | 55.7 | 55.2 | 56.4 | 54.1 |
| | | 72.0 | 76.3 | 86.5 | 10.0 | 1.1 | 78.8 | 83.0 | 86.3 | 85.0 | 80.0 | 77.4 |
| | | 100.0 | 82.1 | 113.0 | 6.0 | 5.2 | 103.0 | 113.0 | 108.0 | 103.0 | 99.9 | 98.8 |
| | 650 | 50.0 | 74.0 | 74.0 | 0.0 | -2.8 | 56.1 | 57.0 | 55.0 | 56.1 | 55.4 | 55.9 |
| | | 72.0 | 77.0 | 91.6 | 8.5 | 1.7 | 81.0 | 87.2 | 91.4 | 86.4 | 80.0 | 78.2 |
| | | 100.0 | 80.8 | 121.0 | 5.5 | 6.7 | 106.0 | 121.0 | 114.0 | 107.0 | 101.0 | 98.8 |

NOTE: Slope at 6 hours relative to initial temperature.     500 lb/yd$^3$ = 297 kg/m$^3$, 650 lb/yd$^3$ = 386 kg/m$^3$
°C = 5/9 (°F-32)

80

**Table 24. Multiple linear regression analysis of early age strengths (4 to 24 hours) on Arrhenius maturity.**

| Regression Equation | Adjusted R-sq. |
|---|---|
| log(f'c) = -9.637 / AR + 0.0011 * CEMENT + 2.733 | 0.910 |
| log(f'c) = -9.681 / AR + 3.390 | 0.900 |
| log(ST) = -12.190 / AR - 3516.370 / FC28 - 0.0157 * T6SLOPE + 3.433 | 0.950 |
| log(ST) = -11.693 / AR + 2.666 | 0.934 |
| log(MR) = -11.227 / AR - 0.0043 * TEMP6 + 3.301E-7 * 10 ^ ( FC28 /1000 ) - 0.014 * PTIME + 3.308 | 0.971 |
| log(MR) = -10.004 / AR + 2.809 | 0.920 |

NOTE: f'c = compressive strength in psi, FC28 = compressive strength at 28 day moist cure in psi,
MR = modulus of rupture in psi, ST = split tensile strength in psi,
AR = Arrhenius maturity in equivalent hours at 68 °F, CEMENT = cement content in lb/yd$^3$,
TEMP6 = temperature at 6 hours in °F, PTIME = time to peak temperature in hours,
T6SLOPE = temperature slope at 6 hours (relative to initial temperature),

1000 lb/yd$^3$ = 593 kg/m$^3$, 1000 psi = 6.9 MPa, °C = 5/9 (°F-32)

**Table 25. Multiple linear regression analysis of early age strengths (4 to 24 hours) on Nurse-Saul maturity.**

| Regression Equation | Adjusted R-sq. |
|---|---|
| $\log(f'c) = -343.817 / NS + 0.0011 * CEMENT + 0.0055 * TRISE + 2.781$ | 0.929 |
| $\log(f'c) = -362.760 / NS + 3.548$ | 0.913 |
| $\log(ST) = -390.621 / NS + 0.0009 * CEMENT + 0.0193 * TEMP0 + 0.684$ | 0.943 |
| $\log(ST) = -404.564 / NS + 2.779$ | 0.910 |
| $\log(MR) = -370.861 / NS - 3.281E\text{-}7 * 10 \wedge ( FC28 / 1000 ) - 0.0118 * PTIME + 2.954$ | 0.965 |
| $\log(MR) = -364.996 / NS + 2.949$ | 0.945 |

NOTE:  f'c = compressive strength in psi, FC28 = compressive strength at 28 day moist cure in psi,
MR = modulus of rupture in psi, ST = split tensile strength in psi,
NS = Nurse-Saul maturity in °F - hours, CEMENT = cement content in lb/yd[3],
TEMP0 = initial temperature in °F, TRISE = Peak minus initial temperature in °F,
PTIME = time to peak temperature in hours

1000 lb/yd[3] = 593 kg/m^{3}, 1000 psi = 6.9 MPa, °C = 5/9 (°F-32)

**Table 26.** Multiple linear regression analysis of early age (4 to 24 hours) strengths on pulse velocity.

| Regression Equation | Adjusted R-sq. |
|---|---|
| $\log(f'c) = 0.153 * (PV/1000) + 0.0198 * TEMP0 + 0.516 * \log(AGE) - 0.981$ | 0.982 |
| $\log(f'c) = 0.192 * (PV/1000) + 0.732$ | 0.973 |
| $\log(ST) = 0.181 * (PV/1000) + 0.374 * GEOM + 0.143 * AGG - 1.889E\text{-}7 * 10 ^\wedge ( FC28/1000 ) - 0.502$ | 0.954 |
| $\log(ST) = 0.178 * (PV/1000) + 0.014$ | 0.931 |
| $\log(MR) = 0.140 * (PV/1000) + 0.128 * GEOM - 1.503 / AGE + 0.757$ | 0.958 |
| $\log(MR) = 0.160 * (PV/1000) + 0.460$ | 0.933 |

NOTE: f'c = compressive strength in psi, FC28 = compressive strength at 28 day moist cure in psi,
MR = modulus of rupture in psi, ST = split tensile strength in psi,
PV = pulse velocity in ft/s,
TEMP0 = initial temperature in °F, AGE = testing age in hours,
GEOM = aggregate geometry (0 for rounded, 1 for crushed),
AGG = type of aggregate (1 for limestone, 2 for quartzite, 3 for river gravel)

$1000 \text{ lb/yd}^3 = 593 \text{ kg/m}^3$, 1000 psi = 6.9 MPa, °C = 5/9 (°F-32), 1000 ft = 305 m

- Time to peak temperature - hours

- Temperature rise - peak minus initial

- Temperature at 6 hours - °F

- Slope of temperature at 6 hours - from initial

- Compressive strength at 28 days - moist cure at 72 °F (22 °C)

Transformations of variables including square root, logarithmic, exponential, and inverse functions were also included. Temperature data used for maturity calculations are summarized in table 23 . As shown in table 23 for 72 and 100 °F (22 and 38 °C) curing, peak temperatures occurred at approximately six hours (minimum). The slope at 6 hours as well as temperature at 6 hours were therefore included as independent variables. The slope at 6 hours is relative to the initial concrete cylinder temperature. Several models were developed for each of the 3 strength types and 2 nondestructive tests. Similar to the mix-specific models relating strength to nondestructive test (NDT) data, the independent variables were related to the logarithmic (base 10) form of strength. Results of the multiple linear regression models relating strength to NDT are summarized in tables 24 through 26 for Arrhenius maturity, Nurse-Saul maturity, and pulse velocity, respectively. For each strength type two models are listed. The first equation is the most statistically significant model. The second equation is the single variable general model (independent of aggregate type and cement content) similar to those developed with the mix-specific data. Strength data at 4 hours cured at 50 °F (10°C) were considered outliers and not used in the maturity data analysis.

As listed in tables 24 through 26 there is no significantly large difference in R-squared between the single variable and multivariable models. The R-squared adjusted values listed in tables 24 through 26 account for effects on R-squared of adding additional independent variables. Differences were minimal for the models with compressive strength. For the three NDT models differences in R-squared between the multivariable and single variable general models averaged 0.012, 0.024, and 0.032 for the compressive, split tensile, and modulus of rupture data, respectively.

For both the Arrhenius and Nurse-Saul maturity models the split tensile and modulus of rupture models were slightly better for predicting strength than the compressive strength model. In developing the maturity models curing temperature and age independent variables (and variable transformations) were not considered. It was assumed that all age and temperature effects were accounted for in the calculation of maturity. The effects on strength prediction of temperature and age data not contained in maturity were later investigated.

For strength-maturity relationships the general single variable (maturity) model can be slightly improved by including other time-temperature factors such as temperature at 6 hours, time to peak temperature, temperature slope at 6 hours (relative to initial temperature), temperature rise, and initial temperature. Cement content and 28-day moist cured compressive strength variables are also significant in predicting some strength types of early ages. The additional time-temperature variables which can improve the models suggests for early age strengths (4 to 24 hours) that the maturity equations do not account for all time and temperature influences on strength. Cement content levels also influence predicted strengths. For models without cement content independent variable terms, the

influences of cement may be indirectly accounted for in the 28-day moist cured (72 °F, 22 °C) compressive strength variables. Cement contents may also be reflected in temperature-time variables which can be affected by heat of hydration effects. The 28-day moist cured compressive strengths are listed in table 21. Aggregate properties (hardness, geometry, type) do not statistically improve the prediction equations for early age concrete strength. This could be expected since failure planes in test specimens passed around and not through the coarse aggregate. Since the mortar content and subsequent maturity behavior for all 6 mixes did not vary over a wide range, aggregate properties should not statistically improve the prediction equations. Any aggregate type influences on strength may be indirectly accounted for in the 28-day moist cured (72 °F, 22 °C) compressive strength variables.

For the strength-pulse velocity models, aggregate properties listed in table 26 can be used to slightly improve split tensile and modulus of rupture predictions. Age has a statistically significant influence on compressive and flexural strengths predicted from pulse velocity. Cement content is not a significant variable in predicting strength. For the split tensile model cement contents may be reflected in the 28-day moist cured compressive strength variable.

Overall for mix-specific models listed in tables 7 through 9 of appendix A the compressive strength models are slightly better than split tensile or modulus of rupture prediction models (higher average R-squared). For the general early age prediction models combining all aggregate types and cement contents, the compressive strength model is the better model for pulse velocity. For the maturity NDT data the compressive strength could not be as well predicted as other strength forms based on coefficients of determination. Maximum differences in R-squared between the single variables compressive strength prediction equation and either the split tensile or modulus of rupture equation were 0.034 and 0.032 for the Arrhenius and Nurse-Saul maturity models, respectively.

Compressive Strength Prediction Models. Since no strength form could be consistently predicted from maturity or pulse velocity data, compressive strength predicted from single independent variable general equations found in tables 24 through 26 were compared to the mix-specific equations previously developed in tables 7 through 9 of appendix A. Comparison was made by computing the difference in absolute value of the prediction errors using the general and mix-specific equations. Compressive strength prediction errors for the general and mix-specific equations are listed in tables 10 through 12 of appendix A for Arrhenius maturity, Nurse-Saul maturity, and pulse velocity, respectively. Differences in prediction errors averaged 167, 128, and 74 psi (1150, 880, and 510 kPa) for the Arrhenius, Nurse-Saul, and pulse velocity data, respectively. This indicates that an overall prediction equation independent of aggregate type and cement content can not be satisfactorily generated as a function of one independent nondestructive test input. If the errors are computed only for lab compressive strength data less than 2000 psi (13.8 MPa), the average errors drop to 68, 56, and 28 psi (470, 390, and 193 kPa) for the Arrhenius, Nurse-Saul, and pulse velocity data, respectively. This corresponds to a 35, 35, and 18 percent difference in prediction error percentages between the general single variable model and mix-specific Arrhenius, Nurse-Saul and pulse velocity models, respectively. Compressive strength and nondestructive data are shown in figures 38 through 46 for compressive strength data less than 2000 psi (13.8 MPa). The general single variable prediction models are also plotted in figures 38 through 46 for compressive strength data less than 2000 psi (13.8 MPa).
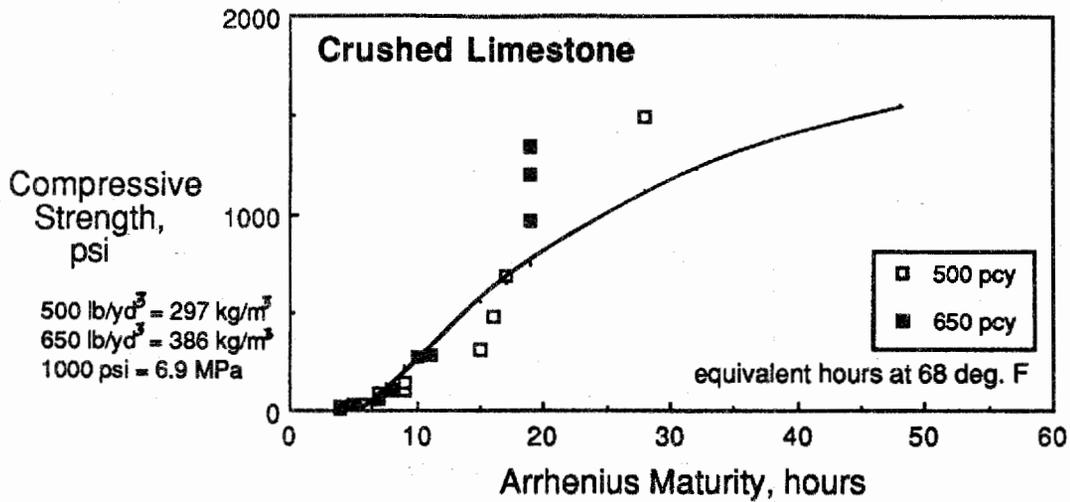
Figure 38.    Arrhenius maturity vs. compressive strength for CS.
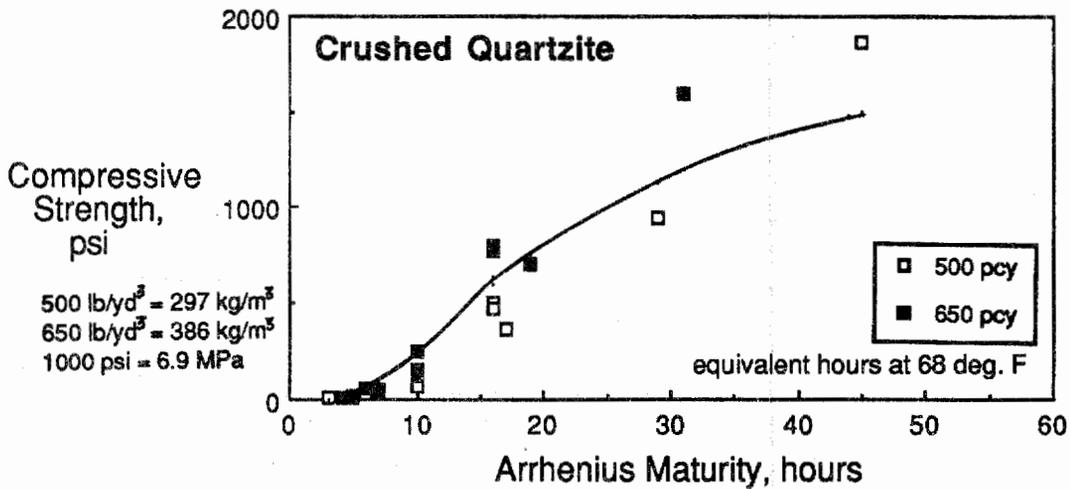


Figure 39.    Arrhenius maturity vs. compressive strength for CH.
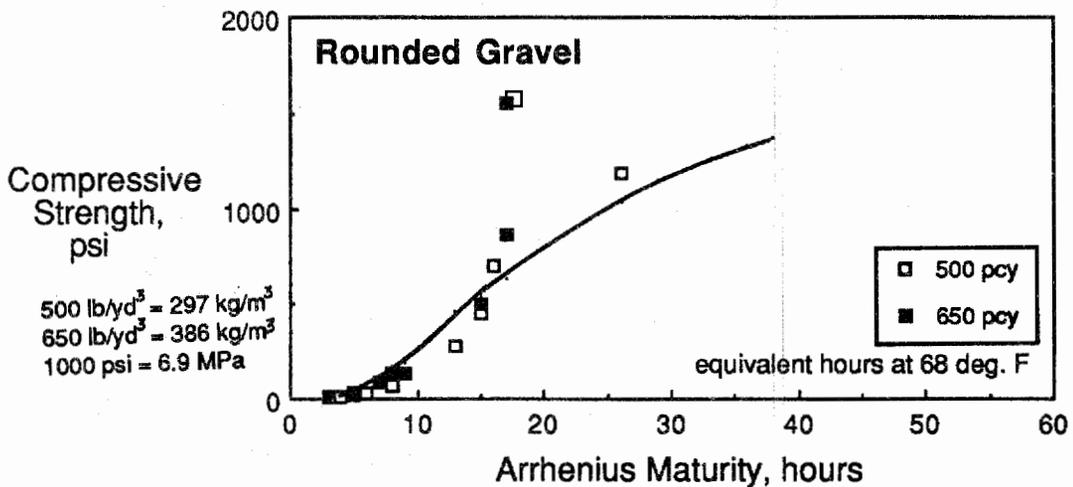


Figure 40.    Arrhenius maturity vs. compressive strength for RH.
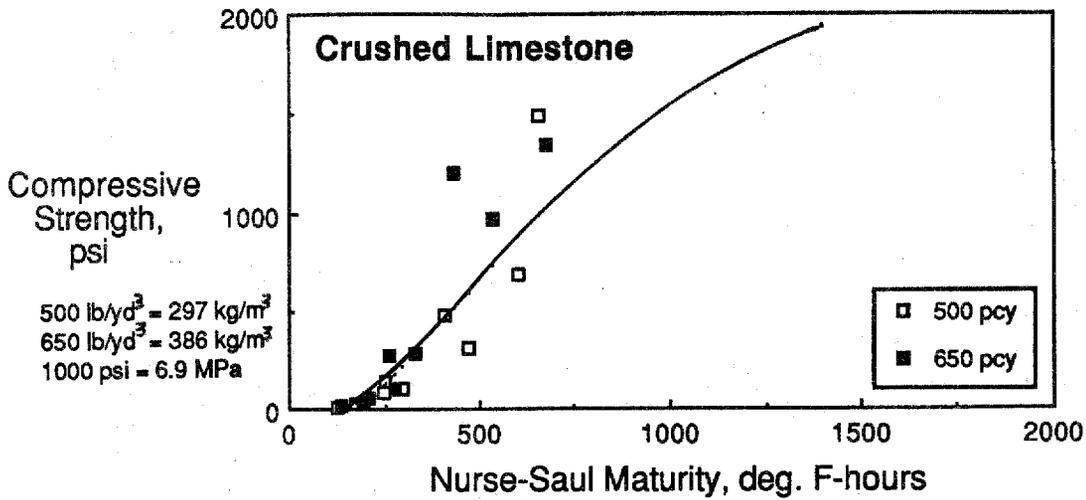
Figure 41.  Nurse-Saul maturity vs. compressive strength for CS.
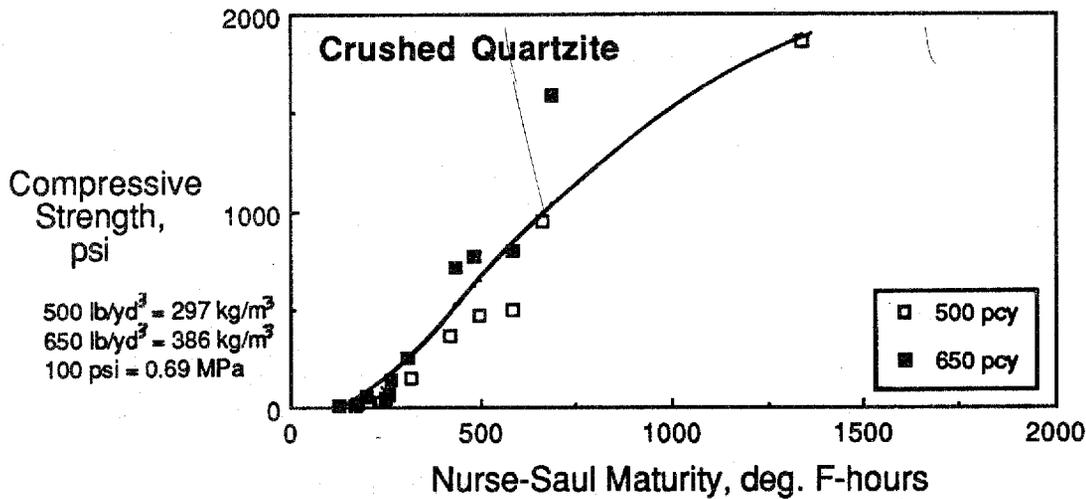


Figure 42.  Nurse-Saul maturity vs. compressive strength for CH.
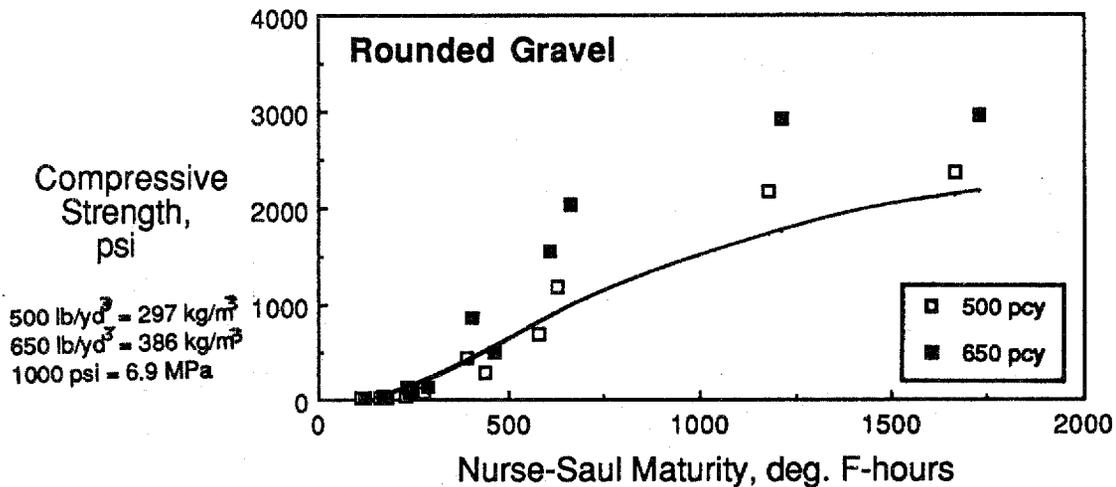


Figure 43.  Nurse-Saul maturity vs. compressive strength for RH.
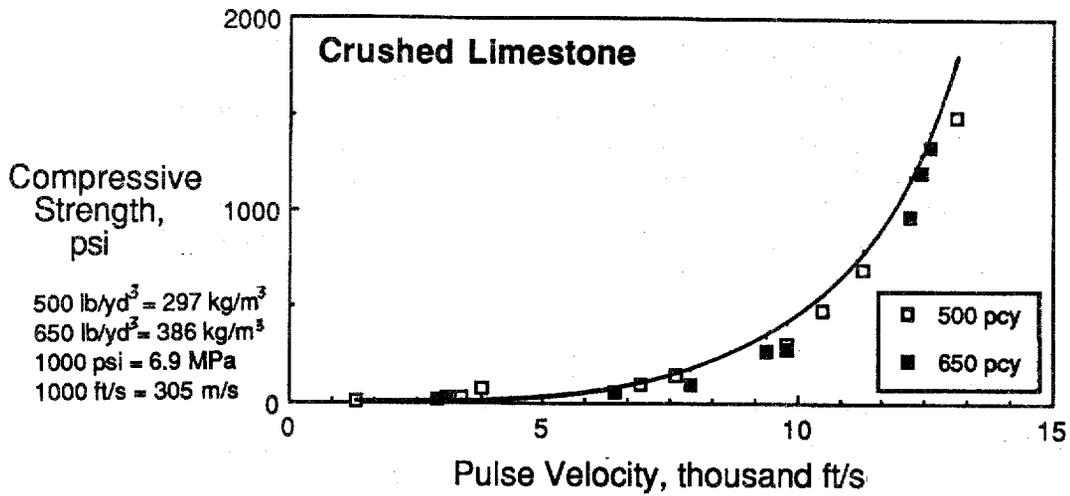
Figure 44.  Pulse velocity vs. compressive strength for CS.
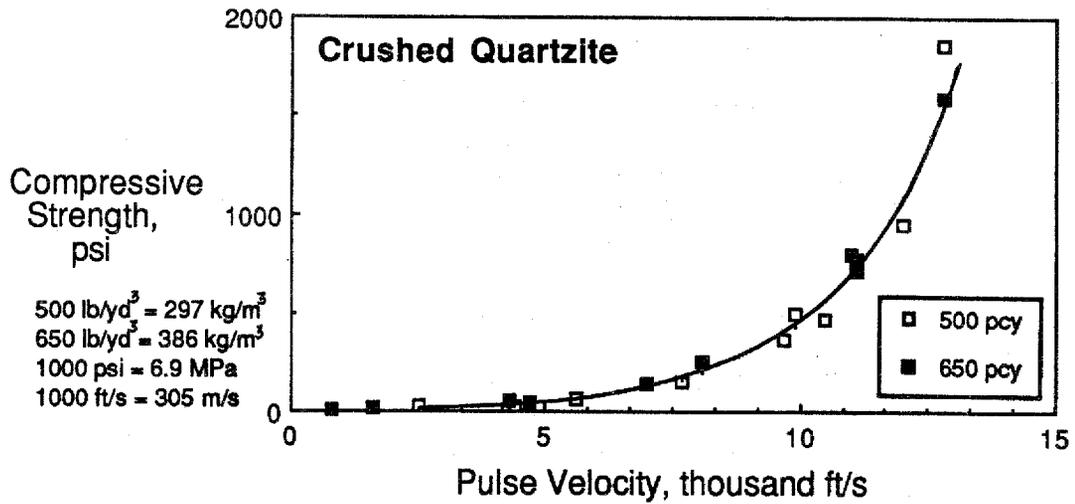


Figure 45.  Pulse velocity vs. compressive strength for CH.
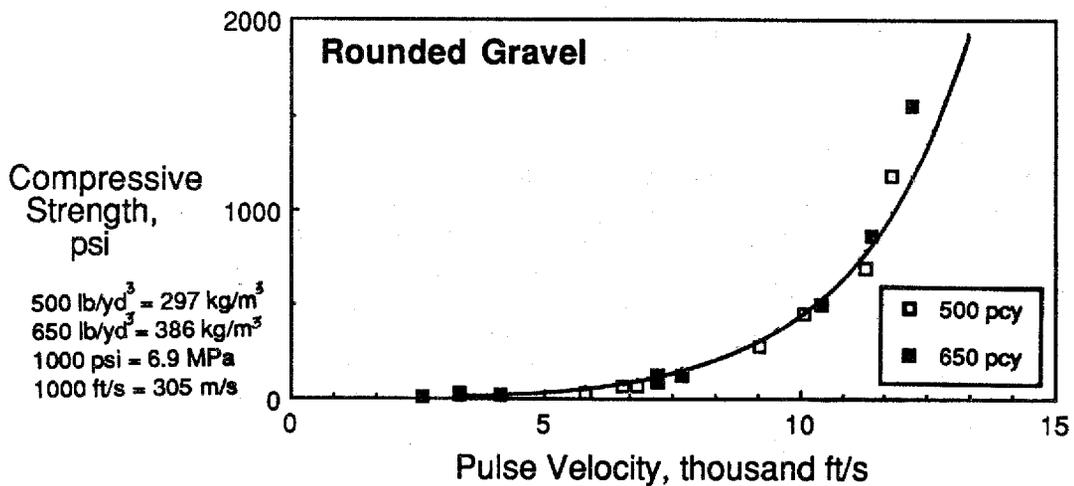


Figure 46.  Pulse velocity vs. compressive strength for RH.

For early age compressive strength (ages 4 to 24 hours) the general single variable models for maturity can predict compressive strength fairly accurately for strengths less than 2000 psi (13.8 MPa). Larger prediction errors for higher compressive strength are expected since the linear regression analysis was conducted on transformed data (log $f_c'$ and inverse of maturity). Prediction error differences between the general single variable and mix-specific pulse velocity models are approximately 50 percent less than those from maturity models. A detailed analysis of other factors affecting early age compressive strength (4 to 24 hours) was next conducted.

The general equation of the multiple linear regression analysis of compressive strength on maturity in tables 24 and 25 did not initially consider time and curing temperature as independent variables. It was assumed that the effects of temperature and time were incorporated into maturity. Other variables such as initial temperature, temperature at 6 hours, peak temperature, slope of temperature at 6 hours, and time to peak temperature were included in the preliminary regression analysis. The multiple regression analysis was repeated for compressive strength on maturity but without suppressing time or temperature variables and variable transformations. As shown in table 27 for Arrhenius maturity when age is included as an independent variable, the concrete temperature at 6 hours, and log (base 10) form of age become statistically significant variables. Cement content is a statistically significant variable when predicting compressive strength from Arrhenius or Nurse-Saul maturity regardless of whether time and temperature variables are suppressed. Coefficients of determination increase from 0.900 for the single variable Arrhenius maturity model to 0.949 when age is included. For Nurse-Saul maturity, including both temperature and age variables increase R-squared from 0.913 (simple general model) to 0.948. Significant models of compressive strength (log base 10) versus Nurse-Saul maturity (inverse) are summarized in table 28.

Table 29 summarizes significant models of predicting compressive strength from pulse velocity measurements (1000 ft/s, 305 m/s). Two additional models not summarized in table 26 are listed in table 29. The increase in coefficient of determination is significantly less than corresponding increases in maturity models when temperature and age are included. Coefficients of determination slightly increased from 0.973 to 0.982 when age and initial temperature effects are considered.

The in-depth analysis of variables affecting compressive strength predictions show that maturity does not incorporate all temperature and age effects. If maturity is combined with age and temperature variables the predictive power of the linear regression equation can be statistically increased. The models can only be slightly improved if other variables (excluding age and temperature) are included with either maturity or pulse velocity.

Within-Test Variability. The within-test standard deviation of the 3 strength types was calculated for each mix at each curing temperature. The variation of concrete strength for a single test is assumed to be attributable to fabricating, handling, curing, and testing conditions. The concrete material variability is minimal if the concrete material is assumed homogeneous. The standard deviation was estimated using the range in strength for each sample. The range was calculated for the 3 compressive, 3 split tensile, and 2 modulus of rupture specimens for each mix at each curing temperature. The range as an estimate of standard deviations is reliable up to specimen sample sizes of 10.[36] A single set of strength data per mix is generally considered insufficient to get a reliable range estimate used to compute a within-test standard deviation. A minimum of 10 strength batches (per

**Table 27. Multiple linear regression analysis of early age compressive strength on Arrhenius maturity.**

| Ind. Variable,[1] X1 | Coefficient [t-statistic] | Ind. Variable,[1] X2 | Coefficient [t-statistic] | Ind. Variable,[1] X3 | Coefficient [t-statistic] | Ind. Variable,[1] X4 | Coefficient [t-statistic] | Constant[1] | R - sq., adjusted |
|---|---|---|---|---|---|---|---|---|---|
| 1/AR | -5.036 [-6.71] | log (AGE) | 1.185 [7.32] | CEMENT | 0.0011 [3.80] | TEMP6 | 0.0084 [4.83] | 0.422 | 0.949 |
| 1/AR | -8.325 [-20.95] | AGE | 0.0212 [5.25] | CEMENT | 0.0012 [3.62] | **** | **** | 2.332 | 0.935 |
| 1/AR | -8.403 [-19.53] | AGE | 0.0207 [4.73] | **** | **** | **** | **** | 3.032 | 0.924 |
| 1/AR | -9.681 [-25.32] | **** | **** | **** | **** | **** | **** | 3.390 | 0.900 |

[1] NOTES:  f'c = compressive strength in psi
AR = Arrhenius maturity in equivalent hours at 68 °F.
AGE = testing age in hours
CEMENT = cement content in lb/yd
TEMP6 = temperature at 6 hours in °F

General equation form log(f'c) = aX1+ bX2 + .... + constant
where X1, X2 ... = independent variables, and a,b ... = coefficients

1000 lb/yd$^3$ = 593 kg/m$^3$ , 1000 psi = 6.9 MPa
68 °F = 20 °C, °C = 5/9 (°F-32)

**Table 28. Multiple linear regression analysis of early age compressive strength on Nurse-Saul maturity.**

| Ind. Variable,[1] X1 | Coefficient [t-statistic] | Ind. Variable,[1] X2 | Coefficient [t-statistic] | Ind. Variable,[1] X3 | Coefficient [t-statistic] | Ind. Variable,[1] X4 | Coefficient [t-statistic] | Constant[1] | R - sq., adjusted |
|---|---|---|---|---|---|---|---|---|---|
| 1/NS | -265.475 [-13.18] | CEMENT HARD | 0.00130 [4.33] -0.0966 [2.05] | 10^(TEMP/1C | 0.0554 [5.25] **** | AGE | 0.0228 [4.72] **** | 1.973 **** | 0.948 |
| 1/NS | -269.291 [-13.12] | CEMENT | 0.00130 [4.22] | 10^(TEMP/1C | 0.0541 [5.01] | AGE | 0.0220 [4.47] | 1.940 | 0.945 |
| 1/NS | -343.749 [-25.31] | CEMENT | 0.00120 [3.50] | 10^(TEMP/1C | 0.0274 [2.69] | **** | **** | 2.631 | 0.930 |
| 1/NS | -361.213 [-29.01] | CEMENT | 0.00120 [3.30] | **** | **** | **** | **** | 2.867 | 0.924 |
| 1/NS | -362.760 [-27.29] | **** | **** | **** | **** | **** | **** | 3.548 | 0.913 |

[1] NOTES: f'c = compressive strength in psi, NS = Nurse-Saul maturity in °F-hours,
CEMENT = cement content in lb/yd , TEMP = curing temperature in °F,
AGE = testing age in hours, HARD = aggregate hardness (0=soft,1=hard)

General equation form log(f'c) = aX1+ bX2 + .... + constant
where X1, X2 ... = independent variables, and a,b ... = coefficients

$1000 \text{ lb/yd}^3 = 593 \text{ kg/m}^3$
1000 psi = 6.9 MPa
68 °F = 20 °C
°C = 5/9 (°F-32)

Table 29. Multiple linear regression analysis of early age compressive strength on pulse velocity.

| Independent Variable,[1] X1 | Coefficient [t-statistic] | Independent Variable,[1] X2 | Coefficient [t-statistic] | Independent Variable,[1] X3 | Coefficient [t-statistic] | Constant[1] | R - sq., adjusted |
|---|---|---|---|---|---|---|---|
| PV/1000 | 0.153 [21.41] | log (AGE) | 0.516 [5.84] | TEMP0 | 0.0198 [5.36] | -0.981 | 0.982 |
| PV/1000 | 0.162 [25.57] | AGE | 0.0150 [5.18] | TEMP0 | 0.0160 [4.56] | -0.446 | 0.981 |
| PV/1000 | 0.183 [36.16] | AGE | 0.00740 [2.76] | **** | **** | 0.733 | 0.975 |
| PV/1000 | 0.192 [50.63] | **** | **** | **** | **** | 0.732 | 0.973 |

[1] NOTES:  $f'c$ = compressive strength in psi,
PV = pulse velocity in ft/s,
AGE = testing age in hours
TEMP0 = initial temperature in °F,

General equation form $\log(f'c) = aX1 + bX2 + \dots + constant$
where X1, X2 ... = independent variables, and a, b ... = coefficients

1000 lb/yd$^3$ = 593 kg/m$^3$ , 1000 psi = 6.9 MPa
68 °F = 20 °C, °C = 5/9 (°F-32)
1000 ft/s = 305 m/s

mix and temperature) is recommended to get a reliable estimate of the range. Therefore, the within-test standard deviations reported reflect additional uncertainty due to ranges computed from a single set of test specimens.

Coefficients of variation for compressive, splitting tensile, and flexural strengths generally were less than 10, 15, and 20 percent, respectively. The aggregate type, cement content, and temperature did not have a consistent effect on the coefficients of variation. Average coefficients of variation for compressive split tensile, and flexural strength tests are summarized in table 30. For the 6 mixes, coefficients of within-test variation averaged 5.7, 9.1, and 10.2 percent for compressive, split tensile and modulus of rupture, respectively. The analysis indicated that at early ages, compressive strength is approximately 50 percent less variable than split tensile and flexural strength tests.

Modulus of Elasticity and Compressive Strength Relationship. Early age (4 to 24 hours) modulus of elasticity was determined for the crushed limestone at the 500 and 650 lb/yd$^3$ (297 and 386 kg/m$^3$) cement contents. The analysis was conducted only for one aggregate type since investigation of moduli at ages of 1 to 28 days indicated that for the data in this study a relationship between compressive strength and modulus of elasticity could be established which is independent of aggregate type and cement content. The modulus of elasticity and compressive strength was determined for 2 specimens at 4, 6, 9, and 24 hours. The modulus of elasticity and compressive strength data was generated in a separate lab batch independent of the other early age lab data shown in figures 11 through 28. The early age modulus of elasticity and companion compressive strengths were batched with a different cement brand than the other early age mixes. Compressive strength data reported for the early age elastic modulus analysis should not be confused with other early age compressive strength data in this report.

Data used in the early age elastic modulus analysis is summarized in table 13 of appendix A. Compressive strength ranged from approximately 30 to 2000 psi (0.2 to 13.8 MPa) for the 2 cement contents at ages of 24 hours and less. Measured modulus of elasticity ranged from approximately 50,000 to 2.8 million psi (345 to 19,300 MPa).

The early age modulus of elasticity can be estimated from compressive strength. Models which are significant in predicting the modulus of elasticity were a function of square root or a function of the logarithm (natural) of compressive strength. Equations relating modulus of elasticity and compressive strength are summarized in table 14 of appendix A. Both models were statistically significant with coefficients of determination of 0.946 and 0.967 for the square root and logarithmic models, respectively. The computed t-statistic of -2.4 on the square root model with a constant term is not significant at the 5 percent level of significance. This suggests that (depending on the level of significance selected) the constant term in the square root model is not statistically different from zero. The square root model with no constant term is:

$$E_c = 61,071 * sqrt\ (f_c') \dots\dots\dots\dots\dots\dots\dots\dots\dots\dots (11)$$

where

$E_c$ = modulus of elasticity, psi (1 million psi = 6890 MPa)
$f_c'$ = compressive strength, psi

**Table 30. Within-test coefficient of variation summary.**

| Aggregate Type | Cement Content, lb/yd$^3$ | | Coefficient of Variation, percent[1] | | |
| --- | --- | --- | --- | --- | --- |
| | | | Compressive Strength | Split Tensile Strength | Modulus of Rupture |
| Crushed Limestone | 500 | minimum | 1.7 | 2.4 | 1.2 |
| | | maximum | 12.3 | 14.2 | 58.3 |
| | | average | 6.1 | 9.1 | 14.7 |
| | 650 | minimum | 1.8 | 2.4 | 1.1 |
| | | maximum | 10.2 | 16.8 | 11.1 |
| | | average | 5.9 | 7.9 | 5.9 |
| Crushed Quartzite | 500 | minimum | 1.6 | 3.2 | 0.0 |
| | | maximum | 12.3 | 19.3 | 16.1 |
| | | average | 5.8 | 8.5 | 6.0 |
| | 650 | minimum | 0.9 | 4.1 | 0.0 |
| | | maximum | 13.5 | 17.9 | 25.3 |
| | | average | 4.7 | 9.1 | 10.0 |
| Rounded Gravel | 500 | minimum | 0.4 | 1.9 | 0.0 |
| | | maximum | 17.0 | 23.8 | 23.1 |
| | | average | 6.5 | 9.6 | 10.8 |
| | 650 | minimum | 1.6 | 4.2 | 0.0 |
| | | maximum | 12.3 | 20.5 | 70.9 |
| | | average | 4.9 | 10.3 | 13.6 |

[1] NOTE: Average of estimated coefficients of variation at ages of 4, 6, 9, and 2 cured at 50, 72, and 100 °F.

500 lb/yd$^3$ = 297 kg/m$^3$ , 650 lb/yd$^3$ = 386 kg/m$^3$
50 °F = 10 °C, 72 °F = 22 °C, 100 °F = 38 °C

As listed in table 13 of appendix A the prediction errors for modulus of elasticity over 100,000 psi (690 MPa) ranged from 1 to 71 percent. This corresponds to errors ranging from 30,000 to 320,000 psi (207 to 2208 MPA) for moduli less than 3 million psi (20,700 MPa).

The model relating modulus to square root of compressive strength (no constant term) was selected since:

- There is no large statistical advantage in using the log or square root models.

- The square root model with constant is easy to calculate.

- The square root no constant equation is similar to the American Concrete Institute (ACI) equation commonly used.[37]

- The constant in the square root model is not statistically significant.

The relationships between compressive strength (at less than 24 hours and from 1 through 28 days) and modulus of elasticity apply to the mixes used in this investigation. Other available data use the same equation form (square root of compressive strength multiplied by a constant) to estimate modulus of elasticity. The constant does change since it may be a function of aggregate type, shape, and properties as well as cement and fly ash source. The constant derived in the study is applicable to the data generated. Caution should be used before applying the relationship to other mixes. It is recommended that a mix-specific relationship be developed to maximize reliability for the prediction of modulus of elasticity.

Coefficient of Thermal Expansion and Contraction. Coefficients of thermal expansion and contraction of concrete measured at 8 and 16 hours are summarized in table 31. Two coefficients are reported for each mix. Coefficients of expansion and contraction were measured on the same specimens. The coefficient of thermal expansion was computed for the nominal temperature range of 72 to 120 °F (22 to 49 °C). The coefficient of thermal contraction was computed for the drop in temperature from approximately 120 to 50 °F (49 to 10 °C). Coefficients averaged 5.6, 6.1, and 6.0 in/in/°F (10.1, 11.0, and 10.8 mm/mm/°C) for the limestone, quartzite, and gravel concrete, respectively. These coefficients do not show a significant range contrary to other data for carbonate and siliceous aggregates. No significant or consistent difference in coefficients between the 500-and 650-lb/yd$^3$ (297-and 396-kg/m$^3$) cement contents was noted.

Thermal coefficients for concrete increase with temperature and are larger in expansion than contraction.[38] At 8 hours the increasing temperature and/or expansion-contraction difference effects are reflected in the larger coefficients of expansion than contraction At 8 hours the difference in expansion (48 °F, 27 °C increase) and contraction (70 °F, 39 °C decrease) averaged 1.4 x 10$^{-6}$ in/in/°F (2.5 x 10$^{-6}$ mm/mm/°C). No significant difference in thermal coefficient of expansion and contraction was observed at 16 hours. At 16 hours the coefficients of expansion generally decreased and coefficients of contraction increased from those measured at 8 hours. For joint sawing operations coefficients of thermal contraction are of interest in computing tensile contraction restraint

## Table 31. Coefficients of thermal expansion and contraction.

| Mix | Cement, lb/yd$^3$ | 8 Hours | | | 16 Hours | | | Change from 8 to 16 hrs, % |
|---|---|---|---|---|---|---|---|---|
| | | Temp., °F Initial | Final | Thermal Coef. | Temp., °F Initial | Final | Thermal Coef.[1] | |
| Limestone | 500 | 74.9 | 123.5 | 6.6 | 72.9 | 127.3 | 5.4 | -17.7 |
| | | 123.5 | 46.7 | 5.0 | 127.3 | 50.1 | 5.7 | 12.6 |
| | 650 | 76.2 | 123.3 | 6.5 | 71.4 | 123.3 | 5.4 | -15.9 |
| | | 123.3 | 47.0 | 4.9 | 123.3 | 55.0 | 5.5 | 11.9 |
| Quartzite | 500 | 76.3 | 121.8 | 6.0 | 72.7 | 123.2 | 6.1 | 1.5 |
| | | 121.8 | 46.9 | 5.7 | 123.2 | 46.5 | 6.0 | 5.0 |
| | 650 | 76.6 | 125.1 | 6.9 | 74.4 | 122.5 | 6.4 | -7.5 |
| | | 125.1 | 45.1 | 5.5 | 122.5 | 44.6 | 6.1 | 12.1 |
| River Gravel | 500 | 75.4 | 123.5 | 7.1 | 74.6 | 123.2 | 5.6 | -21.4 |
| | | 123.5 | 46.4 | 5.3 | 123.2 | 47.1 | 5.7 | 7.1 |
| | 650 | 76.1 | 122.7 | 7.0 | 75.3 | 122.2 | 6.2 | -10.7 |
| | | 122.7 | 45.6 | 5.5 | 122.2 | 46.6 | 5.9 | 7.2 |

[1] NOTE: Thermal coefficients units of in/in/ °F, millionths.

500 lb/yd$^3$ = 297 kg/m$^3$ , 650 lb/yd$^3$ = 386 kg/m$^3$
°C = (1.8 °F) + 32, mm/mm/°C = 1.8 in/in/°F

forces. The coefficients of contraction averaged 5.3, 5.8, and 5.6 x $10^{-6}$ in/in/°F (9.5, 10.4, and 10.1 x $10^{-6}$ mm/mm/°C) for the crushed limestone, crushed quartzite, and rounded gravel, respectively.

**Test Results - Early Loading Time Period:  1 to 28 Days**

Compressive strength, flexural strength (modulus of rupture), and modulus of elasticity testing was conducted at 1, 3, 7, 14, and 28 days. Nondestructive pulse velocity was also done at these ages. Concrete maturity at these ages was calculated from temperatures using both the temperature-time (Nurse-Saul) and equivalent age (Arrhenius function) functions. The datum temperature was 0 °C (32 °F) and activation energy divided by the gas constant was 5000 °K. Two aggregate types, crushed limestone and crushed quartzite, were used in investigation of early loading (1 to 28-day) properties. Cement contents of 500 and 650 lb/yd$^3$ (297 and 386 kg/m$^3$) remained identical to mixes used in the early age laboratory investigation (4 to 24 hours). In addition to the early age curing temperatures of 50, 72, and 100 °F (10, 22, and 38 °C) at 50 percent RH, the 72 °F (22 °C) 100 percent RH (moist cure) condition was selected.

Strength Versus Time. Results of the strength, modulus of elasticity, pulse velocity, and maturity tests are listed in tables 15 and 16 of appendix B. Average values reported are for 3, 3, and 2 specimens for compressive strength, modulus of elasticity, and modulus of rupture, respectively. Modulus of elasticity and compressive strength was determined from the same specimen. Strength and modulus of elasticity as a function of curing age and temperature are summarized in figures 47 through 58.

For compressive strength data, as curing temperatures increased, the strength as well as the percentage of the 28-day strength increased for ages of 1 to 3 days. At ages of 7 and 14 days the effects of curing temperature on strength gain (as a percentage of 28-day strength) were not as significant. At 7 and 14 days the compressive strength ranges from approximately 80 to 90 percent of the 28-day strengths regardless of curing temperatures. Differences in strength percentages between the 2 aggregates were generally less than 5, 5, and 10 percent for compressive, modulus of elasticity, and modulus of rupture, respectively. The strength percentages of the 28-day strengths for the two aggregates were therefore averaged and summarized in table 32.

For cement contents of 650 lb/yd$^3$ (386 kg/m$^3$) the compressive strength at 28 days for curing temperatures of 50 °F (10 °C) are larger than those strengths at 100 °F (38 °C) curing temperatures. For cement contents of 500 lb/yd$^3$ (297 kg/m$^3$) at 28 days the 50 °F (10 °C) strength is still smaller than the 100 °F (38 °C) strength. The trends in compressive strength gain indicate that at ages of greater than 28 days that the 50 °F (10 °C) curing strength will exceed that at the 100 °F (38 °C) curing temperature. The "cross-over" effect of low temperature specimens being weaker at early ages and stronger at 28 days than specimens exposed to higher curing temperatures is frequently observed. The temperature effects are qualitatively explained by the distribution of hydration reaction products.[25] With increased rates of hydration at elevated temperatures, reaction and hydration products are not uniformly distributed. The nonuniform distribution can disrupt further hydration and result in lower later age strength.

Similar to compressive strength data, as curing temperatures increased, the modulus of rupture percentage of the 28-day strength increased for ages of 1 to 3 days. At ages of 7
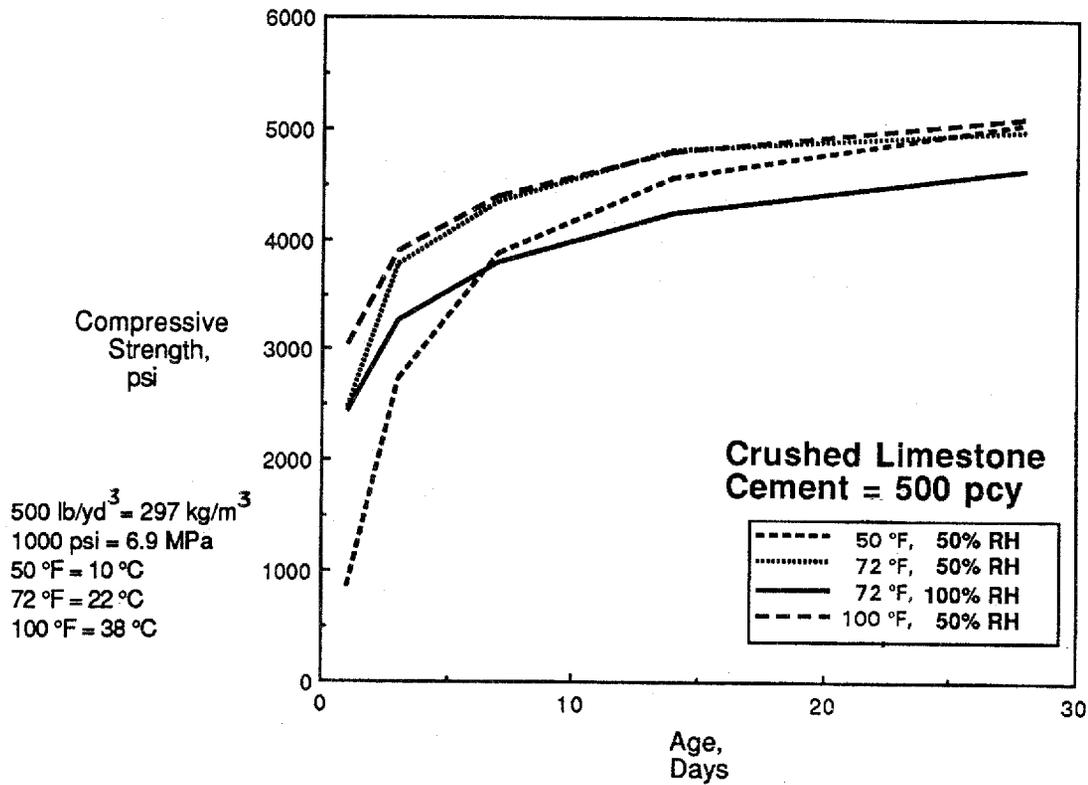
Figure 47. Compressive strength vs. 1 to 28 days for CS 500.
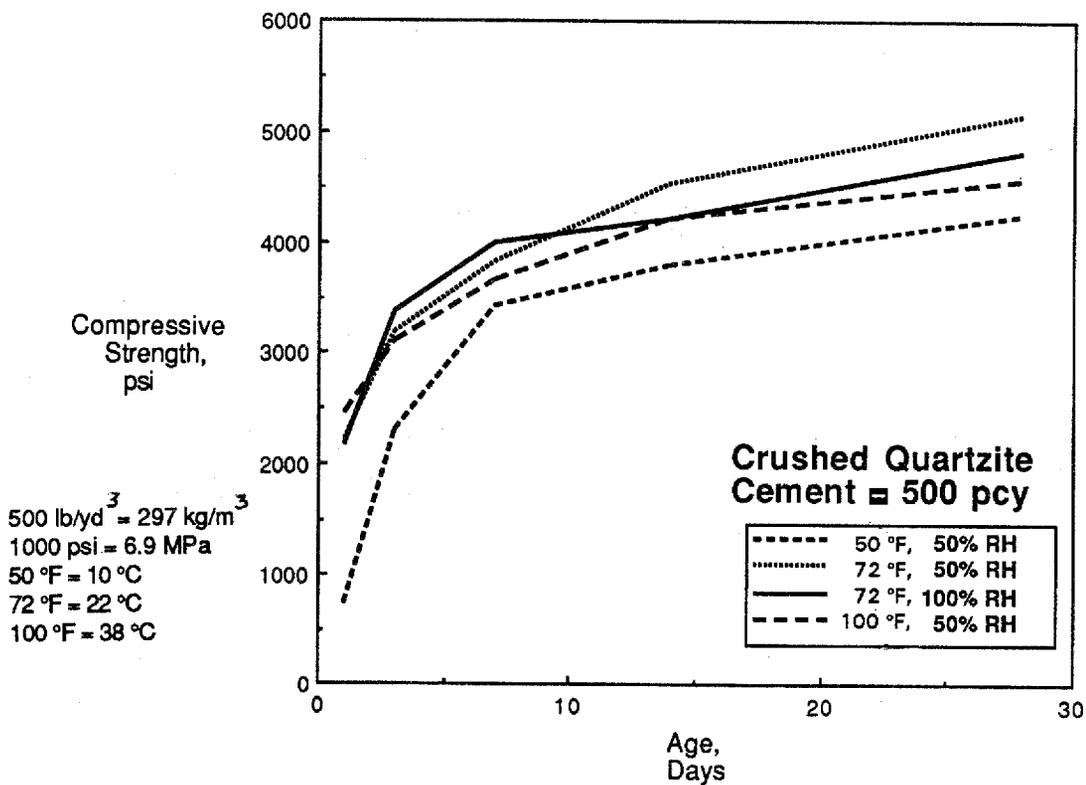


Figure 48. Compressive strength vs. 1 to 28 days for CH 500.
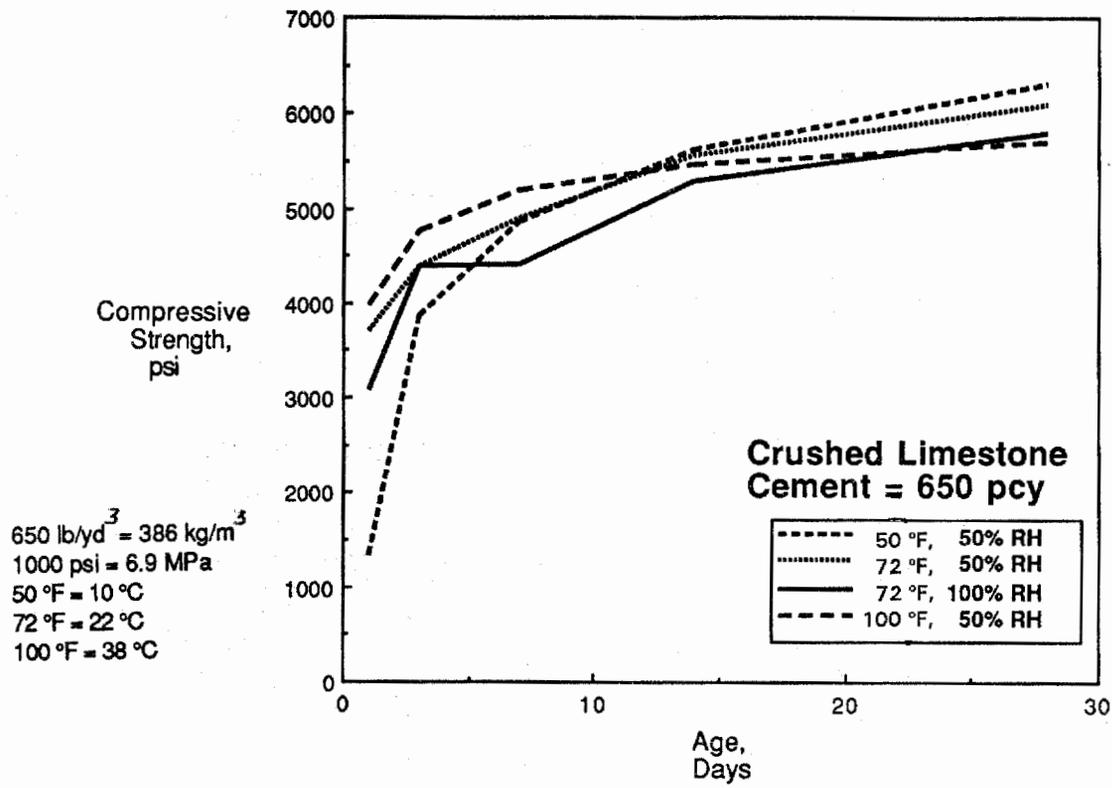
Figure 49. Compressive strength vs. 1 to 28 days for CS 650.
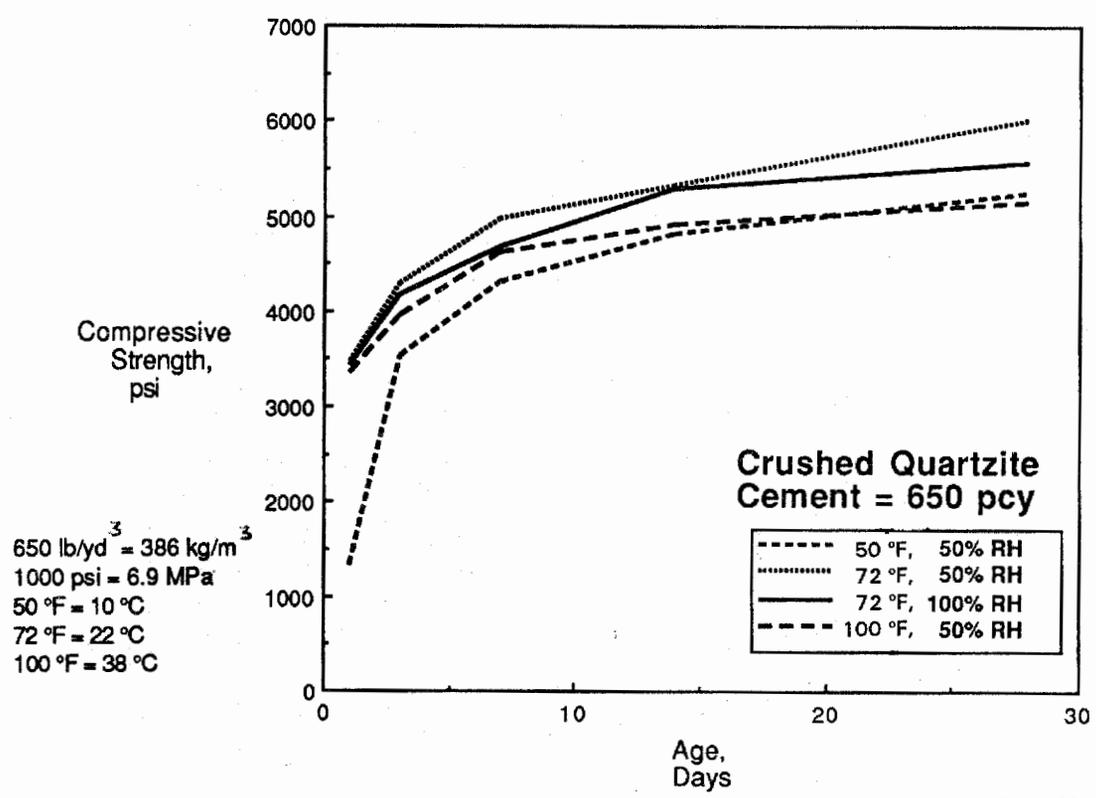


Figure 50. Compressive strength vs. 1 to 28 days for CH 650.
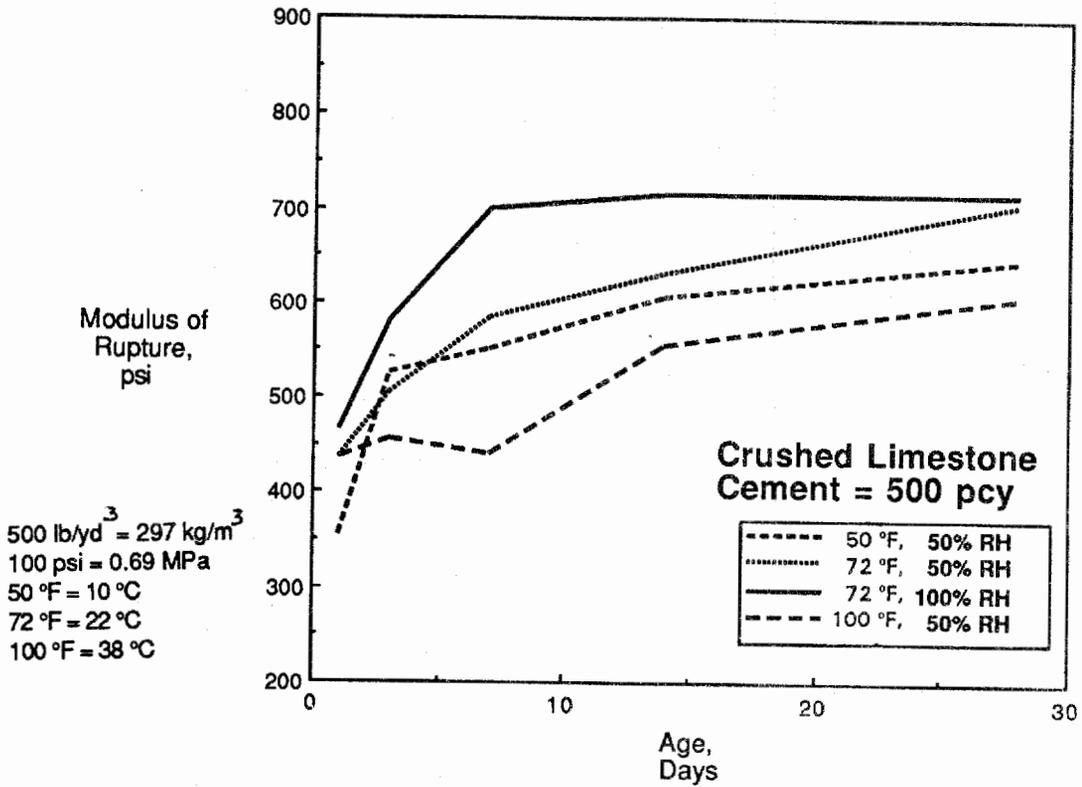
Figure 51.   Flexural strength vs. 1 to 28 days for CS 500.
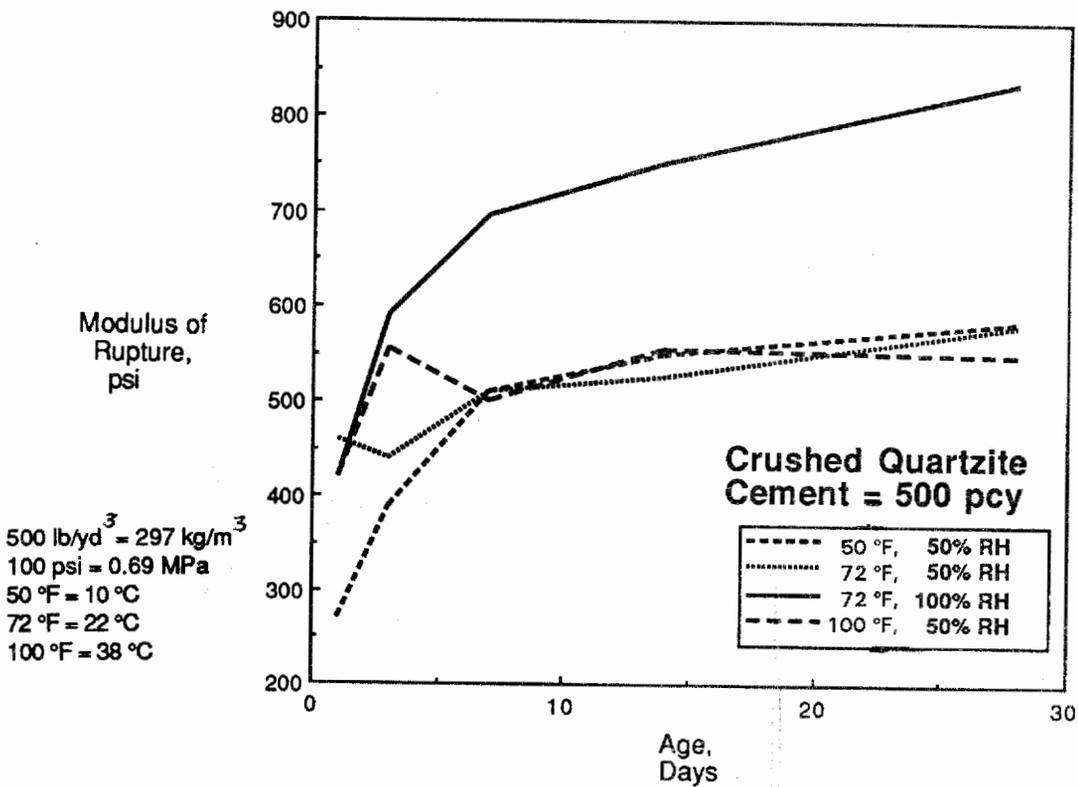


Figure 52.   Flexural strength vs. 1 to 28 days for CH 500.
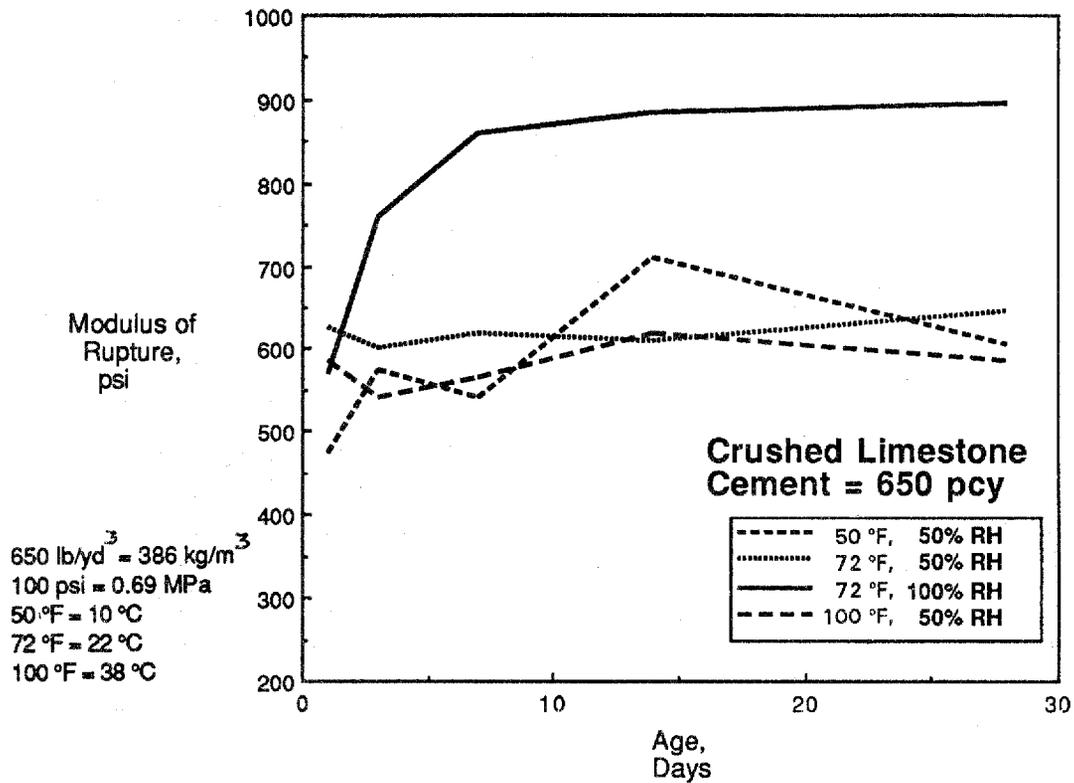
Figure 53.  Flexural strength vs. 1 to 28 days for CS 650.
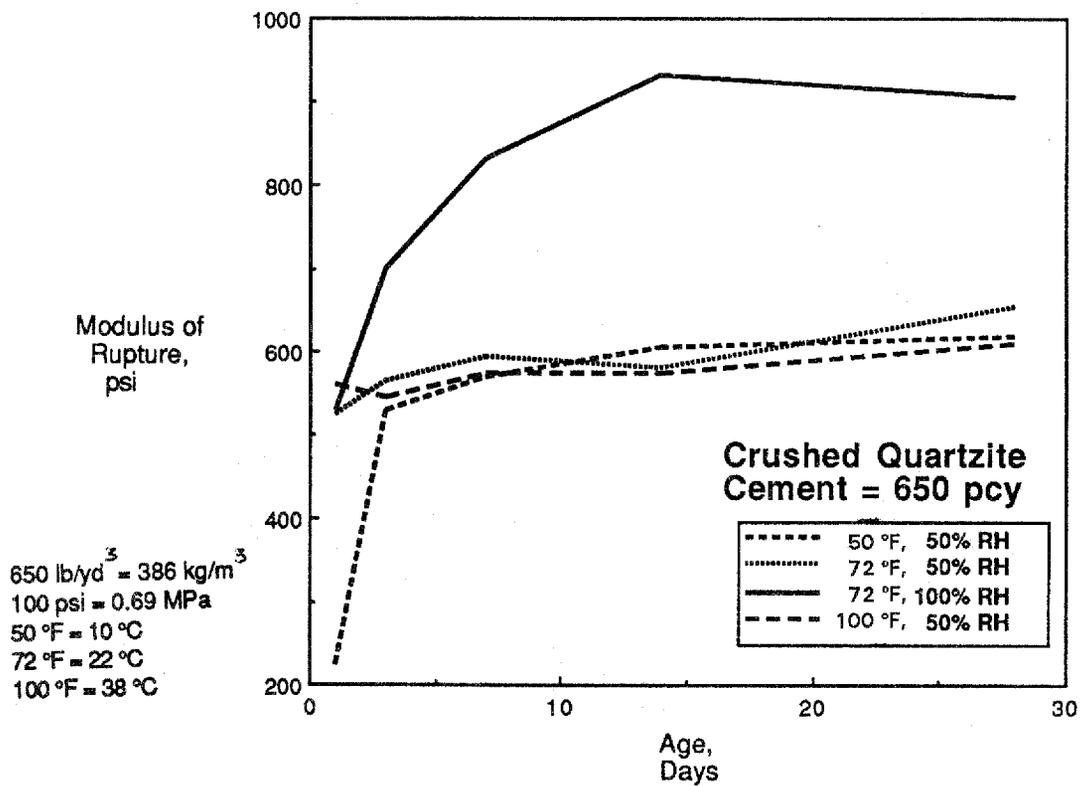


Figure 54.  Flexural strength vs. 1 to 28 days for CH 650.
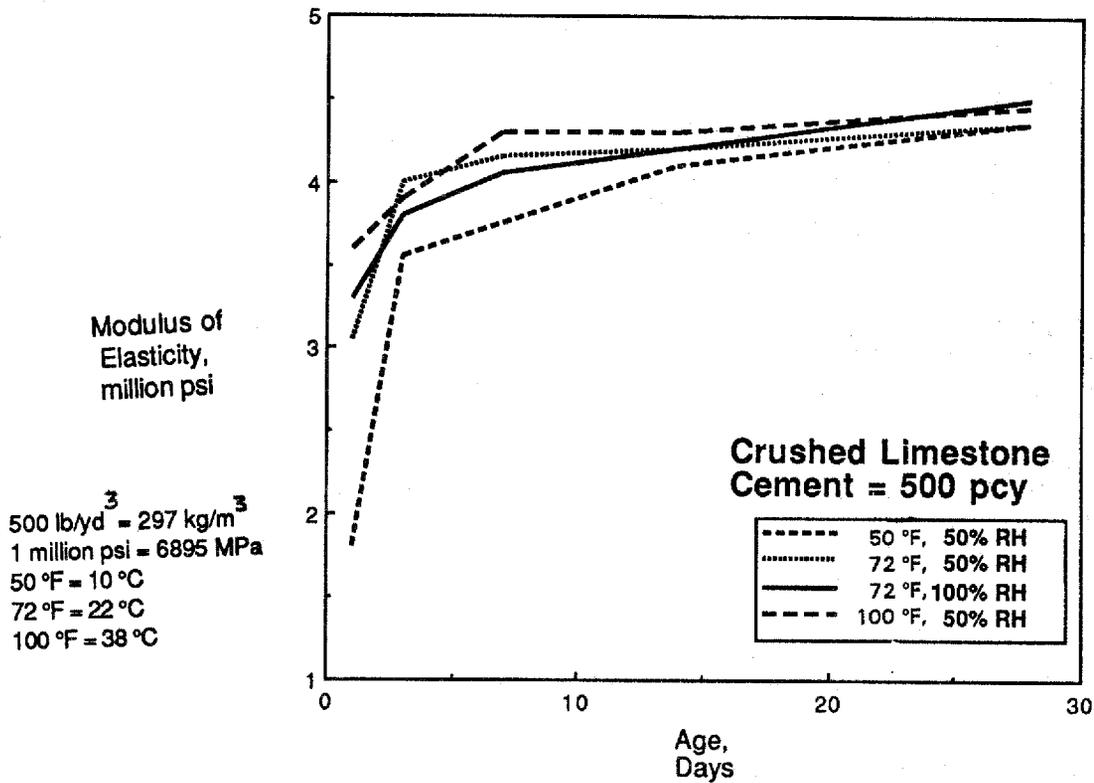
Figure 55.  Elastic modulus vs. 1 to 28 days for CS 500.
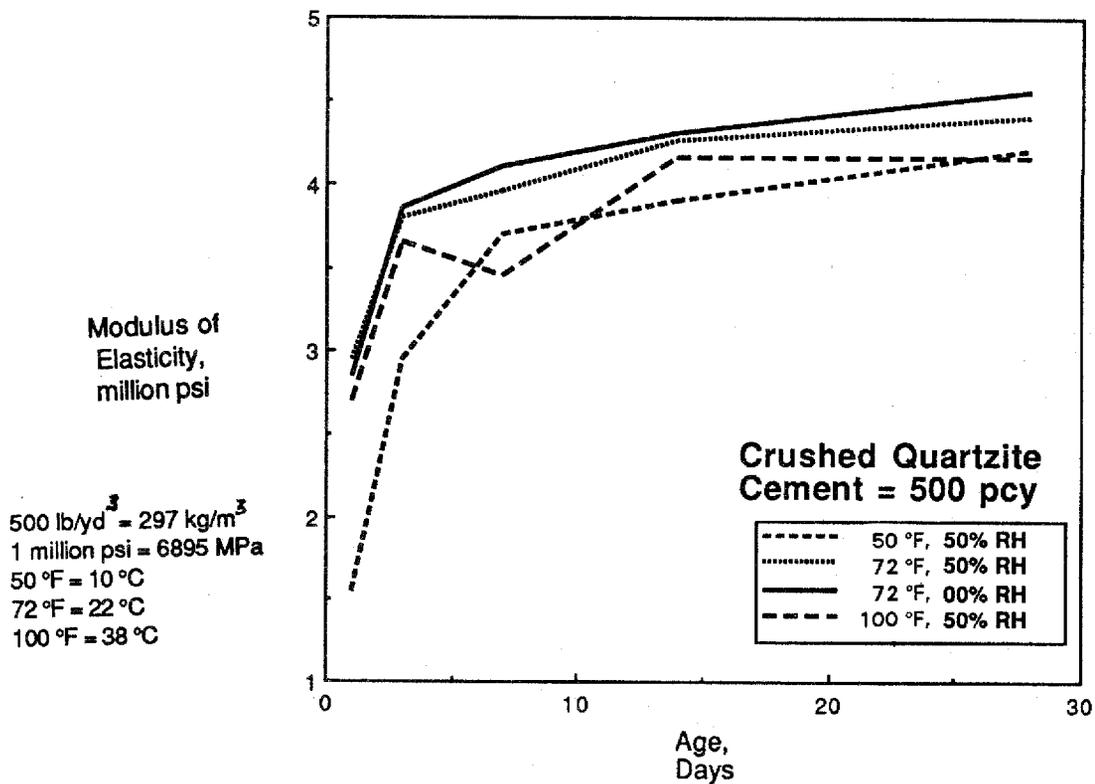


Figure 56.  Elastic modulus vs. 1 to 28 days for CH 500.
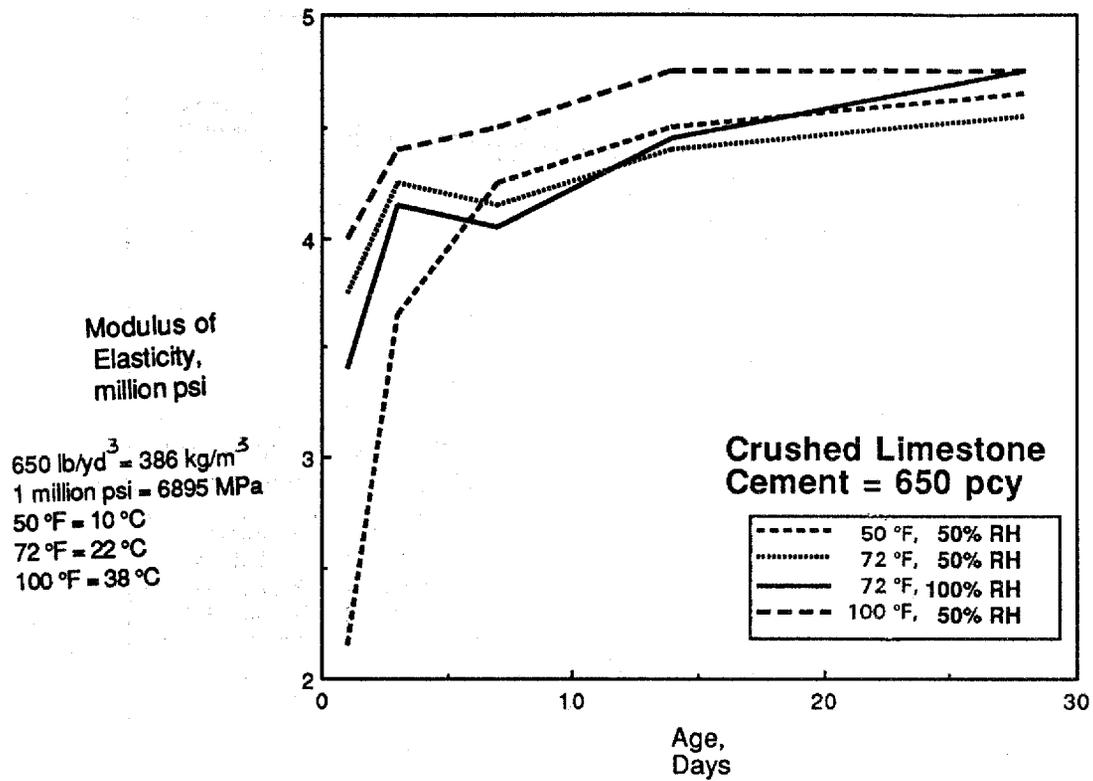
Figure 57.  Elastic modulus vs. 1 to 28 days for CS 650.
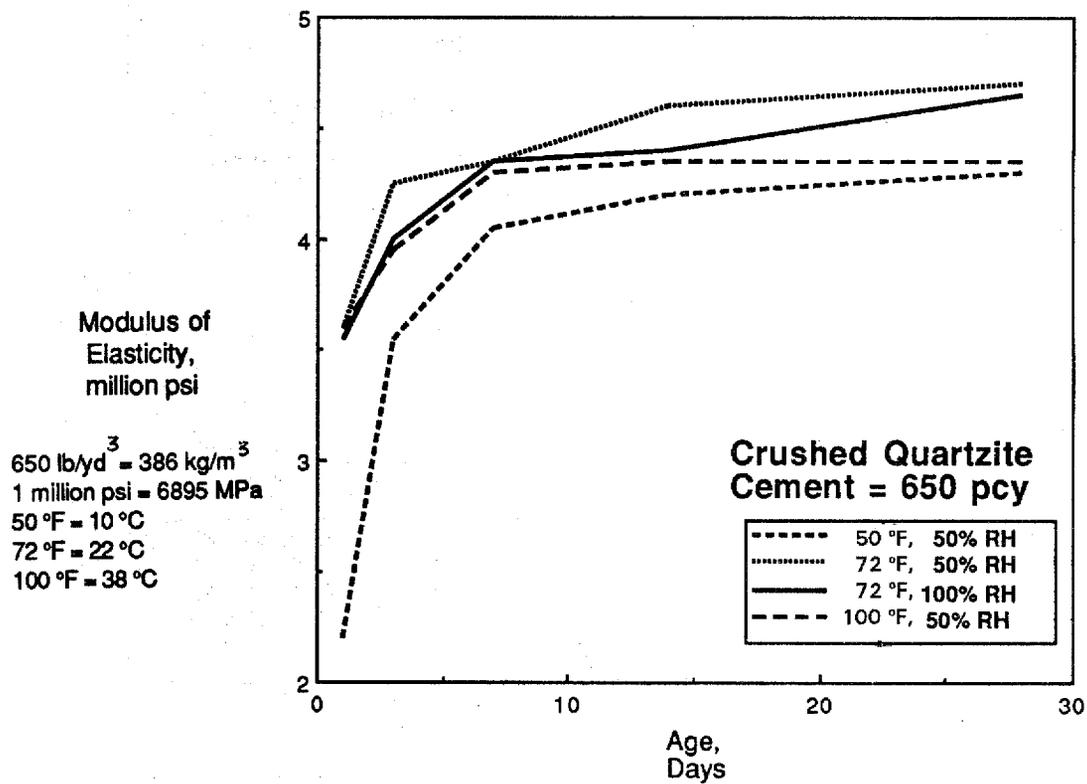


Figure 58.  Elastic modulus vs. 1 to 28 days for CH 650.

## Table 32. Increase In strength and elastic modulus as a percentage of 28-day tests.

| Test | Cement Content, lb/yd$^3$ | Curing Temp., °F | Relative Humidity, percent | Testing Age, days [†] | | | |
|------|------|------|------|------|------|------|------|
| | | | | 1 | 3 | 7 | 14 |
| Compressive Strength | 500 | 50 | 50 | 17 | 54 | 79 | 90 |
| | | 72 | 50 | 46 | 69 | 81 | 92 |
| | | 100 | 50 | 57 | 72 | 83 | 93 |
| | | 72 | 100 | 49 | 70 | 82 | 89 |
| | | | average | 42 | 66 | 81 | 91 |
| | 650 | 50 | 50 | 23 | 64 | 80 | 90 |
| | | 72 | 50 | 59 | 72 | 82 | 90 |
| | | 100 | 50 | 68 | 80 | 91 | 96 |
| | | 72 | 100 | 57 | 75 | 80 | 93 |
| | | | average | 52 | 73 | 83 | 92 |
| Modulus of Rupture | 500 | 50 | 50 | 51 | 74 | 86 | 94 |
| | | 72 | 50 | 71 | 74 | 85 | 90 |
| | | 100 | 50 | 74 | 88 | 82 | 96 |
| | | 72 | 100 | 58 | 76 | 91 | 95 |
| | | | average | 63 | 78 | 86 | 94 |
| | 650 | 50 | 50 | 57 | 90 | 91 | 107 |
| | | 72 | 50 | 89 | 90 | 93 | 92 |
| | | 100 | 50 | 96 | 91 | 95 | 100 |
| | | 72 | 100 | 61 | 81 | 94 | 101 |
| | | | average | 76 | 88 | 93 | 100 |
| Modulus of Elasticity | 500 | 50 | 50 | 39 | 76 | 87 | 94 |
| | | 72 | 50 | 69 | 89 | 93 | 97 |
| | | 100 | 50 | 73 | 88 | 90 | 98 |
| | | 72 | 100 | 68 | 85 | 90 | 94 |
| | | | average | 62 | 84 | 90 | 96 |
| | 650 | 50 | 50 | 49 | 81 | 93 | 97 |
| | | 72 | 50 | 80 | 92 | 92 | 97 |
| | | 100 | 50 | 83 | 92 | 97 | 100 |
| | | 72 | 100 | 74 | 87 | 89 | 94 |
| | | | average | 71 | 88 | 93 | 97 |

[†] NOTE: Percentages are averages of the crushed limestone and crushed quartzite.

500 lb/yd$^3$ = 297 kg/m$^3$ , 650 lb/yd$^3$ = 386 kg/m$^3$
50 °F = 10 °C, 72 °F = 22 °C, 100 °F = 38 °C

and 14 days the effects of curing temperature on strength gain (as a percentage of 28-day strength) are not as significant. At 7 days the modulus of rupture ranges from approximately 80 to 95 percent of the 28 modulus of rupture regardless of curing temperature. At 14 days the percentage ranges from 90 to 107 percent regardless of temperature. Modulus of rupture data expressed as percent of 28-day strengths are summarized in table 32.

Effects of curing temperature on modulus of elasticity were similar to compressive strength. As curing temperature increased, the modulus as well as the percentage of the 28 day value increased for ages of 1 to 3 days. At 7 and 14 days the modulus ranges from approximately 90 to 100 percent of the 28-day values regardless of curing temperature. Moduli of elasticity as a percentage of the 28-day values are summarized in table 32. As observed with compressive strength data at ages greater than 28 days (extrapolated), there is a cross-over effect of the 50 °F (10 °C) curing specimens that have initially lower moduli but have larger values than the 100 °F (38 °C) curing specimens.

Strength and Curing Condition Humidity. For compressive strength data the moist curing (100 percent RH) resulted in lower strengths compared to the 72 °F (22 °C) curing at 50 percent RH. Moist-cured compressive strengths averaged 91.7 and 97.6 percent of strengths at 50 percent RH for limestone and quartzite, respectively. For modulus of rupture data the humidity levels had the reverse effect. The moist-cured beam specimens had higher flexural strengths than those cured at 50 percent RH. The moist-cured modulus of rupture averaged 19.7 and 31.1 percent higher than the 50 percent RH specimens for limestone and quartzite, respectively. Moduli of elasticity due to humidity levels show no significant differences. Average ratios of moduli cured at 100 percent RH to those cured at 50 percent RH averaged 99.6 and 99.4 percent for limestone and quartzite, respectively. The effects of humidity at 72 °F (22 °C) on strength and modulus of elasticity had no consistent trends with curing age. Humidity level effects are summarized in table 33.

Flexural and Compressive Strength Relationships. Relationships between compressive and flexural (modulus of rupture) strengths were evaluated for the 4 individual mixes (2 aggregate types and 2 cement contents). Least squares linear regression analyses indicated that mix-specific relationships between strength types at early ages could be established. For the 4 mixes at ages of 1 through 28 days, the modulus of rupture can be predicted from relative humidity levels and square root of compressive strength. Similar relationships between flexural and square root of compressive strength were previously established for strengths at ages of 24 hours and less.

Models predicting flexural strength are summarized in table 34. Modulus of rupture equations were derived for all data (1 general equation), each aggregate type (2 aggregate-specific equations), and each mix (4 mix-specific equations). Modulus of rupture values at age of 1 day cured at 50 °F (10 °C) were considered leverage (outlier) points and not used in the mix-specific regression analysis. Variables considered in the multiple linear regression analysis of modulus of rupture included:

- Compressive strength

- Cement content - 500, 650 lb/yd$^3$ (297, 386 kg/m$^3$)

- Curing temperature - 50, 72, 100 °F (10, 22, 38 °C)

- Relative humidity - 50, 100 percent

**Table 33. Curing humidity level effects.**

| Aggregate Type | Cement Content, lb/yd$^3$ | Compressive Strength Ratio of 100% to 50% RH, percent | | | Modulus of Rupture Ratio of 100% to 50% RH, percent | | | Modulus of Elasticity Ratio of 100% to 50% RH, percent | | |
|---|---|---|---|---|---|---|---|---|---|---|
| | | minimum | maximum | average[1] | minimum | maximum | average[1] | minimum | maximum | average[1] |
| Crushed Limestone | 500 | 86.2 | 98.8 | 90.7 | 101.4 | 119.7 | 111.3 | 95.0 | 108.2 | 100.8 |
| | 650 | 83.5 | 100.0 | 92.8 | 91.2 | 145.1 | 128.1 | 90.7 | 104.4 | 98.3 |
| | average | 84.9 | 99.4 | 91.7 | 96.3 | 132.4 | 119.7 | 92.9 | 106.3 | 99.6 |
| Crushed Quartzite | 500 | 93.2 | 105.3 | 98.9 | 91.3 | 144.0 | 129.7 | 96.6 | 103.8 | 101.3 |
| | 650 | 92.5 | 99.1 | 96.4 | 101.0 | 160.3 | 132.6 | 94.1 | 100.0 | 97.5 |
| | average | 92.9 | 102.2 | 97.6 | 96.2 | 152.2 | 131.1 | 95.4 | 101.9 | 99.4 |

[1] NOTE: Average of ratios for 1, 3, 7, 14, and 28 days at curing temperature of 72 °F.

500 lb/yd$^3$ = 297 kg/m$^3$ , 650 lb/yd$^3$ = 386 kg/m$^3$ , 72 °F = 22 °C

**Table 34. Multiple linear regression analysis of early load modulus of rupture on compressive strength.**

| Type of Equation | Mix [1] | Ind. Variable, [2,3] X1 | Coef., [3] a | Ind. Variable, [2,3] X2 | Coef., [3] b | Constant [3] | R - sq., adjusted | Maximum Error, [4] percent | Average Error, [4] percent |
|---|---|---|---|---|---|---|---|---|---|
| General | All | sqrt(f'c) | 8.460 | RH | 3.311 | -155.91 | 0.770 | 36 | 8 |
| Aggregate Specific | CS | sqrt(f'c) | 7.063 | RH | 3.165 | -52.92 | 0.673 | 32 | 9 |
| | CH | sqrt(f'c) | 9.773 | RH | 3.355 | -243.52 | 0.844 | 31 | 7 |
| Mix Specific | CS5 | sqrt(f'c) | 10.160 | RH | 2.474 | -224.95 | 0.644 | 30 | 8 |
| | CS6 | sqrt(f'c) | 7.239 | RH | 4.313 | -125.25 | 0.700 | 24 | 8 |
| | CH5 | sqrt(f'c) | 9.956 | RH | 2.827 | -226.83 | 0.778 | 24 | 7 |
| | CH6 | sqrt(f'c) | 10.673 | RH | 3.910 | -335.01 | 0.771 | 29 | 6 |

NOTES:

[1] CS5 = crushed limestone with 500 lb/yd$^3$ cement, CS6 = crushed limestone with 500 lb/yd$^3$ cement
CH5 = crushed quartzite with 500 lb/yd$^3$ cement, CH6 = crushed quartzite with 650 lb/yd$^3$ cement
[2] f'c = compressive strength in psi, RH = relative humidity in percentage
[3] General equation form log(MR) = aX1 + bX2 + constant
where X1, X2 = independent variables, and a, b = coefficients
[4] Statistics based on absolute values of the prediction percentage errors

1000 psi = 6.9 MPa, 500 lb/yd$^3$ = 297 kg/m$^3$, 650 lb/yd$^3$ = 386 kg/m$^3$

- Aggregate type - dummy variable

- Curing age - 1, 3, 7, 14, 28 days

- Compressive strength at 28 days

- Arrhenius concrete maturity - equivalent age, days

- Nurse-Saul concrete maturity - °F-days

Transformations of independent variables including square root, logarithmic, inverse, and exponential functions were also included. To account for the temperature strength cross-over effects where strength at later ages can be higher for lower curing temperatures than strengths cured at higher curing temperatures, a pseudo temperature variable was included. A cross-over variable of absolute value of the quantity curing temperature minus 72 °F (22 °C) was used in the regression analysis.

In addition to relative humidity and square root of compressive strength, curing temperature was a significant variable in the general equation. Including curing temperature only slightly improved modulus of rupture predictions. Coefficient of determination, R-squared, increased from 0.770 to 0.780 when the independent variable temperature is included. Similar to the general equation, the aggregate-specific crushed limestone equation could be improved by including an independent variable with curing temperature. The coefficient of determination increased from 0.673 to 0.726 when the exponential (base 10) of curing temperature divided by 100 was included. The mix-specific prediction equation for limestone at a cement content of 500 lb/yd$^3$ (297 kg/m$^3$), could be improved with the addition of the pseudo temperature variable and logarithmic form (base 10) of age. Coefficients of determination increased from 0.644 to 0.855 with the addition of the two variables. For all other equations listed in table 34 no other variables were statistically significant in improving prediction of modulus of rupture from compressive strength (square root) and relative humidity.

In addition to mix-specific models, curing-specific models for each mix at curing temperatures of 50, 72, and 100 °F (10, 22, and 38 °C) and relative humidity (50 and 100 percent RH) were generated. These modulus of rupture models represent the ideal condition of a mix-specific model cured in a constant temperature and humidity environment. The resulting prediction error percentages (predicted minus measured modulus of rupture) give an indication of minimum expected levels of errors. Minimum error levels under laboratory conditions reflect low levels of variability in mixing, fabricating, handling, curing, and testing of specimens. Prediction percentage errors of curing-specific models therefore mainly represent material variability (reflected in test variability) which can be expected. Although constant curing-specific conditions are unrealistic at highway construction projects, the prediction errors were useful when evaluating the general equation, aggregate-specific, and mix-specific equations. Curing-specific models developed for each mix at each temperature-humidity combination are summarized in table 17 of appendix B.

Average prediction error percentages in table 34 indicate that there is on average no difference between equation types (general, aggregate-specific, mix-specific). Plots of data indicate that the general and aggregate-specific models are similar in prediction of

modulus of rupture. Plots of the general model and mix-specific models show that at 50 percent RH there is very little difference in predicted modulus of rupture. Larger differences do exist at 100 percent RH predictions between the two models. For the 2 mixes at the 500-lb/yd$^3$ (297-kg/m$^3$) cement content the general equation predicted on average a 40 psi (276 kPa) higher modulus of rupture than the mix-specific prediction model. For the 650-lb/yd$^3$ (386-kg/m$^3$) cement content mixes the general model predicted on average a 40 psi (276 kPa) lower modulus of rupture than the mix-specific model. Modulus of rupture and compressive strength plots are shown in figures 59 through 62.

Prediction error percentages (predicted minus actual) for modulus of rupture estimated from the general equation, aggregate-specific, mix-specific, and curing-specific equations are listed in table 18 of appendix B. Averages of the absolute values of the prediction percentage errors were 5.5, 6.1, 6.4, and 2.1 percent for the general, aggregate-specific, mix-specific, and curing condition-specific models, respectively.

Based on the sensitivity of the model type on prediction of moist-cured modulus of rupture, as shown in figures 59 through 62, and on the averages of absolute values of prediction error percentages, the use of the general model for predicting modulus of rupture independent of mixes (aggregate type and cement content) is not recommended. Mix-specific prediction models listed in table 34 should be used instead of the general or aggregate-specific models. For the 4 recommended mix-specific modulus of rupture prediction models, the 90 percent and 95 percent confidence intervals were computed for compressive strengths of 2000, 3000, 4000, and 5000 psi (13.8, 20.7, 27.6, and 34.5 MPa). The predicted modulus of rupture ranges from 338 to 811 psi (2.3 to 5.6 MPa) over the compressive strength range of 2000 to 5000 psi (13.8 to 34.5 MPa). Confidence intervals listed in table 35 are for the conditional expectation of the modulus of rupture. The confidence intervals approximately range from plus or minus 30 to 90 psi (207 to 621 kPa) at the 5 percent level of significance and from plus or minus 20 to 70 psi (138 to 483 kPa) at the 10 percent level of significance.

Modulus of Elasticity and Compressive Strength Relationship. Relationships between 1 to 28 day compressive strength and modulus of elasticity were next established. Similar to data at 4 to 24 hours, the modulus of elasticity can be predicted from the square root of compressive strength. Prediction equations generated for each mix (combining all temperatures and curing humidities) and for the combined data are summarized in table 36. The Y-intercept (constant term) was not statistically significant for any of the prediction equations. For the 4 mixes the coefficients for the square root of compressive strength ranged from approximately 61,000 to 63,000. For a cement content of 500 lb/yd$^3$ (297 kg/m$^3$) the coefficient is approximately 63,000 and for cement content of 650 lb/yd$^3$ (386 kg/m$^3$) the coefficient is approximately 61,000. A general prediction equation independent of aggregate type and cement content fits the data as well as the mix-specific models with no significant difference in constant or coefficient of determination. The coefficient term of 62,000 is close to the coefficient term of 61,000 determined from the 4 to 24 hour data.

Average prediction error using the general mix-independent equation ranged from 2.0 to 4.3 percent for the 4 mixes. The mix-specific prediction of elastic modulus errors ranged 1.8 to 4.0 percent for the 4 mixes. Overall the absolute difference between the general and mix-specific equation percent errors averaged 1.3 percent. This indicates that the loss in predictability using the general equation instead of the mix-specific equations is minimal. For the early load lab data the modulus of elasticity independent of aggregate and
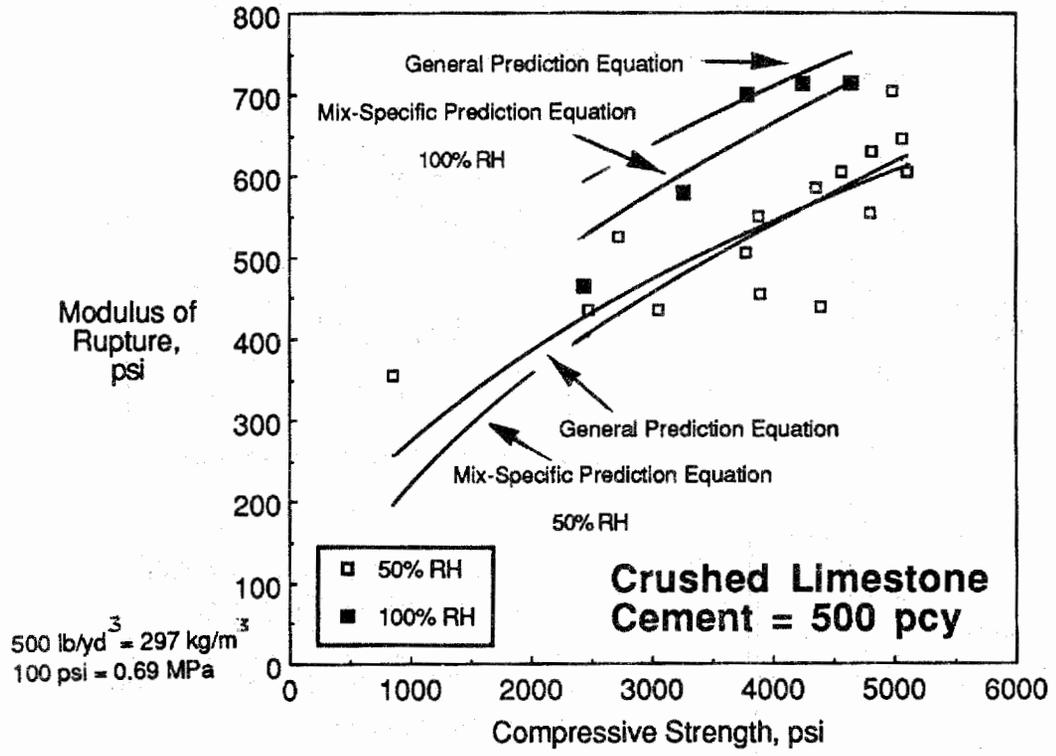
Figure 59. Compressive vs. flexural early load strength for CS 500.
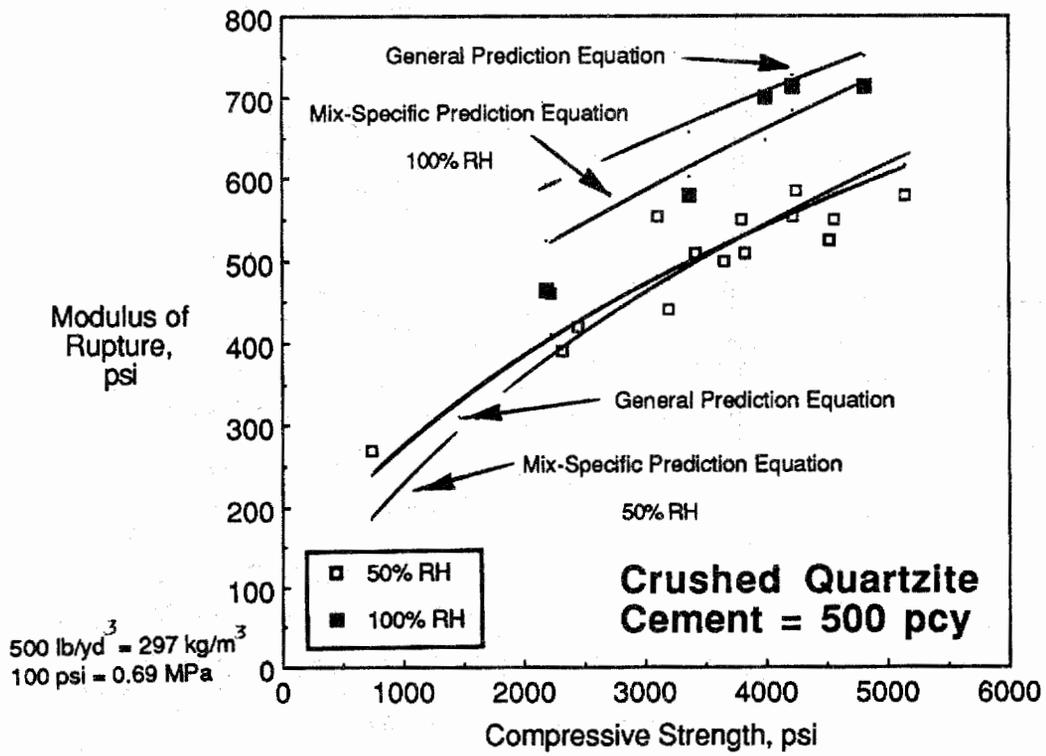


Figure 60. Compressive vs. flexural early load strength for CH 500.
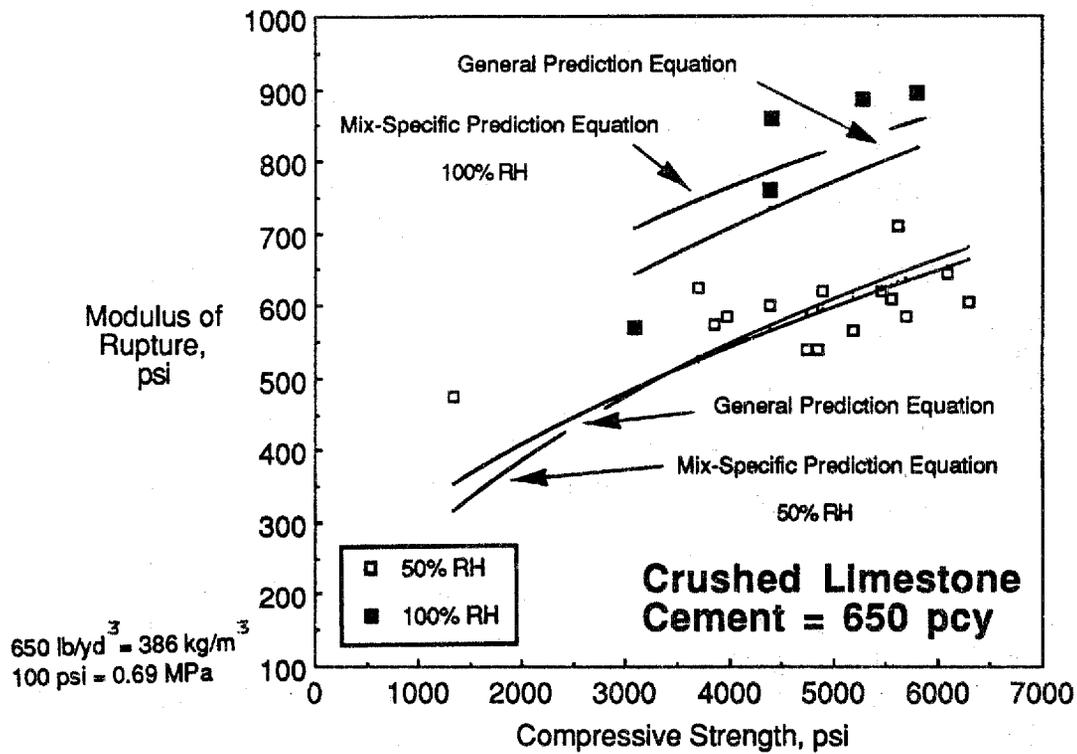
Figure 61. Compressive vs. flexural early load strength for CS 650.
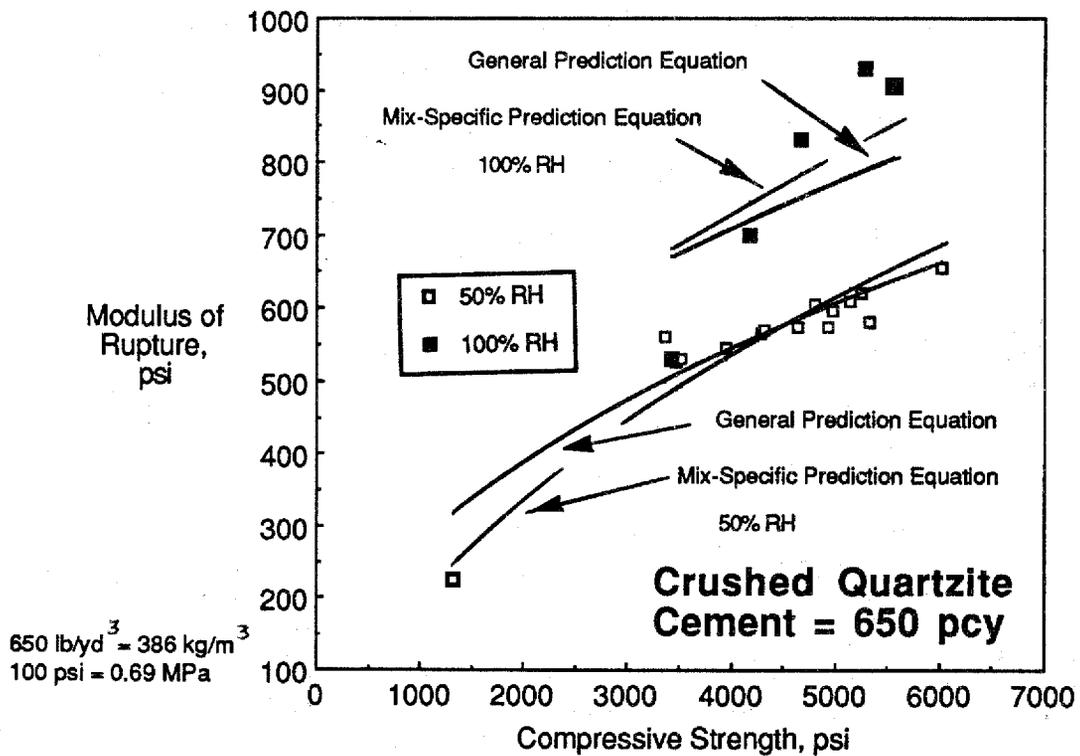


Figure 62. Compressive vs. flexural early load strength for CH 650.

**Table 35. Confidence intervals for prediction of early load (1 to 28 days) modulus of rupture from compressive strength.**

| Mix | Compressive Strength, psi | 50% Curing Humidity | | | 100% Curing Humidity | | |
| | | Modulus of Rupture, [1] psi | Confidence Interval [2] 95% +/- psi | 90% +/- psi | Modulus of Rupture, [1] psi | Confidence Interval [2] 95% +/- psi | 90% +/- psi |
|---|---|---|---|---|---|---|---|
| Limestone 500 lb/yd³ Cement | 2000 | 353 | 86 | 71 | 477 | 85 | 70 |
| | 3000 | 455 | 50 | 41 | 579 | 60 | 49 |
| | 4000 | 541 | 33 | 27 | 665 | 57 | 47 |
| | 5000 | 617 | 43 | 36 | 741 | 70 | 58 |
| Limestone 650 lb/yd³ Cement | 2000 | 414 | 134 | 110 | 630 | 128 | 105 |
| | 3000 | 487 | 87 | 71 | 702 | 86 | 71 |
| | 4000 | 548 | 51 | 42 | 764 | 62 | 51 |
| | 5000 | 602 | 35 | 29 | 818 | 61 | 50 |
| Quartzite 500 lb/yd³ Cement | 2000 | 360 | 60 | 50 | 501 | 74 | 61 |
| | 3000 | 460 | 35 | 29 | 601 | 54 | 45 |
| | 4000 | 544 | 32 | 27 | 686 | 51 | 42 |
| | 5000 | 619 | 48 | 40 | 760 | 62 | 51 |
| Quartzite 650 lb/yd³ Cement | 2000 | 338 | 117 | 97 | 533 | 127 | 105 |
| | 3000 | 445 | 71 | 58 | 641 | 85 | 70 |
| | 4000 | 536 | 39 | 32 | 731 | 60 | 49 |
| | 5000 | 615 | 37 | 31 | 811 | 57 | 47 |

NOTES: [1] Predicition equations listed in table 34.

[2] Confidence interval for conditional expectation of modulus of rupture.

1000 psi = 6.9 MPa, 500 lb/yd³ = 297 kg/m³ , 650 lb/yd³ = 386 kg/m³

**Table 36. Early load (1 to 28 days) modulus of elasticity and compressive strength prediction equations.**

| Aggregate | Cement Content, lb/yd$^3$ | Constant[1] | Coefficient of Determination |
|---|---|---|---|
| Crushed Limestone | 500 | 63,289 | 0.947 |
| | 650 | 61,268 | 0.948 |
| Crushed Quartzite | 500 | 63,130 | 0.943 |
| | 650 | 61,696 | 0.973 |
| General Equation | | 62,249 | 0.948 |

[1] NOTE:   Equation form:  $E = \text{constant} * \text{sqrt}(f'c)$
where $E$ = modulus of elasticity in psi
$f'c$ = compressive strength in psi

500 lb/yd$^3$ = 297 kg/m$^3$
650 lb/yd$^3$ = 386 kg/m$^3$
1000 psi = 6.9 MPa

cement content can be predicted from compressive strength (square root function) using the constant coefficient of 62,000. The general modulus of elasticity prediction equation and early load data are shown in figure 63.

As previously discussed for the 4 to 24 hour data the coefficients were derived from the database generated in this study. A mix-specific relationship should be generated for specific projects for maximum prediction reliability since the coefficient may be dependent on cement source.

Maturity Datum Temperature and Activation Energy. Concrete maturity at 1, 3, 7, 14, and 28 days was calculated from cylinder concrete temperatures. Cylinder concrete temperatures were recorded every half hour until the cylinder reached the isothermal curing condition temperature. As discussed previously for the early age data (4 to 24 hours), ASTM C 1074 describes two methods to calculate maturity. The time-temperature function, commonly referred to as the Nurse-Saul maturity, equation 8, requires that a datum temperature be established for a concrete mix. The datum temperature is the temperature below which no chemical hydration reactions are occurring to increase concrete strength. The second maturity method is an equivalent age (at a specified temperature) function, equation 9, which requires that the activation energy be established for a concrete mix. Suggested values commonly reported in the literature were used in the analysis of early age (4 to 24 hours) data. It is recommended in ASTM C 1074 that for maximum accuracy, the datum temperature and activation energy be experimentally determined. Since the early loading data covered a much larger range in time than the early age data (4 to 24 hours), the activation energy and datum temperatures were estimated from concrete compressive strength data. The datum temperature and activation energy can be experimentally determined from either cement paste, mortars, or concrete test data. For the early loading (1- to 28-day) data the activation energy and datum temperature were determined from cylinder compressive strength data using procedures outlined in reference 25.

The activation energy and datum temperatures were estimated using 2 data sets. The first data set consisted of early age compressive strength combined with early load data at 1 and 3 days. The second set did not include the 3 day early load data. Results of the activation energy and datum temperature analysis are summarized in table 19 of appendix B. The 2 data sets give different values of activation energy and datum temperatures. Differences can be attributed to lack of cylinder temperature control. If tests are done on paste or mortar specimens the curing temperatures are regulated by a controlled water bath. For concrete cylinder specimens temperature control was not as precise. The outer edges of the cylinder had temperatures close to curing room temperatures but the cylinder interior was warmer due to heat of hydration. Activation energy and datum temperatures are easier and more precisely determined using mortar specimen and a controlled water bath. Activation energy (average of 2 trials) ranged from 34.6 to 41.9 kJ/mol for the 4 mixes. This corresponds to an activation energy divided by gas constant, 8.3144 J/(mol-°K), of 4161 to 5039 °K. Average activation energy divided by gas constant for the 4 mixes is 4680 °K. Datum temperature (average of 2 trials) ranged from 30.4 to 31.6 °F (-0.9 to -0.2 °C) and averaged 31.1 °F (-0.5 °C). Average activation energy divided by gas constant of 4680 °K and datum temperature of 31.1 °F (-0 5 °C) determined experimentally are not significantly different than the 5000 °K and 32 °F (0 °C) values assumed in the analysis of early age (4 to 24 hours) strength. To be consistent between the early age (4 to 24 hours) and early load (1- to 28-day) data the 5000 °K activation energy divided by gas constant and 32 °F (0 °C) datum temperature was maintained in the early load analysis.

114
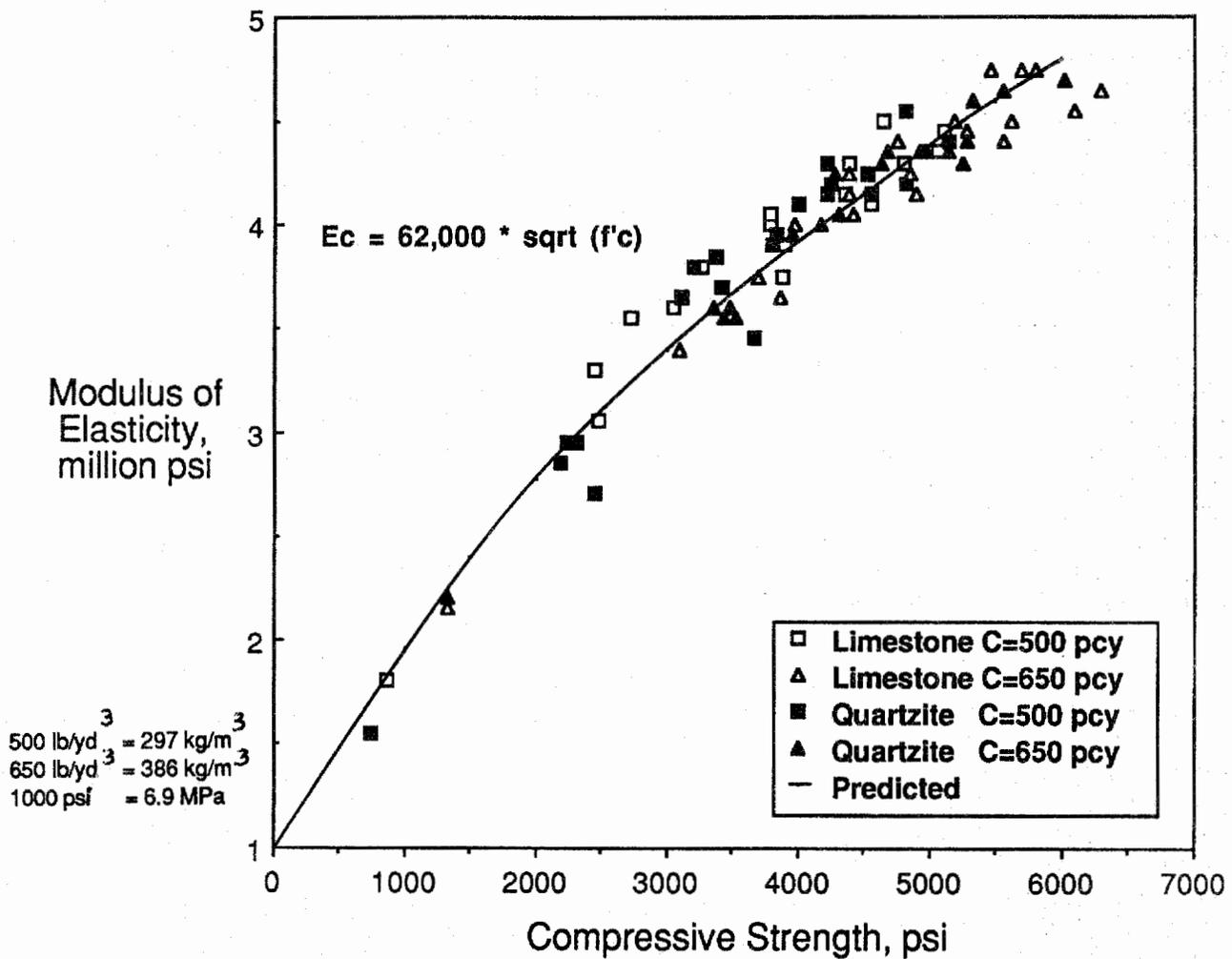
Figure 63.   Compressive strength vs. elastic modulus for early loading.

Compressive Strength Versus NDT Relationship. The concrete compressive strengths at 1 through 28 days were next correlated with nondestructive maturity and ultrasonic pulse velocity data. Compressive strengths were regressed on concrete maturity or pulse velocity using least squares linear regression techniques. The equation fitting the lab data was the hyperbolic form inverse of compressive strength versus inverse of maturity. This equation form has been used to fit other reported laboratory data.[17,32,34] Models were developed for both the Nurse-Saul time-temperature (datum 32 °F, 0 °C) and Arrhenius (equivalent age of 68 °F, 20 °C) exponential maturity function.

A multiple linear regression analysis of early loading (1 to 28) concrete compressive strength on maturity and pulse velocity was done to develop general, aggregate-specific, and mix-specific prediction models. Independent variables included:

- Cement content - 500, 650 lb/yd$^3$ (297, 386 kg/m$^3$)

- Curing temperature - 50, 72, 100 °F (10, 22, 38 °C)

- Pseudo temperature (absolute value of the quantity curing temperature minus 72 °F, 22 °C)

- Relative humidity - 50, 100 percent

- Aggregate type - dummy variable

- Curing age - 1, 3, 7, 14, 28 days

- Compressive strength at 28 days (moist cure)

- Arrhenius concrete maturity - equivalent age, days

- Nurse-Saul concrete maturity - °F-days

- Pulse velocity (1000 ft/s)

- Ratio of strength to 28-day strength (same curing condition)

Transformations for variables including square root, logarithmic, exponential, and inverse functions were also included. For the maturity models the compressive strength (1000 times the inverse) can be predicted as a function of the inverse of maturity (Nurse-Saul or Arrhenius). The relative strength gain, strength divided by limiting strength (maximum), can be predicted also as a function of inverse of maturity. The strength ratio model has been also reported in other studies.[25] The 28-day strength in the evaluation of early loading data was assumed to be the limiting strength.

Both general and mix-specific models were generated to predict compressive strength as a function of maturity. Strengths at 1 day cured at 50 °F (10 °C) were relatively smaller than other strengths. They were considered outlier points and were not used in the analysis. The general models also had a statistically significant variable cement content. Results of the maturity analysis are summarized in tables 37 and 38 for prediction of compressive strength (1000 times the inverse) and compressive strength ratio (inverse of the ratio of compressive strength to strength at 28 days at same curing conditions). As summarized in table 37 based on coefficients of determination mix-specific models (as a

**Table 37. Regression of early loading (1 to 28 days) compressive strength on maturity.**

| Mix | Cement Content, lb/yd$^3$ | $1000 / f'c = (coef.\ 1) / MAT + (coef.\ 2) * CEMENT$ [1] | | | | | | | |
| --- | --- | --- | --- | --- | --- | --- | --- | --- | --- |
| | | 1/AR coef. 1 | CEMENT coef. 2 | const. | R-sq. adj. | 1/NS coef. 1 | CEMENT coef. 2 | const. | R-sq. adj. |
| General | General | 0.2789 | -0.0004 | 0.4149 | 0.834 | 8.8263 | -0.0004 | 0.4182 | 0.853 |
| | | 0.2825 | **** | 0.1933 | 0.656 | 8.8947 | **** | 0.1925 | 0.667 |
| Crushed Limestone | 500 | 0.3264 | **** | 0.1997 | 0.920 | 10.3229 | **** | 0.1990 | 0.934 |
| | 650 | 0.2044 | **** | 0.1744 | 0.833 | 6.4423 | **** | 0.1734 | 0.858 |
| Crushed Quartzite | 500 | 0.3730 | **** | 0.2180 | 0.903 | 12.1370 | **** | 0.2150 | 0.948 |
| | 650 | 0.1910 | **** | 0.1890 | 0.792 | 6.0620 | **** | 0.1880 | 0.864 |

[1] NOTE:   f'c = compressive strength in psi

MAT = Arrhenius (AR in equivalent days) or Nurse-Saul (NS in °F-days) maturity

CEMENT = cement content in lb/yd$^3$

Data at T = 50 °F and t = 1 day not used in regression analysis.

500 lb/yd$^3$ = 297 kg/m$^3$ , 650 lb/yd$^3$ = 386 kg/m$^3$ , 1000 psi = 6.9 MPa, 50 °F = 10 °C

**Table 38. Regression of early loading (1 to 28 days) compressive strength ratio on maturity.**

| Mix | Cement Content, lb/yd$^3$ | $1 / (f'c/f'c\ 28) = (coef.\ 1) / MAT + (coef.\ 2) * CEMENT$ [1] | | | | | | | |
| | | 1/AR coef. 1 | CEMENT coef. 2 | const. | R-sq. adj. | 1/NS coef. 1 | CEMENT coef. 2 | const. | R-sq. adj. |
|---|---|---|---|---|---|---|---|---|---|
| General | General | 1.4504 | -0.0005 | 1.3224 | 0.870 | 45.6436 | -0.0006 | 1.3411 | 0.884 |
| | | 1.4556 | **** | 1.0102 | 0.854 | 45.7450 | **** | 1.007 | 0.866 |
| Crushed Limestone | 500 | 1.5979 | **** | 0.9885 | 0.954 | 50.6571 | **** | 0.9842 | 0.973 |
| | 650 | 1.2770 | **** | 1.0236 | 0.922 | 39.3450 | **** | 1.0228 | 0.904 |
| Crushed Quartzite | 500 | 1.7736 | **** | 1.021 | 0.874 | 57.5829 | **** | 1.0101 | 0.910 |
| | 650 | 1.1043 | **** | 1.028 | 0.856 | 34.3637 | **** | 1.0243 | 0.899 |

[1] NOTE:  f'c = compressive strength in psi

f'c 28 = compressive strength at 28 days in psi

MAT = Arrhenius (AR in equivalent days) or Nurse-Saul (NS in °F-days) maturity

CEMENT = cement content in lb/yd$^3$

Data at T = 50 °F and t = 1 day not used in regression analysis.

500 lb/yd$^3$ = 297 kg/m$^3$ , 650 lb/yd$^3$ = 386 kg/m$^3$ , 1000 psi = 6.9 MPa, 50 °F = 10 °C

118

function of maturity only) can slightly better estimate compressive strength. The mix-specific models were generated from one fourth the data that the general prediction models were generated from. Coefficients of determination averaged 0.049 and 0.048 higher than the general two-variable (maturity and cement content) Arrhenius and Nurse-Saul models, respectively.

By including time and temperature variables in addition to the maturity variables (also a function of time and temperature) the general equation coefficients of determination increased approximately 4-1/2 and 2 percent for the Arrhenius and Nurse-Saul maturity models respectively. This indicates that less than 5 percent of the variability in compressive strength can be further explained with the addition of time and temperature variables (and transformations). Maturity under isothermal curing conditions accounts for most combined time and temperature effects on compressive strength. Based on R-squared values for aggregate-specific maturity functions there is no significant improvement over the general equations.

The mix-specific compressive strength models were generally better than the two variable general prediction models. No other mix-specific independent variables other than maturity statistically helped predict compressive strength.

As summarized in table 38 the strength ratio models (inverse of the ratio of compressive strength to compressive strength at 28 days at the same curing conditions) was better in predicting relative strength than the absolute strength models listed in table 37. Coefficients of determination for both the mix-specific and general equations averaged (for the 2 maturity types) 0.03 higher for the strength ratio models than the absolute compressive strength models. Similar to the general equation absolute compressive strength models, the coefficients of determination for strength ratio models increased less than 0.05 when time and temperature variables (and transformation) were used with the maturity independent variable.

Although the ratio of compressive strengths (strength ratio model) may be slightly better predicted from maturity, an extra unknown variable of 28-day strength under identical curing conditions must be also be estimated. The strength ratio model may statistically be a better prediction model but is less practical to pavement construction projects. The relative small loss in power of prediction is more than offset by uncertainty in estimating 28-day strengths under an assumed curing temperature and humidity.

The general and 4 mix-specific predicted compressive strengths and prediction errors are listed in tables 20 and 21 of appendix B for Arrhenius and Nurse-Saul maturity, respectively. The mix-specific models were significantly better at predicting compressive strength from maturity. Average absolute percentage errors for the Arrhenius maturity models were 9.6 and 6.2 percent for the general and mix-specific models, respectively. Similarly for the Nurse-Saul models the average absolute errors were 8.7 and 5.4 percent for the general and mix-specific models, respectively. The mix-specific prediction equations for compressive strength from Arrhenius and Nurse-Saul maturity are shown in figures 64 through 67. For the Arrhenius and Nurse-Saul maturity plots compressive strength becomes insensitive to changes in maturity (flat slope) at strengths greater than approximately 3500 and 4500 psi (24.1 and 31.0 MPa) for the 500- and 650-lb/yd$^3$ (297- and 386-kg/m$^3$) cement contents, respectively.
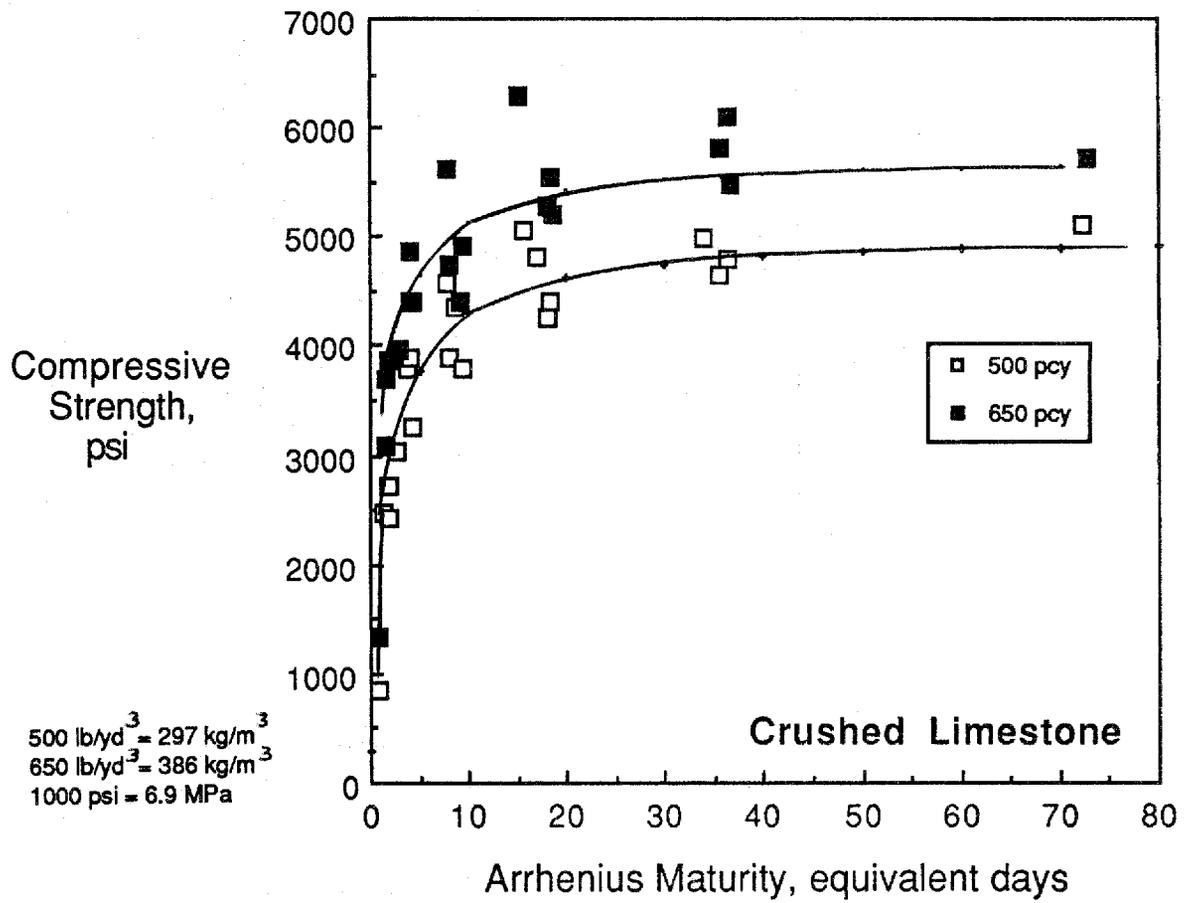
Figure 64. Arrhenius maturity vs. early load compressive strength for CS.
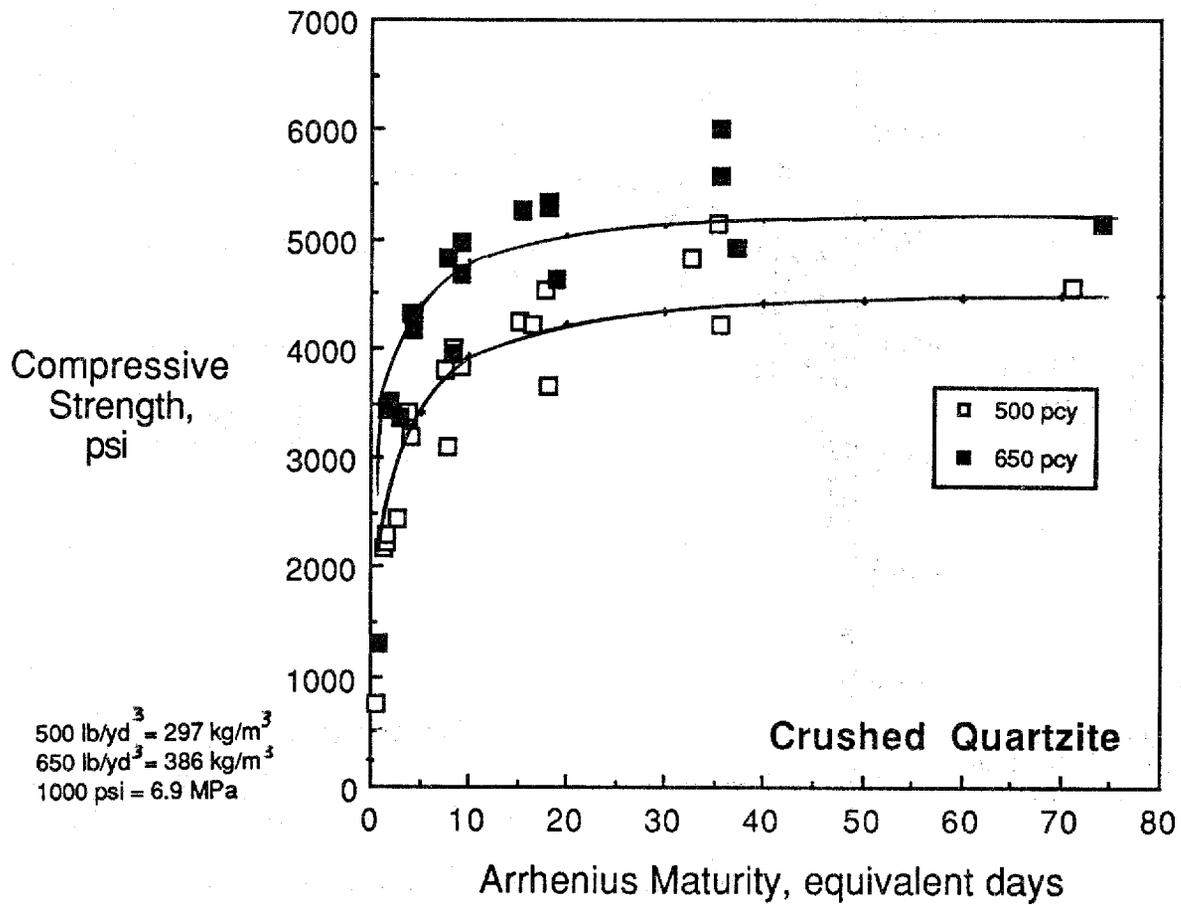
Figure 65. Arrhenius maturity vs. early load compressive strength for CH.
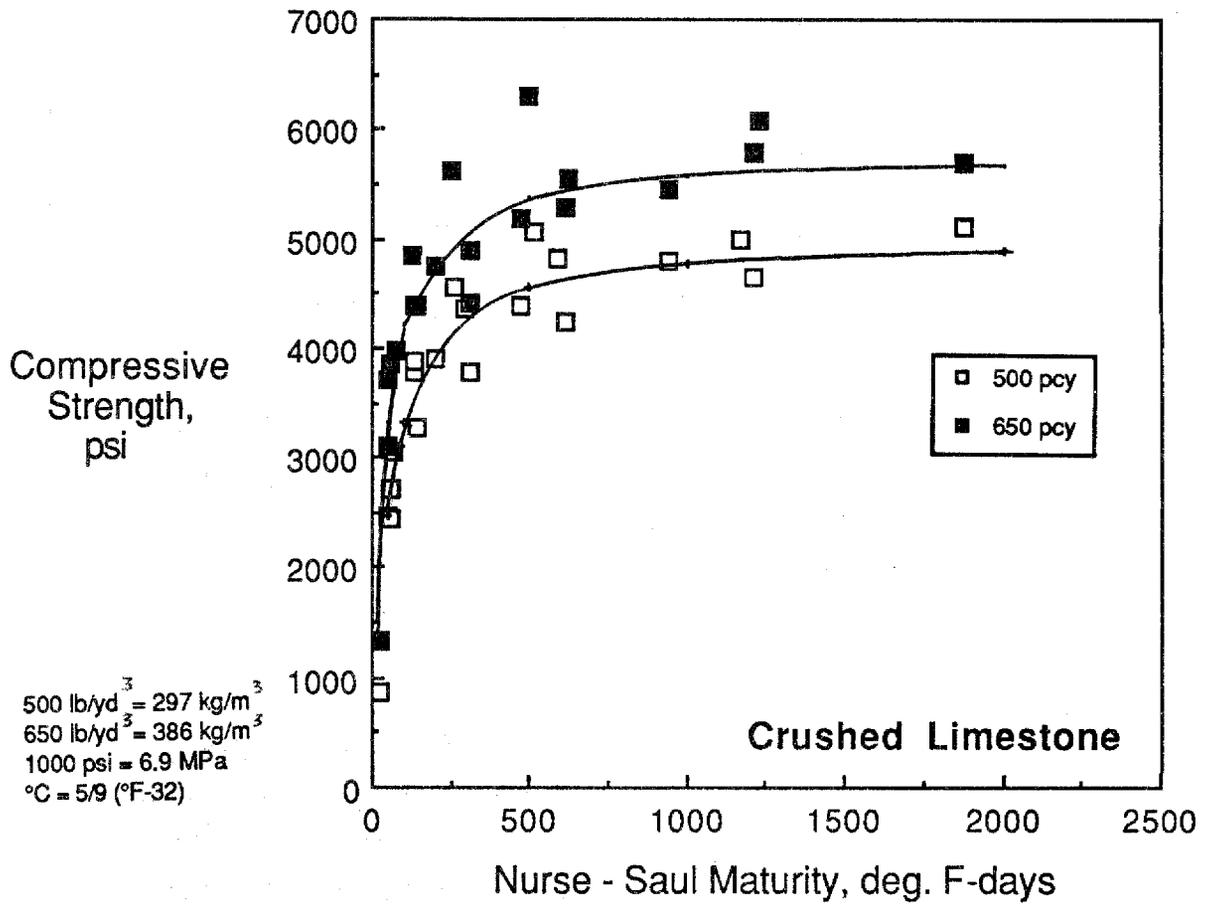
Figure 66.   Nurse-Saul maturity vs. early load compressive strength for CS.
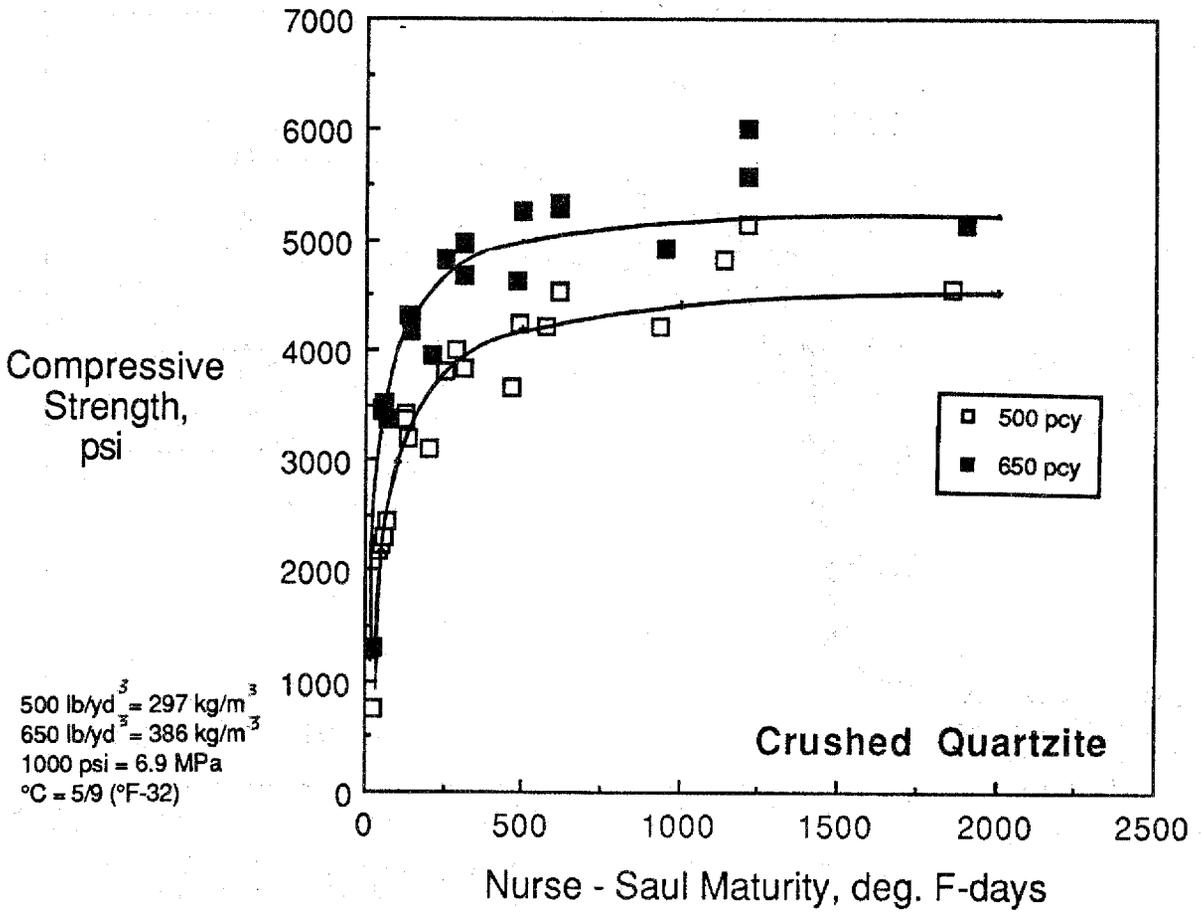
Figure 67. Nurse-Saul maturity vs. early load compressive strength for CH.

Prediction models for compressive strength as a function of nondestructive pulse velocity data were also generated using multiple linear regression techniques. Similar to the early age (4 to 24 hours) pulse velocity analysis, the log of compressive strength can be predicted from pulse velocity (1000 ft/s). Compressive strength data at a curing temperature of 50 °F (10 °C) at 1 day were relatively lower than other early load (1 to 28-day) strengths. These low strength outlier data were not used in the model generation. Similar to the maturity analysis, 2 types of models were generated. The general model considered all compressive strength data from all 4 mixes (2 aggregates and 2 cement contents). The second type of model was mix-specific for the 4 mixes. The mix-specific models predicted compressive strength (log base 10) from pulse velocity (1000 ft/s), curing age (log base 10), and relative humidity (percent). The general equation contained one more significant variable, cement content, in predicting compressive strength. The pulse velocity compressive strength prediction models are summarized in table 39.

For the general prediction model the pulse velocity, age, and cement independent variables are significant in predicting compressive strength. With the addition of relative humidity as a variable the coefficient of determination, R-squared, increases slightly from 0.906 to 0.912. The elimination of any other independent variables significantly reduces R-squared. For the mix-specific models the pulse velocity, age, and relative humidity variables generate models with a relatively high R-squared ranging from 0.944 to 0.967. When the relative humidity variable is eliminated the coefficients of determination slightly decrease ranging from 0.844 to 0.963. With only pulse velocity and relative humidity variables the R-squared values decrease ranging from 0.824 to 0.934. When only pulse velocity is considered the coefficients of determination significantly decrease ranging from 0.669 to 0.906. Largest decreases occurred for the crushed limestone with the progressive elimination of independent variables.

Since relative humidity is difficult to estimate in new concrete construction, is difficult to maintain under lab conditions (to get a correlation), and does not significantly increase the R-squared values, the pulse velocity, age, and cement (general equation only) prediction equations were selected as the optimal models.

The general and 4 mix-specific predicted strengths are listed in table 22 of appendix B. The difference in percent errors between the mix-specific and general equation models is much less than the general and mix-specific maturity models. Average values of absolute percentage errors were slightly less for the mix-specific models than the general equation model. For the 4 individual mix-specific models differences in average absolute percentage errors ranged from 0 to 3 percent less than the general model. Average absolute percentage errors for all 4 mixes were 7 percent for the general equation and 5 percent for the mix-specific models.

The small difference in pulse velocity prediction error percentages could be expected based on the analysis of compressive strength-modulus of elasticity analysis. The analysis showed that compressive strength (square root) could be used to estimate the modulus of elasticity regardless of cement content or aggregate type used in the lab study. Since pulse velocity can mathematically be related to the modulus of elasticity, equation 10, which is empirically related to compressive strength (independent of mix), then pulse velocity-compressive strength relationships may also be mix independent. Since modulus of rupture may need to be predicted from pulse velocity-estimated compressive strength, the relatively smaller minimum error mix-specific model (function of age and pulse velocity) was selected over the general model. The pulse velocity mix-specific prediction model errors are summarized in figure 68.

**Table 39. Regression of early loading (1 to 28 days) compressive strength on pulse velocity.**

| MIX | Cement Content, lb/yd$^3$ | Independent Variable[1] | | | | | R-sq. adj. |
| | | PV / 1000 ft/s | log (AGE) days | RH percent | CEMENT | Constant | |
|---|---|---|---|---|---|---|---|
| General | General | 0.0663 | 0.1251 | -0.0004 | 0.0006 | 2.2634 | 0.912 |
| | | 0.0622 | 0.1292 | **** | 0.0006 | 2.2886 | 0.906 |
| | | 0.0938 | 0.1038 | -0.0005 | **** | 2.2104 | 0.766 |
| | | 0.1388 | **** | **** | 0.0004 | 1.3555 | 0.715 |
| | | 0.1538 | **** | -0.0008 | **** | 1.4454 | 0.644 |
| | | 0.1509 | **** | **** | **** | 1.4386 | 0.624 |
| Crushed Limestone | 500 | 0.1304 | 0.093 | -0.0015 | **** | 1.6966 | 0.958 |
| | | 0.0766 | 0.1355 | **** | **** | 2.3578 | 0.867 |
| | | 0.2188 | **** | -0.0019 | **** | 0.5072 | 0.894 |
| | | 0.1978 | **** | **** | **** | 0.6916 | 0.718 |
| | 650 | 0.0864 | 0.0981 | -0.0011 | **** | 2.3762 | 0.944 |
| | | 0.0514 | 0.1208 | **** | **** | 2.812 | 0.844 |
| | | 0.1897 | **** | -0.0014 | **** | 0.9321 | 0.844 |
| | | 0.1745 | **** | **** | **** | 1.0709 | 0.669 |
| Crushed Quartzite | 500 | 0.1447 | 0.0878 | -0.0004 | **** | 1.475 | 0.967 |
| | | 0.1268 | 0.1047 | **** | **** | 1.6847 | 0.963 |
| | | 0.2211 | **** | -0.0009 | **** | 0.5064 | 0.934 |
| | | 0.2125 | **** | **** | **** | 0.5699 | 0.906 |
| | 650 | 0.1001 | 0.086 | 0.0002 | **** | 2.1405 | 0.957 |
| | | 0.1023 | 0.0843 | **** | **** | 2.1219 | 0.956 |
| | | 0.2014 | **** | 4.87E-05 | **** | 0.7691 | 0.856 |
| | | 0.2015 | **** | **** | **** | 0.7714 | 0.864 |

[1] NOTE: Prediction equation form: log(f'c) = aX1 + bX2 + .... + constant
where X1, X2 .... = independent variables, and a,b .... = coefficients
f'c = compressive strength in psi
AGE = curing age in days
RH = curing relative humidity in percent
CEMENT = cement content in lb/yd$^3$

500 lb/yd$^3$ = 297 kg/m$^3$ , 650 lb/yd$^3$ = 386 kg/m$^3$ , 1000 psi = 6.9 MPa, 1000 ft/s = 305 m/s

125
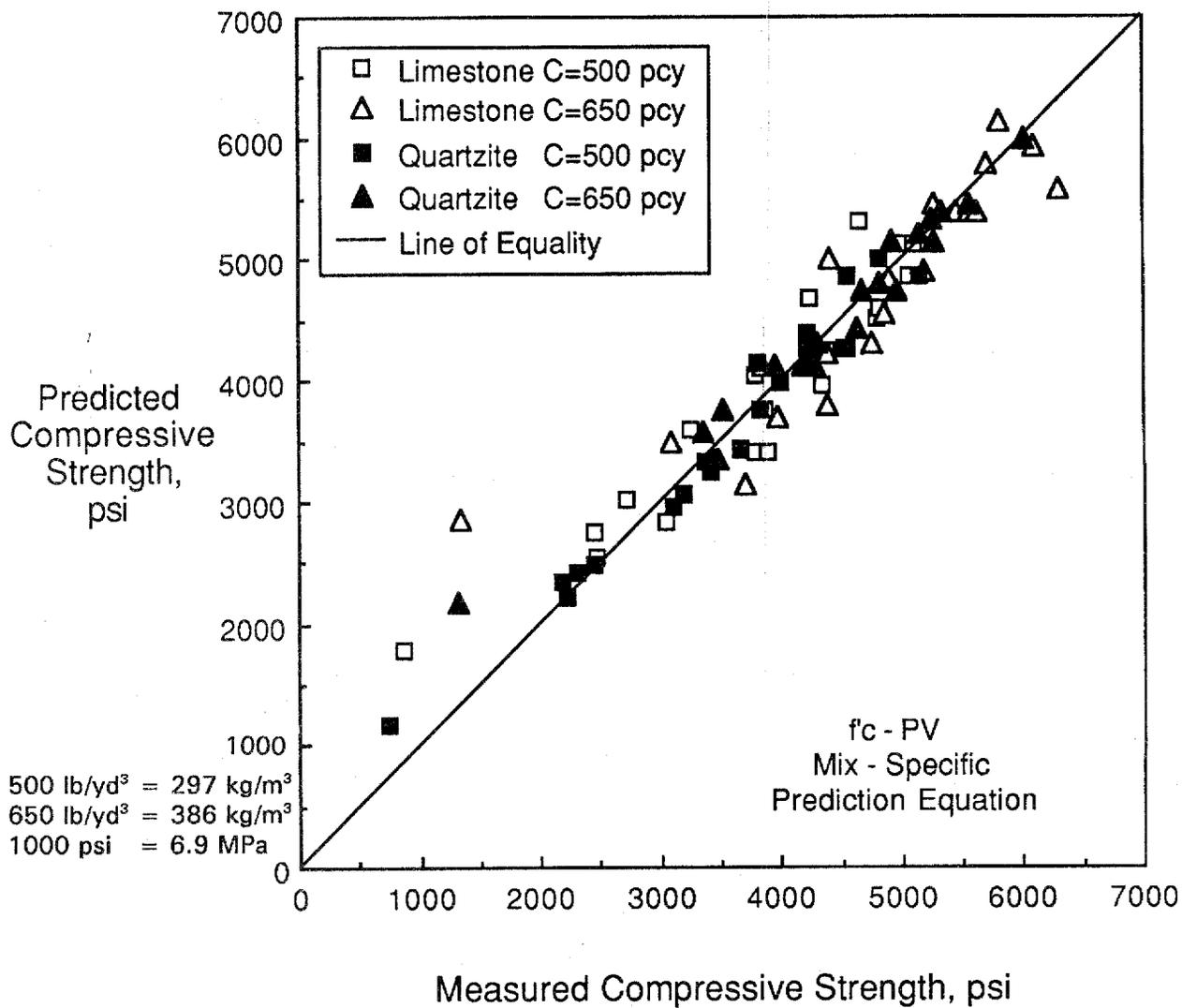
Figure 68. Mix-specific compressive strength prediction errors.

The general prediction equation in table 39, independent of aggregate and cement content, fit the database well relative to the mix-specific models. Theoretically pulse velocity is dependent only on modulus of elasticity (independent of mix). However, for maximum prediction reliability, mix-specific relationships should be developed.

Flexural Strength Versus NDT Relationships. Modulus of rupture was next regressed on nondestructive testing pulse velocity and concrete maturity. Variables considered in the mix-specific model development were the same as those used in the compressive strength prediction models. The modulus of rupture prediction variables for maturity models include relative humidity (percent) and inverse of maturity. For pulse velocity models, modulus of rupture can be predicted from relative humidity and pulse velocity. Prediction models are summarized in table 40. Modulus of rupture values at 50 °F (10 °C) at 1 day were relatively lower and not used in the multiple regression analysis.

For the Arrhenius maturity models coefficients of determination ranged from 0.489 and 0.799 and for the Nurse-Saul models ranged from 0.555 to 0.793. The pulse velocity mix-specific models ranged from 0.451 to 0.752 in calculated coefficients of determination. The quartzite concrete mix models had higher calculated coefficients of determination for both maturity types and pulse velocity models. Average prediction errors (absolute values) were 51, 48, and 50 psi (350, 330, and 350 kPa) for the Arrhenius, Nurse-Saul, and pulse velocity models, respectively. This corresponds to an average of 10, 9, and 10 percent for the Arrhenius, Nurse-Saul, and pulse velocity models, respectively. Modulus of rupture prediction errors for the Arrhenius maturity, Nurse-Saul maturity, and pulse velocity models are shown in figures 69 through 71.

The 95 and 90 percent confidence intervals for the conditional expectation of the predicted modulus of rupture are summarized in table 41. The confidence intervals listed in table 41 for moduli of rupture between 450 and 650 psi (3.1 and 4.5 MPa) ranged from approximately plus or minus 30 to 200 psi (207 to 1380 kPa) for the three nondestructive test methods. Overall average confidence intervals were approximately plus or minus 70 and 80 psi (480 and 550 kPa) for the 10 and 5 percent levels of significance, respectively. The confidence intervals for prediction of modulus of rupture from compressive strength, summarized in table 35 are similar in magnitude to the confidence intervals for prediction from nondestructive test data. The confidence intervals predicted over the compressive strength range of 2000 to 5000 psi (13.8 to 34.5 MPa) generally correspond to the modulus of rupture confidence interval range of 450 to 650 psi (3.1 to 4.5 MPa).

Within-Test Variability. The within-test coefficients of variation (standard deviation divided by average) for each group of tests was calculated for each mix at each curing temperature. The standard deviation was estimated using the range in strength for each sample. The range was calculated for the 3 compressive, 3 moduli of elasticity, and 2 modulus of rupture specimens at each curing temperature. As discussed in the analysis of within-test variability of 1 to 24 hour strength tests, the reported standard deviations reflect additional uncertainty due to ranges computed from a single set of test specimens rather than the desirable average of 10 batches (minimum).

Coefficients of variation for compressive strength, modulus of elasticity and flexural strengths were generally less than 8, 7, and 12 percent, respectively. Similar to the early age data (4 to 24 hours) the aggregate type, cement content, and temperature did not have a consistent effect on the coefficients of variation. Average coefficients of variation for early

127

Table 40. Regression of modulus of rupture on early loading (1 to 28 days) nondestructive test data.

| Mix | Cement Content, lb/yd³ | Arrhenius Maturity [1] | | | | Nurse-Saul Maturity [1] | | | | Pulse Velocity [1] | | | |
|---|---|---|---|---|---|---|---|---|---|---|---|---|---|
| | | 1/AR coef., "a" | RH% coef., "b" | const. | R-sq. adj | 1/NS coef., "a" | RH% coef., "b" | const. | R-sq. adj | PV/1000 coef., "a" | RH% coef., "b" | const. | R-sq. adj |
| Limestone | 500 | -301.65 | 1.74 | 520 | 0.489 | -10163.9 | 1.73 | 525 | 0.555 | 132.63 | 1.17 | -1448 | 0.451 |
| | 650 | -208.39 | 3.96 | 442 | 0.670 | -6550.9 | 3.91 | 446 | 0.674 | 64.14 | 3.82 | -540 | 0.641 |
| Quartzite | 500 | -363.88 | 3.34 | 412 | 0.799 | -11480.4 | 3.19 | 421 | 0.793 | 143.47 | 2.26 | -1605 | 0.733 |
| | 650 | -316.28 | 4.10 | 432 | 0.752 | -9679.8 | 4.05 | 435 | 0.756 | 170.01 | 3.95 | -2051 | 0.752 |

[1] NOTE: General equation form:

$$MR = a / AR + b * RH + constant$$

$$MR = a / NS + b * RH + constant$$

$$MR = a * ( PV / 1000 ) + b * RH + constant$$

where AR = Arrhenius maturity in equivalent days at 68 °F
NS = Nurse -Saul maturity in °F - days
PV = Pulse velocity in ft/s
RH = relative humidity in percent

500 lb/yd³ = 297 kg/m³ , 650 lb/yd³ = 386 kg/m³ , 68 °F = 20 °C, 1000 ft/s = 305 m/s
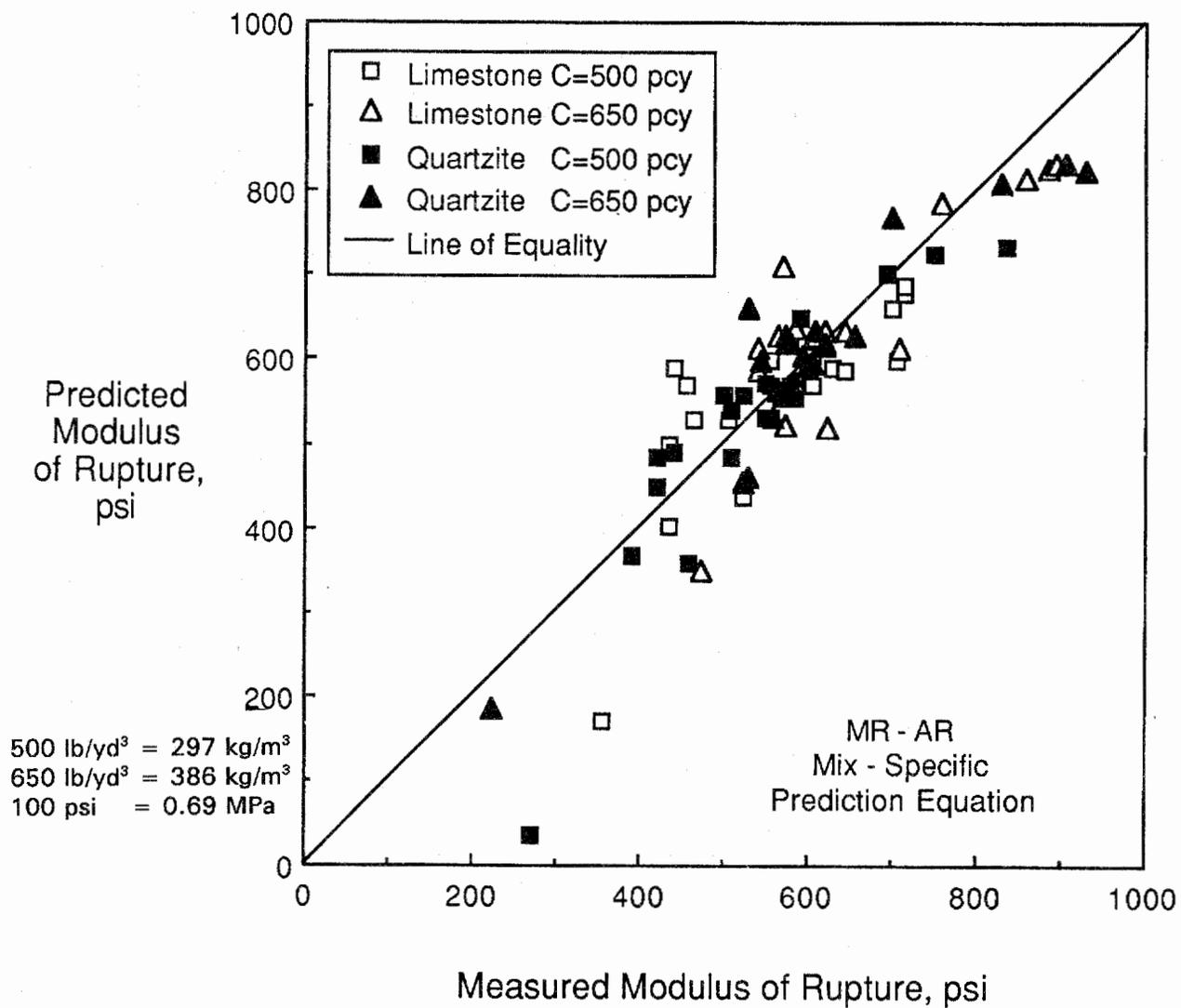
Figure 69. Mix-specific modulus of rupture - Arrhenius maturity prediction errors.
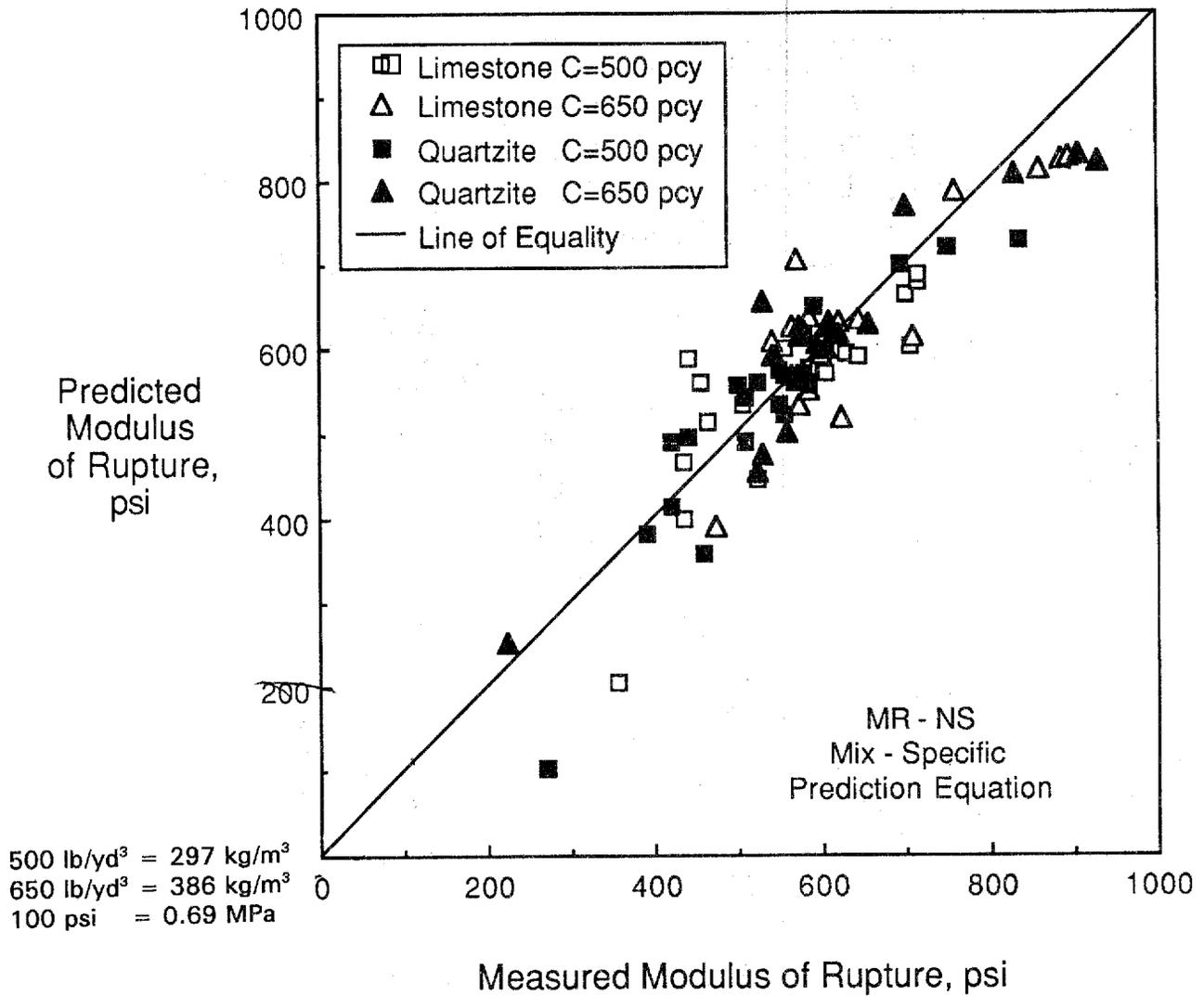
Figure 70.  Mix-specific modulus of rupture – Nurse-Saul
maturity prediction errors.
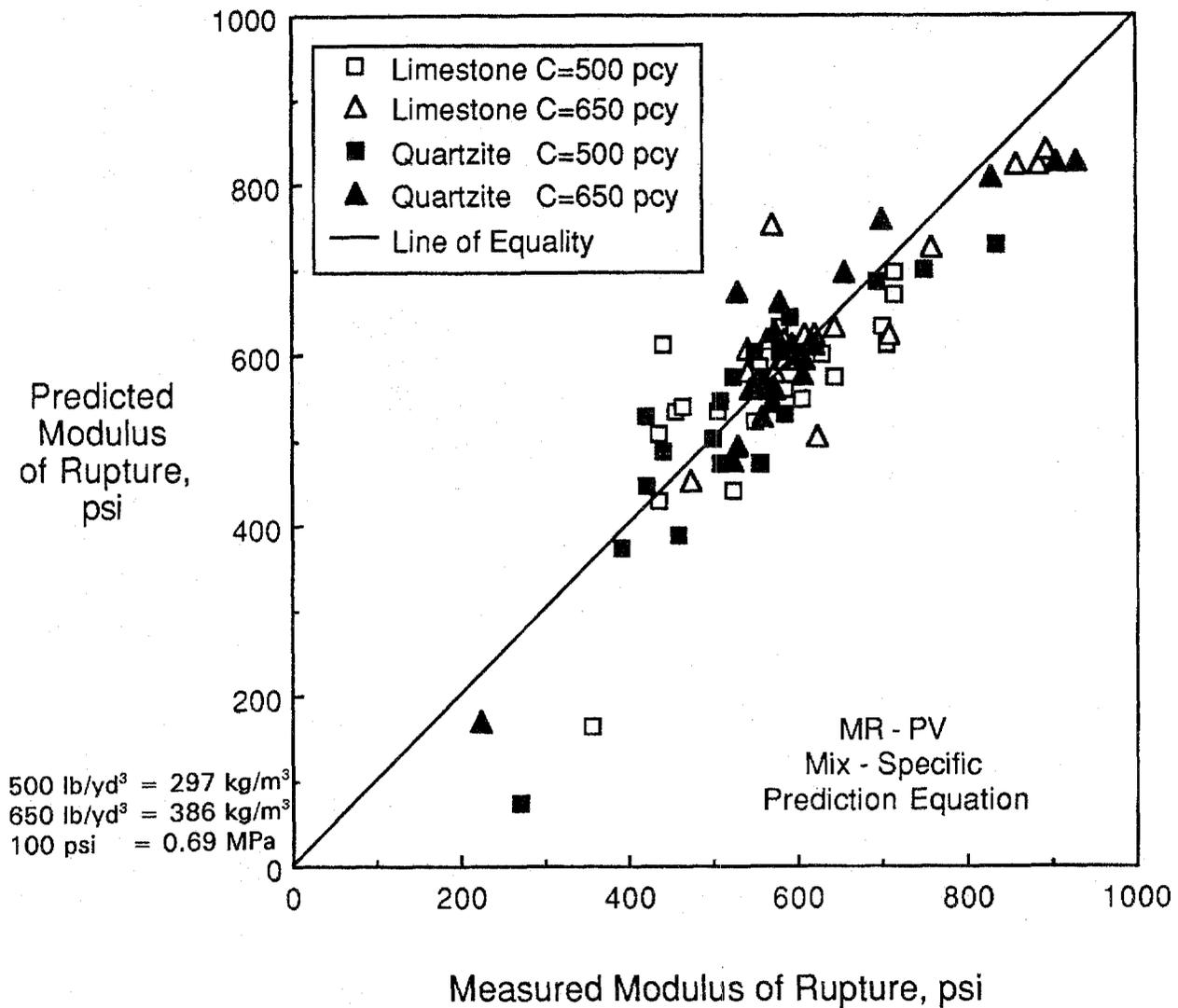
Figure 71.  Mix-specific modulus of rupture - pulse velocity
prediction errors.

**Table 41. Confidence intervals for prediction of early load (1 to 28 days) modulus of rupture from nondestructive test data.**

| Mix | RH, percent | MR, psi | Arrhenius Maturity[1] | | Nurse-Saul Mat.[1] | | Pulse Velocity[1] | |
|---|---|---|---|---|---|---|---|---|
| | | | Con. Int.[2] | | Con. Int.[2] | | Con. Int.[2] | |
| | | | 95% +/- psi | 90% +/- psi | 95% +/- psi | 90% +/- psi | 95% +/- psi | 90% +/- psi |
| Crushed Limestone 500 lb/yd[3] Cement | 50 | 450 | 68 | 57 | 61 | 50 | 73 | 60 |
| | | 550 | 39 | 33 | 37 | 30 | 41 | 34 |
| | | 650 | **** | **** | **** | **** | 75 | 62 |
| | 100 | 450 | 124 | 102 | 110 | 91 | 133 | 110 |
| | | 550 | 82 | 67 | 75 | 62 | 86 | 71 |
| | | 650 | 66 | 55 | 62 | 51 | 69 | 57 |
| Crushed Limestone 650 lb/yd[3] Cement | 50 | 450 | 126 | 104 | 124 | 102 | 145 | 120 |
| | | 550 | 55 | 46 | 54 | 45 | 61 | 51 |
| | | 650 | **** | **** | **** | **** | 59 | 49 |
| | 100 | 450 | 280 | 231 | 275 | 227 | 324 | 268 |
| | | 550 | 203 | 168 | 200 | 165 | 234 | 194 |
| | | 650 | 130 | 107 | 128 | 105 | 148 | 122 |
| Crushed Quartzite 500 lb/yd[3] Cement | 50 | 450 | 34 | 28 | 35 | 29 | 41 | 33 |
| | | 550 | 32 | 26 | 32 | 26 | 37 | 30 |
| | | 650 | **** | **** | **** | **** | 65 | 54 |
| | 100 | 450 | 83 | 68 | 84 | 70 | 100 | 82 |
| | | 550 | 59 | 49 | 60 | 50 | 70 | 58 |
| | | 650 | 48 | 40 | 49 | 40 | 55 | 46 |
| Crushed Quartzite 650 lb/yd[3] Cement | 50 | 450 | 73 | 61 | 72 | 60 | 74 | 61 |
| | | 550 | 37 | 31 | 37 | 31 | 37 | 31 |
| | | 650 | **** | **** | **** | **** | 49 | 41 |
| | 100 | 450 | 175 | 144 | 172 | 142 | 175 | 144 |
| | | 550 | 128 | 106 | 127 | 105 | 129 | 106 |
| | | 650 | 87 | 71 | 86 | 71 | 87 | 72 |

NOTES: [1] Predicition equations listed in table 40.

[2] Confidence interval for conditional expectation of modulus of rupture.

500 lb/yd$^3$ = 297 kg/m$^3$ , 650 lb/yd$^3$ = 386 kg/m$^3$ , 100 psi = 0.69 MPa

132

load tests are summarized in table 42. For the 4 mixes coefficients of within-test variation averaged 4.2, 7.0, and 4.1 percent for compressive strength, modulus of elasticity, and modulus of rupture, respectively.

## Conclusions - Sawing Time Period

An extensive laboratory materials investigation was conducted to study early age (4 to 24 hours) and early loading (1 to 28-day) concrete properties. For the early age study, 3 coarse aggregate types and 2 cement contents were used to produce 6 typical concrete pavement construction mixes. Early age (4 to 24 hour) properties evaluated included compressive, flexural, splitting tensile, modulus of elasticity, and coefficient of thermal expansion. Concrete properties were characterized with nondestructive pulse velocity and concrete maturity measurements. Tests were done at intervals of 4, 6, 9, and 24 hours for concrete cured at 50, 72, and 100 °F (10, 22, and 38 °C). Other tests at early ages included sawability, cube compressive strength, Clegg Impact Hammer, setting time for mortar, and petrographic examination of hardened concrete (at sawed joints). These properties and tests will be discussed in chapter 4. Investigation of Earliest Joint Sawcutting Tests.

Strength interrelationships were developed for 1 to 24 hour modulus of rupture to compressive, modulus of rupture to split tensile, and split tensile to compressive strengths. Strength of one form can be well predicted from both other strength forms. The modulus of rupture is a function of square root of compressive and linear function of split tensile strength. Similar to the modulus of rupture model, the split tensile strength can be predicted from the square root of compressive strength. Models developed for the combined data of all 6 mixes (3 aggregates and 2 cement contents) predicted strengths well compared to models developed for specific mixes. Multiple linear regression analyses indicated that the general single independent variable (strength type) models could only be slightly improved by considering curing age, aggregate geometry, and cement contents.

The concrete maturity and pulse velocity nondestructive testing methods were evaluated for estimating early age strength (4 to 24 hours). Maturity was calculated using the 2 accepted methods of time-temperature (Nurse-Saul) and equivalent age (Arrhenius) functions. Compressive, split tensile, and flexural strengths could be fairly well predicted from nondestructive testing (NDT) data. Mix-specific prediction equations indicated that compressive strength on average (for all mixes and 3 NDT methods) was slightly better than the split tensile or modulus of rupture models. Multiple regression analysis also indicated that compressive strength could also be predicted from pulse velocity better than from the other 2 strength types. For multiple regression analysis of strength (independent from mix design) on maturity data, the compressive strength was the least statistically significant model. All strength type predictions could be statistically improved slightly by considering other variables such as cement content, temperature history characteristics (initial, peak, slope at 6 hours, time to peak, or temperature rise), 28 day moist cured compressive strength, and aggregate characteristics (hardness, geometry).

A detailed analysis of variables affecting early age compressive strength predictions from maturity indicated that when age and temperature factors were included the coefficients of determination increased. When temperature and age variables were suppressed the 2 and 3 variable models developed did not significantly improve the single variable maturity model for the combined data. Maturity does not statistically incorporate all affects of age and temperature since these variables can be significant in addition to maturity. The differences in absolute prediction errors of the general and mix-specific single variable

**Table 42. Early load (1 to 28 days) within-test coefficient of variation summary.**

| Aggregate Type | Cement Content, lb/yd$^3$ | | Coefficient of Variation, percent [1] | | |
|---|---|---|---|---|---|
| | | | Compressive Strength | Modulus of Rupture | Modulus of Elasticity |
| Crushed Limestone | 500 | minimum | 0.5 | 0.0 | 1.1 |
| | | maximum | 11.3 | 15.8 | 12.3 |
| | | average | 5.5 | 5.2 | 4.8 |
| | 650 | minimum | 1.0 | 0.7 | 0.7 |
| | | maximum | 6.8 | 20.4 | 8.9 |
| | | average | 3.0 | 7.1 | 3.1 |
| Crushed Quartzite | 500 | minimum | 0.9 | 1.0 | 0.0 |
| | | maximum | 12.9 | 23.9 | 13.6 |
| | | average | 4.8 | 8.8 | 4.8 |
| | 650 | minimum | 0.5 | 0.0 | 0.6 |
| | | maximum | 12.3 | 17.3 | 6.5 |
| | | average | 3.5 | 6.7 | 3.6 |

[1] NOTE: Average of estimated coefficients of variation at ages of 1, 3, 7, 14, and 28 days cured at 50, 72, and 100 °F.

500 lb/yd$^3$ = 297 kg/m$^3$ , 650 lb/yd$^3$ = 386 kg/m$^3$
50 °F = 10 °C, 72 °F = 22 °C, 100 °F = 38 °C

models computed were significant. However, if the error analysis considers only early age compressive strength data of less than 2000 psi (13.8 MPa), the prediction error increase when the general single variable model (versus the single variable mix-specific model) is used is significantly smaller. For data less than 2000 psi (13.8 MPa) the average difference in absolute prediction percentage errors between the general and mix-specific models is 25 percent for both the Arrhenius and Nurse-Saul maturity.

A detailed analysis of variables affecting early age compressive strength predictions from pulse velocity indicated that age and initial temperature only slightly improve the model. Differences in absolute value of prediction percentage errors between the general single variable and mix-specific pulse velocity models were much less than those computed for the maturity models. Prediction error differences were on the order of 50 percent of those corresponding errors of the maturity models. This suggests that if the general single variable model is used instead of mix-specific prediction models, less error is introduced with the pulse velocity than the maturity methods. If mix-specific models are generated there is only a small advantage of using pulse velocity rather than maturity.

For sawing property evaluation compressive strength was selected over flexural and split tensile strength since:

- Compressive strength testing is a wider accepted test than modulus of rupture or split tensile strength.

- Compressive strength estimated within-test coefficients of variation were approximately 50 percent less than those of split tensile and modulus of rupture tests.

- Flexural and split tensile strength can be well predicted using general single variable compressive strength functions (independent of aggregate type and cement content).

- Compressive strength less than 2000 psi (13.8 MPa) at ages of 4 to 24 hours may be well predicted from maturity or pulse velocity nondestructive testing models for specific mixes.

- Compressive strength less than 2000 psi (13.8 MPa) may be predicted from general single variable maturity equations independent of aggregate type and cement content. Cement content affects are possibly incorporated into maturity by increased heat of hydration temperatures.

- Compressive strength less than 2000 psi (13.8 MPa) may be well predicted from general single variable or mix-specific models incorporating pulse velocity.

Early age modulus of elasticity tests indicate that the modulus can be estimated from a constant multiplied by the square root of compressive strength. The constant is similar to those reported for mature concrete. Coefficients of thermal expansion at early age were similar to those used for mature concrete. The coefficients of contraction ranged from 4.9 to 6.1 millionths in/in /°F (8.8 x $10^{-6}$ to 11 x $10^{-6}$ mm/mm/°C) for the 6 different mixes.

The models from data developed in this study were developed to investigate the influence of mix design parameters (aggregate type, geometry, cement contents, etc.) and curing

conditions (temperature). These models were derived to fit the database used in this study. One parameter not investigated was cement source. Cement type and source will influence maturity and possibly pulse velocity NDT models. Application of models to other project-specific mixes using other cement contents, aggregate sources, and admixture contents and type will not yield reliable results. The models developed should be viewed more as an investigative tool and demonstration of mix-specific applications. Mix-specific models should be developed using similar techniques demonstrated in this study.

General prediction models combining data from aggregate type, cement contents, and curing conditions were used to investigate effects of coarse aggregate on strength. For the database in this study flexural and split tensile strength could be well predicted from compressive strength. The model indicates for the mixes used in this study that mortar properties influence strength prediction more than coarse aggregate properties. The general mix-independent models were anticipated since the failure planes generally passed around coarse aggregate and went through only paste. Use of general models to project -specific mixes should not be used since fine aggregate source, admixture type, admixture quantity, and coarse aggregate quantity were not variables in the strength investigation. Mix-specific relationships should be developed to monitor strength gain for individual projects.

## Conclusions - Early Loading Time Period

An extensive laboratory materials investigation was conducted to study early loading (1-to 28-day) concrete properties. For the early loading study two coarse aggregate types (soft crushed limestone and hard crushed quartzite) and two cement contents were used to produce four typical concrete pavement construction mixes. Early loading properties evaluated included compressive strength, modulus of elasticity, and modulus of rupture. Concrete properties were characterized with nondestructive pulse velocity and concrete maturity measurements. Tests were done at intervals of 1, 3, 7, 14, and 28 days for concrete cured at 50 percent RH at 50, 72, and 100 °F (10, 22, and 38 °C). In addition to the 50 percent RH curing condition, test specimens were stored at 72 °F (22 °C) at 100 percent RH to evaluate the effects of humidity on strength gain. Humidity had a significant effect on modulus of rupture. The moist-cured modulus of rupture averaged 20 to 30 percent higher than the 50 percent RH specimens.

The modulus of rupture could be predicted from compressive strength and relative humidity. No satisfactory general prediction equation for all strength data could be generated. Mix-specific models predicting modulus of rupture from compressive strength and curing humidity were better than the general equation. The 90 percent confidence intervals for the 4 mix-specific models ranged from approximately 20 to 70 psi (138 to 483 kPa).

Similar to prediction model for early age (4 to 24 hours) modulus of elasticity, modulus of elasticity at later ages could be predicted from compressive strength (square root) independent of aggregate, curing condition, and age. The coefficient of 62,000 for early loading (1-to 28-day) is close to the early age (4 to 24 hour) multiplying coefficient of 61,000 (times square root of compressive strength). The coefficient was developed for the database in this study. The square root of compressive strength model is similar to other prediction equations reported in literature. Other cement and aggregate sources will yield a different coefficient. The coefficient should be derived for each project-specific mix using the approved aggregate and cement source.

136

Compressive strength was related to nondestructive Arrhenius maturity, Nurse-Saul maturity, and pulse velocity testing methods. The general equation (independent of aggregate type and cement contents) did not consistently predict actual strengths. Mix-specific strength prediction models were statistically significant. Average mix-specific compressive strength prediction errors (absolute values) were 6.2, 5.4, and 5.2 percent for the Arrhenius, Nurse-Saul, and pulse velocity models, respectively. Compressive strength can be predicted from the inverse of maturity or as a function of pulse velocity and age. Use of either maturity type models becomes insensitive to maturity change at strengths greater than approximately 3500 and 4500 psi (24.1 and 31.0 MPa) for the 500-and 650-lb/yd$^3$ (297-and 386-kg/m$^3$) cement contents, respectively.

Modulus of rupture was also related to nondestructive test data. For concrete maturity data the flexural strength could be predicted from the relative humidity and inverse of maturity. For pulse velocity models the modulus of rupture can be predicted from relative humidity and pulse velocity. Average prediction errors (absolute value) were 10, 9, and 10 percent for the Arrhenius, Nurse-Saul, and pulse velocity models, respectively. The 95 percent and 90 percent conditional expectation of the modulus of rupture were similar for all 3 nondestructive methods as well as similar to the intervals calculated for modulus of rupture prediction from compressive strength. This indicates that if compressive strength can be accurately predicted (low confidence intervals), the modulus of rupture can be estimated from either nondestructive test data correlated directly with flexural strength or indirectly predicted once a relationship between compressive and flexural strength is established.

# CHAPTER 4. INVESTIGATION OF EARLIEST JOINT SAWCUTTING

Objectives of full-scale control joint sawcutting tests and and highway pavement sawcutting operations were to determine the earliest "near" joint sawcutting window of opportunity limit and to determine nondestructive test methods and strength indicators that will predict when sawcutting can be successfully initiated. Full-scale sawcutting tests were made on specially constructed slabs placed in an exterior area. Sawing strip slabs were constructed using the concrete mix proportions and aggregates previously described in Chapter 3. Early Age Concrete Properties From Laboratory Tests. Sawcutting was done for a range of time increments after concrete placement. Companion tests were made to monitor concrete strength at the various sawing times and to measure concrete characteristics by non-destructive methods. The nondestructive tests were made directly on the sawing strip slabs and companion test specimens.

To verify and test the joint sawing criteria and nondestructive test methods developed in construction of full-scale sawcutting test slabs, 3 field sites were selected. The selected sites were U.S. Highway 169 near Fort Dodge, Iowa; Interstate Route 15 near Tremonton, Utah; and Interstate Route 94 near Wisconsin Dells, Wisconsin. The Iowa and Utah projects were new construction and the Wisconsin site was complete removal and reconstruction.

## SAWING STRIP SLABS

To determine the "near" time after concrete placement that sawcutting can be initiated, sawing strip slabs were constructed and sawcut to one-third slab depth for a range of time after concrete placement. By necessity, some sawcuts were made that produced severe sawcut edge concrete ravelling. Premature sawcutting is unacceptable at actual construction sites to highway contractors and owners. Severe ravelling would require, at considerable costs, removal and replacement of complete pavement segments. Construction of the sawing strip slabs concurrently with concrete sawing activities provided access to calibrated laboratory equipment for companion strength testing and also access to a larger technician support crew. Sawing strip slab construction details, companion strength tests and non-destructive tests made on sawing strip slabs, ratings of sawcut concrete edge quality with respect to ravelling, and test results are discussed in this chapter.

### Sawing Strip Slab Construction

Sawing strip slabs, 20 ft long (6.1 m), about 50 in (1.3 m) wide, and 10 in (25 cm) thick, as shown in figure 72, were constructed between two concrete strips that acted as longitudinal edge forms. Top surface elevation of sawing strip slabs were placed and finished to match slave strip surfaces. Slave strips provided support and stability to a 65-(48-kW) horsepower gasoline powered saw when sawcuts were made near sawing strip slab edges.

Concrete used for the sawing strip slab construction was obtained from a nearby ready-mix plant. Concrete was batched to the same proportions using the same fly ash and coarse and fine aggregate as were used for and described in Chapter 3. Early Age Concrete Properties From Laboratory Tests. Type I cement was used for early age laboratory and sawing strip concretes. However, the cement sources were different.

Coarse aggregates from Sioux Falls, South Dakota; Dilles Bottom, Ohio; and McCook, Illinois were stockpiled in segregated bins at the ready-mix producer's yard for mixing concrete used in sawing strip slabs. Batching was done by the producer. Travel
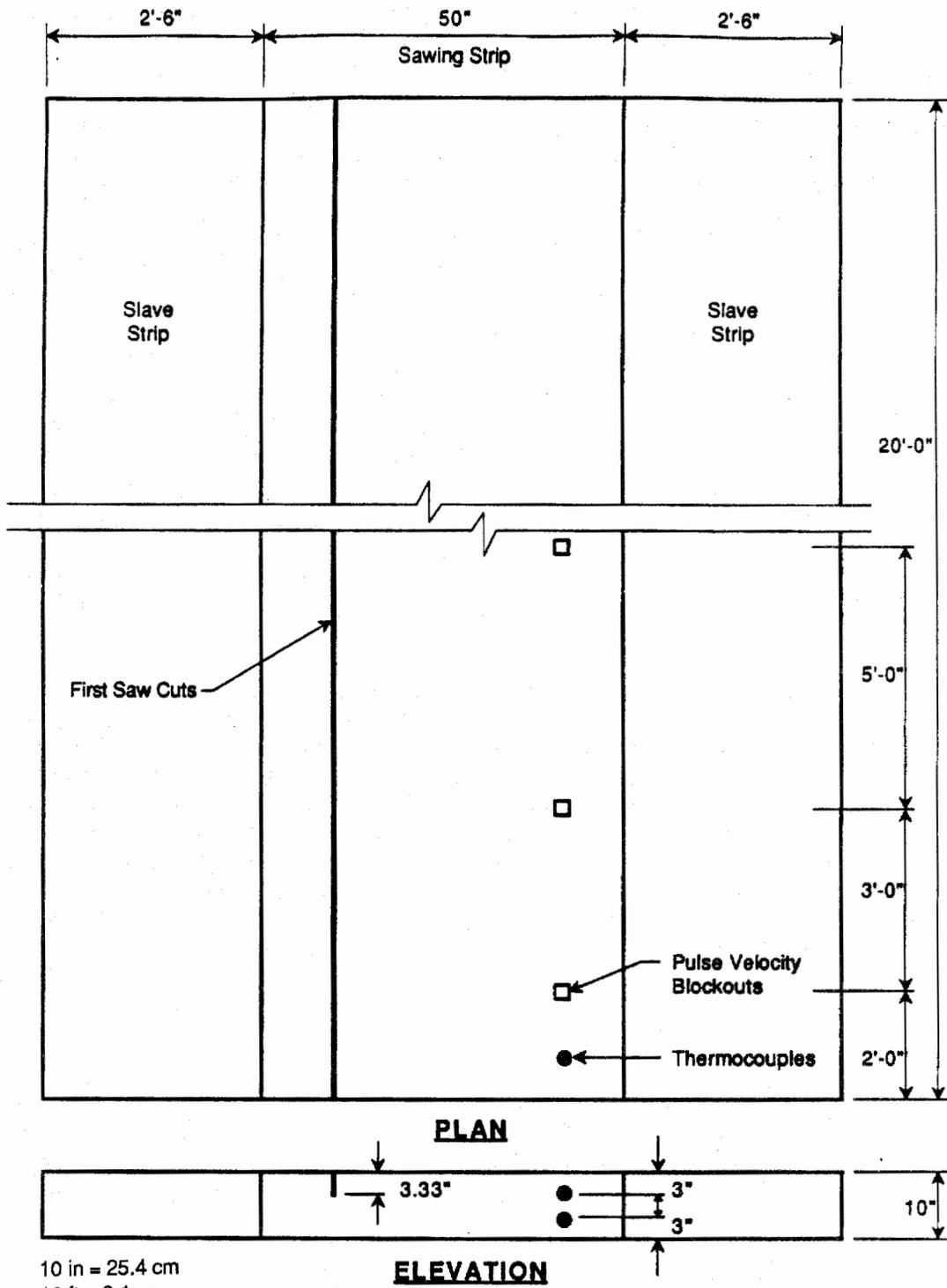
Figure 72.  Sawing strip slab.

time from mixing plant to the sawing site was approximately 30 minutes. After ready-mix truck arrival at sawing slab site, concrete was mixed for about 70 revolutions immediately ahead of discharge and ahead of making slump and air content tests. Additional water was added to the mix if slumps were 1 in (25 mm) or less. After obtaining concrete slumps ranging from about 1 to 3 in (25 to 76 mm), concrete was placed between slave strip edge forms by chuting directly from truck. A polyethylene sheet was located between slab bottom and the below slab existing pavement for ease of after-test sawing strip slab removal.

Seven sawing strip slabs were constructed. The slabs were designated as A through G and were produced with the following constituents and placed on the following dates:

Slab A - CS with 650 lb/yd$^3$ (386 kg/m$^3$) of cement: August  8, 1989
Slab B - CS with 500 lb/yd$^3$ (297 kg/m$^3$) of cement: August 14, 1989
Slab C - CH with 650 lb/yd$^3$ (386 kg/m$^3$) of cement: August 16, 1989
Slab D - CH with 500 lb/yd$^3$ (386 kg/m$^3$) of cement: August 18, 1989
Slab E - RH with 500 lb/yd$^3$ (297 kg/m$^3$) of cement: August 23, 1989
Slab F - RH with 650 lb/yd$^3$ (386 kg/m$^3$) of cement: August 25, 1989
Slab G - CS with 650 lb/yd$^3$ (386 kg/m$^3$) of cement: August 30, 1989

Slab G is a replicate of slab A. However, weather conditions varied during placement. Sawing slab placement temperature conditions and properties are summarized in table 43.

After depositing concrete, it was consolidated with internal vibrators. Strike off and surface finishing was done with a magnesium beam, wood floats, and steel trowels. A minimum of surface finishing was done. Surface texture was achieved with a light broom finish. The light surface texturing was done so that any ravelling occurring as a result of sawcutting could be easily noted and measured. White pigmented curing compound was applied to slab surfaces immediately upon completing light broom surface texturing.

Instrumentation placed in sawing strip slabs included 2 thermocouples to measure temperature used in calculating concrete maturity. Thermocouples were manually located during concrete placement at about 3 in (76 mm) from bottom and top of slab. Blockouts installed to provide access for pulse velocity transducers at distances of about 2, 5, and 10 ft (0.6, 1.5, and 3.1 m) from one slab end were located to one side of the longitudinal slab axis.

Ambient air temperatures were monitored adjacent to the slab placement location. Temperatures were also measured at the center of a 6- by 12-in (15- by 30-cm) concrete cylinder stored adjacent to the slab. The cylinder was molded using concrete delivered for the sawing slab. The black plastic cylinder mold shell was not removed.

Eighteen 6- by 12-in (15- by 30-cm) cylinders were molded for each of the 7 sawing strip slabs. Ten of the 18 cylinders were cast in split cylinder steel molds to avoid damage at early ages during demolding operations. After consolidating concrete in cylinder molds with pencil vibrators, the cylinders were struck off and capped with steel cover disks. The cylinders were stored adjacent to the slabs until testing. Test cylinders were transported in molds to the testing laboratory located within a 3 minute walking distance from slabs. Cylinders were demolded and placed for testing into a compression testing machine.

Clegg Impact Hammer block specimens of 24- by 24- by 10-in (61- by 61- by 25-cm) dimension were cast using concrete from the sawing strip slabs. Three blocks were

**Table 43. Sawing strip slab data.**

| Slab | Coarse Aggregate | Cement Content, lb/yd³ | Fresh Concrete | | | | | | | | Number of Sawcuts | 28 day [1] | |
| | | | Concrete Slump, in | Air Content, percent | Concrete Moisture, percent | Ambient Temp, °F | | Concrete Temp, °F | | | f'c, psi | Pulse Velocity, ft/s |
| | | | | | | Placement | Last Sawcut | Placement | Last Sawcut | | | |
| A | Limestone | 650 | 1.0 | 3.1 | 6.8 | 65 | 79 | 86 | 114 | 4 | 6910 | 16,000 |
| B | Limestone | 500 | 1.7 | 3.9 | 7.4 | 70 | 73 | 70 | 101 | 7 | 6720 | 16,500 |
| C | Quartzite | 650 | 2.0 | 2.5 | 7.3 | 60 | 73 | 60 | 101 | 6 | 5230 | 15,200 |
| D | Quartzite | 500 | 2.9 | 2.0 | 7.3 | 60 | 70 | 77 | 93 | 7 | 6440 | 15,700 |
| E | Gravel | 500 | 2.1 | 3.4 | 7.4 | 71 | 70 | 87 | 100 | 5 | 6170 | 15,100 |
| F | Gravel | 650 | 1.5 | 3.2 | 7.6 | 65 | 75 | 84 | 115 | 6 | 5590 | 14,900 |
| G | Limestone | 650 | 1.5 | 3.5 | 8.2 | 72 | 81 | 83 | 114 | 5 | 5980 | 16,600 |

[1] NOTE: Tests on cylinders cured at 72 °F and 100 % relative humidity.

500 lb/yd³ = 297 kg/m³ , 650 lb/yd³ = 386 kg/m³ , 1000 psi = 6.9 MPa, 1000 ft/s = 305 m/s, 72 °F = 22 °C, 1 in = 25 mm

cast and transported on carts to controlled temperature and humidity chambers. Surface drying of concrete blocks was prevented by covering with polyethylene sheets. Setting time for mortar and cube compressive strength was determined using mortar fraction of each of the concrete mixes. Mortar was placed in a 12-in (30-cm) diameter by 8-in (20-cm) deep mold for setting time and in 2-in (5-cm) steel cube molds for cube compressive strength.

## Companion Tests to Sawcutting Strip Slabs

Companion tests to sawcutting included compressive strength, pulse velocity, maturity monitoring, Clegg Impact Hammer tests, mortar setting time, and mortar compressive strength.

Compressive strength was determined throughout the period that sawcuts were made on sawing strip slabs. Based on analysis of early age laboratory data (4 to 24 hours) compressive strength testing was selected since it could be well predicted (less than 2000 psi, 13.8 MPa) using maturity and pulse velocity NDT data and it correlated well with other strength types. Two cylinders and 2 mortar cubes stored adjacent to the slab were tested on each occasion. In addition, 3 cylinders were used to determine concrete 28-day moist cured compressive strengths. Tests were made according to ASTM Designation: C 39-86 (concrete) and C 109-88 (mortar) methods. To avoid thermal cracking of early age concrete, neoprene cushioned steel caps were used in lieu of capping cylinders with sulphur capping compound, as described for tests for the 4- to 24-hour period.

Pulse velocity tests were made on sawing strip slabs and companion cylinders. Pulse velocity paths were about 2 ft (61 cm) for earliest sawing time that ranged from 2 to 3 hours after placement. To be able to measure velocities for path lengths of about 5 ft (1.5 m), the delays between placement and testing times were generally 3 to 5 hours.

Temperature data to calculate maturity were recorded for sawing strip slabs at about 3 in (76 mm) from slab top and bottom. Maturity data were also collected for a concrete cylinder in a black cylinder mold stored adjacent to the slab. Maturity data were sampled at 30-minute intervals for a 24-hour period. Ambient air temperature data were collected for the same intervals.

Clegg Impact Hammer tests were made throughout the time period that sawcutting was done on sawing strip slab surfaces and companion block specimens stored at 50, 72, and 100 °F (10, 22, and 38 °C). Methods for Clegg Impact Hammer tests are described in Chapter 3. Early Age Concrete Properties From Laboratory Tests.

Setting time for mortar tests were made using ASTM Designation: C 403-88 methods. The cylinder holding the mortar and the equipment for plunger penetration measurements were stored adjacent to the slab.

Three concrete cores, labeled D7, E3, and G3E were cored from slabs D, E, and G respectively. The core from slab D was obtained from the 7th sawcut, the cores from slabs E and G were obtained from the third sawcuts. The cored sawcut from slabs D and E were produced using diamond impregnated blades and the core from slab G was obtained from a sawcut made using an abrasive blade. Sawcuts were made at ages of 11, 5.5, and 3.5 hours for slabs D, E, and G, respectively. Petrographic examinations were done on the three cores using some of the methods described in ASTM Designation: C 856-83 (Reapproved 1988), "Standard Practice for Petrographic Examination of Hardened Concrete." Cores were sawed longitudinally, and resulting core halves lapped to better reveal concrete

142

characteristics, particularly adjacent to sawcuts. The lapped pieces and sawcut edge areas were examined under a stereomicroscope at magnifications of 7 to 45X. Examinations were geared toward locating features possibly indicating damage to the concrete as a result of early sawing.

## Sawcutting Equipment and Sawcutting Tests

A 65-horsepower (48-kW) walk-behind saw was used for making sawcuts on the sawing strip slabs constructed during August 1989. The saw, powered by a gasoline motor, was operated at about 1500 revolutions per minute. To minimize operator bias on sawcutting, the saw was operated by a technician who had limited previous experience with concrete sawing. Guidance for using saws and information on sawing techniques were provided by 2 diamond saw blade manufacturers who also provided the diamond sawing blades. Representatives of the saw blade manufacturers were at the site during sawing of the initial 2 slabs.

Two diamond sawblade manufacturers each supplied two 14.3-in (36-cm) diameter blades. The blades were pre-seasoned by the manufacturers to get representative sawcuts. Each supplied 1 blade designated for sawing concrete produced using crushed limestone coarse aggregate and 1 blade for sawcutting concrete produced using hard coarse aggregate. The diamond impregnated blades made approximately 0.16-in (4 mm) wide sawcuts. Depths of sawcuts were 3-1/3 in (85 mm). Speed of sawcutting was about 3 ft (91 cm) per minute. Sawcut length was about 17 ft (5.2 m) for each cut. At midlength of each cut, after approximately 8-1/2 ft (2.6 m), one manufacturer's blade was removed and the second manufacturer's blade was fixed to the saw mandrel. Sawing was resumed and the cut was completed. Changing blades required about 3 minutes. In slab G, a replicate of slab A, produced using crushed limestone and 650-lb/yd$^3$ (386-kg/m$^3$) cement, the diamond impregnated blade from one manufacturer designated for cutting concrete produced using limestone was used for about an 8-ft (2.4-m) length of sawcut and an abrasive blade was used for dry sawing the other 8 ft (2.4 m) of the sawcut.

Sawcutting for each of the 7 sawing strip slabs was initiated within a time after concrete placement that would produce a sawcut with severe concrete ravelling. A second cut was made to produce a sawcut with some ravelling. About 2 to 5 additional cuts were made to finally produce a sawcut without ravelling. The number of sawcuts installed in a sawing strip slab was determined on the basis of apparent rate of strength gain judged on basis of preliminary Clegg Impact Hammer and pulse velocity data. The slab age in hours to final sawcut, that is a sawcut with no apparent ravelling ranged from 3.9 to 12.1 hours. The number of sawcuts for each slab, weather conditions, concrete slump at placement, and concrete air content are listed in table 43.

Engineers experienced with portland cement concrete pavement construction were requested to qualitatively rate the sawcuts made on each of the sawing strip slabs. The following rating guidelines were provided for each rating panel participant:

> Rating = 1 - Badly spalled: sawcut way too early
> Rating = 2 - Unacceptable
> Rating = 3 - Acceptable if sealant reservoir widening is to be done
> Rating = 4 - Good
> Rating = 5 - Excellent

The rating panel consisted of 15 members. All 15 members rated sawcuts in slabs A through D and 6 of the 15 engineers rated sawcuts in all 7 slabs.

143

Measurements were made on sawcuts to determine the surface area of concrete sawcut edge ravelling. Location of each ravelling occurrence with respect to one end of sawcut was recorded. These data were collected for the full length of each sawcut.

## Joint Sawcut Ratings and Companion Test Results

The discussion of sawcut ratings and companion test results will focus on presentation of panel rating test results and relationship of ratings to quantifiable measurements of sawcuts. The presentation of rating results will be followed by presentation of companion compressive strength results, time of set tests, and nondestructive tests such as pulse velocity, Clegg Impact Hammer, and maturity determinations.

Sawcut Ratings. Sawcut qualitative visual ratings were provided at some time after completing work on slabs A through D and upon conclusion of sawing slab project work. The ratings on a scale of 1 through 5 had standard deviations for ratings ranging from 0.1 to 1.0. These ratings are, of course, somewhat subjective, as they in some measure depend on the rating panel member's visual reaction. Averages of ratings for each sawcut are listed in table 44 along with time after concrete placement when sawcuts were made.

Measurements were made of the plan surface area of individual ravelling instances. Surface area included only ravelled areas and excluded sawcut width. These areas were summed for the full length of each joint. A ravelling index expressed in terms of average ravelled surface area per unit length of sawcut joint is listed for each sawcut in table 44.

Plots of ratings versus average ravelled surface area per unit length of sawcut are shown in figure 73. The exponential best fit curve through the data is

$$Y = 3832 * 10^{-(0.737*R)} \dots\dots\dots\dots\dots\dots\dots\dots\dots\dots (12)$$

where:

$Y = 1 +$ average ravelled area per unit length of sawcut, $mm^2/ft$

$R =$ rating

The coefficient of determination, R-squared, was 0.848 for the rating to ravelling area correlation.

For a sawcut with "good" ratings (R = 4), the amount of concrete sawcut edge ravelling is, according to equation 12, 4.3 $mm^2/ft$ of sawcut length. For a sawcut with "acceptable" rating (R = 3), that is one judged suitable if joint sealant reservoir widening is to be done, the amount of ravelling is about 24 $mm^2/ft$ sawcut length. The visual impact of sawcut ratings is shown in figures 74 and 75. The sawcuts shown in figure 74 were made with a diamond impregnated blade and those shown in figure 75 were made with an abrasive blade. Joint sawcuts rated good, acceptable, and unnacceptable are shown for portions of sawcuts 4, 3, and 2, respectively, from bottom of photographs to top for sawing slabs D and G.

Petrographic Examination of Hardened Concrete Sawcut at Early Ages. Three concrete cores, one each from slabs D, E, and G, were obtained from the seventh, third, and third sawcuts, respectively. The following conclusions are based on results of the petrographic concrete core examinations:

**Table 44. Summary of estimated compressive strength for sawcut slabs.**

| Slab | Agg. | Cement Content, lb/yd$^3$ | Sawcut No. | Cut Age, hours | Ave. Sawcut Rating | Ave. Spall Area,[1] mm$^2$/ft | f'c, from NS Maturity,[2] psi | f'c, from Pulse Velocity,[3] psi | Average f'c, psi |
|---|---|---|---|---|---|---|---|---|---|
| A | Crushed Limestone | 650 | 1 | 2.2 | 1.8 | **** | 67 | 207 | 137 |
|   |   |   | 2 | 3.0 | 3.2 | 12.9 | 290 | 865 | 577 |
|   |   |   | 3 | 3.5 | 4.4 | 1.6 | 432 | 989 | 710 |
|   |   |   | 4 | 3.9 | 4.8 | 0.0 | 574 | 1,034 | 804 |
| B | Crushed Limestone | 500 | 1 | 3.2 | 1.0 | **** | 111 | **** | **** |
|   |   |   | 2 | 4.1 | 1.4 | 414.0 | 267 | 22 | 145 |
|   |   |   | 3 | 4.7 | 2.1 | 28.7 | 361 | 264 | 312 |
|   |   |   | 4 | 5.2 | 3.3 | 15.0 | 461 | 412 | 436 |
|   |   |   | 5 | 6.1 | 4.0 | 0.8 | 673 | 698 | 685 |
|   |   |   | 6 | 7.1 | 4.6 | 0.0 | 885 | 965 | 925 |
|   |   |   | 7 | 8.1 | 4.9 | 0.0 | 1,071 | 1,089 | 1,080 |
| C | Crushed Quartzite | 650 | 1 | 3.6 | 1.0 | **** | 159 | 140 | 150 |
|   |   |   | 2 | 4.6 | 2.0 | 217.6 | 332 | 336 | 334 |
|   |   |   | 3 | 5.3 | 2.7 | 31.0 | 537 | 532 | 535 |
|   |   |   | 4 | 6.3 | 2.9 | 88.3 | 752 | 807 | 780 |
|   |   |   | 5 | 7.3 | 3.7 | 3.7 | 954 | 1,081 | 1,018 |
|   |   |   | 6 | 8.5 | 4.2 | 12.7 | 1,131 | 1,331 | 1,231 |
| D | Crushed Quartzite | 500 | 1 | 5.1 | 1.0 | **** | 426 | 210 | 318 |
|   |   |   | 2 | 6.3 | 1.5 | 260.8 | 720 | 379 | 549 |
|   |   |   | 3 | 7.1 | 2.1 | 188.8 | 814 | 488 | 651 |
|   |   |   | 4 | 8.2 | 2.5 | 55.1 | 993 | 628 | 811 |
|   |   |   | 5 | 9.2 | 2.9 | 56.0 | 1,152 | 776 | 964 |
|   |   |   | 6 | 10.3 | 3.3 | 26.0 | 1,353 | 880 | 1,117 |
|   |   |   | 7 | 12.1 | 4.0 | 5.7 | 1,514 | 957 | 1,235 |
|   |   |   | 8 | 25.1 | 4.7 | 0.0 | 2,138 | 1,286 | 1,712 |

NOTES: [1] Average spall area per linear foot of joint in mm$^2$/ft;
Sawcut with no areas listed had excessive spalling that were not measured.

[2] Nurse-Saul maturity in °F-hours (datum temperature 32 °F);
Estimated compressive strength from sawing slab linear regression analysis.

[3] Estimated compressive strength from early age laboratory developed prediction model.

500 lb/yd$^3$ = 297 kg/m$^3$ , 650 lb/yd$^3$ = 386 kg/m$^3$ , 1000 psi = 6.9 MPa, 32 °F = 0 °C, 25 mm = 1 in

**Table 44. Summary of estimated compressive strength for sawcut slabs (continued).**

| Slab | Agg. | Cement Content, lb/yd$^3$ | Sawcut No. | Cut Age, hours | Sawcut Rating | Ave. Spall Area,[1] mm$^2$/ft | f'c, from NS Maturity,[2] psi | f'c, from Pulse Velocity,[3] psi | Average f'c, psi |
|------|------|------|------|------|------|------|------|------|------|
| E | Rounded Gravel | 500 | 1 | 3.6 | 1.0 | **** | 304 | 123 | 213 |
|   |   |   | 2 | 4.9 | 1.8 | 352.2 | 656 | 377 | 516 |
|   |   |   | 3 | 6.3 | 3.5 | 17.0 | 978 | 626 | 802 |
|   |   |   | 4 | 7.3 | 4.5 | 0.0 | 1,154 | 730 | 942 |
|   |   |   | 5 | 8.3 | 4.9 | 0.0 | 1,303 | 894 | 1,099 |
| F | Rounded Gravel | 650 | 1 | 2.8 | 1.0 | **** | 182 | 135 | 158 |
|   |   |   | 2 | 3.4 | 1.9 | 188.5 | 289 | 212 | 250 |
|   |   |   | 3 | 3.9 | 3.3 | 21.1 | 413 | 384 | 399 |
|   |   |   | 4 | 4.4 | 3.7 | 2.5 | 548 | 572 | 560 |
|   |   |   | 5 | 4.9 | 4.2 | 1.1 | 684 | 771 | 727 |
|   |   |   | 6 | 6.4 | 4.9 | 1.5 | 1,043 | 1,039 | 1,041 |
| G1 | Crushed Limestone (Diamond Blade Cut) | 650 | 1 | 3.0 | 1.7 | **** | 174 | 101 | 138 |
|   |   |   | 2 | 3.5 | 3.2 | 10.5 | 283 | 181 | 232 |
|   |   |   | 3 | 3.9 | 4.1 | 0.0 | 410 | 296 | 353 |
|   |   |   | 4 | 4.4 | 4.6 | 6.5 | 547 | 578 | 563 |
|   |   |   | 5 | 4.9 | 5.0 | 0.0 | 682 | 791 | 737 |
| G2 | Crushed Limestone (Abrasive Blade Cut) | 650 | 1 | 3.0 | 1.2 | **** | 174 | 101 | 138 |
|   |   |   | 2 | 3.5 | 2.2 | 26.4 | 283 | 181 | 232 |
|   |   |   | 3 | 3.9 | 3.7 | 0.0 | 410 | 296 | 353 |
|   |   |   | 4 | 4.4 | 3.7 | 10.2 | 547 | 578 | 563 |
|   |   |   | 5 | 4.9 | 4.4 | 0.0 | 682 | 791 | 737 |

NOTES:  [1] Average spall area per linear foot of joint in mm$^2$/ft;
Sawcut with no areas listed had excessive spalling that were not measured.

[2] Nurse-Saul maturity in °F-hours (datum temperature 32 °F);
Estimated compressive strength from sawing slab linear regression analysis.

[3] Estimated compressive strength from early age laboratory developed prediction model.

500 lb/yd$^3$ = 297 kg/m$^3$, 650 lb/yd$^3$ = 386 kg/m$^3$, 1000 psi = 6.9 MPa, 32 °F = 0 °C, 25 mm = 1 in
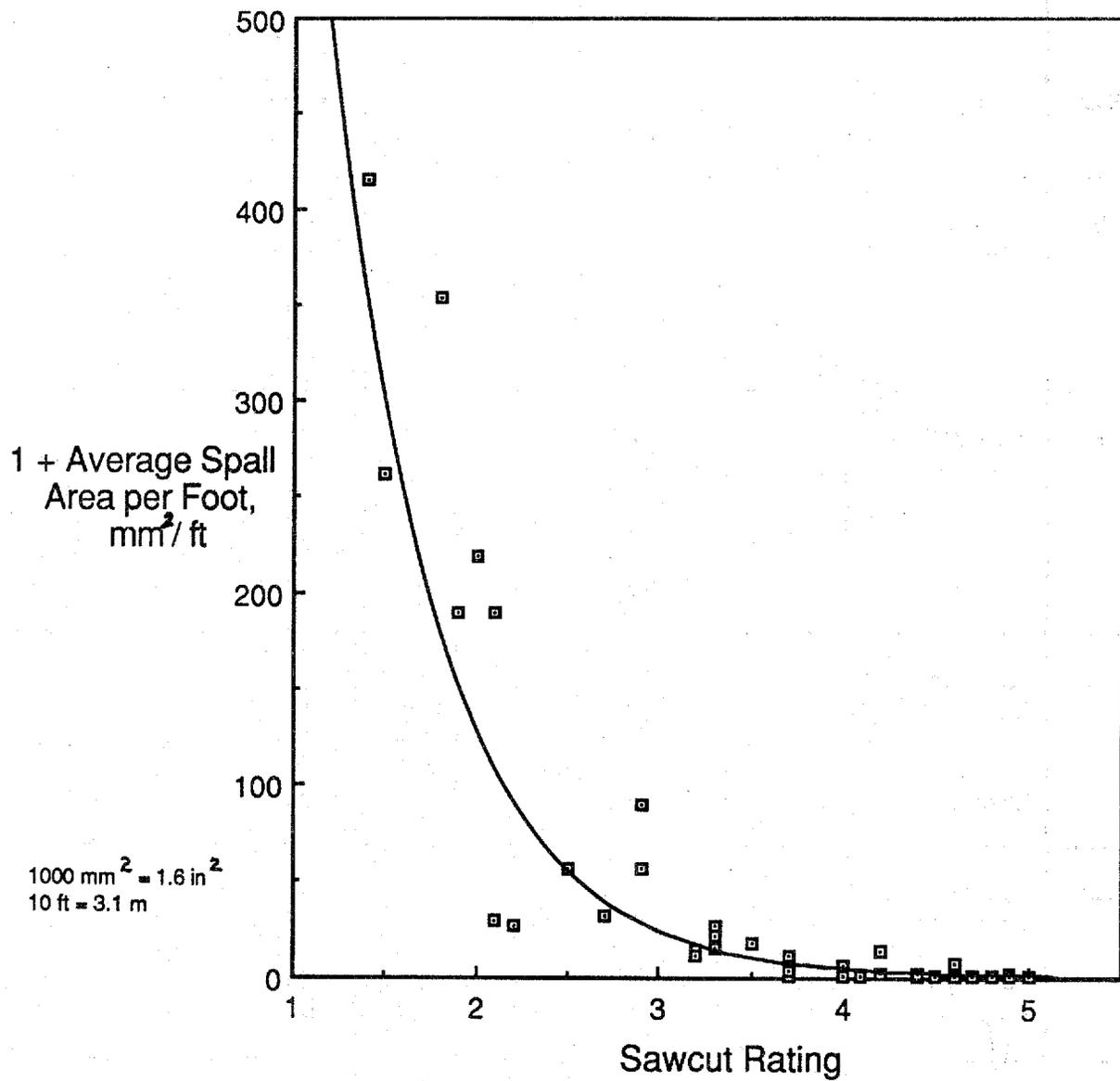
Figure 73. Concrete damage at joint edge vs. sawcut rating.
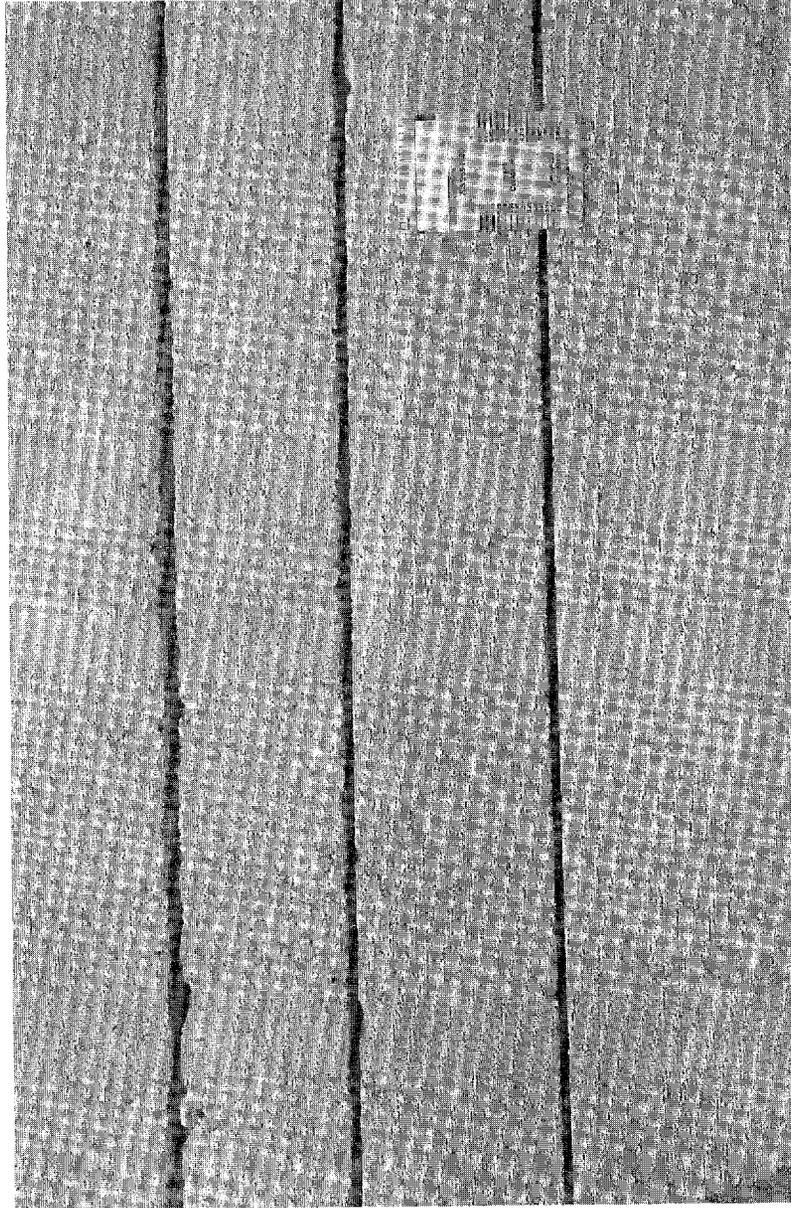
Figure 74. Sawcuts made with diamond-impregnated blade.
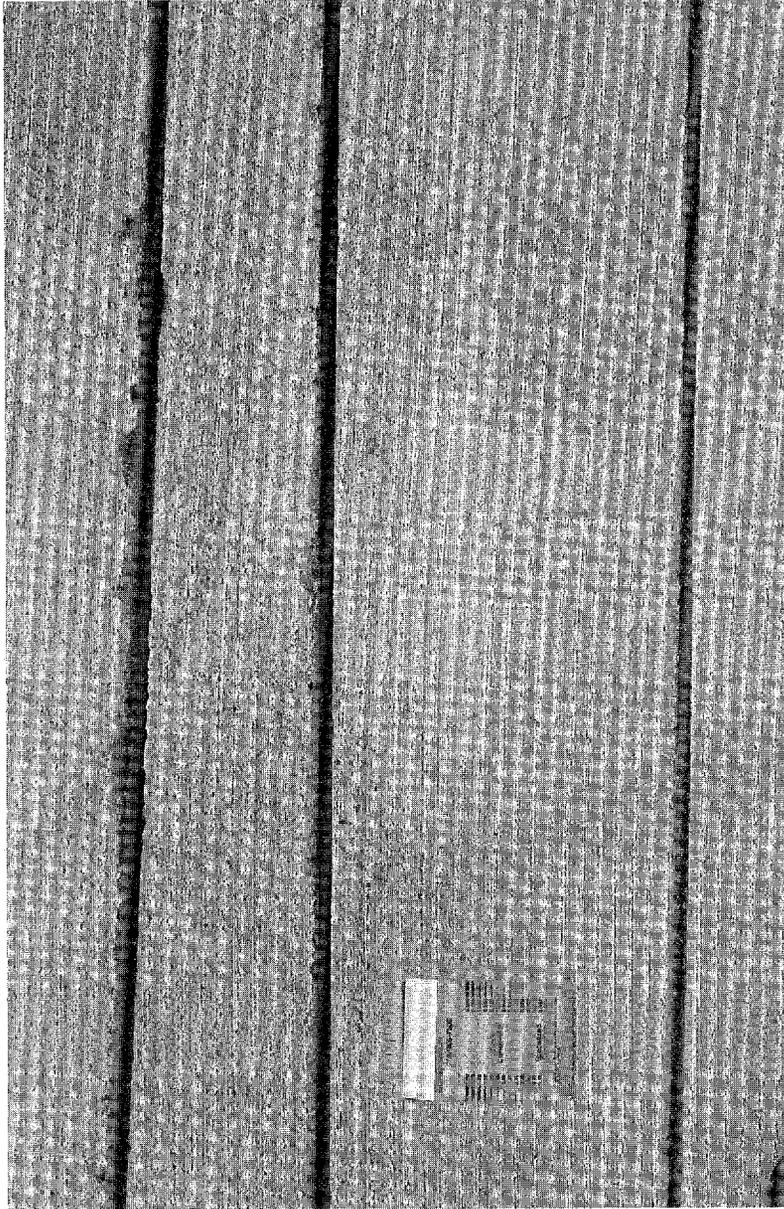
Figure 75. Sawcuts made with abrasive blade.

149

- If no surface ravelling is observed there are no major cracks or spalls associated with sawcutting regardless of time of sawing, cement content, aggregate types, or type of saw blade.

- Concrete immediately adjacent to sawcuts to 0.5 to 0.8 mm (0.02 to 0.03 in) from the edge of sawcut wall is very slightly eroded. The observed erosion is a minor form of damage that is a result of early sawing of soft, incompletely hydrated cement. The small amount of paste and mortar erosion should not affect integrity or durability of concrete adjacent to the sawcuts.

- The observed paste and/or mortar erosion indicates cement paste of all the cores examined was still in early stages of strength development. Core D7 was obtained from sawcut 7 with an average panel rating of 4 ("good"). Average panel ratings for cores E3 (third sawcut) and G3E (third sawcut with abrasive blade) were 3.5 and 3.7 respectively. Cores E3 and G3E showed slightly more paste/mortar erosion than core D7.

Details of petrographic examination are presented in appendix C.

<u>Companion Test Results.</u> Companion test results for cylinder pulse velocity, cylinder compressive strength, cylinder maturity, slab maturity, and slab pulse velocity are reported in tables 23 through 29 of appendix C. These tests were made at intervals for the range of time from about initial sawcuts to about the last sawcut made for each slab. Sawing slab cylinder compressive strength data is summarized in table 45.

Pulse velocity and cylinder compressive strength corresponding for each sawcut age in tables 23 through 29 of appendix C were obtained by interpolating time (age) curves for both slab and cylinder measurements. Compressive strength was estimated using the early age laboratory (4 to 24 hours) pulse velocity prediction equations developed in chapter 3. Analysis of early age data indicated mix-specific pulse velocity prediction equations were slightly better than the general overall equation for predicting compressive strength. For maximum precision the mix-specific equations developed in the lab study as listed in table 9 of appendix A were used to estimate sawing strip slab compressive strength.

Nurse-Saul and Arrhenius maturity relationships established in the early age lab study could predict compressive strength (less than 2000 psi, 13.8 MPa) fairly well. The correlations were established for the Type I cement used in the lab study. A different cement source Type I cement was provided by the ready-mix supplier for sawing slabs. Since different source cements have different rates of chemical reaction and heat of hydration, the maturity equations only apply to concretes made with the same cements. Erratic and unreasonable sawing strip compressive strengths resulted when sawing strip maturity values were input into the laboratory developed maturity equations.

A new prediction equation for compressive strength was developed for the ready-mix suppliers cement using sawing strip cylinders. Analysis of early age lab data indicated that a general prediction equation could be developed that is independent of aggregate type and cement content. Comparison to mix-specific models indicated that differences from the general equation were minimal at strengths of less than 2000 psi (13.8 MPa).

Early age laboratory data indicated that both the Nurse-Saul and Arrhenius maturity methods could predict compressive strength well. The Nurse-Saul method was used in the

150

**Table 45. Summary of cylinder compressive strength tests for sawcut slabs.**

| Slab A | | Slab B | | Slab C | | Slab D | | Slab E | | Slab F | | Slab G | |
|---|---|---|---|---|---|---|---|---|---|---|---|---|---|
| Age, hours | f'c, psi | Age, hours | f'c, psi | Age, hours | f'c, psi | Age, hours | f'c, psi | Age, hours | f'c, psi | Age, hours | f'c, psi | Age, hours | f'c, psi |
| 2.3 | 350 | 3.4 | 70 | 3.8 | 170 | 4.1 | 80 | 4.2 | 140 | 3.1 | 290 | 3.4 | 300 |
| 3.1 | 490 | 4.8 | 310 | 4.8 | 430 | 6.1 | 420 | 5.8 | 270 | 3.8 | 480 | 4.4 | 520 |
| 3.9 | 1210 | 4.2 | 140 | 5.8 | 620 | 7.6 | 810 | 6.7 | 460 | 4.7 | 730 | 5.4 | 1580 |
| 5.3 | 2240 | 5.9 | 640 | 6.8 | 1180 | 8.6 | 1010 | 7.8 | 710 | 6.6 | 1980 | 6.9 | 2110 |
| 8.3 | 2960 | 23.9 | 2920 | 9.0 | 1910 | 9.6 | 1210 | 8.8 | 990 | 8.9 | 2540 | 8.4 | 2530 |
| 23.3 | 4270 | **** | **** | 23.8 | 2590 | 24.3 | 1830 | 23.8 | 2500 | 23.9 | 3480 | 23.4 | 3410 |

1000 psi = 6.9 MPa

151

sawing strip maturity analysis due to ease of computation. The datum temperature was assumed to be 32 °F (0 °C). The general ready-mix concrete Nurse-Saul compressive strength equation is:

$$\log (f_c') = 3.4039 - 203.34*1/NS \dots \dots \dots \dots \dots \dots (13)$$

where

$\log f_c'$ = log (base 10) of compressive strength, psi (1000 psi = 6.9 MPa)
$1/NS$ = reciprocal of Nurse-Saul maturity (°F-hours)

Equation 13 was obtained by linear regression analysis of log (base 10) of compressive strength on the reciprocal of Nurse-Saul maturity from tests on cylinders molded when sawing slab construction occurred. The plot of compressive strength versus Nurse-Saul maturity values is shown in figure 1 of appendix C. The coefficient of determination, R-squared was 0.793.

Concrete insitu slab strengths as listed in column 8 of table 44 were estimated on basis of slab maturity measurements and equation 13. Concrete insitu slab strengths as listed in column 9 of table 44 were estimated on basis of slab pulse velocity measurements and use of table 9 of appendix A mix-specific equations. Estimated compressive strength, as determined by the above described method from Nurse-Saul maturity and pulse velocity correlations, are listed in table 44 along with previously discussed sawcut ratings. Average compressive strengths in table 44 were obtained by averaging the estimates of compressive strength estimated via Nurse-Saul maturity and pulse velocity.

Clegg Impact Hammer ratings obtained on sawing slabs and block specimens cured at 50, 72, and 100 °F (10, 22, and 38 °C) spanning the sawing slab sawcutting period are listed in table 30 of appendix C. Regression of the square root of compressive strength cylinder compressive strength on Clegg Impact Hammer tests are described by the following general (mix independent) equation:

$$(f_c')^{1/2} = 7.0748 + 0.15173 * (CH) \dots \dots \dots \dots \dots (14)$$

where

$f_c'$ = concrete average compressive strength, psi (1000 psi = 6.9 MPa)
CH = Clegg Impact Hammer reading

Coefficient of determination, R-squared, for equation 14 is 0.802. The plot of test data and the best fit line for the compressive strength versus Clegg Impact Hammer values is shown in figure 76.

Setting time for mortar penetration, ASTM Designation: C 403-88, test results are listed in table 31 of appendix C. Initial set, defined as 500-psi (3.4-MPa) penetration resistance, occurred within a range of 1 to 3.1 hours after concrete placement. Final set, corresponding to 4000-psi (27.6-MPa) penetration resistance, occurred within a range of 2 to 4 hours after concrete placement. The data shows that sawcuts made at about time of final set had a rating of 1.8 or less. Thus it is concluded that mortar penetration test results are not suitable for judging near sawing time.
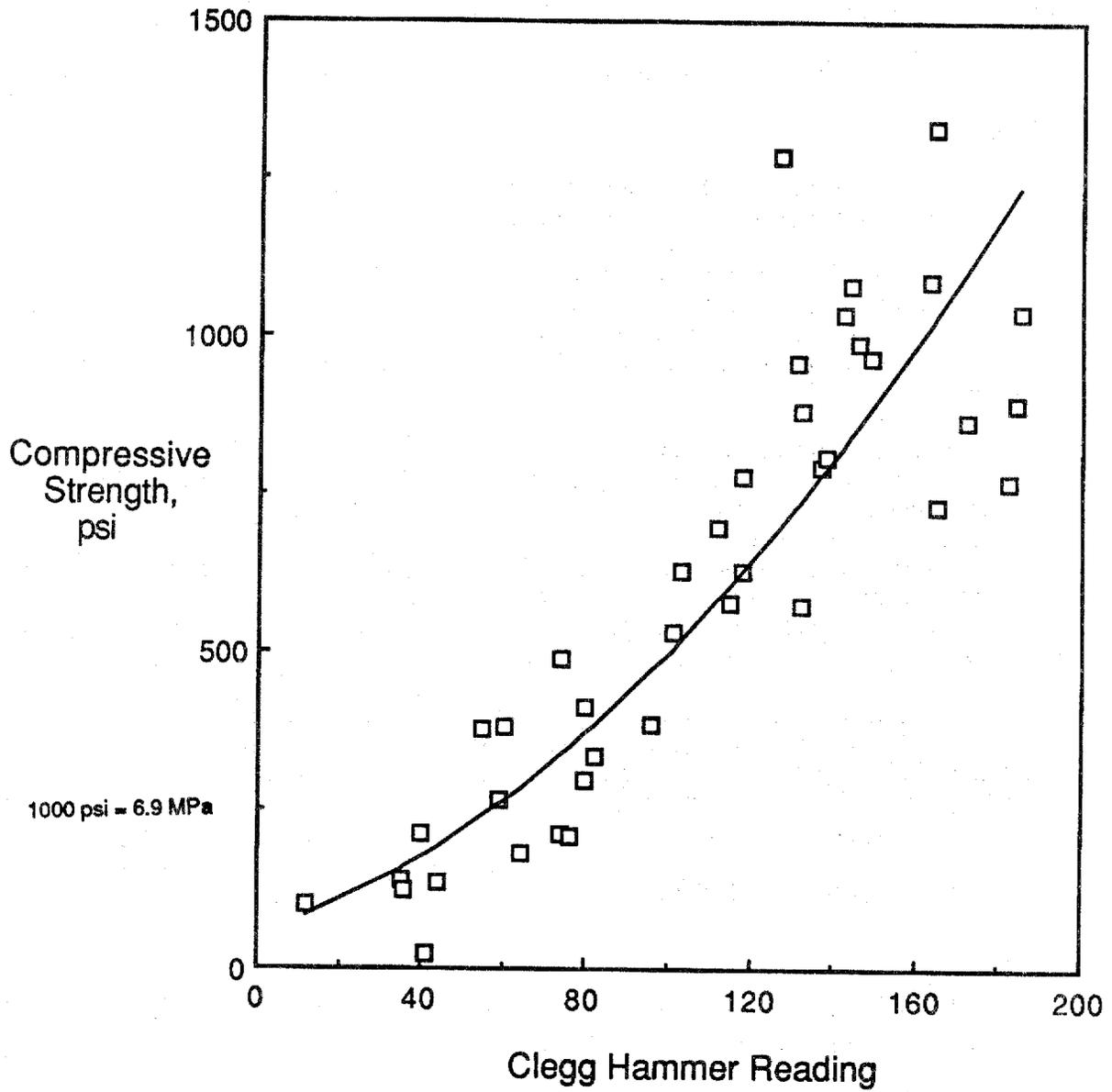
Figure 76.  Clegg hammer impact on sawing slabs vs. compressive strength.

Compressive strengths of mortar cube specimens molded using sawing slab mortar are listed in table 32 of appendix C. A plot of cube compressive strength versus sawcut rating is shown in figure 2 of appendix C for the following regression equation:

$$(f_c')^{1/2} = -11.3768 + 7.3002*R + 10.7674*H + 14.8604*G \dots \dots (15)$$

where:

$f_c'$ = cube compressive strength, psi (1000 psi = 6.9 MPa)
R = sawcut rating
H = coarse aggregate hardness
    soft = 0
    hard = 1
G = coarse aggregate geometry
    round = 0
    crushed = 1

Cement content is not significant. The coefficient of determination is 0.796. The "round soft" coarse aggregate type was not part of the slab sawing study. Effects of this aggregate type should be further investigated since the dummy variables for aggregate hardness and geometry only account for qualitative not quantitative effects on cube compressive strength. For individual mixes the cube mortar strength correlated well with cylinder compressive strength. Individual mix regression analysis of cube strength on cylinder compression strength resulted in coefficients of determination ranging from 0.869 to 0.993. Since mortar cube and concrete cylinder compressive strengths were highly correlated a multiple linear regression analysis of compressive strength on aggregate hardness, geometry, cement content, and sawcut rating was conducted. Equation 16 for concrete cylinder compressive strength better describes (higher R-squared) the effect of compressive strength than equation 15 relating the same factors to compressive mortar cube strength.

Sawcut Ratings and Concrete Strength Required for Sawcuts. Sawcut ratings and companion test results showing promise for being indicators of slab readiness for sawing can be correlated by the following regression equation:

$$(f_c')^{1/2} = 13.9432 + 5.1931*R + 8.7086*H +$$
$$5.4198*G - 0.0263*C \dots \dots \dots \dots \dots \dots \dots \dots \dots (16)$$

where

$f_c'$ = average concrete compressive strength, psi (1000 psi = 6.9 MPa)
R = sawcut rating
H = coarse aggregate hardness
    soft = 0
    hard = 1
G = coarse aggregate geometry
    round = 0
    crushed = 1
C = cement content, lb/yd$^3$ (500 lb/yd$^3$ = 297 kg/m$^3$)

Equation 16 relates sawcut rating, compressive strength, concrete coarse aggregate shape and hardness, and cement content. The coefficient of determination, for equation 16 is 0.917. Curves showing the best fit equation for a range of mixes are presented in figure 77. The curves indicate that required concrete strengths to produce sawcuts with acceptable or

154
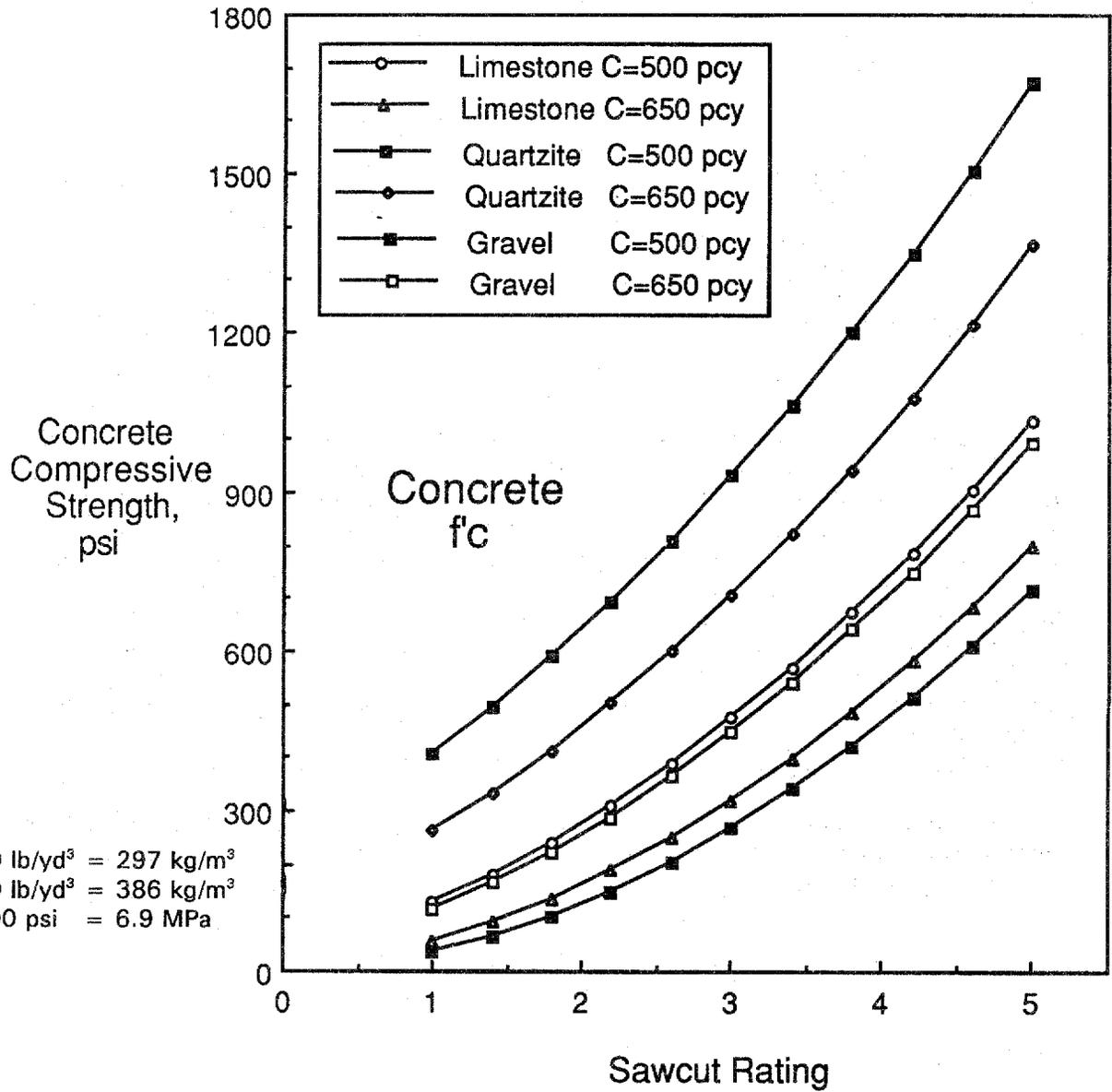
Figure 77. Sawcut rating vs. concrete compressive strength.

better ratings are greater for mixes made with 500 lb/yd³ (297 kg/m³) of cement than those made with 650 lb/yd³ (386 kg/m³) of cement. The "round soft" coarse aggregate type was not investigated in the slab sawing study. Effects of this aggregate type should be further investigated since the dummy variables for aggregate hardness and geometry only account for qualitative not quantitative effects on concrete compressive strength.

Equation 16 was used to generate required concrete compressive strengths for producing acceptable (rating 3) and good (rating 4) sawcuts. These required strengths are listed in table 46 for a range of concrete mix constituents. The required strength range to produce acceptable or good sawcuts between 500 and 650 lb/yd³ (297 and 386 kg/m³ ) of cement for a given coarse aggregate geometry and hardness can be attributed to amount of cement past volume. If the amount of paste volume is set proportional to cement weight/yd³, then a ratio of 500 to 650 or a 0.769 paste volume adjustment factor can be considered for adjusting strength requirements for sawcutting. For example, the concrete mix produced with crushed hard coarse aggregate and 500 lb/yd³ (297 kg/m³) of cement listed in table 46 had a required 930-psi (6.4-MPa) strength for making an "acceptable" (rating 3) sawcut. To normalize the required strength by paste volume referenced to 650 lb/yd³ (386 kg/m³) cement content, the 930 psi (6.4 MPa) is multiplied by the paste volume adjustment factor to adjust required strength for the lesser paste volume. This produces the 715-psi (4.9-MPa) required strength in table 47. Similar adjustments as indicated in table 47 to account for the reduced 500-lb/yd³ (297-kg/m³) mix paste volume will significantly narrow the spread between strength requirements for 500- and 650-lb/yd³ (297- and 386-kg/m³) mixes observed in figure 77.

## HIGHWAY PAVEMENT SAWCUTTING OBSERVATIONS

To verify and test the joint sawing criteria for earliest joint sawcutting and selected nondestructive test methods 3 field sites were selected. The selected sites were near Fort Dodge, Iowa; Tremonton, Utah; and Wisconsin Dells, Wisconsin.

For the Iowa and Utah sites, the temperature data from pavement slabs were used for estimating strength development and also to calculate pavement restraint stresses.

### Project Details

Details of the 3 sites are summarized in table 48. Sites were selected to evaluate numerous variables on joint sawcutting.

### Sawcutting Details

Differences between the sites which were of interest in evaluating sawcutting are summarized in table 49. Mix design data are summarized in tables 33 through 35 of appendix D.

Iowa Route 169. Approximately 500 lineal ft (153 m) of paving were monitored August 14, 1990. Paving was observed from approximately 10:30 a.m. to 12:30 p.m. Compressive strength development at 23 joints was monitored using the Clegg Impact Hammer tester and the ultrasonic pulse velocity methods. Two joints were selected for temperature monitoring. Concrete compressive strength was monitored using the time-temperature maturity method. Cylinder pulse velocity and maturity were also evaluated at the 2 joint locations.

**Table 46. Required compressive strength for acceptable ratings for different mixes.**

| Aggregate Geometry | Aggregate Hardness [2] | Cement Content, lb/yd [3] | Sawcut Rating [1] | |
|---|---|---|---|---|
| | | | 3 | 4 |
| Crushed | Soft | 500 | 480 | 730 |
| | | 650 | 320 | 530 |
| Crushed | Hard | 500 | 930 | 1270 |
| | | 650 | 700 | 1010 |
| Rounded | Soft | 500 | 270 | 470 |
| | | 650 | 150 | 310 |
| Rounded | Hard | 500 | 630 | 920 |
| | | 650 | 450 | 690 |

NOTES:

[1]   Rating "3" = acceptable if sealant reservoir is to be widened
    Rating "4" = good
    Minimum compressive strength in psi.

[2]   Estimated "rounded soft" aggregate-type required strength from qualitative dummy variable regression analysis. Aggregate type not investigated in sawing study.

500 lb/yd$^3$ = 297 kg/m$^3$, 650 lb/yd$^3$ = 386 kg/m$^3$, 1000 psi = 6.9 MPa

**Table 47. Required compressive strength for acceptable ratings for different mixes (normalized for paste volume).**

| Aggregate Geometry [3] | Aggregate Hardness | Cement Content, lb/yd [3] | Sawcut Rating [1] | |
|---|---|---|---|---|
| | | | 3 | 4 |
| Crushed | Soft | 500 [2] | 370 | 560 |
| | | 650 | 320 | 530 |
| Crushed | Hard | 500 [2] | 715 | 980 |
| | | 650 | 700 | 1010 |
| Rounded | Soft | 500 [2] | 210 | 360 |
| | | 650 | 150 | 310 |
| Rounded | Hard | 500 [2] | 480 | 710 |
| | | 650 | 450 | 690 |

NOTES:

[1]   Rating "3" = acceptable if sealant reservoir is to be widened
Rating "4" = good
Minimum compressive strength in psi.

[2]   Reduce table 46 500-lb cement content strengths by cement reduction factor 0.769 (500 to 650 cement content ratio).

[3]   Estimated "rounded soft" aggregate-type required strength from qualitative dummy variable regression analysis. Aggregate type not investigated in sawing study.

500 lb/yd$^3$ = 297 kg/m$^3$, 650 lb/yd$^3$ = 386 kg/m$^3$, 1000 psi = 6.9 MPa

**Table 48. Joint sawcutting project description.**

| | Iowa | Utah | Wisconsin |
|---|---|---|---|
| Project | U.S. Highway 169 | Interstate 15 | Interstate 94 |
| Location | Webster County | Box Elder County | Sauk County |
| Cement Content, lb/yd$^3$ | 487 | 611 | 530 |
| Slab Thickness, in | 10 in | 10 in | 12 in |
| Lane Width | 12 and 14 ft (truck) | 12 ft | 12 and 14 ft (truck) |
| Shoulder | 10 in asphalt | 4 and 10 ft x 10 in concrete | 4 and 8 ft (truck) asphalt |
| Base Course | 6-9 in granular | 4 in LCB over granular layer | 4 in open graded |
| Transverse Joints | 20 ft skewed | 15,11,10,14 ft skewed | 13,19,18,12 ft skewed |
| | 1-1/4 dia. dowels at 12 in | aggregate interlock | 1-1/2 dia. dowels at 12 in |
| | 3/8 in x 3-1/3 in (measured) | 1/8 in x 3-1/3 in (min.) | 1/8 in x 3 in |
| | Abrasive blade, no widening | 3/8 in wide second cut | - |
| Longitudinal Joints | 3/8 in x 3-3/4 in (measured) | 1/8 in x 3-1/3 in (min.) | Plastic parting strip at 4 in |
| | #5 tie bars at 36 in | #5 tie bars at 30 in | #4 tie bars at 24 in |

1 in = 25 mm, 10 ft = 3.1 m, 100 lb/yd$^3$ = 59 kg/m$^3$

159

**Table 49. Field study sawcutting variables.**

| | Iowa | Utah | Wisconsin |
|---|---|---|---|
| Coarse Aggregate Type | crushed limestone | crushed granite and quartzite | crushed limestone virgin and recycled |
| Max. Air Temp., °F | low 80's | low 90's | low 70's |
| Max. Concrete Temp., °F | 105 | 118 | 98 |
| Absolute Air Humidity | high | low | medium |
| Cement Content, lb/yd$^3$ | 487 | 611 | 530 |
| Paving Date | mid-August | late-August | early-October |
| Sawing Time | early p.m. | early a.m. and p.m. | early to late p.m. |
| Sawblade | abrasive | diamond | diamond |
| Sawing Equipment | walk behind | spansaw | walk behind |
| Slab Thickness, in | 10 | 10 | 12 |
| Joint Type | dowels | aggregate interlock | dowels |
| Subbase | granular | lean concrete | granular |

NOTE: 30 in from slab edge at sawcut depth.

10 in = 25 cm, 100 lb/yd$^3$ = 59 kg/m$^3$, °C = 5/9(°F-32)

Sawcutting with 3/8-in (10-mm) wide abrasive blades mounted on 65-horsepower (48-kW) walk-behind saws was done at ages ranging from 6.1 to 7.6 hours. Weather between concrete placement and sawcutting was sunny with gusting winds, and air temperatures ranged from the upper 70's to mid 80's. The sawcutting was simultaneously done with 2 saws cutting transverse joints at 20-ft (6.1-m) joint spacing and 1 saw for the longitudinal centerline joint. Blades were, with wear, frequently changed to maintain an approximately 3-3/4-in (10-cm) deep cut. Sawing was initiated and stopped at the discretion of the sawing crew superintendent.

Utah I-15. Approximately 1700 lineal ft (519 m) of pavement were evaluated August 24, 28, and 29, 1990. Sawcutting at 74 joints was observed and compressive strength evaluated at moment of cutting. Twelve joints were also selected to monitor compressive strength development between placement and sawcutting using the 3 nondestructive testing methods. Four joints were selected for temperature monitoring. Compressive strength was monitored using the maturity method. Cylinder pulse velocity and maturity were also evaluated at 3 of the 4 joint locations.

Sawcutting was observed in the early morning (7:00 - 9:00 a.m.) for paving placed between 10:00 p.m. and 12:00 a.m. Observations were made in the early afternoon (12:00 - 2:00 p.m.) and early evening (5:30 - 7:00 p.m.) for paving placed between 8:00 a.m. and 1:00 p.m. Daylight air temperatures ranged from the low 60's to mid 90's during paving observations. Weather was mostly sunny, slightly windy, with low humidity during sawcutting. Saw-cutting was done with diamond impregnated blades. Transverse joint sawcutting was done with a spansaw. Longitudinal shoulder and centerline joints were simultaneously sawed with 65-horsepower (48 kW) saws mounted on self-propelled buggies. Buggie saws were interconnected with a steel channel framework. Sawing was initiated and stopped at the discretion of the sawing crew superintendent.

Wisconsin I-94. Sawcutting observations were made over 1360 lineal ft (415 m) of paving at the Wisconsin project on October 2, 1990. Strength development was monitored at 23 joints using nondestructive test methods. Clegg Impact Hammer and ultrasonic pulse velocity readings were done at all 23 joint locations. Three joints were selected for temperature monitoring. Cylinder maturity was also done at all 3 joints. Pulse velocity monitoring was done on 1 cylinder and 1 maturity joint.

Paving was observed between 7:00 a.m. and 12:00 p.m. Sawcutting was done between 7:00 and 10:00 p.m. Weather during paving was partly sunny, no wind, and air temperatures ranged from the upper 40's to mid 70's. Transverse joint sawcutting was done with two 65-horsepower (48-kW) walk-behind saws. Use of a plastic parting strip eliminated the longitudinal centerline sawcut.

## Companion Testing Results and Control Joint Observations

The Clegg Impact Hammer tester, concrete maturity (ASTM C 1074-87), and ultrasonic pulse velocity (ASTM C 597-83) methods were used to monitor compressive strength development. As summarized in table 46, concrete compressive strength can be used as an indicator for earliest time for sawcutting joints. Compressive strengths from Clegg Impact Hammer readings were estimated using the laboratory developed relationship (equation 14).

Separate models for each project were developed for estimating compressive strength from either pulse velocity or concrete maturity. Similar to the early age (4 to 24 hours) laboratory study, concrete temperatures were recorded every half hour for 24 hours.

161

Concrete maturity using the time-temperature Nurse-Saul function was calculated at 30 minute intervals. A datum temperature of 32 °F (0 °C) was assumed for all 3 projects. Similar to the early age analysis reported in chapter 3, the log of compressive strength can be predicted from the inverse of the Nurse-Saul maturity. The log of compressive strength can be predicted from pulse velocity. This model form is the same as those developed in the early age (4 to 24 hours) laboratory study reported in Chapter 3.

For the Iowa joint sawing study, the compressive strength prediction models were established in the laboratory using job site aggregates, cement, and fly ash. Thirty-seven 6- by 12-in (15- by 30-cm) cylinders were tested at ages ranging from 5 hours to 31 days. Testing at ages greater than 12 hours was done to establish relationships used in the analysis of construction traffic loading discussed in Chapter 6. Evaluation of Early Concrete Pavement Loading.

For the Utah compressive strength relationships, models were developed from 24 6- by 12-in (15- by 30-cm) cylinders fabricated and tested at the batch plant. Cylinders were stored, until tested, in an on-site semi-controlled air conditioned room with temperatures maintained at approximately 70 °F (21 °C). After 1 week the remaining cylinders were shipped back to Illinois and stored at 72 °F (22°C) moist curing conditions until tested. Twenty-four cylinders from the batch plant and 4 cylinders used to monitor concrete maturity during joint sawing observations were tested using a manually operated hydraulic cylinder testing machine. Testing was done at ages ranging from 8 hours to 4 days. Similar to the Iowa data analysis, testing at ages greater than 24 hours was done to establish relationships used in the analysis of construction traffic loading discussed in chapter 6. Due to lack of temperature data when cylinders were left at the batch plant and shipped back to Illinois, 2 maturity models were developed. The early age joint sawing model used temperature data less than 24 hours. Temperature data was recorded every 30 minutes during the initial 24 hour period. After 1 day, the cylinders were stored in the semi-controlled room. Since the temperature data logger was required at the joint sawing and load testing sites, no temperature data was recorded at ages greater than 1 day. The second maturity model developed used maturity data greater than 1 day. A constant curing temperature of 70 °F (21 °C) was assumed from 1 through 41 days. A single pulse velocity model for ages through 41 days was developed since temperature and age do not significantly increase the predictive power in compressive strength estimation.

For the Wisconsin compressive strength development model, 39 6- by 12-in (15- by 30-cm) cylinders were fabricated and tested using the portable compression testing equipment. Similar to the Utah study, cylinders were fabricated and stored either at the joint sawing observation sites or at the batch plant. Temperature for cylinder maturity was recorded at 30 minute intervals for the first 24 hours. From 24 to 48 hours the cylinder temperature was either automatically or manually recorded (using digital thermocouple meters) approximately every hour. After 2 days, the remaining cylinders were transported back to the lab and stored at 72 °F (22 °C) moist curing. Compressive strength and pulse velocity tests were done at ages ranging from 5 hours to 28 days. Although no load testing was done at the Wisconsin project, prediction models necessary for analysis of early loading effects were developed.

Companion Test Results. Pulse velocity and maturity models developed are summarized in table 50. Data for prediction models are summarized in tables 36 through 38 of appendix D. Resulting standard error of estimates and coefficients of determination are similar to those reported in chapter 3. Early Age Concrete Properties From Laboratory Tests. With the exception of the Utah maturity model, all models cover a strength range larger than that required for joint sawcutting. As discussed in chapter 6, models also were required for analysis of early loading criteria. Due to limitations on fabricating, storing, transporting,

**Table 50. Summary of the regression equations.**

| State | Dep. [2,3] Variable, Y | Ind. [2,6] Variable, X | Coefficient, a | t-stat. | Constant, b | R - sq. | SEE [7] | No. of Points |
|---|---|---|---|---|---|---|---|---|
| Iowa | log(f'c) | PV/1000 | 0.302 | 37.65 | -0.933 | 0.977 | 0.0838 | 35 |
| | log(f'c) | 1/MAT | -415.706 | 49.41 | 3.885 | 0.989 | 0.0639 | 30 |
| Utah | log(f'c) | PV/1000 | 0.291 | 36.29 | -0.514 | 0.984 | 0.0540 | 23 |
| | log(f'c)[4] | 1/MAT | -1442.926 | 8.89 | 4.955 | 0.929 | 0.0644 | 8 |
| | log(f'c)[5] | 1/MAT | -818.747 | 27.87 | 3.822 | 0.979 | 0.0316 | 19 |
| Wisconsin | log(f'c) | PV/1000 | 0.289 | 28.46 | -0.614 | 0.960 | 0.0867 | 36 |
| | log(f'c) | 1/MAT | -357.239 | 25.27 | 3.650 | 0.948 | 0.0906 | 37 |
| All [1] | sqrt(f'c) | Clegg | 0.152 | 12.42 | 7.075 | 0.802 | 3.6337 | 40 |

NOTES:  [1]Equation 14 developed in sawing slab study.
[2]General equation form: $Y = aX + b$.
[3]f'c = compressive strength in psi.
[4]Developed using data for age less than or equal to 1 day.
[5]Developed using data for age greater than 1 day.
[6]PV = pulse velocity in ft/s, MAT = Nurse-Saul maturity in °F-hours.
 Clegg = Clegg Impact Hammer reading.
[7]SEE = standard error of estimate.

1000 psi = 6.9 MPa
°C = 5/9 (°F-32)
1000 ft/s = 305 m/s

and curing test specimens; the models developed cover both the joint sawing and early loading compressive strength ranges. For specific projects the development and use of separate models may increase the strength prediction accuracy.

Pulse velocity was measured on cylinders immediately prior to testing for compressive strength. Pulse velocity was determined on cylinders removed from the molds since it can be influenced by cylinder mold material. For instance, if the equipment is used on high grade structural steel, velocities can be as high as 19,000 to 20,000 ft/s (5795 to 6100 m/s). For early age concrete measured pulse velocities are on the order of 10,000 to 13,000 ft/s (3050 to 3965 m/s). Thus, pulse velocity measured on cylinders left in molds may be that of the mold rather than that of the concrete.

For the Utah project, disposable tin cylinder molds were used. Plastic disposable molds were used for companion testing at the Iowa and Wisconsin sites. To eliminate the relatively higher effects of metallic molds, all pulse velocity testing in Utah was made on cylinders removed from molds. For the Wisconsin project the effects of plastic cylinder molds were evaluated by testing 33 specimens with cylinders in the molds, stripping the cylinders, and then testing the cylinders without the molds. Mold bottom was approximately 3/32 in (2 mm) thick. Travel path decreased approximately 0.8 percent when tested without the molds. A linear regression of pulse travel time without molds on time measured in molds at ages ranging from 6 hours through 4 days indicated that an adjustment factor can be developed for mold effects. For the plastic molds used in Wisconsin, the measured travel time should be multiplied by a factor of 0.9746 (coefficient of determination 0.973) to account for plastic mold effects.

It is recommended that cylinders be removed from plastic cylinder molds prior to testing with pulse velocity. If tin or steel molds are used to evaluate pulse velocity, specimens must be removed prior to testing. If plastic molds are used and cannot be easily removed without specimen damage prior to pulse velocity testing, a correction factor should be established by testing with and without molds.

Slab Test Results. Compressive strength estimated using the equations in table 50 was calculated for all Clegg Impact Hammer, pulse velocity, and maturity data. Compressive strength at sawcutting estimated using the three NDT methods are summarized in table 51. Concrete temperatures for the slabs were recorded using the automatic data logger or were manually recorded using digital thermocouple meters. Temperatures were converted into maturity (32 °F, 0 °C datum temperature) to estimate compressive strength. Thermocouples for maturity data were positioned at approximately 2 in (5 cm) below the surface and 30 in (76 cm) from the slab edge.

Pulse velocity was measured by using the semi-direct transmission path. One transducer was positioned on the pavement surface 12 in (30 cm) from the slab edge. The second transducer was positioned approximately 2 to 3 in (5 to 8 cm) below the surface on the vertical edge. The actual depth was dependent on surface roughness. The transducer positions were marked so that the same path was used during strength monitoring. The vertical position of the transducer was recorded to accurately compute the angled path length used to calculate pulse velocity. Other path length pulse velocities were also calculated at 6, 12, 18, and 24 in (15, 30, 46, and 61 cm) from slab edge. These results, as reported in table 52, show that pulse velocity is sensitive to path length. As the total transducer path length (offset from edge) decreases from 12 to 6 in (30 to 15 cm), the transit time decreases at a larger percentage rate than the travel distance. As the travel path decreases, the pulse velocity and estimated compressive strength increases. For the Iowa and Wisconsin projects as the offset decreased from 12 to 6 in (30 to 15 cm) the estimated strength increased 108 and 57 percent, respectively. As the travel path increased from the 12-in (30-cm) off-

**Table 51. Summary of estimated compressive strengths at sawcutting.**

|  | Iowa | Utah | Wisconsin |
|---|---|---|---|
| Paving Date<br>Paving Length, ft | 14 Aug 90<br>500 | 24,28,29 Aug 90<br>1700 | 2 Oct 90<br>1360 |
| Average Age, hours<br>Minimum Age, hours<br>Maximum Age, hours | 6.8<br>6.1<br>7.6 | 9.1<br>8.4<br>9.6 | 10.9<br>9.8<br>11.7 |
| Average Rating<br>Minimum Rating<br>Maximum Rating | 3.4<br>2.7<br>5.0 | 4.2<br>2.1<br>5.0 | 4.3<br>2.8<br>5.0 |
| No. Clegg Joints<br>Average f'c, psi [1]<br>Min. f'c, psi<br>Max. f'c, psi | 23<br>653<br>415<br>1036 | 74<br>787<br>478<br>1278 | 23<br>401<br>294<br>567 |
| No. PV Joints<br>Average f'c, psi [2]<br>Min. f'c, psi<br>Max. f'c, psi | 23<br>498<br>215<br>996 | 74<br>910<br>250<br>1746 | 23<br>310<br>137<br>485 |
| No. MAT Joints<br>Average f'c, psi [3]<br>Min. f'c, psi<br>Max. f'c, psi | 2<br>823<br>690<br>956 | 4<br>213<br>154<br>303 | 3<br>773<br>760<br>788 |

NOTES:  [1] Clegg Hammer estimated compressive strength.

[2] Pulse velocity estimated compressive strength.

[3] Nurse-Saul maturity estimated compressive strength.

1000 ft = 305 m, 1000 psi = 6.9 MPa.

**Table 52. Effects of path length on pulse velocity.**

| Project | Number of Joints Tested | No. of Tests | Maximum Age, h | Ave. f'c at 12 in Path, psi | Max. f'c at 12 in Path, psi | Path Distance Ratio, in to in | PV Ratio, percent | f'c Ratio, percent |
|---|---|---|---|---|---|---|---|---|
| Iowa | 23 | 93 | 8.4 | 360 | 960 | 6 to 12 | 113 | 208 |
| Utah | 10 | 56 | 11.1 | 560 | 1740 | 24 to 12 | 76 | 60 |
| Wisconsin | 23 | 51 | 11.7 | 210 | 480 | 6 to 12 | 107 | 157 |

10 in = 25.4 cm

set, the velocity and estimated strength decreases. For the Utah project as the path increased from 12 to 24 in (30 to 60 cm) the estimated strength decreased 40 percent. Similar results are noted on cylinders and beams tested in Iowa where at early ages the computed velocities increase with decreases in travel distance. Since the developed models are based on 12-in (30-cm) cylinder travel paths, the slab compressive strength should also be estimated using the 12-in (30-cm) edge offset transducer position. For the transducer positioned on the vertical slab edge 2.5 in (6 cm) from the surface, the diagonal travel path is 12.5 in (32 cm).

As summarized in table 51 for Wisconsin and Iowa data, the Clegg Impact Hammer compressive strength was significantly higher on average than corresponding pulse velocity data. The Utah data showed higher average strengths estimated using the pulse velocity method. Differences in average strength estimated using the Clegg and pulse velocity method ranged from 91 to 155 psi (627 to 1069 kPa) and averaged 123 psi (848 kPa) for the 3 projects. Differences can be attributed to the general model developed in the sawing strip laboratory study, relatively poorer degree of correlation (lower R-squared on prediction model), and the use of impact resistance of the slab surface that may not be a consistent measure of cylinder compressive strength.

Due to the limitations of temperature recorders, concrete maturity was monitored on only a few joints. Therefore, the average strength should not be directly compared to the average pulse velocity strength reported in table 51. The maturity estimated strengths are later discussed when the calculation of restraint stresses are addressed in Chapter 5. Investigation of Latest Joint Sawcutting.

Slab and Cylinder Test Comparison. Compressive strengths of cylinders and slabs using all 3 NDT methods were monitored at a total of 9 joints for the 3 projects. Compressive strengths estimated from Clegg Impact Hammer readings (slab only), pulse velocity, and maturity at time of sawcutting are listed in table 53. Differences between compressive strength of slabs and cylinders ranged from 0 to 262 psi (0 to 1.8 MPa) excluding the Wisconsin site pulse velocity data. Average absolute difference between slab strengths and cylinder strength was 132 psi (910 kPa).

For the Wisconsin data, cylinder pulse velocity and maturity compressive strength was always greater than slab strengths. Due to cooler air temperatures, use of black plastic molds on a sunny day, and relatively low initial concrete temperatures; the estimated cylinder strengths were higher than slab strengths. Maximum near surface concrete temperatures, 30 in (76 cm) from edge, ranged from 81 to 84 °F (27 to 29 °C). Maximum cylinder temperatures at the same location ranged from 96 to 103 °F (36 to 39 °C).

Similar to the Wisconsin data, the estimated cylinder compressive strength in Iowa was higher than the corresponding slab strength. Maximum slab temperatures for the 2 joints monitored were 104 and 101 °F (43 and 38 °C). Corresponding cylinder temperatures were 109 and 100 °F (43 and 38 °C). Differences in temperature as well as in estimated strengths were significantly smaller than the Wisconsin differences. The differences in cylinder and slab strengths can be attributed to the temperature history as well as maximum temperatures. Temperature plots with time are illustrated in chapter 5. Investigation of Latest Joint Sawcutting.

For the Utah project the pulse velocity strength measured on the slab was larger than the cylinder strength. The reverse was true for maturity estimated strengths. Since accumulated temperatures were slightly higher for cylinders, the pulse velocity estimated cylinder strength should also be higher than slab strengths. The lower cylinder strength from pulse velocities may be explained by considering the increase in pulse velocity (increase in

**Table 53. Comparison of three nondestructive estimated strengths.**

| Project | Station | Joint Number | Clegg Slab f'c, psi | Pulse Velocity f'c, psi | | | Nurse-Saul Maturity | | |
|---|---|---|---|---|---|---|---|---|---|
| | | | | Slab | Cylinder | Slab/Cyl Difference | Slab | Cylinder | Slab/Cyl Difference |
| Iowa | 375+50 | 3 | 650 | 650 | 656 | -6 | 956 | 1024 | -68 |
| | 372+70 | 17 | 520 | 270 | 495 | -225 | 685 | 727 | -42 |
| Utah | 2532+20 | 65 | 799 | 835 | 683 | 152 | 204 | 289 | -85 |
| | 2530+00 | 70 | 973 | 835 | 835 | 0 | 288 | 305 | -17 |
| | 2529+00 | 72 | 696 | 835 | **** | **** | 213 | **** | **** |
| | 2528+00 | 74 | 776 | 623 | 439 | 184 | 155 | 232 | -77 |
| Wisconsin | 152+50 | 6 | 438 | 325 | 1505 | -1180 | 760 | 981 | -221 |
| | 155+60 | 11 | 354 | 485 | **** | **** | 771 | 1020 | -249 |
| | 161+20 | 20 | 423 | 348 | **** | **** | 788 | 1050 | -262 |

Note: 1000 psi = 6.9 MPa

strength) with time at the time of joint sawing. At the time of joint sawing the temperature change (increase in maturity) is fairly constant. Cylinder pulse velocity with time for the Utah data were significantly increasing. Increase in pulse velocity strength with time were such that within 25 minutes after joint sawing the estimated cylinder strength would be approximately that of the slab strength at time of sawing. Based on trends in pulse velocity it appears that the rate in cylinder strength gain was faster than the rate of strength gain in the slab.

The comparison between companion cylinder and slab strengths indicate that if similar temperature histories (both magnitude and rate) are exhibited, estimated strengths are similar. If the temperature trends and magnitudes are significantly different, such as in the case of the Wisconsin data, significant errors can be introduced in estimating slab compressive strength with cylinders. Based on analysis of the slab and companion cylinder data, it is recommended that cylinders not be used in estimating slab strength unless common temperature histories can be assured.

Differences in slab strength estimates using the Clegg Impact Hammer and pulse velocity at the 9 joints listed in table 53 ranged from 0 to 250 psi (0 to 1724 kPa). Average difference (absolute value) was 115 psi (793 kPa) for the 9 joints. This is within the range of 91 to 155 psi (627 to 1069 kPa) average difference calculated for the 3 projects, as listed in table 51

Larger differences in strength listed in table 53 were estimated between both the Clegg and maturity and the pulse velocity and maturity test methods. The maturity estimated slab and cylinder strengths were significantly higher for the Wisconsin and Iowa projects but lower for the Utah project. Differences can mainly be attributed to the relatively small number of maturity cylinders tested. Due to limited testing facilities, manpower, and materials, only a limited number of maturity cylinders could be tested at early ages. As demonstrated in the early age (4 to 24 hours) laboratory study, maturity models can be developed which will predict early age compressive strength.

Control Joint Observations. Sawing was done with 65-horsepower (48-kW) walk-behind saws at the Wisconsin and Iowa project. In Utah, transverse joints were cut with a spansaw. The longitudinal centerline and shoulder joints were cut with buggie saws. The Iowa pavement joints were cut using abrasive saw blades.

Compressive strengths were estimated at joints at the time of sawing using the 3 nondestructive testing methods. Measurements of spalled and ravelled areas at sawcut joints were made shortly after cutting. These measurements and corresponding joint condition ratings were later correlated with each other.

Most spalling observed was at sawcut intersections. Intersecting sawcuts occur when longitudinal joint sawing crosses the sawed transverse joint. At the Iowa and Utah sites, longitudinal sawing was done immediately following transverse joint sawing. Use of a plastic insert strip in Wisconsin eliminated the longitudinal sawed joint. Spalling at joint intersections consisted of small corner breaks of mortar or aggregate dislodgement, generally less than 1/2-in² (3.3-cm²) area.

Intersecting sawcuts and minor spalling occurred at the Utah site when spansaw cuts overlap. Multiple blades on the spansaw, used to cut short segments, overlap to form a single cut joint. Due to slight shifting of equipment and/or alignment of the spansaw frame, cuts do not always coincide and hence small slivers of concrete can be formed. The dimen-

sions of concrete wedges are dependent on the degree of horizontal saw misalignment and when the operator raises the spansaw from the pavement. Some small thin wedges of broke off or may potentially break in the future.

Other types of noted distress occurred at sawcuts crossing relatively deep tine marks. Since joints were skewed, the angle of cut crossing tining marks tended to ravel small concrete wedges. These ravelled areas did not appear to be deeper than the tining marks and should not affect the overall future joint integrity. In Wisconsin the use of a weighted ribbon placed on the surface at the joint location prior to tining reduced subsequent sawcut ravelling. At joints where the sawcut did not coincide with the ribbon location, some ravelling at joints crossing deeper tining marks was observed.

Small minor amounts of surface joint ravelling were observed in Iowa. Ravelling due to the abrasive blade was minor and did not appear to extend deeper than the surface mortar layer. Use of the abrasive blades did require frequent replacement. As blade wear occurred the depth of cut was reduced. To maintain the specified minimum sawcut depth, joint depth and blade wear was frequently checked.

Cracking below sawed joints was noted the next day at the Iowa and Utah projects at all joints where sawcutting was observed. Joint depth and crack widths measured in Iowa are listed in table 39 of appendix D. For the 23 joints, crack widths at 2 days ranged from 0.002 to 0.050 in (0.05 to 1.3 mm) and averaged 0.011 in (0.3 mm).

Cracking observations at the Wisconsin site was not performed until 1 week later. Of the 50 joints surveyed in the area where joint sawcutting was monitored, only 29 joints were cracked. This may be attributed in part to the fact that for the 12-in (30-cm) thick pavement, sawcut depth was only 25 percent of slab thickness. Another contributing factor could be the relatively cooler weather during paving. The larger temperature drops in Iowa and Utah during the first night after paving help induce cracking at all joints. Crack widths in Wisconsin ranged from 0.010 to 0.190 in (0.25 to 5 mm) and averaged 0.090 in (2.3 mm) at the time of survey. Crack widths were significantly larger than those in Iowa, where all the joints were active. This points out the importance of inducing cracking uniformly among all joints to maintain load transfer effectiveness and extend sealant life. Joint crack widths and surface condition data for the Wisconsin project are listed in table 40 of appendix D.

## Sawcut Joint Ratings and Compressive Strength

Results of field observed joint ravelling from sawcutting operations and nondestructive compressive strength testing were compared to data from the laboratory sawing strips. Amount of joint ravelling, subjective sawcut joint acceptability ratings, and compressive strengths (as a function of aggregate hardness and cement content) were investigated in the full-scale sawing strip tests. Results of the petrographic examinations on cores through sawcuts indicated that if no major surface ravelling is observed there is only minor paste and erosion damage resulting from early sawing of concrete with incompletely hydrated cement. The petrographic report also states that the small amount of observed erosion should not affect the integrity or durability of concrete adjacent to the sawcuts.

Measurements of ravelled areas and corresponding compressive strength estimates at time of sawcutting for the Iowa, Utah, and Wisconsin studies are summarized in tables 41

through 43 of appendix D, respectively. Ratings of each sawcut were back-calculated from measured surface distress using equation 12. Ratings based on measured sawcut surface distress were defined as follows:

Rating = 1 - Badly spalled.
Rating = 2 - Unacceptable.
Rating = 3 - Acceptable if sealant reservoir widening is done.
Rating = 4 - Good.
Rating = 5 - Excellent.

Joint sawcut ratings for Iowa ranged from 2.7 to 5.0 and averaged 3.4 for the 23 joints surveyed. Compressive strength sawcutting estimated from pulse velocity for the crushed limestone mix ranged from 200 to 1000 psi (1.4 to 6.9 MPa) and averaged 500 psi (3.4 MPa) at the time of sawing. As previously discussed, most observed surface distress at sawcuts in Iowa was due to sawing at skewed angles to tine marks and consisted of minor surface ravelling extending no deeper than the surface mortar layer. If shallow edge ravelling distress is excluded, since the overall future joint integrity should not be affected, the average rating in Iowa increased to approximately 4.0.

For the Utah study, the sawcut ratings ranged from 1.9 to 5.0 and averaged 4.1 for the 74 joints surveyed. Most surface distress occurred where the multiple blades on the spansaw, used to cut short segments, overlapped at a slight angle causing small wedge shaped slivers of concrete to break off. If this distress due to equipment operation rather than material properties is excluded, the joint ratings would be slightly better. Pulse velocity estimated compressive strength at the time of sawing at the Utah site ranged from 250 to 1750 psi (1.7 to 12.1 MPa) and averaged 910 psi (6.3 MPa).

For the Wisconsin data, approximately every fourth joint was monitored for compressive strength development. The compressive strengths for the previous joint and the 2 joints ahead were considered as 1 test location. The compressive strength monitored at 1 joint was assumed representative of the 4 joint samples. The condition survey ravelling areas and ratings reported in table 43 of appendix D reflect 4 transverse joints. Ratings for Wisconsin were similar to those in Iowa. Sawcut condition ratings ranged from 2.8 to 5.0 and averaged 4.3 for the 23 areas (4 joints per sample) surveyed. Pulse velocity estimated compressive strength at the time of sawing ranged from 140 to 485 psi (0.7 to 3.3 MPa) and averaged 310 psi (2.1 MPa). Most observed spalling occurred at the skewed joints where the sawcut deviated from the untined surface strip (produced with a weighted ribbon placed on pavements at contraction joint alignments prior to tining operation).

Compressive strength at the time of sawcutting was estimated in the field studies using nondestructive test methods. Compressive strength corresponding to the back-calculated rating (from spall/ravelling areas) at each joint was also calculated using equation 16. Compressive strength as a function of rating, coarse aggregate geometry, coarse aggregate hardness, and cement content was calculated for each joint. Required minimum compressive strength (sawing strip model) for observed rating was calculated and listed in tables 41 through 43 of appendix D.

As previously discussed, the maturity estimated strength model can be improved if enough cylinders are used in the correlation. The Clegg Impact Hammer estimated compressive strengths were on average within the range of strengths estimated by the pulse velocity method. Clegg Hammer strength differences were mainly attributed to using an equation developed in the laboratory sawing strip study with a relatively low prediction

equation coefficient of determination. Both the Clegg Hammer and maturity nondestructive test methods to estimate compressive strength can be improved with increased data and verification.

Pulse velocity field estimated compressive strength was selected for comparison with laboratory full-scale sawing strip data. Pulse velocity strength was selected as representative of slab strength due to:

- Good laboratory and field developed compressive strength models over a wide strength range.

- Less sensitive than the maturity method to effects of solar radiation.

- Indicative of compressive strength rather than Clegg Impact Hammer (surface) strength.

- Larger amounts of available data (compared to maturity).

- Relatively lower percentage of within-test variance than Clegg Impact Hammer tests.

- Project specific model rather than the general (all lab mixes) Clegg Impact Hammer model developed.

The pulse velocity estimated compressive strengths at sawcutting versus ratings back-calculated from ravelled areas are shown in figures 78 through 80 for the Iowa, Wisconsin, and Utah projects, respectively. The sawcut ratings are based on surface distress area measurements correlated in the laboratory sawing strip investigation. If the laboratory model could perfectly relate compressive strength, surface sawcutting distress, coarse aggregate hardness, and cement content; the pulse velocity strength would be equal to the corresponding surface distress rating. As shown in figures 78 through 80, the majority of the ratings data is above the predicted rating. This indicates that the laboratory compressive strength-sawcut rating model is somewhat conservative. The resulting sawcut surface rating was generally less than what the laboratory model would predict given the compressive strength. For the Iowa, Utah, and Wisconsin field studies, 83, 68 and 100 percent of the joints, respectively, could be cut at a lower strength than that predicted by the sawing strip model.

Of the joints with ratings of less than 5 the laboratory developed rating model over-estimated (higher than measured rating) by more than one-half a rating point 4, 0, and 36 percent of the joints for the Iowa, Wisconsin, and Utah projects, respectively. Of the 13 joints in Utah where the rating model overpredicted the observed surface ravelling, 7 corresponded to joints where deep tine marks were broken off or where the spansaw blade overlapped at a slight angle. Distress at these joints was caused by equipment rather than material properties. Excluding these 7 joints, the percentage of overestimated ratings for the Utah project decreases from 36 to 26 percent. Average overestimation of surface ratings was 0.8 and 1.3 for the Iowa and Utah projects, respectively.

The laboratory rating and strength correlation model was somewhat conservative when applied to field observations. Excluding joints in Utah where equipment rather than strength properties influenced observed ravelling and ratings, most data in figures 78 through 80 lie above the ratings model.
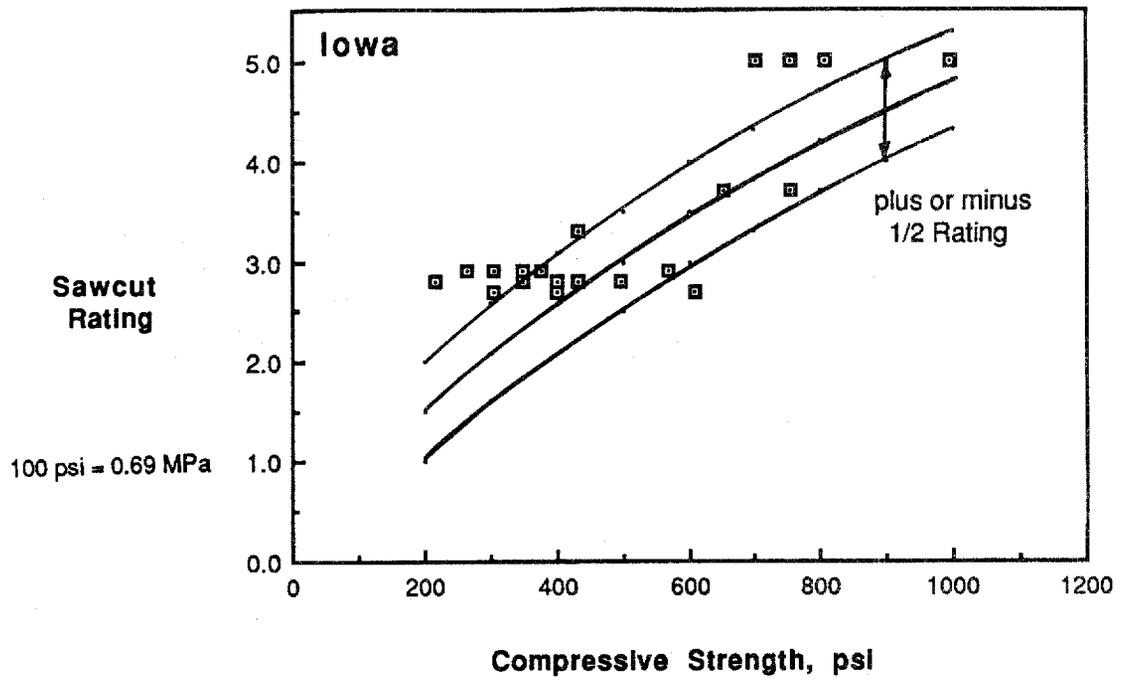
Figure 78.   Field study of compressive strength vs. sawcut rating in Iowa.
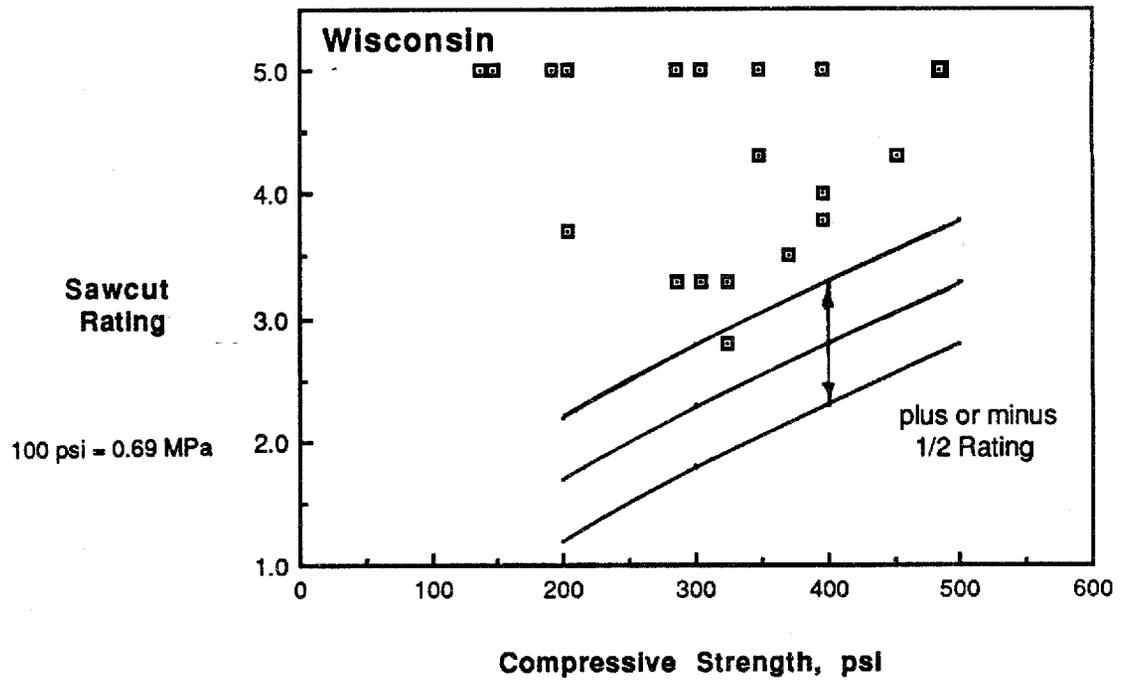


Figure 79.   Field study of compressive strength vs. sawcut rating in Wisconsin.

173
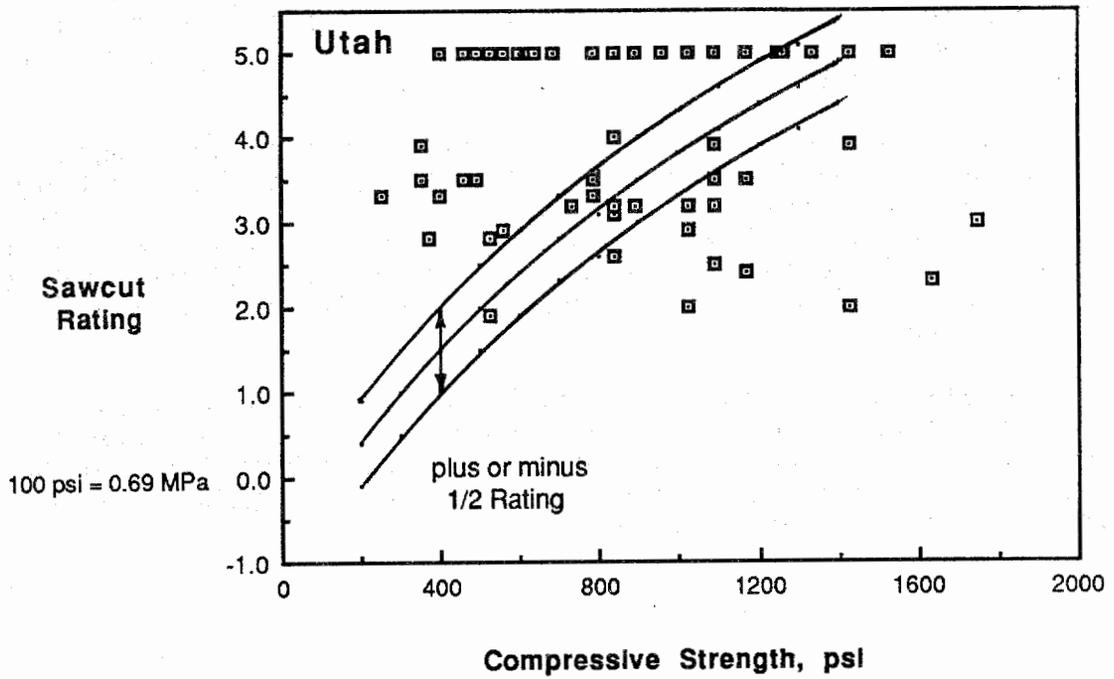
Figure 80.  Field study of compressive strength vs. sawcut
rating in Utah.

## SUMMARY OF EARLIEST JOINT SAWCUTTING

Full-scale sawcutting tests were made to investigate the strength required for earliest joint sawcutting. Sawcuts were made at increasing strengths to produce joints with various quantities of surface ravelling. Petrographic examination of sawed joint faces revealed that if no surface spalling, ravelling, or cracking is observed; minimal erosion of paste and mortar occurs. The small amount of erosion should not affect the integrity or durability of concrete adjacent to the sawcuts.

A relationship between ravelled area per unit length and expert panel joint ratings was established. A second relationship between concrete compressive strength, rating, aggregate hardness, aggregate geometry, and cement content was also derived. Minimum required strengths for acceptable and good ratings were established.

The joint rating and compressive strength model was evaluated at 3 paving projects. Compressive strength relationships between concrete maturity, pulse velocity, and Clegg Impact Hammer were developed and demonstrated. Measured joint ravelling was used to calculate joint ratings as developed in the laboratory investigation. Compressive strength estimated using pulse velocity data at time of sawing indicated that the laboratory model is conservative. For a given compressive strength, the predicted rating of surface distress is lower than observed in the field.

Equations 12 and 16 can be used in initially setting guidelines for minimum compressive strengths which must be achieved in the field prior to sawing. As discussed further in Chapter 8. Guidance Recommendations for Timing of Control Joint Sawcutting, adjustments may be required during construction to account for changes in visual joint distress, mix design, and sawcutting production rates.

# CHAPTER 5. INVESTIGATION OF LATEST JOINT SAWCUTTING

Joint sawcutting must be done after the concrete has developed enough strength to prevent ravelling and before the slab restraint stresses exceed the concrete tensile and flexural strength. Axial restraint stresses resulting from average slab temperature changes develop due to frictional resistance between slab bottoms and subbase or subgrade surfaces. Bending restraint stresses are due to differences between slab surface and slab bottom temperatures. When the combination of axial restraint and bending restraint stresses exceed the concrete strength, slab cracking occurs. If joints are not cut deep enough or not soon enough random cracking will occur.

As discussed in chapter 2, observations of cracking occurring in slabs installed at exterior locations and in beams under controlled laboratory conditions indicate that cracking occurs when surface cooling from maximum concrete temperature during early hydration exceeds about 15 °F (8 °C). At the time of slab cracking near top surface temperature was about equal to slab bottom. However, the top surface was about 7 °F (4 °C) cooler than slab mid-depth. Calculated curing restraint stresses due to the temperature gradient exceeded the concrete tensile strength when cracking was observed. The 7 °F (4 °C) differential occurred when the surface temperature dropped by approximately 21 °F (12 °C). To minimize potential for cracking it was recommended that surface temperature cooling in excess of 7 to 10 °F (4 to 6 °C) should be avoided.

Field site temperature data were used to investigate strength development and compared to calculated restraint stresses. Temperature data were recorded for about 12 hours from concrete placement at the Utah site, about 10 hours at the Iowa site, and about 14 hours at the Wisconsin site. The recorded temperatures are shown in figures 81 and 82 for Utah and Iowa concrete pavements. Slab surface temperatures were measured by placement of a thermocouple weighted with a wood block on the slab surface. Thermocouples were also positioned at 2 in (5 cm) below slab surface approximately 30 in (76 cm) from the edge, at slab mid-depth and near slab bottom at the slab edge. Thermocouples were also placed at the interior of concrete cylinders stored at side of pavement slabs. Ambient temperatures were monitored with a thermocouple located near pavement edge. The bottom of slab thermocouple at the Iowa site provided inconsistent temperature data and was not analyzed. Temperature data were used to calculate pavement restraint stresses. Slab bottom versus slab surface temperature differences needed to cause cracking below sawcut notches were calculated by balancing concrete tensile strength with sum of restraint stresses.

Temperatures monitored at 3 joints at the Wisconsin project did not show significant temperature fluctuation for the first 14 hours after placement. Maximum temperature difference between top and mid-depth was less than 7.5 °F (4 °C). Average temperature difference for the 3 joints monitored ranged from 3.2 to 3.8 °F (1.8 to 2 °C). Small temperature differentials within the slab did not cause high restraint stresses to initiate cracking below sawcut notches. The low thermal restraint stresses during the first night when split tensile strength is lowest and temperature decrease is relatively high, was in part confirmed by the lack of joint cracking observed 1 week after construction. As discussed in chapter 4, of the 50 joints surveyed only 29 joints were cracked. Crack widths averaged 0.090 in (2.3 mm) and were significantly larger than those measured at the Utah and Iowa projects where all joints were active within 24 hours of sawing.
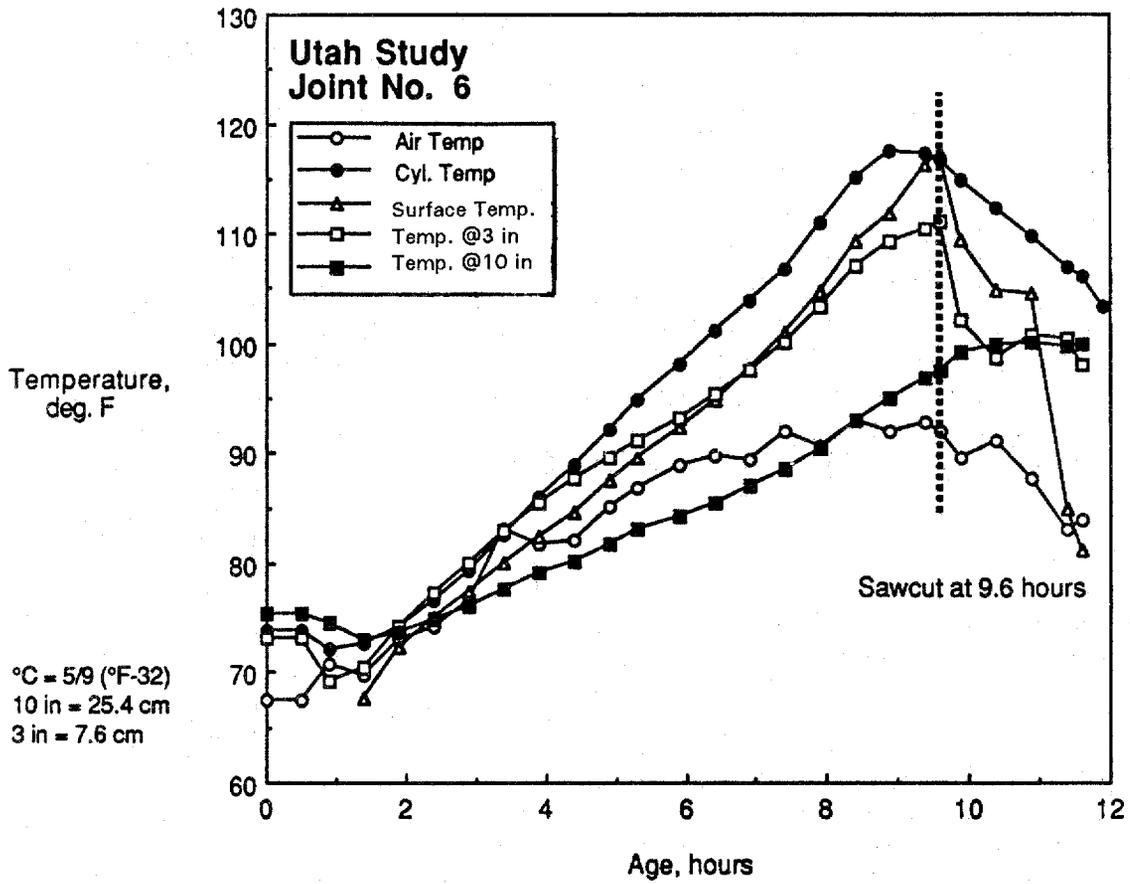
Figure 81.  Utah I-15 slab temperatures after concrete placement.
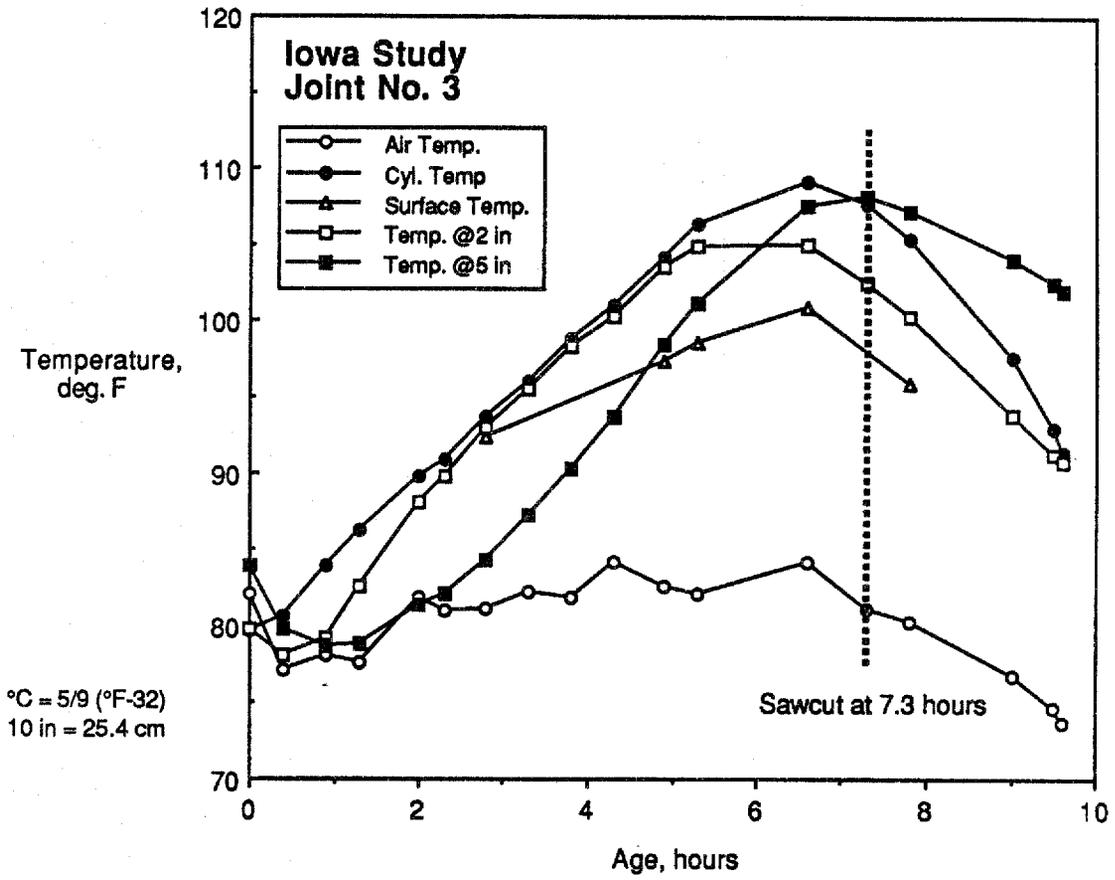
Figure 82.   Iowa Route 169 slab temperatures after concrete placement.

## Temperature Observations

Irregular concrete temperature trends were observed during the first hour after concrete placement for the Iowa and Utah sites. For the Utah site, initial as-placed concrete temperature was somewhat higher than air temperature. This may explain the slight drop of concrete temperatures following placement. In Iowa, air temperature decreased following concrete placement and concrete temperatures followed suit. Concrete and air temperatures at both sites increased along with air temperature starting about 1 hour after placement. The initial temperature fluctuations observed for the concrete pavement are considered to be inconsequential to buildup of pavement stresses as they occurred while the concrete was still plastic. No measurements of initial concrete set were made, but based on measurements made during sawing slab construction reported in chapter 4, initial set had not occurred at less than 1.4 hours after placement.

For the Utah pavement, as shown in figure 81, air and within concrete slab temperature followed a rising trend until about 9 hours after concrete placement. Maximum concrete surface temperature, about 118 °F (48 °C), was attained at about 9.5 hour age. Based on concrete temperature data it may be concluded that the concrete was in a compression mode at least up to the moment of maximum concrete temperature. Near slab bottom temperatures lagged near surface temperatures and levelled off at about 100 °F (38 °C) at about 10.5 hours after concrete placement. Maximum cylinder temperature was about equal to maximum slab surface temperature. Cylinder temperature trends followed slab surface trends. Surface temperature showed a precipitous drop starting about 9 hours after concrete placement and the surface had cooled to about 85 °F (29 °C) just after the 11-hour age. This rapid concrete surface cooling can be attributed to pavement surface evaporation or cooling when joint sawing activities caused pavement wetting. Concrete temperature at 3 in (7.6 cm) from the surface followed the same trend as the surface temperature. The temperature below the surface peaked at the same time but was about 6 °F (3 °C) cooler than the surface temperature. Air temperatures gradually increased from 68 °F (20 °C) and peaked at 93 °F (34 °C). The air, cylinder, surface, and near-surface temperatures all peaked between 8-1/2 and 9-1/2 hours.

For the Iowa pavement, as shown in figure 82, a rising concrete temperature trend was observed to start at 1 hour slab age and extended to about 6 to 7 hours after concrete placement. The recorded surface temperature was lower than temperatures recorded at 2 in (5 cm) below slab surface. This is not a reasonable scenario since surface temperatures on clear days with summertime solar radiation exposure are usually higher than below surface temperatures. To obtain near surface and near slab bottom temperatures, the cylinder temperature data was used as a surrogate for surface temperature. Slab bottom temperature is estimated at the time of maximum surface temperature by assuming a linear temperature gradient passing from slab top (cylinder) through mid-slab temperature to slab bottom. For a maximum 109 °F (42 °C) surface (cylinder) temperature at age 6.6 hours and 107 °F (41 °C) at mid-slab, the bottom temperature was estimated at about 105 °F (41 °C). Bottom slab temperature can be assumed to be constant, similar to the Utah condition, for several hours following top surface maximum temperature observations. The top surface temperature (surrogate cylinder temperature) and midslab temperatures indicate that slab cooling started at about 6.5 to 7 hours slab age. At about 9.8 hours, slab top (cylinder) had cooled to about 92 °F (33 °C) and slab bottom had cooled to about 102 °F (39 °C) from 105 °F (41 °C) at concurrent top surface maximum temperature condition. Slab bottom temperature was assumed equal to temperature at mid-depth.

179

## Pavement Restraint Stresses

Shortly after initiation of concrete cooling, the concrete slabs are considered to pass from a state of compression to a state of tension. Tensile stresses are due to both subgrade friction restraints to axial contraction and restraints to bending (curling) deformations. These pavement restraint stresses can be calculated using equations 1 and 2 in figure 2 (axial restraint) and equations 5 and 6 in figure 3 (bending restraint).

Full axial restraint stresses, $E\alpha\Delta T$, occur, depending on magnitudes of early age modulus of elasticity, average concrete slab cooling, and slab to subbase friction factor at a range of distances from slab ends. For example, for the Utah pavement, full restraint (equation 3) is calculated to occur at a distance of about 29 ft (8.8 m) from slab end when an average cooling of 15 °F (8 °C) occurs, a 2-million psi (13,800-MPa) concrete modulus, and a slab to subbase friction factor of 5 (lean concrete base) is used. For the Iowa pavement with a 10 °F (6 °C) average cooling, a subgrade friction value of 3 (granular base), and a concrete modulus of 2.5-million psi (17,200-MPa) concrete modulus, the distance from slab end to mobilize full axial restraint stress is about 40 ft (12.2 m). A coefficient of thermal contraction of 5 x 10$^{-6}$ in/in/°F (9 x 10$^{-6}$ mm/mm/°C) and a concrete density of 150 lb/ft$^3$ (13.8 kg/m$^3$) was used for the calculations. Thermal contraction coefficients for a range of highway concrete pavement mixes at early ages are listed in table 31 of chapter 3. The lower magnitude of the range of coefficients was used in this report as measured slab end movements are generally less than those calculated.

Full bending restraint stresses occur at distances from free edges as a function of radius of relative stiffness, L. As shown in figure 3 equation 6, L is a function of concrete elastic modulus, slab thickness, modulus of subgrade reaction, and Poisson's ratio. A modulus of subgrade reaction of 250 lb/in$^3$ (67.5 MPa/m) and 700 lb/in$^3$ (190.0 MPa/m) was assumed for the Iowa (granular subbase) and Utah (lean concrete base) pavements, respectively. Using equation 6 the fully restrained curling stresses occurs at distances greater than 6-1/4 ft (1.9 m) and 8-1/2 ft (2.6 m) from slab edges for the Utah and Iowa pavements, respectively. The elastic modulus used in equation 6 was 2 million psi (13,800 MPa) and 2.5 million psi (17,200 MPa) for the Utah and Iowa pavements respectively.

Restraint Stresses at Time of Utah Joint Sawcutting. Joint sawing, as shown in figure 81 was done at about 9.6-hours concrete age. At that moment concrete surface temperature was about 117 °F (47 °C) slowly cooling from a maximum of 118 °F (48 °C). At slab bottom concrete temperature was about 97 °F (36 °C). No significant slab cooling had occurred prior to sawcutting and slab near surface temperatures exceeded near slab bottom temperatures. Thus, it is concluded that the slab concrete was in compression when sawing was done.

Restraint Stresses at 2 Hours after Utah Joint Sawcutting. Curling restraint stresses at 11-1/2 hours in the transverse direction for the 10-in (25-cm) thick pavement were about 78 psi (538 kPa) for the 15 °F (8 °C) slab bottom to top temperature difference. Since 1/2 the pavement width is greater than the 6-1/4 ft (1.9 m) minimum distance required to develop stresses, equation 5 shown in figure 3 can be used to calculate bending restraint stress. A 2.0-million psi (13,800-MPa) modulus of elasticity obtained from figure 83 for the 10 hour concrete age was used for the curling stress calculation. The axial restraint stress in the transverse direction, using a slab to subbase friction value of 5, was about 99 psi (683 kPa) for the 38-ft (11.6-m) wide pavement. Axial restraint was calculated using equation 1 since 1/2 of the 38-ft (11.6-m) pavement width is less than the 29 ft (8.8 m) needed to develop

180
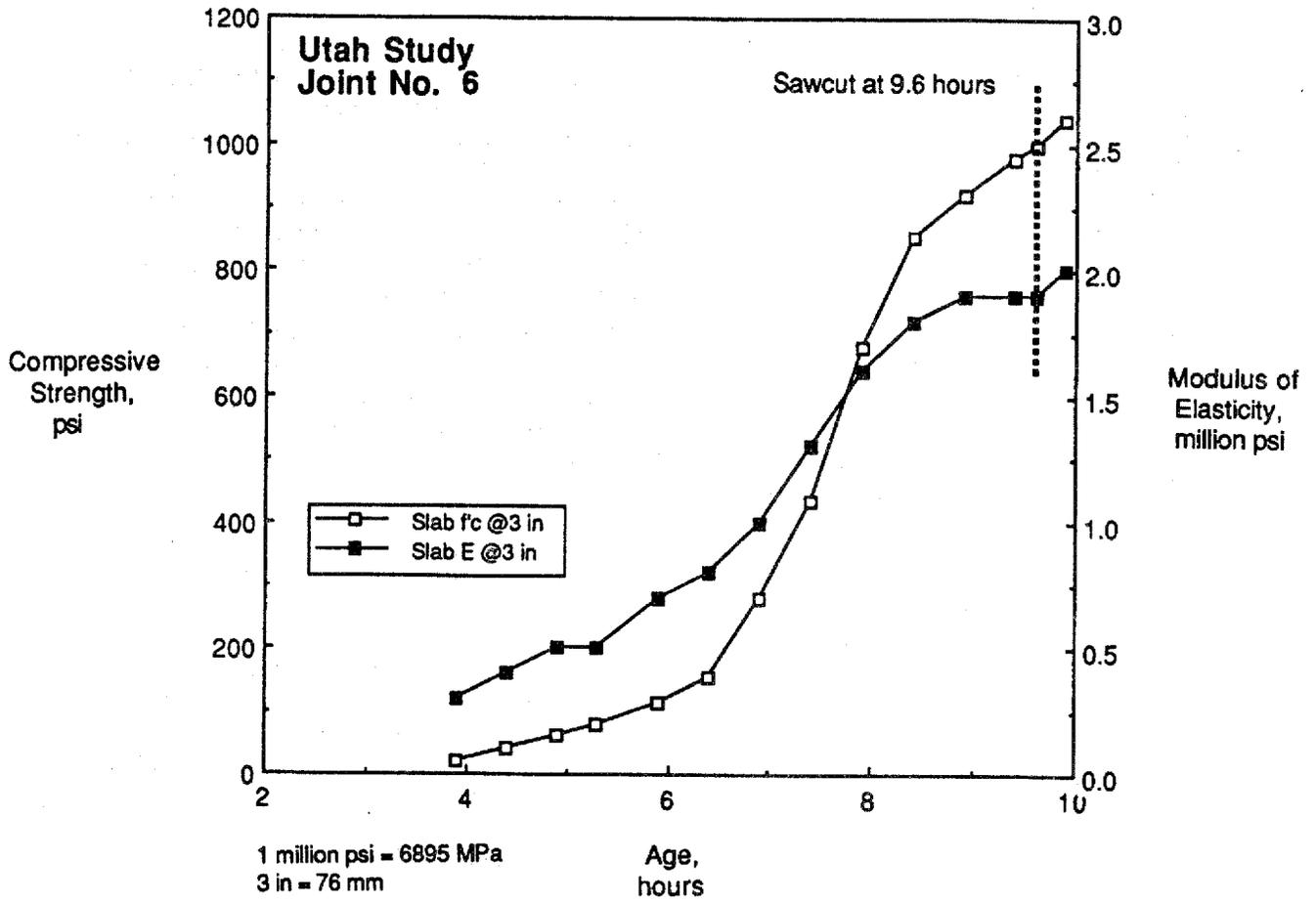
Figure 83.  Utah I-15 early age concrete properties.

full axial restraint stresses. A friction value of 5 was used for the pavement placed on top of a lean concrete base. The total maximum restraint stress (at mid-width) was about 177 psi (1.2 MPa) for the 10-in (25-cm) pavement thickness cross-section.

For the 38-ft (11.6-cm) wide pavement, the longitudinal joint in closest proximity to pavement mid-width is 16 ft (4.9 m) from a free edge. At this distance from the free edge fully developed bending restraint stresses still occur. For the 10-in (25-cm) full-depth slab cross-section, total restraint stress at the longitudinal joint alignment was 161 psi (1.1 MPa) for the above conditions of friction factor of 5, 15 °F (8 °C) temperature difference, and 2.0-million psi (13,800-MPa) elastic modulus. After sawcutting the joint to 1/3-slab depth, the total restraint stress at the reduced section was increased by 50 percent to 242 psi (1.7 MPa). This was greater than the approximately 190 psi (1.3 MPa) split tensile strength, as shown in figure 84, for the 9.8-hour insitu concrete age. Slab compressive strength was estimated using pulse velocity data. Modulus of elasticity and split tensile strength were estimated using early age general prediction equation relationships reported in chapter 3.

Fully developed axial restraint stresses in the longitudinal direction using equation 2 were 140 psi (966 kPa) for an average temperature drop of 14 °F (8 °C). Average temperature (top, near top, and bottom) at peak surface temperature was 109 °F (43 °C) and at 11-1/2 hours was 95 °F (35 °C). Bending restraint stress was 78 psi (538 kPa). Total full section restraint stress was 218 psi (1.5 MPa). After sawcutting the total restraint stress was increased by 50 percent to 327 psi (1.6 MPa). Since the reduced section stress was greater than the 190-psi (1.3-MPa) strength some transverse joints 2 hours after sawcutting would be cracked to relieve restraint stresses.

If every other joint cracked the effective slab length was reduced to approximately 25 ft (7.6 m) for the staggered joint spacings. At 12.5 ft (3.8 m) from slab ends in the longitudinal direction axial restraint calculated using equation 1 (partial restraint) was reduced to 65 psi (449 kPa). Total full section restraint was 143 psi (987 kPa). Reduced section restraint stresses of 215 psi (1.6 MPa) exceeded the 190 psi (1.3 MPa) strength.

After cracking at all transverse joints axial restraint stresses were reduced to 33 psi (228 kPa). Total full section restraint stresses for a 15 °F (8 °C) temperature differential were reduced to 111 psi (766 kPa). Reduced section restraint stresses of 167 psi (1.2 MPa) were less than the concrete strength 2 hours after sawing.

Restraint Stresses at Time of Iowa Joint Sawcutting. Joint sawing, as shown in figure 82, was done at about 7.3 hours concrete age. At that moment the temperature at the concrete surface (surrogate cylinder temperature) was about 108 °F (42 °C). At slab mid-depth, temperature was also about 108 °F (42 °C). Slab bottom temperature, as discussed above was about 105 °F (41 °C). At the moment of sawing, as shown in figure 82, concrete temperature had, on average, dropped by less than 2 °F (1 °C). Thus it is concluded that the slab was at or very near a zero stress condition, that is it was in transition from a compression mode coinciding with rising average concrete temperature to a tension mode coinciding with cooling average concrete temperature.

Restraint Stresses at 2 Hours After Iowa Joint Sawcutting. Curling restraint stresses in the transverse direction for the 10-in (25 cm) thick pavement were about 65 psi (449 kPa) for the 10 °F (6 °C) slab bottom to top temperature difference. Since 1/2 the pavement width is greater than the minimum 8-1/2-ft (2.6-m) distance to develop maximum bending restraint, equation 5 was used. A 2.5-million psi (17,250-MPa) modulus of elasticity obtained from figure 85 for the approximately 9.3-hour concrete age was used for the curling stress calculation.
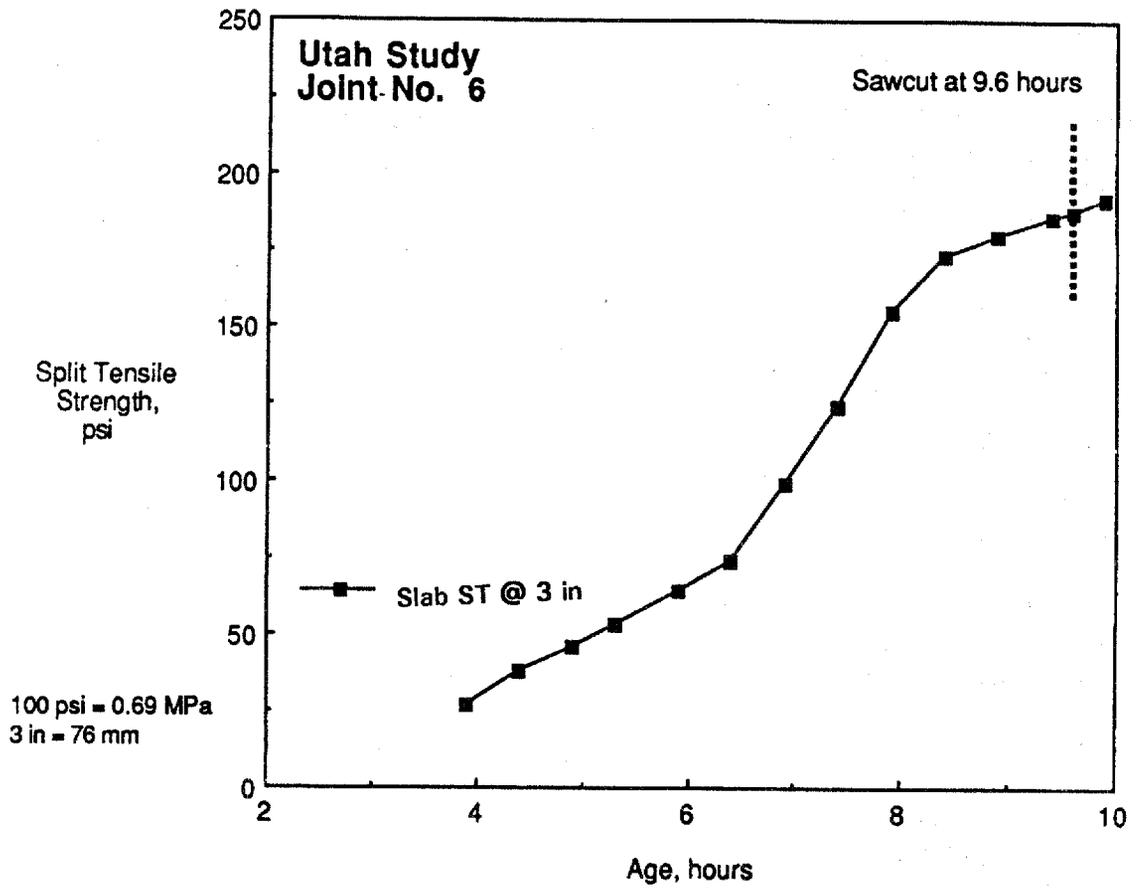
Figure 84. Utah I-15 early age split tensile strength.
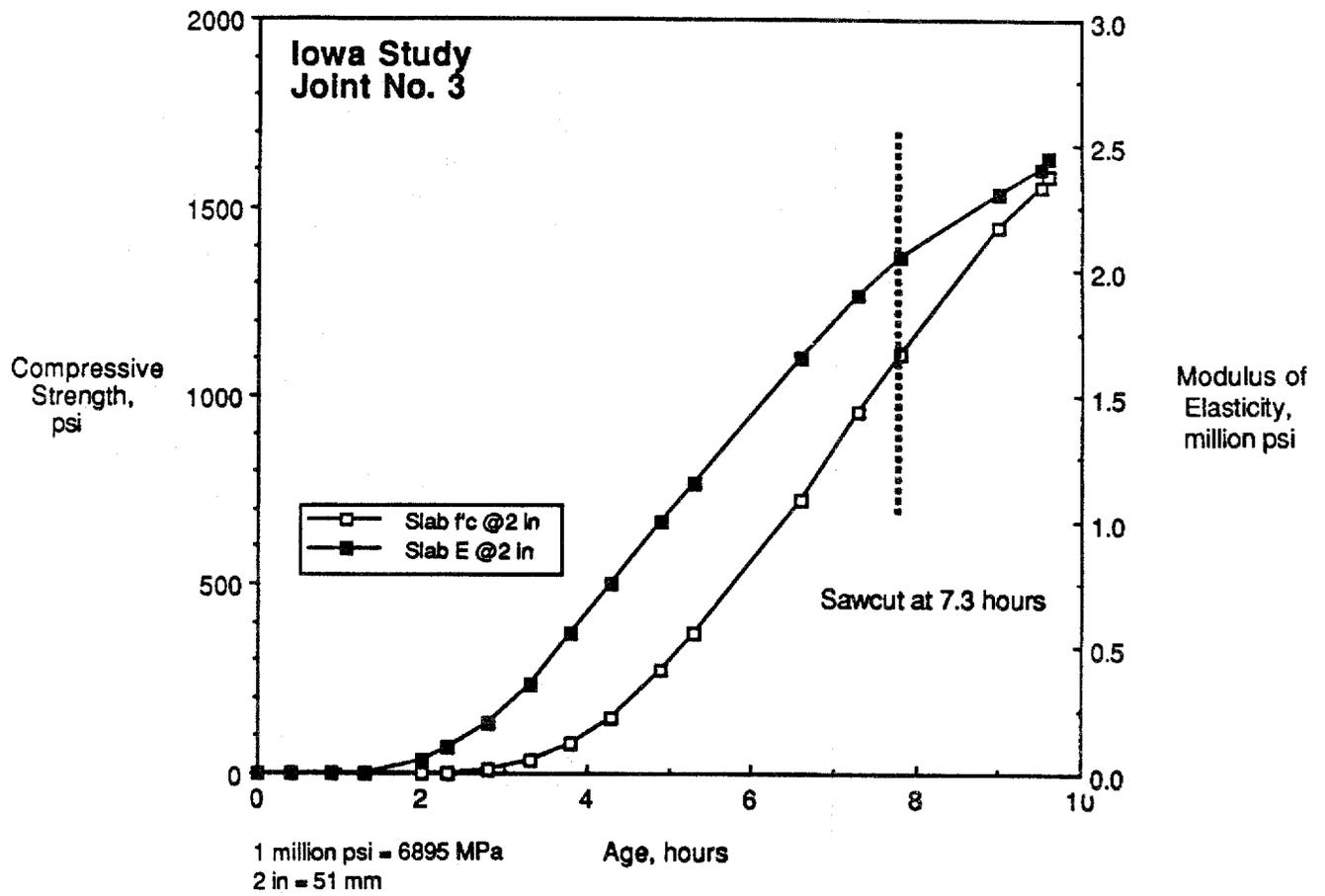
**Figure 85. Iowa Route 169 early age concrete properties.**

The axial restraint stress, using a subbase friction value of 3, in the transverse direction was 37 psi (255 kPa). Partially developed axial restraint stresses were calculated using equation 1 since 1/2 the pavement width was less than the 40 ft (12.2 m) needed to develop full restraint. A friction value of 3 was used for the crushed stone subbase as the concrete will key to subbase surface. Total full section restraint was 102 psi (704 kPa) in the transverse direction. For the Iowa pavements the joints were sawcut to 1/3-slab thickness and the total restraint stress at the reduced section was increased by 50 percent to 153 psi (1.1 MPa). This was less than the 235-psi (1.6-MPa) split tensile strength as shown in figure 86 for the 9.3-hour age insitu concrete. Slab compressive strength was estimated using maturity data. Modulus of elasticity and split tensile strength were estimated using early age general prediction equations reported in chapter 3.

The curling restraint stress for the 10 °F (6 °C) temperature differential in the longitudinal direction as calculated above was 65 psi (449 kPa). Axial restraint stress, fully developed was 125 psi (863 kPa) as calculated using equation 2 with an average temperature decrease of 10 °F (6 °C). Average temperature (top, near top, middle, and bottom) at peak surface temperature was 107 °F (42 °C) and at 9.3 hours was 97 °F (36 °C) Total full section restraint was 190 psi (1.3 MPa). Reduced section restraint stresses of 285 psi (2.0 MPa) exceeded the concrete strength.

If every other transverse joint cracked the effective slab length becomes 20 ft (6.1 m). Axial restraint stress is reduced to 62 psi (428 kPa). Total restraint stress at the sawcut location midway between joints with assumed cracks was 127 psi (876 kPa). Reduced section restraint stresses were 192 psi (1.3 MPa). This is less than the 235-psi (1.6-MPa) split tensile strength, as shown in figure 86 for the 9.3-hour age insitu concrete.

## Cracking Below Sawcut Notches

Cracks were observed below all sawcut notches at about 24 hours concrete age, that is the morning following the paving day for both the Utah and Iowa pavements. Crack and joint depth measurements in Iowa are summarized in table 39 of appendix D. Cracking is anticipated to occur when restraint stresses exceed concrete tensile strength. Split tensile strength is considered to be equivalent to direct tensile strength. For a slab without sawcuts at the moment of incipient cracking, split tensile strength balances the sum of curling and axial restraint stresses as shown in the following equation:

$$ST = \sigma_c + \sigma_f \dots\dots\dots\dots\dots\dots\dots\dots\dots\dots (17)$$

where

$ST$ = split tensile strength, psi

$\sigma_c$ = bending restrait stress (curling)

$\sigma_f$ = frictional restraint stress (axial)

Using equation 1 in figure 2 and equation 4 in figure 3 and transposing

$$\Delta T = 2 (ST - wh\mu x/h) / CE\alpha \dots\dots\dots\dots\dots\dots\dots\dots (18)$$
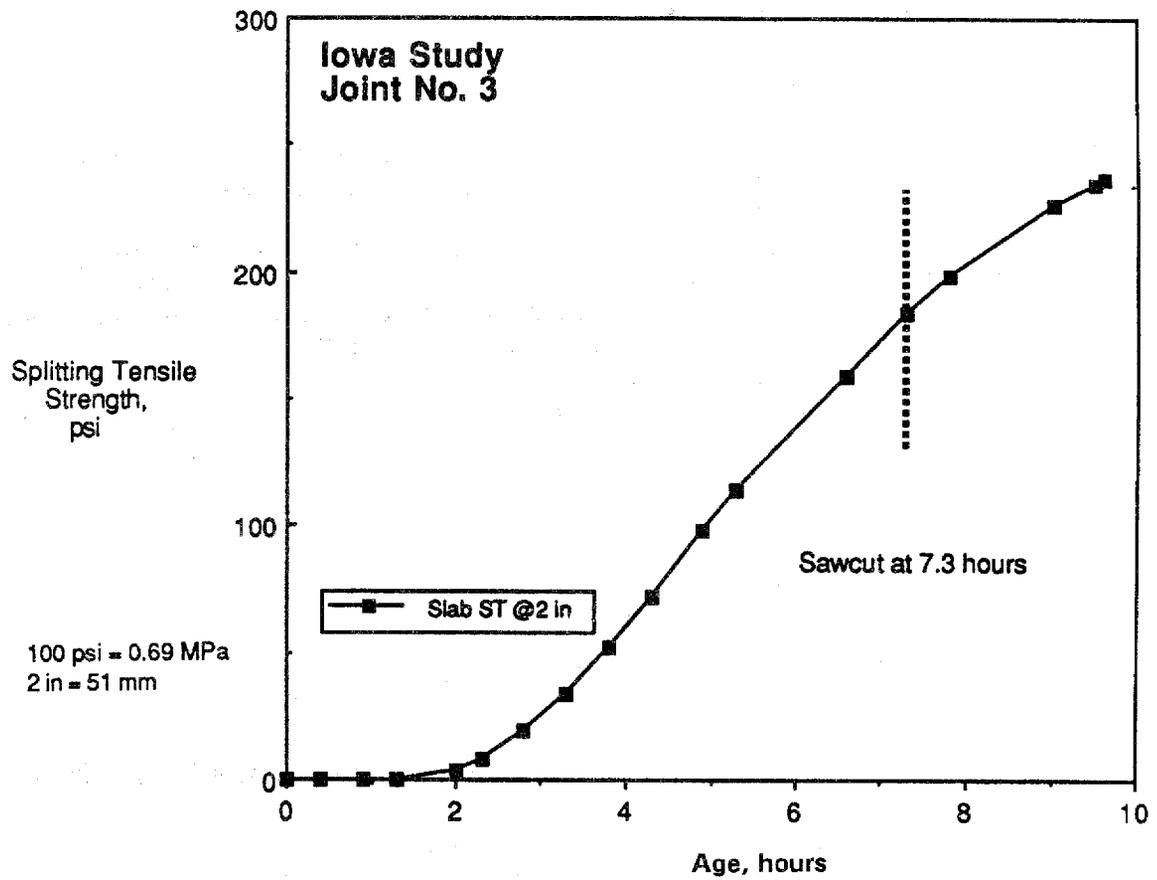
**Figure 86. Iowa Route 169 early age split tensile strength.**

where

$\Delta T$ = slab top to bottom temperature differential, °F
ST = split tensile strength, psi
w = density of concrete, lb/in³
h = slab thickness, in
$\mu$ = coefficient of subgrade friction
x = distance from slab end, in
C = curling stress coefficient (figure 4)
E = modulus of elasticity, psi
$\alpha$ = coefficient of thermal expansion, in/in/°F

The slab bottom versus slab surface temperature difference, t, at time of crack formation is obtained for a full-depth slab cross section, that is a slab without sawcut.

Where the pavement cross section is reduced by a sawcut notch the axial and curling restraint stresses are increased at the weakened plane cross section by the ratio of slab thickness to slab depth below sawcut. To determine slab bottom to top temperature difference when cracks occur below sawcuts the following equation is used:

$$\Delta T = 2 \ (ST - w\mu xn) \ / \ nCE\alpha \dots\dots\dots\dots\dots\dots\dots\dots\dots\dots (19)$$

where

n = h/(h-z)
h = total slab thickness, in
z = sawcut depth, in

For the Utah pavement using the following values:

$\mu$ = 5
E = 2.0 million psi (13,800 MPa)-(assuming cracking at about 10 to 12 hours concrete age)
$\alpha$ = 5 millionths in/in/°F (9 millionths mm/mm/°C)
x = 120 in (3.1 m) for shortest transverse joint spacing of staggered joints
h = 10 in (25 cm)
w = 0.0868 lb/in³ (0.024 MPa/m)
ST = 200 psi (1.4 MPa)
C = 1.04
z = 10/3 = 3.3 in (8.4 cm) sawcut depth

cracking below sawcut notches occurred for a slab bottom to slab surface temperature difference of about 15 °F (8 °C). For the Utah pavement, concrete elastic modulus and split tensile strength versus concrete age are shown in figures 83 and 84. If the slab bottom temperature remained at about 100 °F (38 °C) then slab surface temperature cooled to about 85 °F (29 °C) at time of below sawcut notch concrete cracking.

For the Iowa pavement using the following values:

$\mu$ = 3

E = 2.5 million psi (17,250 MPa) - (assume cracking about 9 to 10 hours after concrete placement

$\alpha$ = 5 millionths in/in/°F (9 millionths mm/mm/°C)

x = 240 in (6.1 m) for 20 ft (6.1 m) joint spacings with cracks

h = 10 in (25 cm)

w = 0.0868 lb/in$^3$ (0.024 MPa/m)

ST = 250 psi (1.7 MPa)

C = 1.04

z = 10/3 = 3.3 in (8.4 cm) sawcut depth

cracking below sawcut notches occurred for a slab bottom to slab surface temperature difference of about 16 °F (9 °C). For the Iowa pavements, concrete modulus and split tensile strength versus concrete age are shown in figures 85 and 86. If the slab bottom temperature cools from maximum bottom temperature of about 105 °F (41 °C) to about 103 °F (39 °C), the slab surface temperature cooled to about 87 °F (31 °C) at time of below sawcut notch concrete cracking.

## SUMMARY

As discussed in chapter 2 observations of slab cracking occurs when a temperature differential of 7 °F (4 °C) occurs. This corresponded to approximately a 21 °F (12 °C) drop in surface temperature from peak temperature. Temperatures were measured in Utah and Iowa to monitor gradients and thermal histories. Axial and curling restraint stresses calculated in both the longitudinal and transverse directions 2 hours after joint sawing were compared to split tensile strengths.

For the Utah pavement 2 hours after sawcutting the temperature differential was 15 °F (8 °C). Average overall temperature drop from peak surface temperature was 14 °F (8 °C). Restraint stresses at both the longitudinal and transverse joints exceeded the concrete split tensile strength. For the Iowa pavement 2 hours after sawcutting the temperature differential was 10 °F (6 °C). Average overall temperature drop from peak surface temperature was also 10 °F (6 °C). Restraint stresses at longitudinal joints were less than the split tensile strength. For the transverse joints fully restrained axial and curling stresses exceeded the concrete strength. If every other joint cracked the restraint stresses were less than the concrete strength.

By balancing split tensile strength with curling and frictional restraint stresses the temperature differential (top and bottom) to cause cracking below sawcut notches can be solved. For both the Utah and Iowa pavements the calculated temperature differentials were about 15 °F (8 °C). This corresponds to an estimated 33 °F (18 °C) and 22 °F (12 °C) surface temperature drop for the Utah and Iowa pavements, respectively.

Both average temperature drops and temperature gradients contribute to random cracking. As shown in figures 81 and 82 the temperature at 2- or 3-in (5-or 8-cm) depth does not decrease as rapidly as the surface temperature. Bending restraint stresses will therefore be more sensitive than average slab temperature decreases (frictional restraint) to surface temperature changes.

# CHAPTER 6. EVALUATION OF EARLY CONCRETE PAVEMENT LOADING

## INTRODUCTION

Newly placed concrete pavements are often subjected to traffic loading shortly after they have hardened but long before they have attained their design strength. For example, construction traffic may use the young pavement as a "working platform" to facilitate subsequent construction activities. Lighter construction equipment, such as joint sawing equipment, may also load the pavement at a very early age when it is critical that the joints be established in the pavement.

The early trafficking of young concrete pavements raises several questions regarding the potential reduction in the service life of the pavement due to the early loading. While some argue that the pavement should not be loaded until it has achieved its design strength, others contend that light loads or a small number of heavier load repetitions will not cause any appreciable damage which can significantly reduce the service life of the pavement.

Other issues regarding the early loading of concrete pavements that frequently arise include:

- The age or strength the pavement may be loaded by construction traffic without causing significant damage to the pavement.

- The damage done to a pavement if it is subjected to only a few repetitions of a heavy load.

- The early loading by light traffic causing any appreciable damage.

- The damage done if the pavement is only loaded in the interior portions of the slabs as opposed to the edge position.

This chapter will present a methodology for addressing the above issues and demonstrate how it can be used in practical applications.


## APPROACH TO EARLY LOADING EVALUATION

In order to determine the damage caused by early loading, a fatigue analysis of concrete pavements subjected to early loading was conducted. The fatigue analysis compares the actual number of traffic load applications to the allowable number of load applications that the pavement may sustain before cracking. This latter value depends on the flexural stress produced in the slab by the construction traffic and the existing strength of the slab. The higher the pavement strength, the higher the number of allowable load applications that the slab may sustain before cracking.

Determination of stresses is presented as a demonstration of a procedure which can be used to estimate fatigue damage at early ages. Assumptions used in determining stresses include the relationship developed from this study database between compressive strength and elastic modulus. A second relationship between modulus of rupture and both compressive strength and curing relative humidity was also assumed. Specific relationships using project materials should be established. The method described in this chapter can be followed to develop a procedure to investigate effects of early opening of pavements to traffic.

## Determining Stresses and Compressive Strength

The maximum tensile stresses occurring at the bottom of the slab, which are the critical stresses that can produce flexural fatigue cracking, were determined for typical construction traffic loadings using the ILLI-SLAB finite element computer program. This program has been in use since 1977 and has undergone numerous revisions and verifications.[39 through 43] The program was also evaluated under this study using field-measured stress data and provided favorable results. Comparison of measured with calculated stresses are discussed in chapter 7. Full-Scale Highway Pavement Load Tests.

In the laboratory study presentation of figure 63 of Chapter 3, the following relationship was developed between the concrete elastic modulus and the concrete compressive strength:

$$E_c = 62,000 * (f_c')^{0.5} \dots\dots\dots\dots\dots\dots\dots\dots\dots\dots (20)$$

where:

$E_c$ = concrete elastic modulus, psi
$f_c'$ = concrete compressive strength, psi

Since the ILLI-SLAB program requires an elastic modulus value for the determination of pavement stresses, those stresses can now be related directly to the compressive strength of the pavement. By knowing the compressive strength of a concrete slab at any time, the modulus of elasticity at that time can be predicted, and an estimate of the stresses developing in the slab can be made.

The most common procedure for monitoring compressive strength gain of the newly-placed concrete calls for casting cylinders from the material as it is placed and testing the cylinders in compression with time. However, since the mass of the concrete in the slab can generate a much higher heat of hydration than the concrete in the cylinder molds, its compressive strength may be higher than those of the cylinders. This results in a "built-in" factor of safety when using cylinders to estimate the strength of the concrete pavement.

Other ways of estimating the strength of the in-place concrete are the concrete maturity and the pulse velocity nondestructive testing methods. Both methods can be used to predict concrete strength as it is curing in-place once mix-specific relationships are established.

## Determining Modulus of Rupture

The modulus of rupture is the concrete strength in flexure. As such, it is an important parameter in the estimate of fatigue damage. Since this test is not performed by most State highway agencies, it is recommended that each agency develop a relationship between the compressive strength of the concrete and the modulus of rupture. A general relationship for all laboratory mixes was developed in the laboratory analysis in table 34 of chapter 3 for the purposes of this study and is given below:

$$MR = [8.460 \times (f_c')^{0.5}] + (3.311 \times RH) - 155.91 \dots\dots\dots\dots\dots\dots (21)$$

190

where:

MR = concrete modulus of rupture, psi
$f_c'$ = concrete compressive strength, psi
RH = relative humidity during curing, percent

The model was derived for a number of different concrete mixes with different aggregate types, relative humidities, and cement contents. Since the relationship depends upon the mix, it is recommended that agencies develop their own unique relationships for each individual mix design.

## Estimating Concrete Fatigue Damage

Both the stresses developing in a concrete slab for a given loading (function of elastic modulus) and the concrete modulus of rupture can be related to the compressive strength of the concrete. Since compressive strength can be monitored for a newly-placed pavement, it is possible to obtain an estimate of the amount of fatigue damage that will occur in a slab if it is subjected to early loading.

To determine the fatigue damage of concrete pavements subjected to early loading, a fatigue-consumption approach similar to the one first proposed by Miner was employed.[44] This approach theorizes that a concrete pavement has a finite life and can withstand some maximum number of load repetitions, N, of a given traffic loading before fracture. Every individual traffic loading applied, n, decreases the life of the pavement by an infinitesimal amount. Thus, damage is defined as:

$$\text{Damage} = \Sigma \, (n \, / \, N) \quad \dots\dots\dots\dots\dots\dots\dots\dots\dots\dots\dots\dots\dots\dots\dots \quad (22)$$

where:

Damage = Proportion of life consumed (50 percent of slabs cracked when damage is 1.0).
n = Actual number of applied traffic loadings.
N = Maximum allowable number of traffic loadings before failure.

This damage value provides the percentage of life that is consumed by the actual number of traffic loads up to a given point in time. Theoretically, when $\Sigma \, n/N = 1$, fracture of the concrete would occur; however, because of variability in traffic loading and material properties, fracture of some concrete slabs can occur at values less than 1. Thus, because average values of numbers of loadings are used in the fatigue damage analysis, 50 percent of the slabs (on average) will be cracked when the fatigue damage is 1.0.

The allowable number of traffic loadings before 50 percent of the slabs are cracked can be estimated from the following fatigue damage model:

$$\text{Log}_{10} \, N = 2.13 \, (1 \, / \, SR)^{1.2} \quad \dots\dots\dots\dots\dots\dots\dots\dots\dots\dots\dots\dots\dots \quad (23)$$

where:

N = allowable number of traffic loadings before failure

SR = stress ratio = $\sigma$ / MR

$\sigma$ = stress in slab due to given loading, psi

MR = concrete modulus of rupture, psi

It is noted that N is calculated for a given strength level and stress combination. During the early stages of construction and curing, the concrete slab can experience relatively large percentage increases in flexural strength, but the rate of strength gain falls off after reaching a certain point. It is because of the rate of strength gain at the early ages of a newly-placed concrete pavement that the considerations for early loading are important.

Figure 87 shows how actual slab cracking can be related to accumulated fatigue damage. This figure is based on the field performance of 52 jointed plain concrete pavements (JPCP) sections and shows the wide variability in cracking for different accumulated fatigue damages. The $\log_{10}$ (n/N) = 0 corresponds to a fatigue damage of n/N = 1.

The fatigue damage model was developed from full-scale field slab data. It is a more realistic model than fatigue models developed from laboratory beam testing since the field-developed model represents supported slab conditions, whereas laboratory beams do not. Also, while in theory when the stress ratio is greater than or equal to one, a crack will result in a single loading. While a crack can occur in a slab after one loading, the fully supported slab in the field may sustain many more loadings before the crack propagates to the surface. Finally, the model is also based on many slabs that were loaded with high stresses that approached or exceeded the concrete strength, which is often the case in early loading.

The previous relationships show that, by knowing the compressive strength of a given slab at any given time, an estimate of the proportion of pavement life consumed by a certain number of load applications can be obtained. This will be illustrated in the following section, where a specific load is evaluated and relationships were developed showing the effect of early loading on the fatigue life of the concrete.

## EVALUATION OF EARLY CONSTRUCTION TRAFFIC LOADING

An 20,000-lb (9080-kg), single axle with dual tires was selected as the critical load for the evaluation of early construction traffic loading on the fatigue damage of the newly-placed concrete pavement. This was assumed to be typical of the type of early loading to which a concrete pavement might be subjected. Since the stresses produced by tandem loads are generally less than those for single axles the procedure can easily be applied to tandem axle loads using a loading adjustment factor. Only one contact pressure 100 psi (690 kPa) was evaluated. An agency could further evaluate additional factors such as contact pressures, axle types, and axle loads for each type of traffic expected on the pavement.

Three loading conditions (edge, interior, and transverse joint) were evaluated as shown in figures 88 through 90. Stresses for each of the 3 loading conditions were determined using the ILLI-SLAB program for a range of slab thicknesses, elastic modulus values, and effective k-values. Table 54 provides a summary of the input variables used in the ILLI-SLAB evaluation of early construction loading.

192
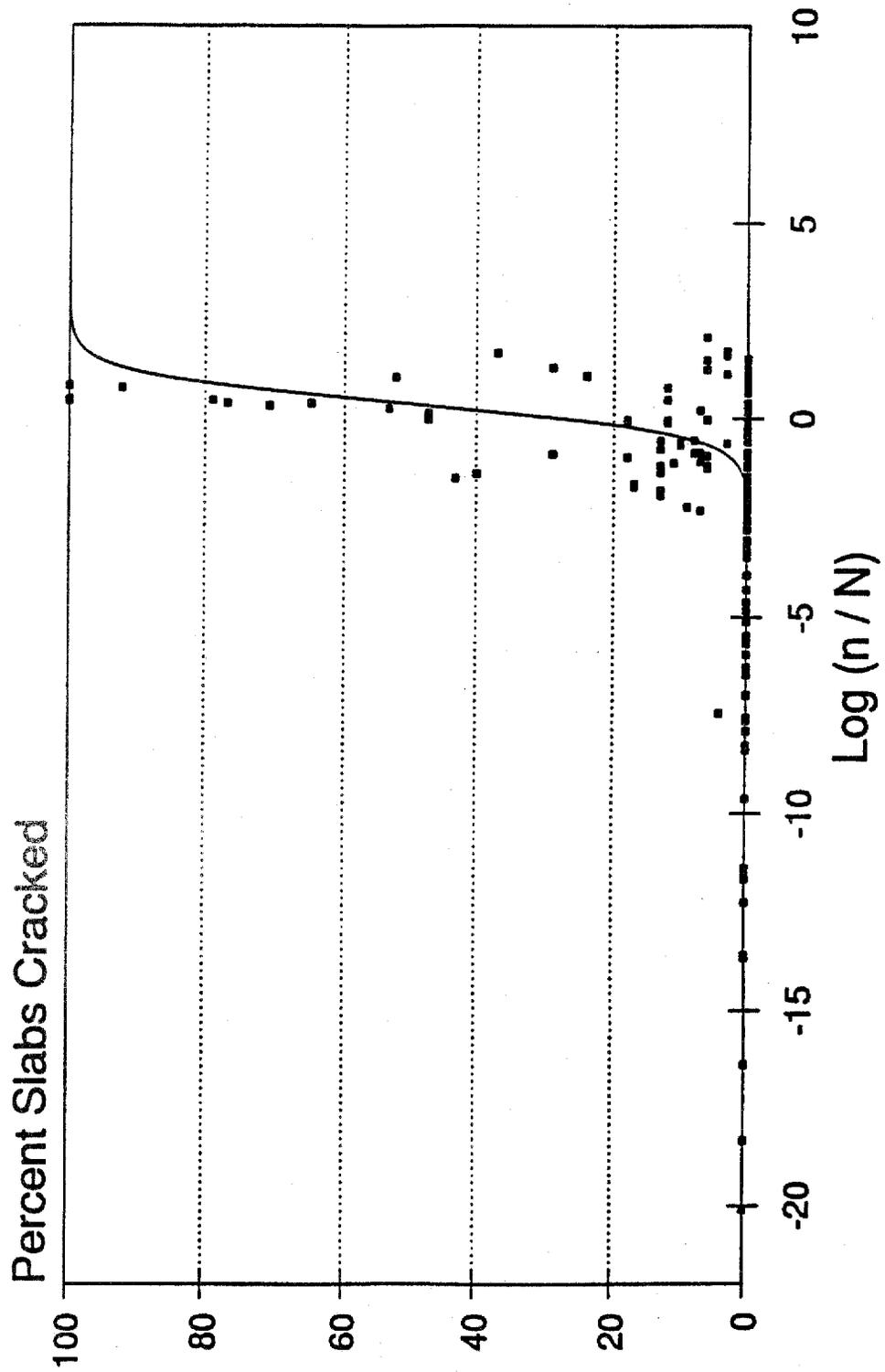
Figure 87. Observed slab cracking vs. accumulated fatigue damage for 52 JPCP sections.

## EDGE LOADING CONDITION
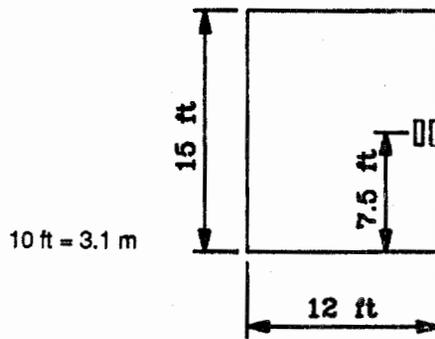


Figure 88.   Edge loading condition for early loading analysis.

## INTERIOR LOADING CONDITION
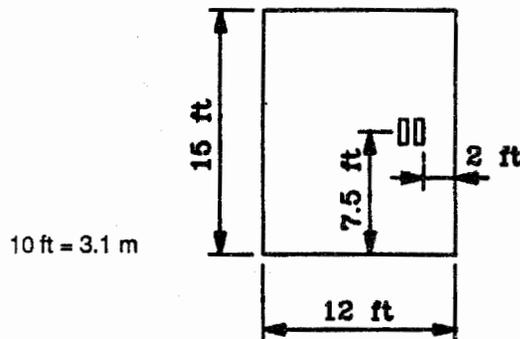


Figure 89.   Interior loading condition for early loading analysis.

## TRANSVERSE JOINT LOADING CONDITION
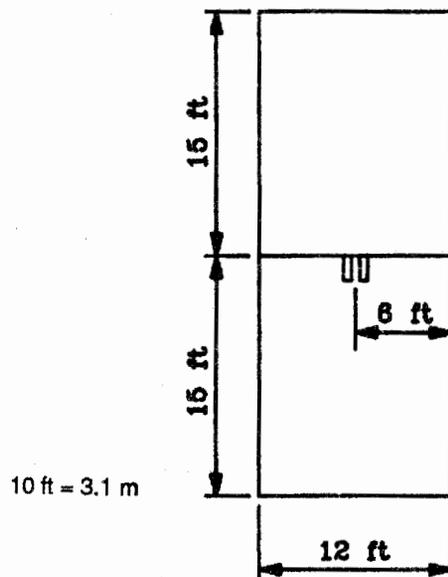


Figure 90.   Transverse joint loading condition for early loading analysis.

194

**Table 54. Summary of input variables used in ILLI-SLAB evaluation of early construction traffic loading.**

| Pavement Type | Jointed Plain Concrete Pavement | |
|---|---|---|
| Pavement Surface Properties | Thickness, in<br>Poisson's Ratio<br>Elastic Modulus, million psi<br>Temperature Gradient | 8, 10, and 12<br>0.15<br>1, 2, 3, 4, and 5<br>none |
| Subgrade Properties | Model<br>k-value, lb/in$^3$ | Winkler<br>100, 300, and 500 |
| Pavement Joint Data | Joint Spacing, ft<br>Lane Width, ft<br>Joint Width, in<br>Dowel Diameter,[1] in<br>Dowel Spacing,[1] in<br>Modulus of Dowel Support,[1] lb/in$^3$<br>Dowel Modulus of Elasticity,[1] psi<br>Dowel Poisson's Ratio[1]<br>Dowel Concrete Interaction,[1] lb/in$^3$<br>Aggregate Interlock Factor[2] | 15<br>12<br>0.125<br>1.25<br>12<br>1,500,000<br>29,000,000<br>0.3<br>1,490,000<br>0 (free edge) |
| Wheel Loading | Type of Axle<br>Weight of Axle, lb<br>Tire Imprint, in$^2$<br>Contact Pressure, psi | Single, Dual Wheel<br>20,000<br>45<br>100 |

NOTES:  [1] For doweled joint.

[2] For undoweled joint.

10 in = 25 cm
100 lb/in$^3$ = 27.1 MPa/m$^3$
1000 psi = 6.9 MPa

## Edge Loading Condition

The edge loading condition occurs when the load is placed at the midpoint of the slab at the edge. This typically represents the most critical loading position, in that the highest flexural stresses develop at this location for an unsupported edge. Calculated stresses are generally higher at midslab at the edge than for a corner, interior, or joint load.

Based on the relationship in equation 20 between the concrete elastic modulus and concrete compressive strength, the computed stresses were related directly to the compressive strength. For example, based on the previous relationship in equation 20 between elastic modulus and compressive strength, the back-calculated compressive strength corresponding to a concrete elastic modulus of 2 million psi (13,800 MPa) would be 1041 psi (7.2 MPa).

Table 55 summarizes the maximum longitudinal free edge stress determined by ILLI-SLAB for the inputs listed in table 54. Stresses rapidly increase non-linearly for elastic moduli values up to 3 million psi (20,700 MPa). For moduli of 3 to 5 million psi (20,700 to 34,500 MPa) the rate of stress decreases to more of a linear trend. For example, a 10-in (25 cm) slab with a k-value of 300 lb/in³ (81 MPa/m) and a compressive strength of 1041 psi (7.2 MPa) would develop a maximum stress of 223 psi (1.5 MPa) for a 20,000-lb (9080-kg) single-axle load with a contact pressure of 100 psi (690 kPa). A 1300-psi (9-MPa) increase in compressive strength from 1041 to 2341 psi (7.2 to 16.1 MPa) increases the stress 6 percent. A further increase of 1821 psi (12.6 MPa) in compressive strength increases the stress 4 percent. Another increase of 2342-psi (16.1-MPa) compressive strength increases the stress only 2 percent. Other stress-compressive strength relationships can easily be derived using the ILLI-SLAB program for various axle loads, configurations, and contact pressures.

If the modulus of rupture corresponding to a given compressive strength is estimated, then the stress ratio (stress/modulus of rupture) can be calculated and an estimate of the fatigue damage done to the pavement by the given construction loading could be obtained. As previously discussed, the relationship between the compressive strength and the modulus of rupture is dependent upon the concrete mix design and should be developed by each agency. For purposes of illustration, the general relationship between modulus of rupture and compressive strength that was presented earlier will be used, assuming 80 percent relative humidity. Studies have shown that this is a typical value for the curing of concrete, and may in fact be a conservative estimate for a slab that has been coated with curing compound.[45]

The resulting modulus of rupture estimate was then used in the fatigue model to obtain the mean allowable number of load applications before slab fracture. For example, a slab with a compressive strength of 1041 psi (7.2 MPa) and a curing relative humidity of 80 percent, the modulus of rupture would be:

$$MR = [8.460 \times (1041)^{0.5}] + (3.311 \times 80) - 155.91 = 382 \text{ psi } (2.6 \text{ MPa})$$

Using this modulus of rupture estimate and the 223-psi (1.5-MPa) critical stress value previously obtained for the 10-in (25-cm) slab, the resulting allowable number of edge load applications is:

196

# Table 55. Summary of fatigue damage for edge loading condition.

| t, in | k, lb/in³ | Ec, million psi | f'c, psi | MR, psi | Stress, psi | Allowable N | Percent Fatigue Damage Consumed at Different Loading Levels | | | | |
|---|---|---|---|---|---|---|---|---|---|---|---|
| | | | | | | | 1 | 10 | 100 | 1000 | 10,000 |
| 8 | 100 | 1 | 260 | 245 | 322 | 3.44E+01 | 3 | 29 | 100+ | 100+ | 100+ |
| 8 | 100 | 2 | 1041 | 382 | 370 | 1.63E+02 | 1 | 6 | 61 | 100+ | 100+ |
| 8 | 100 | 3 | 2341 | 518 | 390 | 9.92E+02 | 0 | 1 | 10 | 100+ | 100+ |
| 8 | 100 | 4 | 4162 | 655 | 404 | 6.27E+03 | 0 | 0 | 2 | 16 | 100+ |
| 8 | 100 | 5 | 6504 | 791 | 414 | 4.25E+04 | 0 | 0 | 0 | 2 | 24 |
| 8 | 300 | 1 | 260 | 245 | 270 | 7.93E+01 | 1 | 13 | 100+ | 100+ | 100+ |
| 8 | 300 | 2 | 1041 | 382 | 317 | 4.64E+02 | 0 | 2 | 22 | 100+ | 100+ |
| 8 | 300 | 3 | 2341 | 518 | 336 | 3.88E+03 | 0 | 0 | 3 | 26 | 100+ |
| 8 | 300 | 4 | 4162 | 655 | 361 | 2.24E+04 | 0 | 0 | 0 | 4 | 45 |
| 8 | 300 | 5 | 6504 | 791 | 361 | 2.88E+05 | 0 | 0 | 0 | 0 | 3 |
| 8 | 500 | 1 | 260 | 245 | 247 | 1.31E+02 | 1 | 8 | 76 | 100+ | 100+ |
| 8 | 500 | 2 | 1041 | 382 | 292 | 8.64E+02 | 0 | 1 | 12 | 100+ | 100+ |
| 8 | 500 | 3 | 2341 | 518 | 311 | 8.51E+03 | 0 | 0 | 1 | 12 | 100+ |
| 8 | 500 | 4 | 4162 | 655 | 326 | 8.44E+04 | 0 | 0 | 0 | 1 | 12 |
| 8 | 500 | 5 | 6504 | 791 | 336 | 9.17E+05 | 0 | 0 | 0 | 0 | 1 |
| 10 | 100 | 1 | 260 | 245 | 229 | 2.07E+02 | 0 | 5 | 48 | 100+ | 100+ |
| 10 | 100 | 2 | 1041 | 382 | 258 | 2.59E+03 | 0 | 0 | 4 | 39 | 100+ |
| 10 | 100 | 3 | 2341 | 518 | 270 | 4.56E+04 | 0 | 0 | 0 | 2 | 22 |
| 10 | 100 | 4 | 4162 | 655 | 277 | 9.75E+05 | 0 | 0 | 0 | 0 | 1 |
| 10 | 100 | 5 | 6504 | 791 | 282 | 2.18E+07 | 0 | 0 | 0 | 0 | 0 |
| 10 | 300 | 1 | 260 | 245 | 193 | 6.85E+02 | 0 | 1 | 15 | 100+ | 100+ |
| 10 | 300 | 2 | 1041 | 382 | 223 | 1.13E+04 | 0 | 0 | 1 | 9 | 88 |
| 10 | 300 | 3 | 2341 | 518 | 237 | 2.86E+05 | 0 | 0 | 0 | 0 | 3 |
| 10 | 300 | 4 | 4162 | 655 | 246 | 8.14E+06 | 0 | 0 | 0 | 0 | 0 |
| 10 | 300 | 5 | 6504 | 791 | 252 | 2.50E+08 | 0 | 0 | 0 | 0 | 0 |
| 10 | 500 | 1 | 260 | 245 | 178 | 1.37E+03 | 0 | 1 | 7 | 73 | 100+ |
| 10 | 500 | 2 | 1041 | 382 | 208 | 2.64E+04 | 0 | 0 | 0 | 4 | 38 |
| 10 | 500 | 3 | 2341 | 518 | 220 | 9.05E+05 | 0 | 0 | 0 | 0 | 1 |
| 10 | 500 | 4 | 4162 | 655 | 229 | 3.30E+07 | 0 | 0 | 0 | 0 | 0 |
| 10 | 500 | 5 | 6504 | 791 | 237 | 1.16E+09 | 0 | 0 | 0 | 0 | 0 |
| 12 | 100 | 1 | 260 | 245 | 173 | 1.71E+03 | 0 | 1 | 6 | 58 | 100+ |
| 12 | 100 | 2 | 1041 | 382 | 190 | 8.36E+04 | 0 | 0 | 0 | 1 | 12 |
| 12 | 100 | 3 | 2341 | 518 | 197 | 6.52E+06 | 0 | 0 | 0 | 0 | 0 |
| 12 | 100 | 4 | 4162 | 655 | 201 | 6.05E+08 | 0 | 0 | 0 | 0 | 0 |
| 12 | 100 | 5 | 6504 | 791 | 203 | 7.53E+10 | 0 | 0 | 0 | 0 | 0 |
| 12 | 300 | 1 | 260 | 245 | 146 | 9.70E+03 | 0 | 0 | 1 | 10 | 100+ |
| 12 | 300 | 2 | 1041 | 382 | 167 | 5.76E+05 | 0 | 0 | 0 | 0 | 2 |
| 12 | 300 | 3 | 2341 | 518 | 176 | 6.44E+07 | 0 | 0 | 0 | 0 | 0 |
| 12 | 300 | 4 | 4162 | 655 | 182 | 7.67E+09 | 0 | 0 | 0 | 0 | 0 |
| 12 | 300 | 5 | 6504 | 791 | 187 | 1.13E+12 | 0 | 0 | 0 | 0 | 0 |
| 12 | 500 | 1 | 260 | 245 | 136 | 2.20E+04 | 0 | 0 | 0 | 5 | 45 |
| 12 | 500 | 2 | 1041 | 382 | 156 | 1.81E+06 | 0 | 0 | 0 | 0 | 1 |
| 12 | 500 | 3 | 2341 | 518 | 164 | 2.80E+08 | 0 | 0 | 0 | 0 | 0 |
| 12 | 500 | 4 | 4162 | 655 | 171 | 4.57E+10 | 0 | 0 | 0 | 0 | 0 |
| 12 | 500 | 5 | 6504 | 791 | 176 | 9.40E+12 | 0 | 0 | 0 | 0 | 0 |

20,000 lb = 9080 kg, 10 in = 25 cm, 1000 psi = 6.9 MPa, 100 lb/in³ = 27.1 MPa/m

$$N = 10 \exp[2.13(382/223)^{1.2}] = 11,572 \text{ applications}$$

This indicates that, at a compressive strength of 1041 psi (7.2 MPa) corresponding to a 382-psi (2.6-MPa) modulus of rupture, the slab can sustain 11,572 edge load applications of a 20,000-lb (9080-kg) single axle load until 50 percent of the slabs are cracked. To calculate the damage done to the pavement by 1000 loads along the unsupported edge, the actual number of load applications (n) is divided by N, so that the percent life consumed would be:

$$\text{Damage} = (1000 / 11,572) \times 100 = 8.6 \text{ percent}$$

As the damage value indicates, the amount of damage from 1000 applications of a 20,000-lb (9080-kg) single-axle with a tire pressure of 100 psi (690 kPa) along an unsupported edge would be 8.6 percent at that point in time when the concrete possesses a compressive strength of 1041 psi (7.2 MPa). To show the importance of early strength development on concrete fatigue, the damage done by the same 1000 loads for pavements with a compressive strength of 2341 and 4162 psi (16.1 and 28.7 MPa) would be 2.2 and 0.1 percent, respectively.

Table 55 provides a summary of the fatigue damage calculations for each combination of slab thickness (t), k-value, and elastic modulus value (E). The table also shows the corresponding compressive strength ($f_c'$) and modulus of rupture (MR) values, the critical stress in the slab ($\sigma$), and the allowable number of load applications (N). The allowable load applications were calculated using the assumed compressive strength-elastic modulus, compressive strength-modulus of rupture, and fatigue relationships.

The fatigue damage results of table 55 are plotted in figures 91 through 99 for only those cases where significant fatigue damage occurs. These charts allow for the immediate determination of the fatigue damage done by the standard truck loading 20,000-lb (9080-kg), single-axle and 100-psi (690-kPa) contact pressure on a pavement of known compressive strength. For simplification in graphing, the compressive strength values have been rounded off to the nearest 50 psi (345 kPa).

As an example in using the charts, it is observed that, from figure 91, which is for an 8-in (20-cm) slab with a k-value of 100 lb/in³ (27.1 MPa/m), 100 loads of the standard truck loading will consume 61 percent of the concrete fatigue life if the slab is loaded when it has a compressive strength of only 1050 psi (7.2 MPa). However, if the pavement is not loaded until the concrete has attained a compressive strength of 4150 psi (28.6 MPa) then 100 load applications of the standard loading will reduce the fatigue life by only about 2 percent. Other comparisons can be made as to the relative damage done at different concrete strengths by a different number of load applications.

## Interior Loading Condition

An analysis similar to the one conducted for the edge loading condition was conducted the interior loading condition. The interior loading condition is when the wheel loading is situated at some distance from the edge. The position of the interior load was placed 2 ft (61 cm) from the edge to represent the case where an 8-ft (2.4-m) wide truck would center itself in a 12-ft (3.7-m) wide lane, as shown in figure 89. The ILLI-SLAB

**t=8 in, k=100 pci**

■ 250 psi   □ 1050 psi   ◆ 2350 psi   ◇ 4150 psi   ▲ 6500 psi
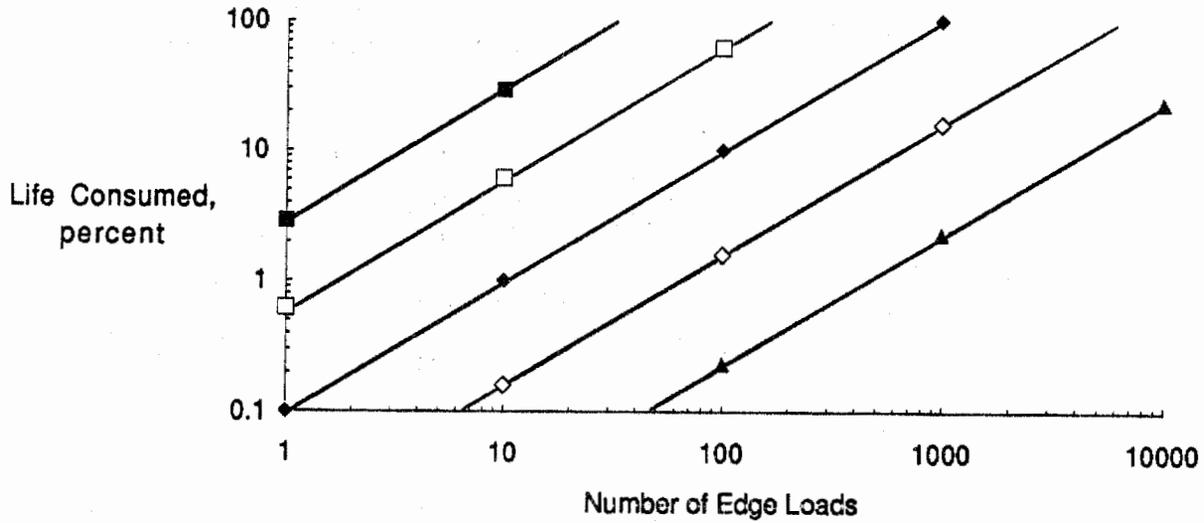


Figure 91.  Percent life consumed vs. number of 20,000-lb (9080-kg) single-axle edge load applications for an 8-in (20-cm) slab (k = 100 pci, 27.1 MPa/m).

**t=8 in, k=300 pci**

■ 250 psi   □ 1050 psi   ◆ 2350 psi   ◇ 4150 psi   ▲ 6500 psi



Figure 92.  Percent life consumed vs. number of 20,000-lb (9080-kg) single-axle edge load applications for an 8-in (20-cm) slab (k = 300 pci, 81.3 MPa/m).

8 in = 20 cm
500 pci = 136 MPa/m
1000 psi = 6.9 MPa

**t=8 in, k=500 pci**

■ 250 psi   □ 1050 psi   ◆ 2350 psi   ◇ 4150 psi   ▲ 6500 psi

Life Consumed, percent

Number of Edge Loads
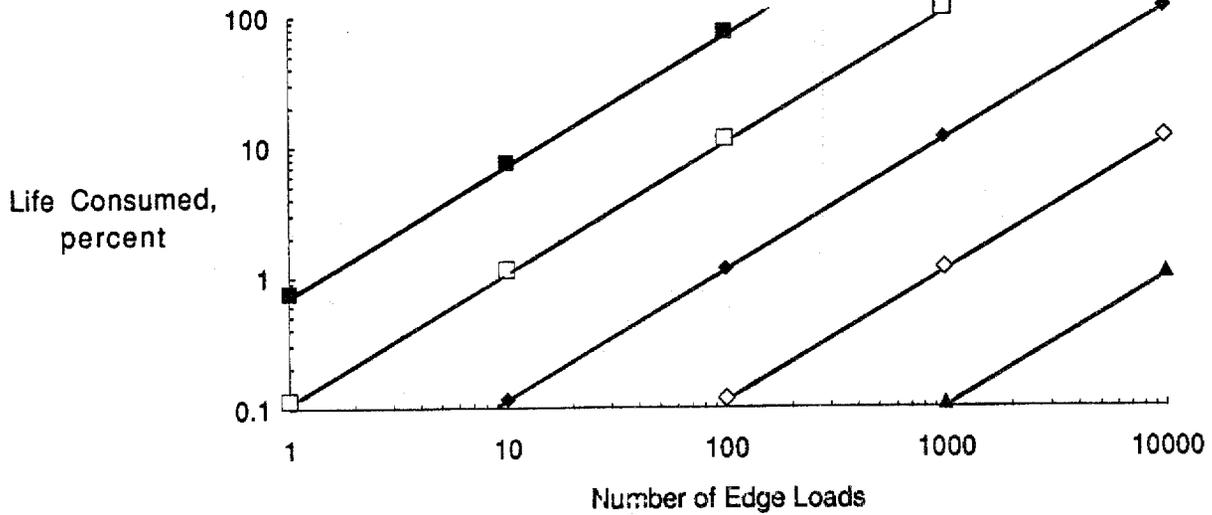
Figure 93.  Percent life consumed vs. number of 20,000-lb (9080-kg) single-axle edge load applications for an 8-in (20-cm) slab (k = 500 pci, 135.5 MPa/m).



10 in = 25.4 cm
100 pci = 27.1 MPa/m
1000 psi = 6.9 MPa

**t=10 in, k=100 pci**

■ 250 psi   □ 1050 psi   ◆ 2350 psi   ◇ 4150 psi   ▲ 6500 psi

Life Consumed, percent

Number of Edge Loads
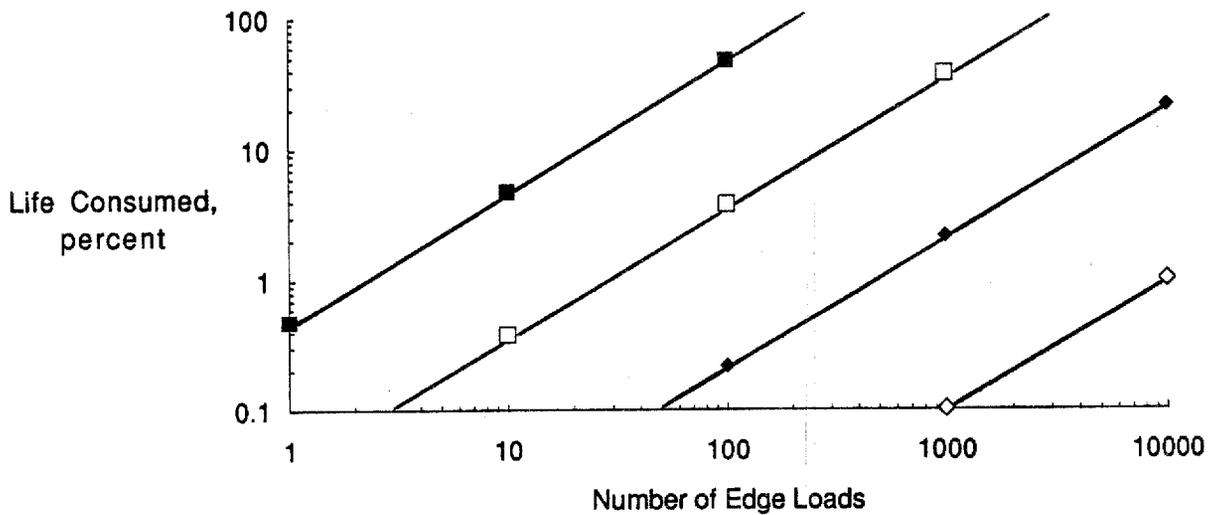
Figure 94.  Percent life consumed vs. number of 20,000-lb (9080-kg) single-axle edge load applications for a 10-in (25-cm) slab (k = 100 pci, 27.1 MPa/m).

200

t=10 in, k=300 pci

■ 250 psi   □ 1050 psi   ◆ 2350 psi   ◇ 4150 psi   ▲ 6500 psi

Life Consumed, percent

Number of Edge Loads
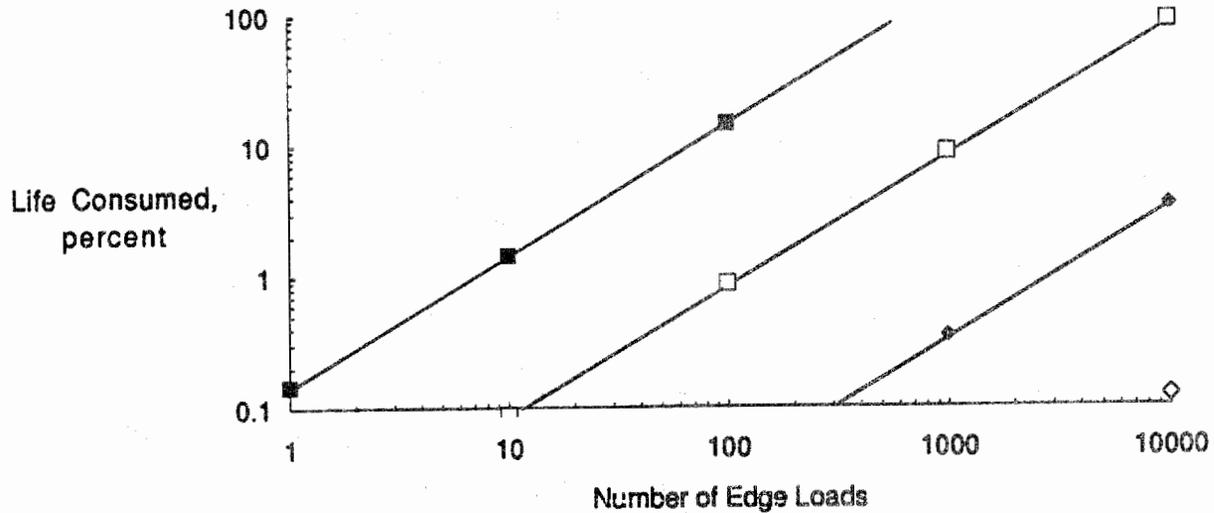
Figure 95.   Percent life consumed vs. number of 20,000-lb (9080-kg) single-axle edge load applications for a 10-in (25-cm) slab (k = 300 pci, 81.3 MPa/m).

10 in = 25.4 cm
500 pci = 136 MPa/m
1000 psi = 6.9 MPa

t=10 in, k=500 pci

■ 250 psi   □ 1050 psi   ◆ 2350 psi   ◇ 4150 psi   ▲ 6500 psi

Life Consumed, percent

Number of Edge Loads
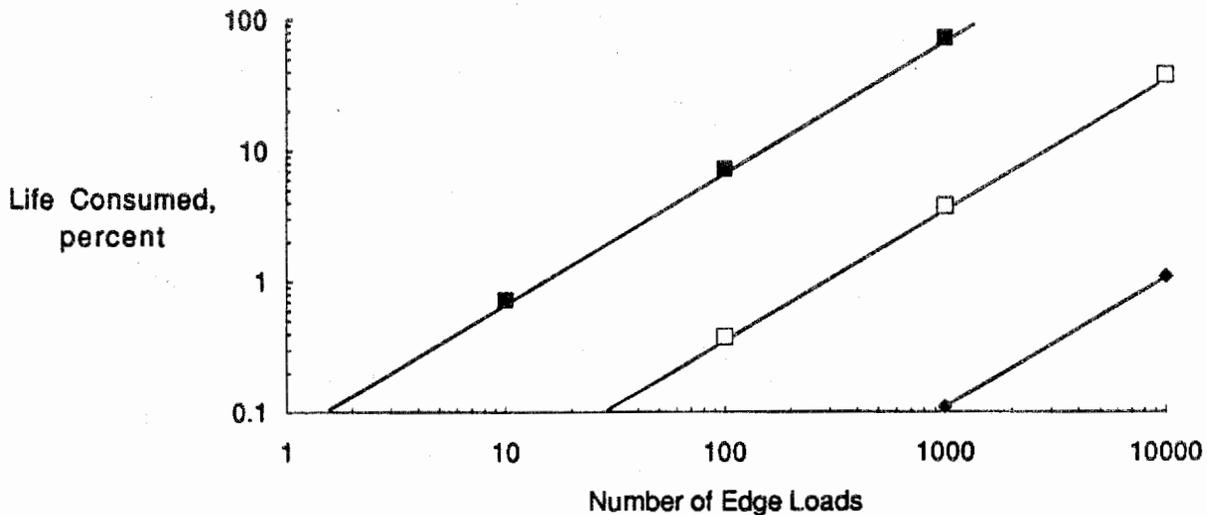
Figure 96.   Percent life consumed vs. number of 20,000-lb (9080-kg) single-axle edge load applications for a 10-in (25-cm) slab (k = 500 pci, 135.5 MPa/m).

201

12 in = 30 cm
100 pci = 27.1 MPa/m
1000 psi = 6.9 MPa

**t=12 in, k=100 pci**

■ 250 psi   □ 1050 psi   ◆ 2350 psi   ◇ 4150 psi   ▲ 6500 psi
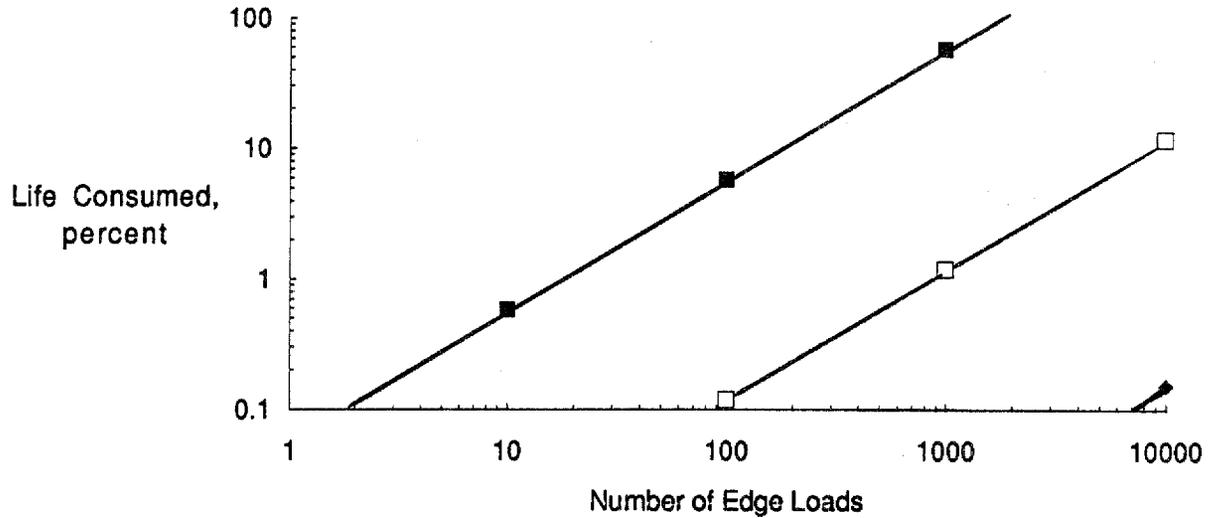
Figure 97.  Percent life consumed vs. number of 20,000-lb (9080-kg) single-axle edge load applications for a 12-in (30-cm) slab (k = 100 pci, 27.1 MPa/m).



12 in = 30 cm
300 pci = 81.4 MPa/m
1000 psi = 6.9 MPa

**t=12 in, k=300 pci**

■ 250 psi   ⊞ 1050 psi   ◆ 2350 psi   ◇ 4150 psi   ▲ 6500 psi
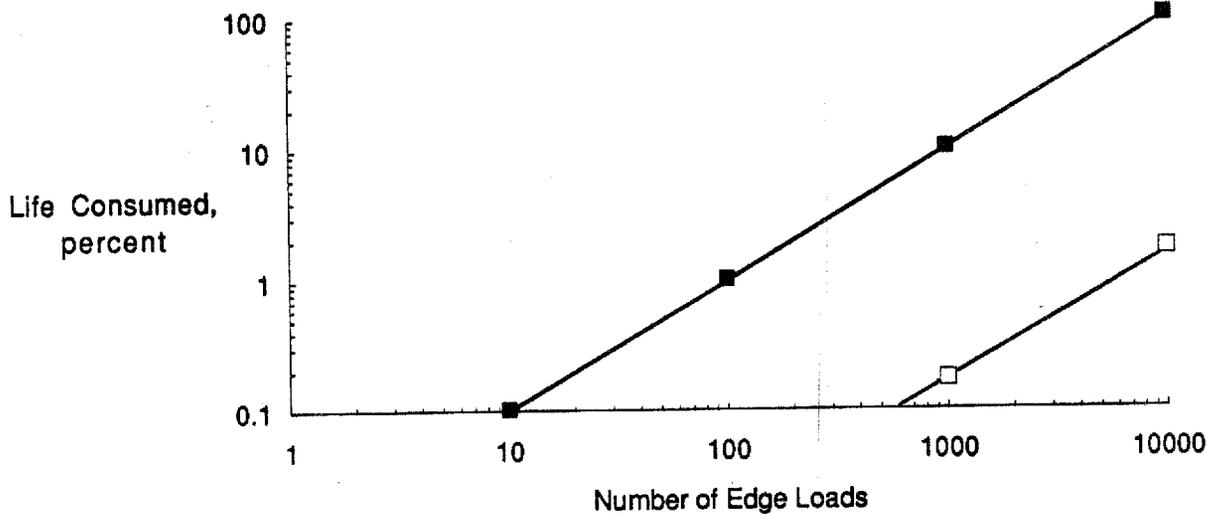
Figure 98.  Percent life consumed vs. number of 20,000-lb (9080-kg) single-axle edge load applications for a 12-in (30-cm) slab (k = 300 pci, 81.3 MPa/m).

202
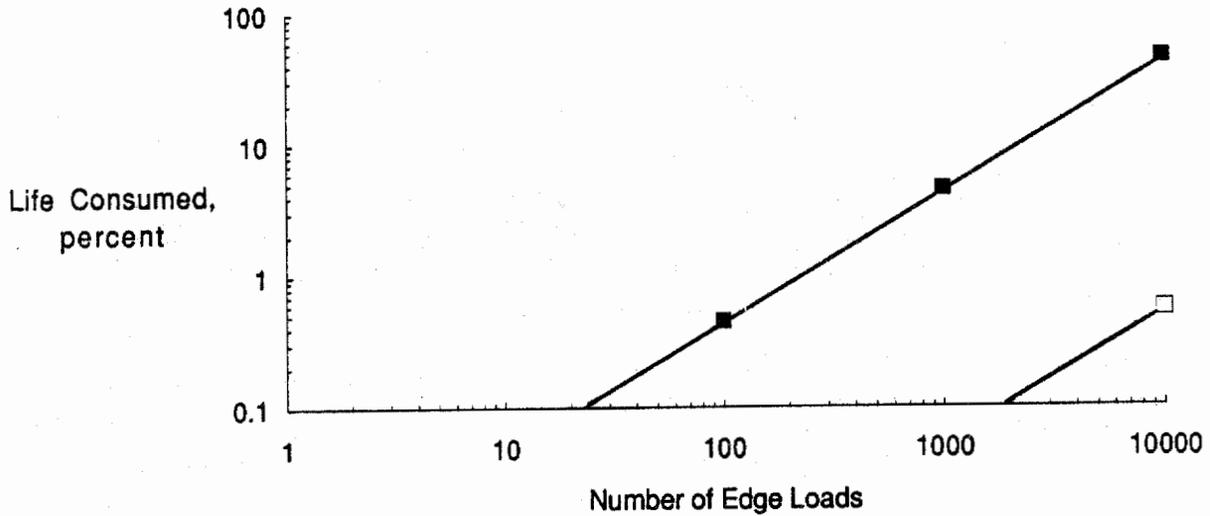
Figure 99. Percent life consumed vs. number of 20,000-lb (9080-kg) single-axle edge load applications for a 12-in (30-cm) slab (k = 500 pci, 135.5 MPa/m).

program was used to determine the stresses occurring in the pavement for the 20,000-lb (9080-kg) single-axle load with a contact pressure of 100 psi (690 kPa). These stresses are summarized in table 56.

Using the same relationship between compressive strength and elastic modulus, the maximum stress in the slab as a function of the compressive strength of the concrete was computed. Then, again for purposes of demonstration, the modulus of rupture was estimated from the general laboratory relationship with compressive strength using 80 percent relative humidity. These results were then evaluated using the fatigue damage model to obtain an estimate of the slab fatigue damage for a range of slab thicknesses and load applications, as summarized table 56.

The interior loading condition produces much less damage than the edge loading condition, and indicates that if the trucks that load a pavement early stay 2 ft (61 cm) away from the edge little damage may result. In the edge loading condition example, it was noted that 100 applications of the 20,000-lb (9080-kg) single-axle load consumed 291 percent of the life of an 8-in (20-cm) slab with a k-value of 100 lb/in$^3$ (27.1 MPa/m) and a compressive strength of 250 psi (1.7 MPa). However, if those same 100 applications are positioned 2 ft (61 cm) from the edge of the slab, only about 9 percent of the fatigue life would be consumed.

## Transverse Joint Loading Condition

In addition to the edge and interior loading conditions, the case of a wheel load placed at the transverse joint was also considered. The results of the field investigations showed that, for both doweled and nondoweled joints, the stresses developing at the transverse joints at early ages were actually less than those developing at the slab interior. This is believed to be due to the presence of the dowels (for the doweled joints) and also to the fact that, at very early ages before concrete drying shrinkage, there is a large amount of aggregate interlock at the joints. This results in good load transfer across the joint that serves to reduce the magnitude of the transverse joint stresses.

Although the transverse joint loading condition was not considered to be as critical as the edge or even the interior loading condition, it was still evaluated with the ILLI-SLAB program for a few selected cases. A 10-in (25-cm) slab (with and without dowel bars) was evaluated for k-values of 100, 300, and 500 lb/in$^3$ (27.1, 81.4, and 135.7 MPa/m) and concrete elastic modulus values of 2 million and 4 million psi (13,790 and 27,580 MPa). The transverse joint was loaded with an 20,000-lb (9080-kg) single-axle load at a distance of 6 ft (92 cm) from the slab edge. The load was placed at midslab to calculate maximum flexural stress. Similar to edge loading conditions maximum stresses occur at midslab. Loads placed at a corner or in the wheel path will result in lower calculated stresses.

Doweled Transverse Joint. The results of the analysis for the doweled trans-verse joint loading condition are shown in table 57. The doweled transverse joint was analyzed ass uming zero aggregate interlock at the joint with load transfer only provided by dowel bars. This provides for a conservative estimate of the actual stresses because a por-tion of the load will be transferred through aggregate interlock. Typical stress transfer effi-ciencies measured in the field study for the doweled joints ranged between 46 and 58 percent.

# Table 56. Summary of fatigue damage for interior loading condition.

| t, in | k, lb/in³ | Ec, million psi | f'c, psi | MR, psi | Stress, psi | Allowable N | Percent Fatigue Damage Consumed at Different Loading Levels | | | | |
|---|---|---|---|---|---|---|---|---|---|---|---|
| | | | | | | | 1 | 10 | 100 | 1000 | 10,000 |
| 8 | 100 | 1 | 260 | 245 | 183 | 1.05E+03 | 0 | 1 | 9 | 95 | 100+ |
| 8 | 100 | 2 | 1041 | 382 | 206 | 3.01E+04 | 0 | 0 | 0 | 3 | 33 |
| 8 | 100 | 3 | 2341 | 518 | 219 | 9.84E+05 | 0 | 0 | 0 | 0 | 1 |
| 8 | 100 | 4 | 4162 | 655 | 228 | 3.65E+07 | 0 | 0 | 0 | 0 | 0 |
| 8 | 100 | 5 | 6504 | 791 | 236 | 1.31E+09 | 0 | 0 | 0 | 0 | 0 |
| 8 | 300 | 1 | 260 | 245 | 154 | 5.17E+03 | 0 | 0 | 2 | 19 | 100+ |
| 8 | 300 | 2 | 1041 | 382 | 172 | 3.45E+05 | 0 | 0 | 0 | 0 | 3 |
| 8 | 300 | 3 | 2341 | 518 | 183 | 2.59E+07 | 0 | 0 | 0 | 0 | 0 |
| 8 | 300 | 4 | 4162 | 655 | 192 | 1.87E+09 | 0 | 0 | 0 | 0 | 0 |
| 8 | 300 | 5 | 6504 | 791 | 199 | 1.48E+11 | 0 | 0 | 0 | 0 | 0 |
| 8 | 500 | 1 | 260 | 245 | 143 | 1.15E+04 | 0 | 0 | 1 | 9 | 87 |
| 8 | 500 | 2 | 1041 | 382 | 159 | 1.26E+06 | 0 | 0 | 0 | 0 | 1 |
| 8 | 500 | 3 | 2341 | 518 | 170 | 1.31E+08 | 0 | 0 | 0 | 0 | 0 |
| 8 | 500 | 4 | 4162 | 655 | 178 | 1.52E+10 | 0 | 0 | 0 | 0 | 0 |
| 8 | 500 | 5 | 6504 | 791 | 183 | 2.07E+12 | 0 | 0 | 0 | 0 | 0 |
| 10 | 100 | 1 | 260 | 245 | 131 | 3.31E+04 | 0 | 0 | 0 | 3 | 30 |
| 10 | 100 | 2 | 1041 | 382 | 146 | 5.99E+06 | 0 | 0 | 0 | 0 | 0 |
| 10 | 100 | 3 | 2341 | 518 | 154 | 1.28E+09 | 0 | 0 | 0 | 0 | 0 |
| 10 | 100 | 4 | 4162 | 655 | 160 | 3.58E+11 | 0 | 0 | 0 | 0 | 0 |
| 10 | 100 | 5 | 6504 | 791 | 163 | 1.40E+14 | 0 | 0 | 0 | 0 | 0 |
| 10 | 300 | 1 | 260 | 245 | 110 | 3.80E+05 | 0 | 0 | 0 | 0 | 3 |
| 10 | 300 | 2 | 1041 | 382 | 122 | 2.28E+08 | 0 | 0 | 0 | 0 | 0 |
| 10 | 300 | 3 | 2341 | 518 | 131 | 1.22E+11 | 0 | 0 | 0 | 0 | 0 |
| 10 | 300 | 4 | 4162 | 655 | 137 | 9.13E+13 | 0 | 0 | 0 | 0 | 0 |
| 10 | 300 | 5 | 6504 | 791 | 142 | 5.04E+16 | 0 | 0 | 0 | 0 | 0 |
| 10 | 500 | 1 | 260 | 245 | 101 | 1.49E+06 | 0 | 0 | 0 | 0 | 1 |
| 10 | 500 | 2 | 1041 | 382 | 113 | 1.41E+09 | 0 | 0 | 0 | 0 | 0 |
| 10 | 500 | 3 | 2341 | 518 | 120 | 2.13E+12 | 0 | 0 | 0 | 0 | 0 |
| 10 | 500 | 4 | 4162 | 655 | 127 | 1.96E+15 | 0 | 0 | 0 | 0 | 0 |
| 10 | 500 | 5 | 6504 | 791 | 131 | 2.60E+18 | 0 | 0 | 0 | 0 | 0 |
| 12 | 100 | 1 | 260 | 245 | 99 | 2.19E+06 | 0 | 0 | 0 | 0 | 0 |
| 12 | 100 | 2 | 1041 | 382 | 109 | 3.99E+09 | 0 | 0 | 0 | 0 | 0 |
| 12 | 100 | 3 | 2341 | 518 | 114 | 1.12E+13 | 0 | 0 | 0 | 0 | 0 |
| 12 | 100 | 4 | 4162 | 655 | 118 | 4.88E+16 | 0 | 0 | 0 | 0 | 0 |
| 12 | 100 | 5 | 6504 | 791 | 119 | 5.12E+20 | 0 | 0 | 0 | 0 | 0 |
| 12 | 300 | 1 | 260 | 245 | 83 | 6.10E+07 | 0 | 0 | 0 | 0 | 0 |
| 12 | 300 | 2 | 1041 | 382 | 93 | 3.56E+11 | 0 | 0 | 0 | 0 | 0 |
| 12 | 300 | 3 | 2341 | 518 | 99 | 3.55E+15 | 0 | 0 | 0 | 0 | 0 |
| 12 | 300 | 4 | 4162 | 655 | 103 | 3.35E+19 | 0 | 0 | 0 | 0 | 0 |
| 12 | 300 | 5 | 6504 | 791 | 107 | 3.88E+23 | 0 | 0 | 0 | 0 | 0 |
| 12 | 500 | 1 | 260 | 245 | 77 | 4.03E+08 | 0 | 0 | 0 | 0 | 0 |
| 12 | 500 | 2 | 1041 | 382 | 86 | 6.65E+12 | 0 | 0 | 0 | 0 | 0 |
| 12 | 500 | 3 | 2341 | 518 | 91 | 1.43E+17 | 0 | 0 | 0 | 0 | 100+ |
| 12 | 500 | 4 | 4162 | 655 | 96 | 2.80E+21 | 0 | 0 | 0 | 0 | 0 |
| 12 | 500 | 5 | 6504 | 791 | 99 | 6.80E+25 | 0 | 0 | 0 | 0 | 0 |

20,000 lb = 9080 kg, 10 in = 25 cm, 1000 psi = 6.9 MPa, 100 lb/in³ = 27.1 MPa/m

**Table 57. Maximum transverse stresses computed by ILLI-SLAB for transverse joint loading condition for doweled joint.**

| Slab Thickness, inches | k-value, lb/in $^3$ | Maximum Transverse Stress, psi | |
|---|---|---|---|
| | | Concrete Modulus of Elasticity, million psi | |
| | | 2 | 4 |
| 10 | 100 | 137 | 157 |
| | 300 | 128 | 144 |
| | 500 | 119 | 137 |

100 lb/in$^3$ = 27.1 MPa/m$^3$
10 in = 25 cm
1000 psi = 6.9 MPa

**Nondoweled Transverse Joint.** Table 58 shows the results of the analysis for the nondoweled transverse joint loading condition. The analysis was conducted assuming a "free edge" and then the various stresses corresponding to selected load transfer efficiencies were determined using the following relationship:

$$\sigma = \sigma_{fe} / (1 + LTE) \quad\ldots\ldots\ldots\ldots\ldots\ldots\ldots\ldots\ldots\ldots\ldots\ldots\ldots\ldots\quad (24)$$

where:

$\sigma$ = calculated edge stress for a given LTE of

$\sigma_{fe}$ = maximum free edge stress (zero LTE)

LTE = stress load transfer efficiency across transverse joint (unloaded divided by loaded slab stress, percentage)

Stress load transfer efficiencies ranging from 0 to 100 percent were evaluated and the resulting stresses are shown in table 58. As would be expected, the amount of the LTE greatly influences the magnitude of the stresses.

**Comparison of Interior and Transverse Joint Stresses.** The stresses for the doweled and nondoweled joints (assuming 50 percent LTE) are plotted in figures 100 through 102 along with the corresponding interior stresses. Generally, there is little difference in the magnitude of the stresses. It is observed that, for a k-value of 100 lb/in$^3$ (27.1 MPa/m), the doweled transverse joint stresses were less than the interior stresses. As the k-value increased, the doweled stresses became slightly larger than the corresponding interior loading condition, although the differences are not substantial.

The nondoweled transverse joint stresses were generally higher than those for the doweled joint or the interior loading condition. Again, however, the nondoweled transverse joint stresses were not substantially different than those for the interior loading condition. The biggest differences between the nondoweled transverse joint stresses and the interior stresses occurred for the stiffer k-value of 300-and 500-lb/in$^3$ (81-and 136-MPa/m) foundations, respectively.

For the purposes of this comparison, 50-percent stress load transfer was assumed for the nondoweled transverse joint. In actuality, this value may be much higher due to the high level of aggregate interlock that exists immediately after construction. As observed from table 58, an increase in stress load transfer efficiency to even 75 percent greatly reduces the magnitude of the stresses to values much less than these for interior loading condition. The same argument can be made for the stresses developing in the doweled joint, as these were determined assuming no aggregate interlock load transfer. Thus, since there does not appear to be significant differences between the transverse joint stresses (relatively low 50 percent load transfer efficiency) and the interior stresses, the fatigue table developed for the interior loading condition is probably applicable to the transverse joint loading condition as well.

**Table 58. Maximum transverse stresses computed by ILLI-SLAB for transverse joint loading condition for undoweled joint with varying stress load transfer efficiencies.**

| Slab Thickness, in | Modulus of Subgrade Reaction (k-value), lb/in³ | Maximum Transverse Stress, psi [1] | | | | | | | |
|---|---|---|---|---|---|---|---|---|---|
| | | Concrete Modulus of Elasticity, million psi | | | | | | | |
| | | 2 | | | | 4 | | | |
| | | 0% LTE | 50% LTE | 75% LTE | 100% LTE | 0% LTE | 50% LTE | 75% LTE | 100% LTE |
| 10 | 100 | 226 | 150 | 129 | 113 | 240 | 160 | 137 | 120 |
| | 300 | 198 | 132 | 113 | 99 | 217 | 144 | 123 | 109 |
| | 500 | 181 | 121 | 103 | 91 | 202 | 134 | 116 | 101 |

NOTE: [1] Stresses corresponding to 50-, 75-, and 100-percent stress load transfer efficiencies (LTE) were determined from the equation: S = Sfe/(1 + LTE/100)

where S = calculated joint stress for a given value of LTE

Sfe = maximum free joint stress (zero LTE)

LTE = stress load transfer efficiency across transverse joint in percentage

100 lb/in³ = 27.1 MPa/m³, 10 in = 25 cm, 1000 psi = 6.9 MPa

**Transverse and interior stresses t = 10 in, k = 100 pci**
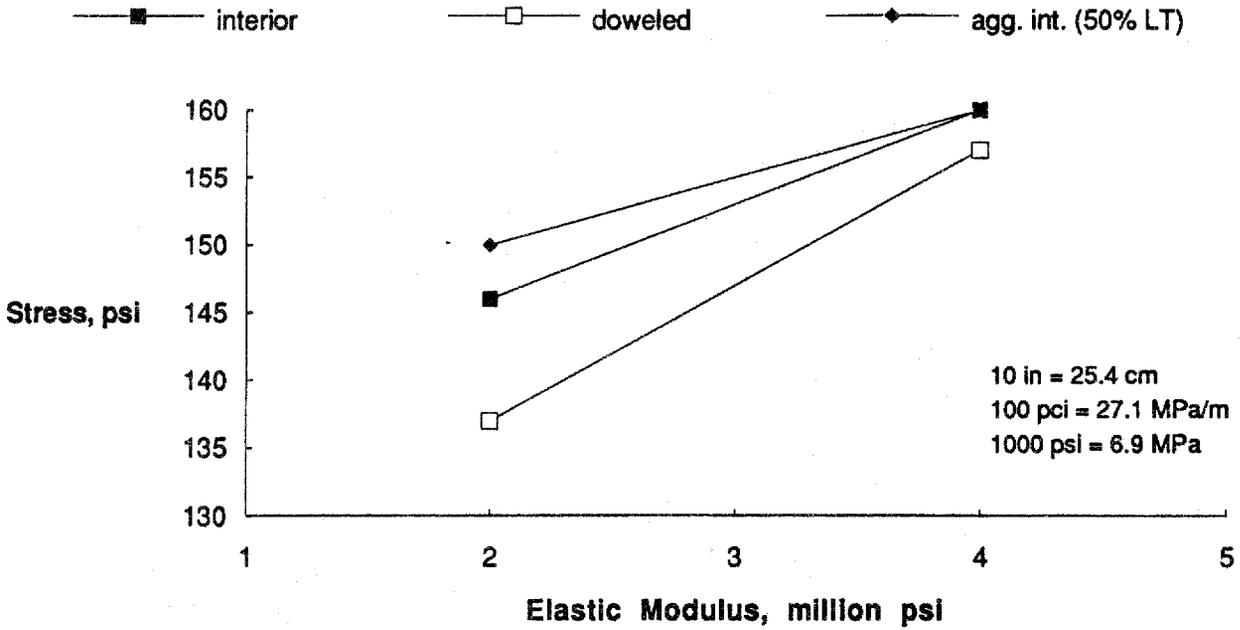


Figure 100. Comparison of interior and transverse joint stresses for a 10-in (25-cm) slab (k = 100 pci, 27.1 MPa/m).

**Transverse and interior stresses t = 10 in, k = 300 pci**
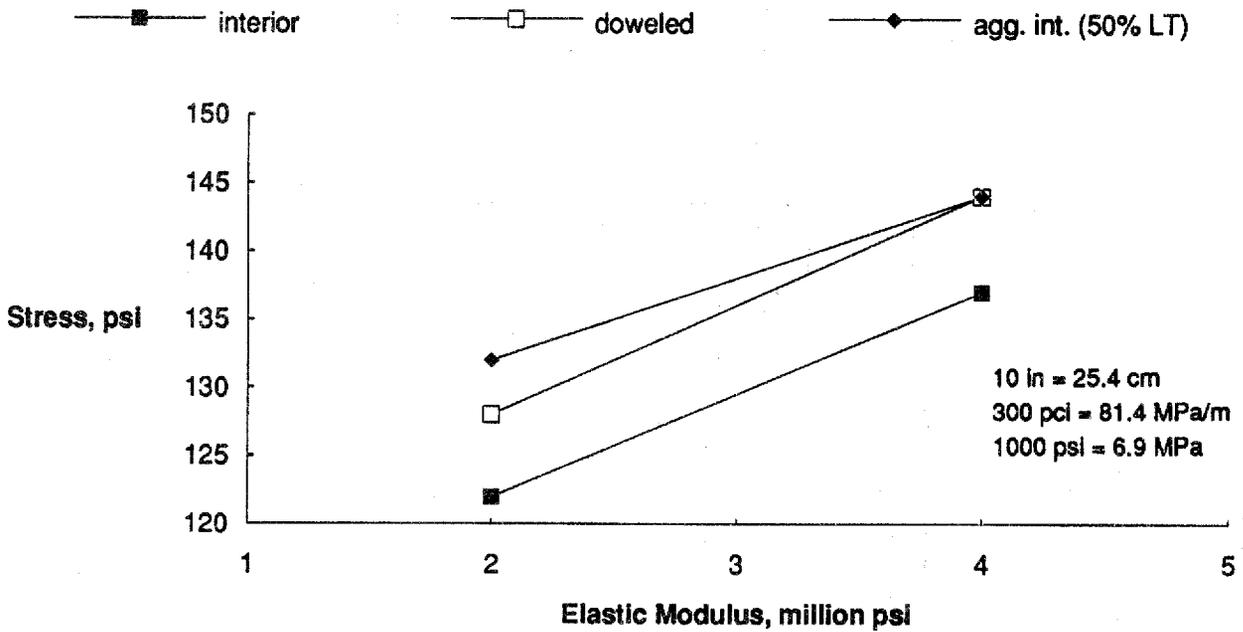


Figure 101. Comparison of interior and transverse joint stresses for a 10-in (25-cm) slab (k = 300 pci, 81.3 MPa/m).

209

**Transverse and interior stresses t = 10, k = 500 pci**
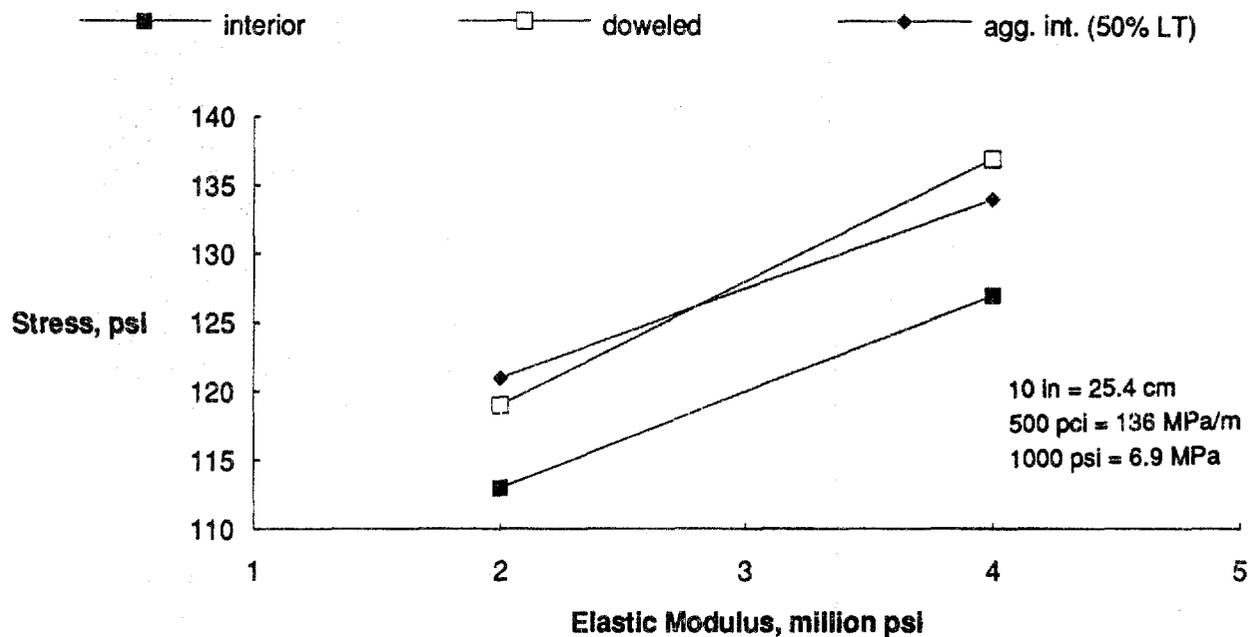


Figure 102. Comparison of interior and transverse joint stresses for a 10-in (25-cm) slab (k = 500 pci, 135.5 MPa/m).

## Tandem-Axle Loading Condition

Single-axle loadings at the edge of a slab induce higher stresses than tandem-axle loads of equal axle load magnitude. Since early construction traffic may consist of tandem-axle load vehicles the fatigue consumption at early ages will be less than for single-axle vehicles of equal load magnitude. The ILLI-SLAB analysis was repeated for a 40,000-lb (18,160-kg) tandem-axle load at the slab edge.

The tandem-axle load edge stresses for inputs listed in table 54 ranged from 72 to 81 percent of the single-axle load stresses. Average reduction in stress was 24 percent. Eighty percent of the 45 combinations of thickness, subgrade support, and elastic modulus ranged from 21 to 27 percent edge stress reduction. For the interior loading tandem-axle load stresses ranged from 75 to 85 percent of the single-axle load stresses. Average interior stress reduction was 22 percent. Seventy-one percent of the 45 combinations of thickness, subgrade support, and elastic modulus ranged from 19 to 25 percent interior stress reduction. Overall (edge and interior) stress reduction was 23 percent. If a significant portion of construction traffic is 40,000-lb (18,160-kg) tandem-axle loadings the fatigue damage can be easily determined using the procedure previously outlined. The stresses in tables 55 and 56 should be reduced by 23 percent (multiplied by 0.77) and fatigue damage recalculated using equation 23. The table and figures for the single-axle edge loading may also be used for tandem-axle loading if a 23 percent load factor of safety is desired.

## Stresses at Loads Other than 20,000 lb (9080 kg)

Similar to the tandem-axle analysis, the fatigue for loads different than 20,000-lb (9080 kg) can be easily determined. For instance if the maximum single-axle load is 15,000 lb (6810 kg) then the stresses in tables 55 and 56 would be multiplied by the ratio of 15 to 20 (0.75). The resulting fatigue per axle loading would then be calculated using equation 23. For a 30,000-lb (13,620-kg) tandem-axle load the stresses in tables 55 and 56 would be multiplied by 0.77 to convert from a 20,000-lb (9080 kg) single to 40,000-lb (18,160-kg) tandem-axle load and again multiplied by the ratio of 30 to 40 (0.75) to convert from a 40,000-to 30,000-lb (18,160-to 13,620-kg) tandem-axle load. Fatigue per loading is then calculated using equation 23.

For mixed traffic tandem- and single-axle vehicles (including front axles of tandem-axle vehicles) at various loads, the analysis would be repeated. The fatigue damage would be summed for all loads anticipated at each concrete modulus of elasticity. The mixed traffic analysis would be repeated as the elastic modulus changes with time, using equation 22 to determine damage done by anticipated traffic.

## Warping Restraint Stresses

Warping stresses were not considered in the evaluation of stresses at early ages. Warping restraint stresses occur at slab edges and corners due to volumetric changes in the concrete. Warping restraint stresses occur as slabs lose moisture creating a moisture gradient. If moisture is lost out the the slab surface the volumetric changes will cause slab edges to curl up causing a bottom compressive restraint stress. These stresses would then be subtracted from the load induced bottom tensile stresses adding a factor of safety to the

early loading analysis. Since the slabs are generally cured using curing compound, wet burlap, or polyethylene sheeting, the moisture gradient effects are minimized. Any loss of moisture through the slab surface due to inadequate curing compound coverage would induce stresses of opposite sign of those due to load.

Studies on moisture gradients in slabs indicate that the changes in moisture can cause significantly less change in volume than corresponding changes due to temperature.[46] It is very difficult to reliably measure moisture changes with depth and to calculate effects of warping stresses. Most engineers recognize that warping restraint stresses exist but do not account for them in a quantitative mechanistic design procedure.

Warping restraint stresses in the early loading analysis were not accounted for since:

- Any moisture gradients are non-linear and constantly changing.

- Effects of moisture gradient changes are difficult to compute for non-linear gradients.

- Proper curing procedure will minimize volumetric moisture gradient related changes at early ages.

- If a moisture gradient causes slabs to warp up, the restraint stresses act in opposite direction to load induced stresses (subtractive).

## Curling Restraint Stresses

Curling stresses were also not considered in the early loading analysis. Differential temperatures between the top and bottom of the slab result in a thermal gradient. The gradient causes a volumetric difference which will cause the slab to curl up or down. The degree of curling is dependent on coefficients of thermal expansion, presence of shoulders, joint spacing, thermal gradient magnitude, and thermal distribution.

Slabs which curl up at night when air tempeatures cool the surface cause a bottom compressive curling restraint stress and is subtractive from load induced bottom tensile stresses at slab edges (critical for flexural fatigue) and transverse joints. Slabs curl down during the day as solar radiation causes a greater temperature increase at the surface than at the bottom resulting in a positive gradient. Since the slab weight adds to tensile stresses at the slab bottom for convex curl they are additive to bottom tensile load induced stresses.

Curling restraint stresses were not accounted for in the early loading analysis since:

- Stresses depend on material variables such as unit weight and coefficient of thermal expansion which may vary from project to project.

- Stresses also depend on design variables such as thickness, subbase support, shoulders, and joint spacing.

- Theoretical calculations assume a linear temperature gradient which may not be realistic of actual conditions.

212

- Gradients are constantly changing which could introduce variables of magnitude and distribution of temperature gradient. Also gradients are dependent on seasonal, air temperature, and solar radiation effects.

- Theoreteical curling stresses are sensitive to joint spacing effects.

The early loading analysis outlined in this study can easily incorporate effects of thermal gradients. Curling restraint stresses can be calculated using the procedures outlined in chapter 2. Other techniques of calculating curling stresses are also available. Westergaard developed a closed form solution for calculating curl stresses for jointed pavements.[47] The ILLI-SLAB computer program is also capable of computing curing restraint stresses with or without the addition of wheel loads assuming a linear temperature gradient. Restraint stresses are a function of temperature gradient, joint spacing, coefficient of thermal expansion, slab support, and slab thickness. Stresses are mainly a fraction of joint spacing and slab subbase support.[46]

For a particular project a temperature gradient would be assumed. Coefficients of thermal expansion measured in the laboratory study indicated that at ages of 16 hours, the coefficients were not significantly different than those normally assumed in mature concrete. Coefficients will be a function of aggregate type. Curling stresses can then be estimated for the given pavement design. For daytime construction traffic, when the slab surface is warmer than the bottom and slabs are curled downward, the calculated stresses should be added to the load stresses. Commonly the slabs are curled upward until mid to late morning. This time is dependent upon solar radiation, subbase type, slab thickness, and slab temperature gradients. For traffic when slabs are curled upward, the stresses are subtracted from load stresses.

To calculate fatigue an analysis similar to that for tandem-axle and loads other than 20,000 lb (9080 kg) would be conducted. The calculated curling restraint stress (no load) for a slab curled downward would be added to the load stress in tables 55 and 56. For each load the fatigue damage can be recalculated using equation 23. Similarily for a slab curled upward the curling restraint stress would be subtracted from the load stress in tables 55 and 56.

## EVALUATION OF DOWEL BEARING STRESSES

The maximum bearing stresses exerted by the dowel on the concrete can be a critical aspect in the design of doweled concrete pavements. The magnitude of the bearing stresses can have a large impact on the development of transverse joint faulting.[48,49] Of particular interest to this study is the magnitude of the bearing stresses due to early loading. If the bearing stresses due to early loading exceed the compressive strength of the concrete, fracture of the concrete below the dowels will occur.

The modified Friberg analysis was used to calculate the maximum bearing stresses.[50,51] The maximum bearing stress is given by the formula:

$$\sigma_{max} = G * \delta_o \quad \dots \dots \dots \dots \dots \dots \dots \dots (25)$$

where:

$G$   = modulus of dowel support, $lb/in^3$

$\delta_0$   = deflection of the dowel at the face of the joint, in

   = $P_t (2 + \beta z) / 4\beta^3 E_s I$

in which

$P_t$   = shear force acting on dowel, lb

$z$   = width of joint opening, in

$E_s$   = modulus of elasticity of dowel bar, psi

$I$   = moment of inertia of dowel bar cross-section, $in^4$

   = $0.25 * \pi * (d/2)^4$ for dowel diameter d, in

$\beta$   = relative stiffness of the dowel concrete system, 1/in

   = $[ (Gd) / (4E_s I) ]0.25$

$d$   = dowel diameter, in

The analysis considers the case of a 10,000-lb (4540-kg) wheel load placed at the corner, which will produce stress in the outermost dowel bar. Only dowel bars within a distance of 1.0*L from the center of the load are considered to be active, where L is the radius of relative stiffness, defined in equation 6 of figure 3.

The modified Friberg analysis is based on the assumption that 45 percent of the load (not the stress) was transferred across the joint, which has been shown to provide conservative results.[49]

One parameter required for the determination of dowel bearing stresses that is very difficult to determine is the modulus of dowel support, G. This value has been suggested to range from 300,000 to 1,500,000 $lb/in^3$ (81,400 to 407,200 MPa/m), with a value of 1,500,000 $lb/in^3$ (407,200 MPa/m) typically assumed in design. For newly-placed concrete pavements this value is probably much less than 1,500,000 $lb/in^3$ (407,200 MPa/m). A recent study that conducted laboratory studies on the modulus of dowel support determined that G increased with increasing compressive strength.[52] Since G is a measure of the support provided to the dowel bar by the slab, it is intuitive that this support value will increase with increasing compressive strength. It would follow then, that the parameter also increases with increasing concrete elastic modulus (function of compressive strength), and that different G values corresponding to increases in the concrete elastic modulus should be used in the evaluation of early age bearing stresses.

Very little research has been done on the relation between the modulus of dowel support and PCC compressive strength or elastic modulus. There was, however, the limited data from reference 52 that indicated that G increased with increasing compressive strength. This data was used to develop some very crude approximations of the modulus of dowel support at various compressive strengths. Since only 28-day compressive strengths were measured in that study, strengths at earlier times when the modulus of support value was actually measured were obtained using the concrete strength development model provided in reference 53. Based upon the measured modulus of support values and the corresponding compressive strengths, the average modulus of dowel support values shown in table 59 were estimated for the corresponding elastic modulus values evaluated in this study.

214

**Table 59. Modulus of dowel support estimated from concrete elastic modulus.**

| Concrete Modulus of Elasticity,[1] psi | Concrete Compressive Strength, psi | Modulus of Dowel Support, lb/in$^3$ |
|---|---|---|
| 1,000,000 | 260 | 375,000 |
| 2,000,000 | 1,041 | 650,000 |
| 3,000,000 | 2,341 | 1,000,000 |
| 4,000,000 | 4,162 | 1,750,000 |
| 5,000,000 | 6,504 | 2,500,000 |

[1] NOTE: Elastic modulus estimated from compressive strength
$$Ec = 62,000 * sqrt (f'c)$$

1000 psi = 6.9 MPa
1000 lb/in$^3$ = 271 MPa/m

It must be reiterated that the values shown in table 59 are based on very limited data, particularly in the area of early concrete strengths. Additional research is recommended to more accurately quantify the relationship between elastic modulus (or compressive strength) and the modulus of dowel support. The elastic modulus was determined from compressive strength using equation 20 which was developed from the laboratory database used in this study.

Reference 52 also indicated that the modulus of dowel support decreased with increasing dowel bar diameter. However, for the purposes of this evaluation, the modulus of support values shown in table 59 were based on 1-1/4 in- (32-mm-) diameter dowel bars.

Assuming the modulus of dowel support values listed in table 59, dowel bearing stresses were computed for a range of concrete pavement design conditions. Dowel bar diameters were assumed to be one-eighth of the slab thickness. The resulting bearing stresses are plotted in figures 103 through 105 for a range of design factors. The diagonal lines shown in figures 103 through 105 represent the line of equality between the bearing stress and the compressive strength; those bearing stresses that fall to the left of the line are unacceptable (i.e., bearing stress exceeds compressive strength) and those that fall to the right of the line are acceptable (i.e., compressive strength exceeds bearing stress).

There are several general trends observed from figures 103 through 105. Perhaps the most important observation is that the magnitude of the bearing stresses decrease with increasing slab thickness (and dowel bar diameter since larger dowels were assumed for thicker slabs). For example, an 8-in (20-cm) slab with a compressive strength of 3000 psi (20.7 MPa) has a maximum bearing stress of about 3200 psi (22.1 MPa) for a k-value of 100 lb/in$^3$ (27.1 MPa/m). A 10-in (25-cm) slab with the same compressive strength and k-value has a maximum bearing stress of about 1900 psi (13.1 MPa). Because of this, the thinner slabs are much more susceptible to bearing stress fracture due to early loading than the thicker slabs. Considering the 8-in (20-cm) slab, the compressive strength does not equal the maximum bearing stress until the concrete has reached a strength of about 3200, 4000, and 4500 psi (22.1, 27.6, and 31.1 MPa) for foundation support values of 100, 300, and 500 lb/in$^3$ (27.1, 81.4, and 135.7), respectively. These same critical strength values for the 10-in (25-cm) slab are 1800, 2200, and 2500 psi (12.4, 15.2, and 17.3 MPa), while for the 12-in (30-cm) slab they are 1200, 1400, and 1600 psi (8.3, 9.7, and 11.0 MPa). The combination of greater slab thickness and larger dowel bars greatly reduce the magnitude of the bearing stresses, so that early loading of such slabs is much less likely to cause damage than on a thinner slab with smaller diameter dowel bars.

Another observation from figures 103 through 105 is that the bearing stress increases with an increase in the foundation support. For example, for an 8-in (20-cm) slab with 1-in (25-mm) diameter dowels, the maximum bearing stress corresponding to a compressive strength of 3000 psi (20.7 MPa) ranges from about 3200 to about 4200 psi (22.1 to 29 MPa) for k-values of 100 and 500 lb/in$^3$ (27.1 and 135.7 MPa/m), respectively. However, the impact of the foundation support on the dowel bearing stresses is not as substantial for thicker slabs with larger dowel bars. Figure 105 shows that the maximum bearing stress for a 12-in (30-cm) slab with 1.5-in (38-mm) diameter dowels ranges from only 1200 to 1700 psi (8.3 to 11.7 MPa) for the same k-values.

As the modulus of subgrade reaction increases the radius of relative stiffness, L, will decrease. With a decrease in L the number of dowel bars considered to be active (within a distance of L from center of load) will decrease. With the decreased number of active bars

## 8-in slab, 1-in dia. dowels

**k = 100 pci**   **k = 300 pci**   **k = 500 pci**
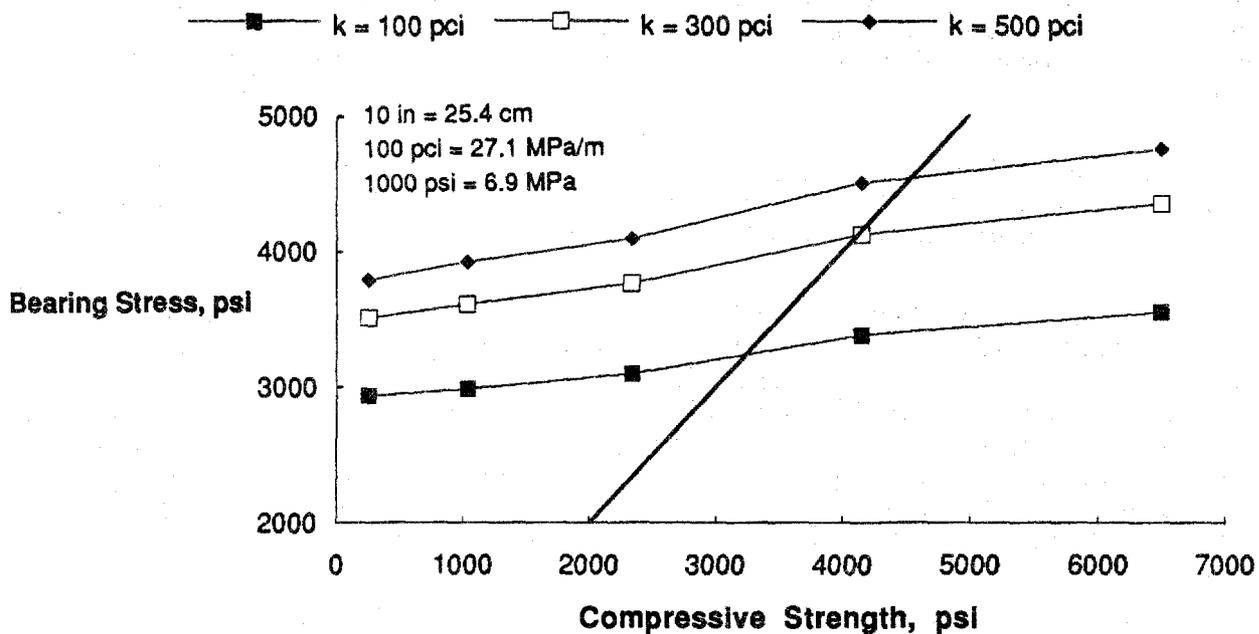


Figure 103. Maximum bearing stress vs. compressive strength
(8-in (20-cm) slab).

## 10-in slab, 1.25-in dia. dowels

**k = 100 pci**   **k = 300 pci**   **k = 500 pci**
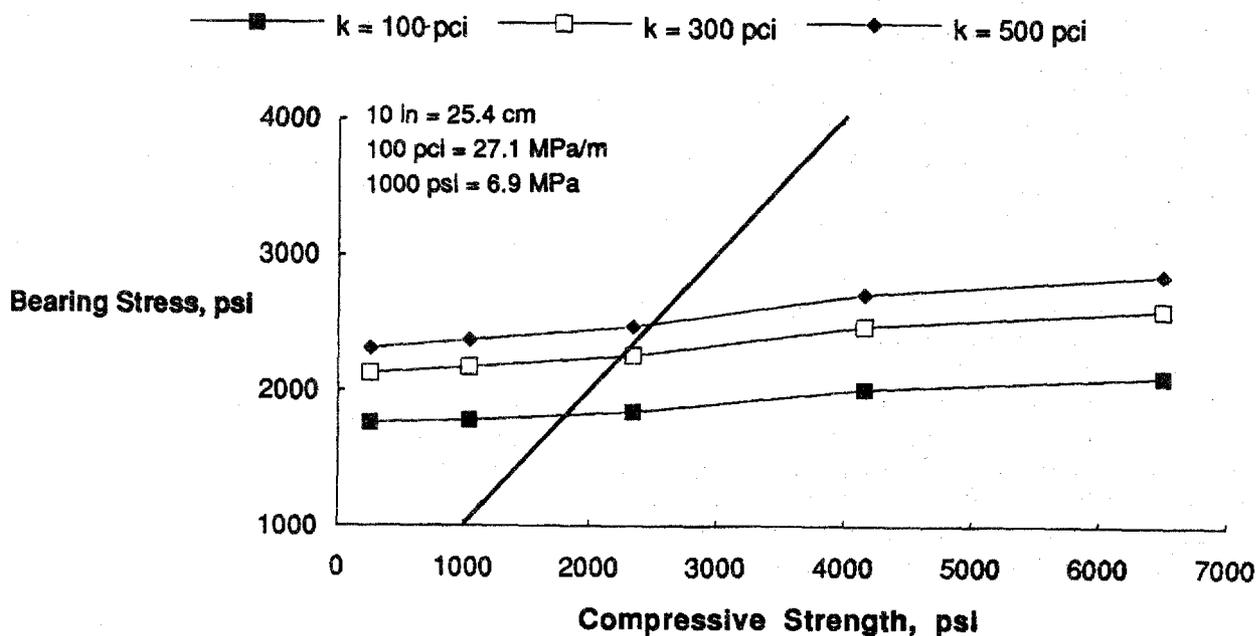


Figure 104. Maximum bearing stress vs. compressive strength
(10-in (25-cm) slab).

217

**12-in slab, 1.5-in dia. dowels**
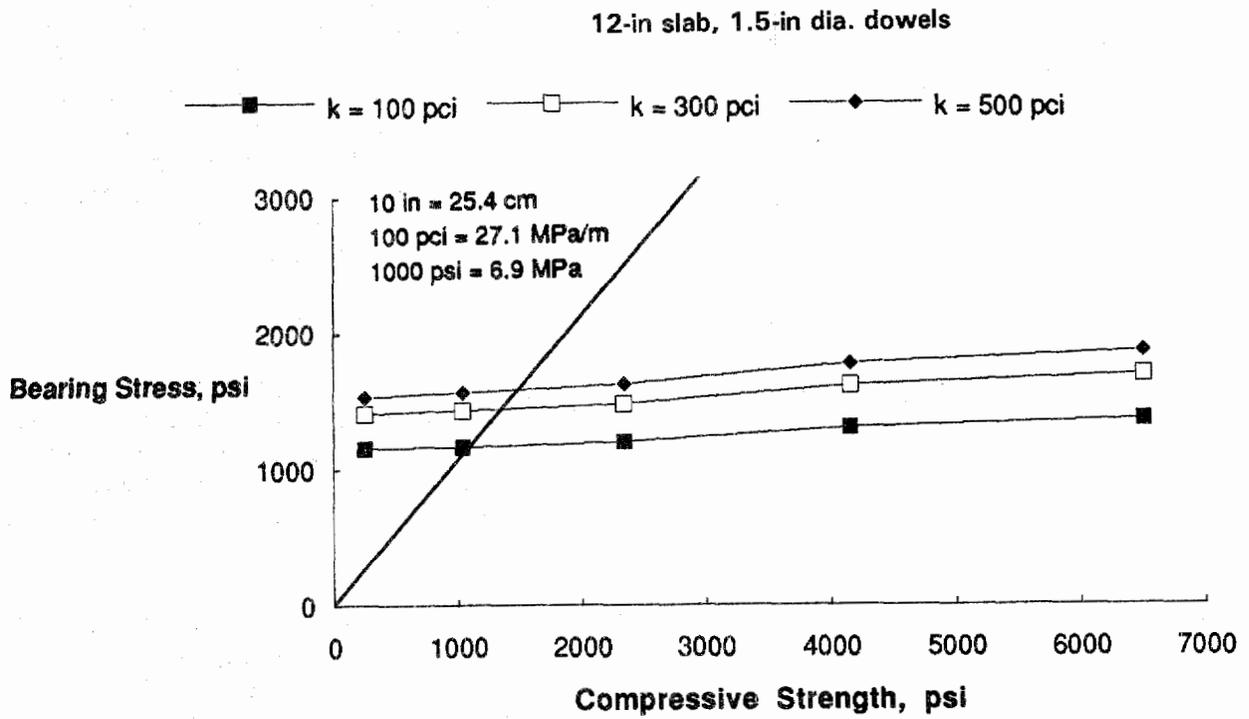


Figure 105.   Maximum bearing stress vs. compressive strength (12-in slab).

the shear force acting on the active dowels will increase thereby increasing the dowel deflections. An increased dowel deflection in equation 25 results in an increased dowel bearing stress.

It has been shown that dowel diameters are an important factor influencing the magnitude of the bearing stresses. To illustrate this, maximum bearing stresses as shown in table 60 were determined for a 10-in (25-cm) slab with 1, 1-1/4, and 1-1/2-in (25, 32, and 38-mm) dowel diameters. Larger dowel diameters resulted in lower bearing stresses, with a large reduction in bearing stresses obtained by moving from a 1-in (25-mm) dowel to a 1-1/4-in (32-mm) diameter dowel. For a k-value of 300 lb/in$^3$ (81.4 MPa/m) and elastic modulus of 3 million psi (20,700 MPa) the dowel bearing stresses decreased 33 and 51 percent as the dowel diameter increased from 1 to 1-1/4 and 1-1/2 in, (25 to 32 and 38 mm) respectively. Since they are so effective in reducing the bearing stresses, the use of larger diameter dowel bars greatly reduces the potential damage from early loading.

## EVALUATION OF LOADING BY SAWING EQUIPMENT

In addition to construction truck traffic, there is other equipment that may be driven or moved across the concrete at early ages. Other than construction truck traffic, the spansaw, used to cut the transverse joints in the slab, is probably the heaviest piece of equipment. An evaluation of the fatigue damage done by the spansaw was also conducted. The loading pattern assumed for the spansaw is shown in figure 106. A list of the inputs for the ILLI-SLAB evaluation is provided in table 61.

The spansaw configuration and input variables were run through ILLI-SLAB, and the resulting maximum stresses listed in table 62 were obtained. Examination of table 62 indicates that the stresses are less than half of the stresses obtained for the standard 20,000-lb (9080-kg) single-axle truck loading condition. Using the relationship between compressive strength and elastic modulus in equation 20, data in table 62 were developed which show how the stresses in the slab change as a function of compressive strength.

A fatigue damage analysis was conducted following the procedure previously described. Results of that analysis are listed in table 62. It is noted that no fatigue damage occurs for any combination, even up to a maximum of 10,000 load applications of the spansaw (which would never occur). Thus, it is assumed that none of the lighter construction equipment or spansaw load positioning at other slab locations causes any damage on the pavement after the pavement has obtained a minimum compressive strength of 250 psi (1720 kPa) corresponding to an elastic modulus of 1 million psi (6900 MPa).

## SUMMARY

A methodology has been demonstrated that allows for the estimation of concrete fatigue damage due to early loading. The procedure considers stress development in the slab and its corresponding compressive strength to estimate the fatigue damage. With this information, the fatigue damage sustained by a pavement of known compressive strength due to a certain number of early load applications can be estimated, or, conversely, the minimum compressive strength required to minimize the fatigue damage caused by a certain number of early load applications can be determined.

219

**Table 60. Maximum dowel-bearing stresses for 10-in (25-cm) slab with varying dowel diameters.**

| Slab Thickness, in | k-value, lb/in$^3$ | Maximum Bearing Stress, psi | | | | |
|---|---|---|---|---|---|---|
| | | Concrete Modulus of Elasticity, million psi [1] | | | | |
| | | 1 | 2 | 3 | 4 | 5 |
| 10 | 100 | 2612 | 2643 | 2731 | 2977 | 3120 |
| 1.00-in dowels | 300 | 3156 | 3224 | 3350 | 3664 | 3852 |
| | 500 | 3426 | 3518 | 3664 | 4017 | 4228 |
| 10 | 100 | 1764 | 1784 | 1843 | 2009 | 2106 |
| 1.25-in dowels | 300 | 2131 | 2178 | 2261 | 2473 | 2599 |
| | 500 | 2314 | 2376 | 2474 | 2711 | 2853 |
| 10 | 100 | 1281 | 1296 | 1338 | 1458 | 1527 |
| 1.50-in dowels | 300 | 1547 | 1580 | 1641 | 1794 | 1886 |
| | 500 | 1680 | 1724 | 1796 | 1967 | 2069 |

[1] NOTE: Modulus of elasticity estimated from compressive strength
Ec = 62,000 * sqrt (f'c)

100 lb/in$^3$ = 27.1 MPa/m$^3$
1000 psi = 6.9 Mpa
10 in = 25 cm
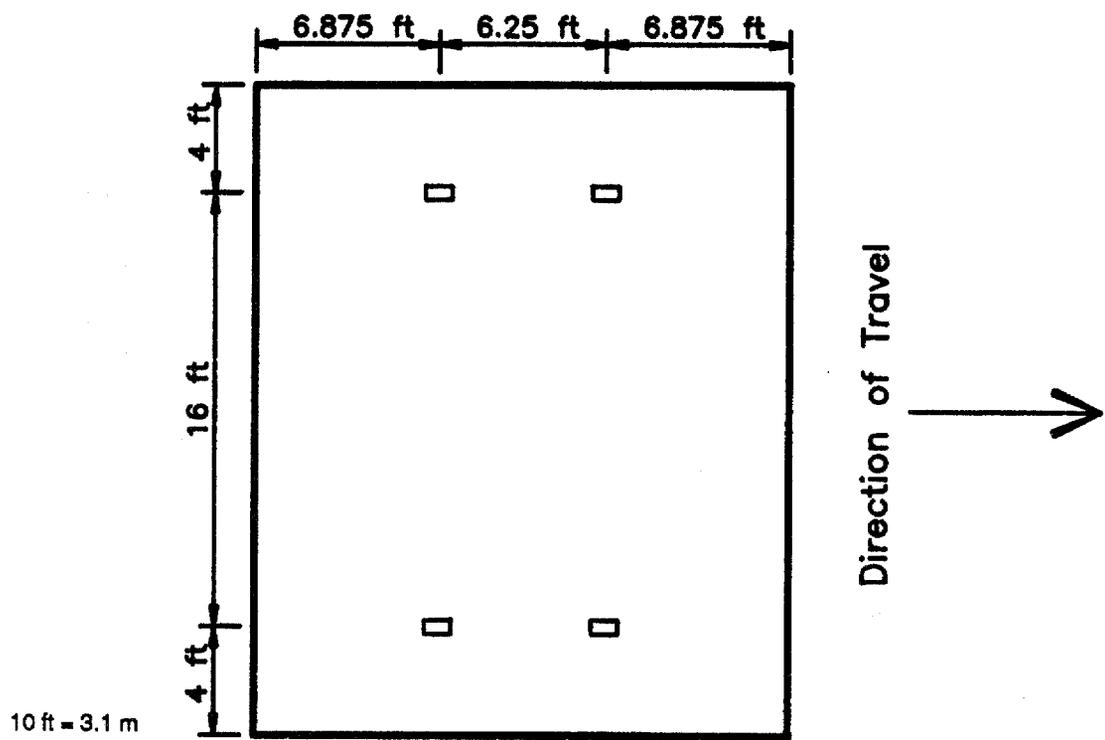
Figure 106.  Spansaw load pattern assumed for early loading analysis.

**Table 61. Summary of input variables used in ILLI-SLAB evaluation of spansaw interior loading.**

| Pavement Type | Jointed Plain Concrete Pavement | |
|---|---|---|
| Pavement Surface Layer Properties | Thickness, in | 8, 10, and 12 |
| | Poisson's Ratio | 0.15 |
| | Elastic Modulus, million psi | 1, 2, 3, 4, and 5 |
| | Temperature Gradient | none |
| Pavement Subgrade Properties | Model | Winkler |
| | k-value, lb/in$^3$ | 100, 300, and 500 |
| Pavement Joint Data | Joint Spacing, ft | 20 |
| | Lane Width, ft | 24 |
| Wheel Loading | Gross Weight of Spansaw, lb | 14,500 |
| | Number of Tires | 4 |
| | Tire Imprint, in$^2$ | 48 |
| | Contact Pressure, psi | 75.5 |

10 in = 25 cm
1 million psi = 6895 MPa
100 lb/in$^3$ = 27.1 MPa/m
10 ft = 3.1 m
14,500 lb = 6580 kg
48 in$^2$ = 310 cm

## Table 62. Summary of fatigue damage for spansaw loading condition.

| t, in | k, lb/in³ | Ec, million psi | f'c, psi | MR, psi | Stress, psi | Allowable N | Fatigue Damage Consumed at Different Loading Levels | | |
|---|---|---|---|---|---|---|---|---|---|
| | | | | | | | 1 | 10 | 100 |
| 8 | 100 | 1 | 260 | 245 | 83 | 6.65E+07 | 0 | 0 | 0 |
| 8 | 100 | 2 | 1041 | 382 | 88 | 2.49E+12 | 0 | 0 | 0 |
| 8 | 100 | 3 | 2341 | 518 | 90 | 2.57E+17 | 0 | 0 | 0 |
| 8 | 100 | 4 | 4162 | 655 | 91 | 5.53E+22 | 0 | 0 | 0 |
| 8 | 100 | 5 | 6504 | 791 | 92 | 1.48E+28 | 0 | 0 | 0 |
| 8 | 300 | 1 | 260 | 245 | 74 | 9.51E+08 | 0 | 0 | 0 |
| 8 | 300 | 2 | 1041 | 382 | 80 | 7.92E+13 | 0 | 0 | 0 |
| 8 | 300 | 3 | 2341 | 518 | 73 | 2.41E+22 | 0 | 0 | 0 |
| 8 | 300 | 4 | 4162 | 655 | 85 | 4.81E+24 | 0 | 0 | 0 |
| 8 | 300 | 5 | 6504 | 791 | 87 | 1.33E+30 | 0 | 0 | 0 |
| 8 | 500 | 1 | 260 | 245 | 70 | 3.96E+09 | 0 | 0 | 0 |
| 8 | 500 | 2 | 1041 | 382 | 76 | 6.04E+14 | 0 | 0 | 0 |
| 8 | 500 | 3 | 2341 | 518 | 79 | 2.28E+20 | 0 | 0 | 0 |
| 8 | 500 | 4 | 4162 | 655 | 82 | 5.89E+25 | 0 | 0 | 0 |
| 8 | 500 | 5 | 6504 | 791 | 83 | 7.50E+31 | 0 | 0 | 0 |
| 10 | 100 | 1 | 260 | 245 | 56 | 3.50E+12 | 0 | 0 | 0 |
| 10 | 100 | 2 | 1041 | 382 | 58 | 2.78E+20 | 0 | 0 | 0 |
| 10 | 100 | 3 | 2341 | 518 | 59 | 7.92E+28 | 0 | 0 | 0 |
| 10 | 100 | 4 | 4162 | 655 | 59 | 1.79E+38 | 0 | 0 | 0 |
| 10 | 100 | 5 | 6504 | 791 | 60 | 1.12E+47 | 0 | 0 | 0 |
| 10 | 300 | 1 | 260 | 245 | 51 | 1.08E+14 | 0 | 0 | 0 |
| 10 | 300 | 2 | 1041 | 382 | 55 | 6.16E+21 | 0 | 0 | 0 |
| 10 | 300 | 3 | 2341 | 518 | 56 | 5.84E+30 | 0 | 0 | 0 |
| 10 | 300 | 4 | 4162 | 655 | 57 | 7.41E+39 | 0 | 0 | 0 |
| 10 | 300 | 5 | 6504 | 791 | 58 | 1.01E+49 | 0 | 0 | 0 |
| 10 | 500 | 1 | 260 | 245 | 48 | 1.24E+15 | 0 | 0 | 0 |
| 10 | 500 | 2 | 1041 | 382 | 52 | 2.03E+23 | 0 | 0 | 0 |
| 10 | 500 | 3 | 2341 | 518 | 54 | 1.38E+32 | 0 | 0 | 0 |
| 10 | 500 | 4 | 4162 | 655 | 55 | 4.13E+41 | 0 | 0 | 0 |
| 10 | 500 | 5 | 6504 | 791 | 56 | 1.29E+51 | 0 | 0 | 0 |
| 12 | 100 | 1 | 260 | 245 | 40 | 6.09E+18 | 0 | 0 | 0 |
| 12 | 100 | 2 | 1041 | 382 | 41 | 9.97E+30 | 0 | 0 | 0 |
| 12 | 100 | 3 | 2341 | 518 | 42 | 2.83E+43 | 0 | 0 | 0 |
| 12 | 100 | 4 | 4162 | 655 | 44 | 2.48E+54 | 0 | 0 | 0 |
| 12 | 100 | 5 | 6504 | 791 | 45 | 2.81E+66 | 0 | 0 | 0 |
| 12 | 300 | 1 | 260 | 245 | 37 | 4.23E+20 | 0 | 0 | 0 |
| 12 | 300 | 2 | 1041 | 382 | 39 | 8.24E+32 | 0 | 0 | 0 |
| 12 | 300 | 3 | 2341 | 518 | 40 | 1.18E+46 | 0 | 0 | 0 |
| 12 | 300 | 4 | 4162 | 655 | 41 | 1.60E+59 | 0 | 0 | 0 |
| 12 | 300 | 5 | 6504 | 791 | 41 | 2.00E+74 | 0 | 0 | 0 |
| 12 | 500 | 1 | 260 | 245 | 36 | 2.07E+21 | 0 | 0 | 0 |
| 12 | 500 | 2 | 1041 | 382 | 38 | 9.08E+33 | 0 | 0 | 0 |
| 12 | 500 | 3 | 2341 | 518 | 39 | 3.11E+47 | 0 | 0 | 0 |
| 12 | 500 | 4 | 4162 | 655 | 40 | 9.65E+60 | 0 | 0 | 0 |
| 12 | 500 | 5 | 6504 | 791 | 40 | 3.44E+76 | 0 | 0 | 0 |

1000 psi = 6.9 MPa, 10 in = 25 cm, 100 lb/in³ = 27.1 MPa/m

A series of charts were generated for several slab thicknesses, subgrade support values, and compressive strengths. These charts allow for the damage from a given number of 20,000-lb (9080-kg) single axle loadings at a given concrete strength to be estimated. Charts were prepared for the edge loading condition. Interior stresses and fatigue consumption were significantly smaller as listed in table 56. Calculations for damage from other load levels, other tire pressures, other concrete strengths, and different elastic modulus-compressive strength models could be performed in a manner similar to what is described herein. The fatigue analysis assumes a relatiionship between modulus of elasticity and compressive strength and modulus of elasticity and modulus of rupture. As discussed, project specific relationships should be developed and input into the fatigue analysis. The procedure is easily adaptable to consider tandem axle loads, different load magnitudes, warping and curling restraint stresses, and other fatigue consumption models.

An evaluation of the transverse joint loading condition showed that the maximum stresses for both the nondoweled and doweled joints were comparable to the stresses developed for the interior loading condition. If higher levels of aggregate interlock were assumed (which is not unrealistic for a new concrete pavement), the critical transverse joint stresses would even be less than the interior loading condition. Thus, use of the fatigue table generated for the interior loading condition appears to be applicable to joint loading conditions.

An evaluation of dowel bearing stresses at early ages indicated that thinner slabs, which typically use smaller diameter dowel bars, may be more susceptible to early loading damage than thicker slabs. Larger dowel diameters were noted to be very effective in reducing bearing stresses. All of the work evaluating bearing stresses were based on modulus of dowel support values that were assumed to change with compressive strength. More research on this topic is needed since rough approximations of the modulus of dowel support value were made based on compressive strength.

A fatigue damage analysis was also conducted for the use of spansaws. The evaluation indicated that this equipment causes no fatigue damage to a slab (for a minimum compressive strength of 250 psi, 1720 kPa). Since the spansaw is the heaviest of the various pieces of equipment that may load a slab at a very early age, the fatigue damage caused by other pieces of light equipment is also assumed to be zero.

It occasionally becomes desirable or necessary to place loads on a newly-placed slab. One consideration when doing so is to determine at what the maximum amount of fatigue damage that the slab should sustain from early loading. That maximum tolerable amount of early loading damage is ultimately up to the State agency, but it is critical that the agency consider the design traffic and the performance period of the pavement when determining the maximum amount of fatigue damage from early loading.

As an example, consider a pavement that was designed for 10 milion 18,000-lb (8172-kg) equivalent single-axle load (ESAL) applications over a 20-year period. Of those 10 million ESAL applications, only about 6 percent (600,000) of these would be edge loads. If early edge loading consumed 10 percent of the fatigue damage, this would mean that about 60,000 edge load applications were consumed. This translates to a reduction in life of roughly 2 years. For this particular example, with the unknowns in actual traffic loadings and the historic inaccuracies of traffic projections, the loss of 2 years of service life

is probably unacceptable. Thus, the design traffic and the performance period must be evaluated for each design in order to evaluate what may be an acceptable level of fatigue damage from early loading.

# CHAPTER 7. FULL-SCALE HIGHWAY PAVEMENT LOAD TESTS.

Objectives for making full-scale highway pavement load tests soon after concrete placement were to generate pavement strain response data for loads placed at slab interiors, along free edges, at longitudinal joints, and at transverse joints. The pavement response data from the load tests were compared to pavement stresses calculated using the finite element ILLI-SLAB pavement analysis computer program with measured material properties.

The ILLI-SLAB finite element computer program was utilized in the analysis of the early loading of concrete pavements presented in Chapter 6. Evaluation of Early Concrete Pavement Loading. Since its introduction in 1977, this model has undergone continuous modifications and verifications to improve the accuracy of the model.[39-43] Several comparisons have been made in the past that have shown good agreement between field-measured stresses and the ILLI-SLAB predicted stresses.

Full-scale highway pavement load tests were made on newly constructed portland cement concrete pavements in Iowa and Utah. Load tests were made in Iowa during the week of August 13, 1990 and in Utah during the week of August 24, 1990.

This chapter will demonstrate the ability of the ILLI-SLAB program to predict actual, field-measured stresses. While a complete evaluation of the model is beyond the scope of the study, this limited comparison of the field-measured stresses and the ILLI-SLAB predicted stresses for selected loading conditions will illustrate the reasonableness of the program in predicting stress development for early loading of new concrete pavements.

## DESCRIPTIONS OF TEST PAVEMENTS

The Iowa pavement was located near Fort Dodge on U.S. Route 169 near station 2208. The plain doweled 10-in (25-cm) thick concrete pavement was placed over a 6- to 9-in (15-to 23-cm) thick drainable granular subbase located over a clay loam subgrade. The 1-1/4-in (3.2-cm) diameter coated dowels spaced at 12 in (30 cm) were located at slab mid-depth. Transverse skewed joints were spaced at 20 ft (6.1 m). The load test site was located near an access driveway. In the area of the load site, transverse joints were perpendicular to the longitudinal pavement axis and were spaced at 14 ft (4.3 m). Joints were dry sawed with a carborundum saw blade. Sawcut depths at transverse joints were about 2-1/4 in (6 cm). Sawcut depths were 3-1/3 in (8 cm) at longitudinal joints. The longitudinal centerline joint was a tied warping joint with no. 5 tiebars at 36 in (91 cm). During load test periods no shoulder had been placed at the pavement free edge. Lane widths were 12 and 14 ft (3.7 and 4.3 m). Concrete for the Iowa pavement was produced using 487 lb/yd$^3$ (289 kg/m$^3$) of cement and 82 lb/yd$^3$ (49 kg/m$^3$) of Class C fly ash. Concrete mix design is listed in table 33 of appendix D.

The Utah load test slabs were located near Tremonton on I-15 near stations 2455, 2463, and 2441. The Utah 10-in (25-cm) thick plain concrete pavement was placed over a 4-in (10 cm) thick lean concrete base located over a 4-in (10-cm) thick untreated granular subbase course. The lean concrete base had been placed about 1 month ahead of concrete paving and was cured with a bituminous cure coat. The cure coat was observed to be worn away in numerous areas by construction traffic at the time paving concrete was placed. Epoxy coated no. 5 tiebars were located at 30-in (76-cm) spacings in longitudinal warping joints. Transverse skewed joints were spaced at random 15-, 11-, 10-, and 14-ft (4.6-, 3.4-, 3.1-, and 4.3-m) intervals. The pavement consisted of two 12-ft (3.7-m) wide traffic lanes, a 4-ft (1.2-m) wide inside (passing lane) shoulder, and a 10-ft (3.1-m) wide outside (truck

lane) shoulder. The pavement was placed full width with a slipform paver. Transverse joints were sawed to about 3-1/3-in (8-cm) depth with spansaws using diamond impregnated blades producing about a 1/8-in (3-mm) wide sawcut. Self-propelled buggy saws were used to cut longitudinal warping joints to about 3-1/3-in depth (8 cm). Concrete for the Utah pavement was produced using a specified minimum 611 lb/yd$^3$ (277 kg/m$^3$)of cement. Concrete mix properties are listed in table 34 of appendix D.

## PAVEMENT LOAD TESTS AND COMPANION TESTS

Pavement full-scale load tests were made using a loaded truck with an approximately 20,000-lb (9080-kg) rear single axle with dual tires. The pavements were instrumented with 120-mm (4.7-in) long PL-120-11 Tokyo Sokki Kenkyuso Co. surface mounted strain gauges. Pavement surfaces at strain gauge locations were ground smooth and level with a carborundum wheel and treated with acetone ahead of installing gauges with an epoxy glue. Strain gauges were protected with wax waterproofing applications. Loads were applied and strains were measured at slab interiors, along free edges, at longitudinal joints (Utah only), and at transverse joints for various hours of the day. Slabs were loaded in Utah from 7:30 hours in the morning to 15:00 hours in the afternoon. In Iowa, load tests were done between 8:00 and 15:00 hours. In both Iowa and Utah, strains were measured for both standing (static) and creep speed loading conditions. For static loads, the strain gauge "zero" reading was for truck wheel away from the loading position. A second strain gauge reading was obtained after applying load and providing sufficient time for slab response. Creep speeds were for wheel movement past load position at about 2 m/h (3.2 km/h).

Load tests were made 2, 3, 7, and 8 days after concrete placement for the Iowa pavements. For the Utah pavements, load tests were made on slabs at 3, 4, 5, 6, 7, and 8 days after concrete placement. In addition, in Utah, load tests were made for comparison on a nearby 1-year-old slab. The 1-year-old location, part of the first phase of the Utah project, was not yet opened to public traffic. Strains were recorded using a digital strain box, peak meter, and switchbox.

For the Iowa study, companion compressive strengths with time were obtained from 6- by 12-in (15- by 30-cm) cylinder tests made by Iowa DOT staff and from cylinders fabricated and tested in the laboratory using job-site materials. For the Utah study, cylinders were fabricated and tested on-site. Remaining cylinders at ages of 14 days were shipped back from Utah to Illinois and tested. Elastic moduli were obtained during compressive strength testing at ages of greater than 24 hours. Pulse velocity measurements made on the pavement slabs were used to determine slab modulus of elasticity at the time of load testing. Temperature data were obtained with thermocouples installed on slab surface and bottom near the slab edge to monitor slab temperature differential throughout the load test period.

## COMPANION TEST RESULTS

Companion tests concentrated on developing models to predict the modulus of elasticity from compressive strength. Early age (4 to 24 hours) and early load (1 to 28 days) laboratory data described in chapter 3 indicated that the modulus of elasticity could be well predicted from compressive strength (square root function). As demonstrated with the early loading data (1 through 28 days) in chapter 3, compressive strength models as a function of either concrete maturity (inverse) or pulse velocity can be established. Since the automatic temperature data logger was simultaneously required in monitoring joint sawing operations, the moduli of elasticity at load testing sites were estimated using the pulse velo-

city rather than the maturity predicted compressive strength. Maturity models were generated from the companion test cylinder data even though they were not used in predicting the modulus of elasticity. From compressive strength data the modulus of elasticity can be estimated at load testing. The modulus of elasticity multiplied by the measured strain data gives the concrete flexural stress under load.

Due to limited amounts of field testing and materials which could be shipped to Illinois for further laboratory testing, the pulse velocity and maturity models developed as a function of compressive strength incorporated tests done both for joint sawing as well as load testing time periods. Pulse velocity and maturity models were presented in table 50 of Chapter 4. Investigation of Earliest Joint Sawcutting. Models were presented for the Iowa, Utah, and Wisconsin projects. Models for Wisconsin data in table 50 were developed to illustrate that the maturity or pulse velocity monitoring could be used to evaluate when to safely allow construction traffic on the pavement. Due to lack of continuous temperature data at ages greater than 24 hours, 2 maturity models were developed for the Utah project. The model using data at ages less than 24 hours was used for the joint sawcutting analysis. The second Utah maturity model assumes a constant cylinder temperature during on-site storage and in transit back to the laboratory.

## Modulus of Elasticity

The modulus of elasticity can be predicted as a function of the square root of compressive strength. Models generated from tests on 6- by 12-in (15-by 30-cm) cylinders are summarized in table 63. Cylinder data is presented in tables 44 through 46 of appendix E. Prediction errors, standard error of estimate, and coefficients of determination are similar to those reported in the early load laboratory study of chapter 3. The early load laboratory study data indicated that 1-through 28-day moduli of elasticity could be predicted from a constant (62,000) multiplied by the square root of compressive strength. As listed in table 63 the y-intercept term is statistically significant for the Iowa data and cannot be assumed equal to zero. The Utah and Wisconsin cylinder data agreed with the early load laboratory data with the y-intercept term being statistically insignificant.

For estimating compressive strength during joint sawing operations, 1 pulse velocity transducer was set on the surface at 12 in (30 cm) from the slab edge and the other transducer was positioned on the vertical pavement edge within a few inches of the surface. The vertical edge transducer was set near the surface since it was used to estimate strength near the surface. It was also observed during joint sawing observations that for concrete at early ages (less than 1 day) the pulse velocity decreased as the travel path increased. The 12-in (30-cm) edge offset travel path during joint observations was selected since early age compressive strength models were generated on 12-in (30-cm) long cylinders.

For the monitoring of compressive strength and modulus of elasticity using pulse velocity, the vertical pavement edge transducer was positioned more toward the bottom of the slab. This forced the pulse to travel on a diagonal path through more of a representative cross-section of concrete than when joint sawcutting is considered. Similar to early age (less than 24 hours) pulse velocity monitoring, the velocity is sensitive to the travel distance and/or angle between the transducers. As the pavement surface transducer offset was increased from 1 to 3 ft (30 to 90 cm) from the edge the velocity decreased. For Iowa field data ranging in age from 2 through 8 days, the estimated compressive strength decreased an average of 16 and 22 percent as the edge offset of the surface transducer increased from 1 to 2 and 3 ft (30 to 61 and 91 cm), respectively. This corresponds to only a 5- and 7-percent decrease in the elastic modulus estimate for the 2- and 3-ft (61-and 91-cm) offsets, respectively.

**Table 63. Regression equations of elastic modulus on compressive strength.**

| Project | Dep.[1,2] Variable, Y | Ind.[1,3] Variable, X | Coefficient, a | t-stat. | Constant, b | R - sq. | SEE[4] | No. of Points |
|---------|----------------------|----------------------|---------------|---------|-------------|---------|--------|---------------|
| Iowa | Ec | sqrt (f'c) | 42,700 | 12.74 | 1,508,000 | 0.915 | 207,000 | 17 |
| Utah | Ec | sqrt (f'c) | 53,100 | 59.43 | 0 | 0.904 | 251,000 | 18 |
| Wisconsin | Ec | sqrt (f'c) | 65,200 | 15.49 | 0 | 0.956 | 70,000 | 10 |

NOTES: [1] Prediction equation form: $Y = aX + b$

[2] Ec = concrete modulus of elasticity in psi

[3] f'c = compressive strength in psi

[4] SEE = standard error of estimate in psi

1000 psi = 6.9 MPa

For the Utah pulse velocity estimated compressive strength at ages of greater than 2 days, similar trends as with the Iowa data were noted. As the travel distance increased from the 1-ft (30-cm) edge transducer offset to 2 and 3 ft (61 and 91 cm), the pulse velocity decreased. The corresponding compressive strength decreased an average of 19 and 21 percent as the offset distance increased from 1 to 2 and 3 ft (30 to 61 and 91 cm), respectively. This corresponds to a 10 and 12 percent decrease in the elastic modulus estimate for the 2- and 3-ft offsets (61 and 91-cm), respectively.

To evaluate the effect of the angle changing between the transducers (as the offset distance increases) on the decreasing estimates of compressive strength, the compressive strength was also estimated near the slab surfaces at the Utah site. Pulse velocity was evaluated with the vertical slab edge transducer placed within 2 in (5 cm) of the slab surface. The exact elevation of the slab edge was marked for future monitoring tests with time and to calculate the exact diagonal nominal pulse travel path distance. At each offset, the resulting compressive strengths measured near the surface were slightly higher than the lower path compressive strength. Average decrease in compressive strength and modulus of elasticity were 9 and 5 percent, respectively. The decreases in strength are likely due more to the increase in travel path (for a given transducer offset) that the lower path pulse must travel rather than the increase in angle between transducer surfaces. The higher strength near the surface may also be attributed to solar radiation effects. During the summer paving the higher slab surface temperatures can promote rapid strength increases.

Further research is recommended to determine the effects of the offset distance from surface transducer to slab edge transducer. Since the correlation between elastic modulus and compressive strength was based on 12-in (30-cm) long cylinders the power of prediction can not be evaluated for actual path lengths. Using a 1-ft (30-cm) surface offset distance with the other pulse velocity transducer near the slab bottom at 9 in (23 cm) results in a 1-1/4-ft (38-cm) travel path. The modulus of elasticity as a function of compressive strength model was based on testing 12-in (30-cm) long cylinders. One recommended offset distance is therefore testing at a pulse travel distance close to the cylinder travel distance. The second offset distance for the surface transducer would be 2 to 3 ft (61 to 91 cm) from the slab edge. Load induced strains and deflections can be measured at a distance of up to several feet from a load. The use of a longer travel path, therefore, is more realistic in that compressive strength is estimated over a larger material volume. In addition to testing a more representative material volume, the longer path will evaluate concrete away from the slab edges. For ages greater than 1 day, the concrete slab under certain solar radiation, heat of hydration, and temperature conditions will have a higher (or lower) strength away from the edge than at the edge. The use of a longer path may be advantageous in monitoring a more representative condition.

For the load tests, the modulus of elasticity was estimated from pulse velocity compressive strength data averaged for the 1-, 2-, and 3-ft (30; 61; and 91-cm) offsets. Compressive strength estimated from pulse velocity using equations listed in table 50 was input into the modulus of elasticity equations listed in table 63. For the Iowa load tests at ages of 2, 3, 7, and 8 days, the modulus of elasticity was 3.0, 3.1, 3.2, and 3.2 million psi (20,700; 21,400; 22,100; and 22,100 MPa), respectively. For the Utah load tests at ages of 3, 4, 5, 6, 7, and 8 days, the modulus of elasticity was 3.1, 2.9, 3.25, 3.4, 3.15, and 3.4 million psi (21,400; 20,000; 22,400; 23,400; 21,700; and 23,400 MPa), respectively. At the approximately 1-year-old site the estimated modulus was 4.6 million psi (31,700 MPa). The inconsistent increasing trend in modulus of elasticity is due to testing 4 different slabs at various ages. Load testing several slabs at various ages allowed for pavement strain measurements over a wider time range.

## LOAD TEST RESULTS

Load test site details for Iowa and Utah are summarized in table 64. Load test results obtained from Iowa and Utah slabs selected for full-scale loading are summarized in tables 65 and 66, respectively. Pavement full-scale tests were made using a loaded truck with an approximately 20,000-lb (9080-kg) rear single axle with dual tires. Load truck details for both the Iowa and Utah test sites are listed in table 47 of appendix E. Average slab strains listed in tables 65 and 66 were obtained by averaging slab strain data for several loading periods. Slab strain data for each of the loading times are listed in tables 48 through 51 for Iowa and 52 through 58 for Utah in appendix E. For example, for the Iowa data in table 65 the average unit strain of 0.000048 was monitored for a static 20,100-lb (9120-kg) dual wheel load at slab edge (load case 8) was obtained from strains measured for 11:30-, 13:30-, and 14:00-hour loadings made on slab 1 on the second day after placing concrete. Locations of wheel loads and strain gauges for the various load cases described in the third and fouth columns of tables 65 and 66 are shown in figures 3 through 34 of appendix E.

Strains were measured throughout the day to evaluate the effects of slab temperature curl on measured load induced strains. Curl at slab edges and corners occur due to temperature gradients. At night if slab surfaces become cooler than the slab bottom the edges and corners will curl upwards. As the solar radiation heats the slabs during daylight the temperature gradient (top minus bottom temperature per slab thickness) becomes less negative. At some maximum thermal gradient the slab curl downwards with time essentially ceases. Typically curl will affect magnitudes of corner and edge deflections under load. Maximum curl influences on load induced deflection are usually observed late at night or early in the morning. Field testing studies have shown that curl influences on load induced strain are less than on load induced deflections.

For the Iowa data, average strain magnitude for the 4 time periods and 10 load cases was 23 microstrain. Average daily difference between the maximum and minimum measured strain for each load case was less than 5 microstrain. Since the average maximum difference is small relative to strain magnitudes and the measured strains did not consistently or significantly change with time, the average strain throughout the day was used to calculate stress.

For the Utah strain data average magnitude for the 6 time periods (ages less than 10 days) and 22 load cases was 9 microstrain. Average difference between daily maximum and minimum measured strain for each load case was less than 3 microstrain. Similar to the Iowa data, average strain during the test day was used to calculate stress.

Slab stresses due to wheel loads were calculated using averaged strain data measured and the concrete modulus of elasticity data determined from companion tests and pulse velocity nondestructive testing. Pulse velocity data, as summarized in table 64, indicate that a 3-million psi (20,700-MPa) modulus of elasticity is obtained for the Iowa concrete at 2 days. The corresponding stress for load case 8, when unit strain is 0.000048 for slab 1 at 2 days, is 143 psi (986 kPa), as listed in column 6 of table 65. Load case 8 is for a wheel load position at 2 in (5 cm) from slab edge and a strain gauge with longitudinal orientation (parallel to free slab edge) at the slab edge.

Maximum stress for loads positioned on test slabs 1 and 2 in Iowa occurred for the static load case 8 loading in slab 1 at 3 days. Static loads produced somewhat higher average stresses than creep loads. Average creep stresses were 74 percent of average static load stresses at the free edge.

231

**Table 64. Load test slab description.**

| Site | Slab No. Station | Thick., in | Test Date | Age, days | Testing Time | f'c,[1] psi | Modulus of Elasticity,[2] million psi | Air Temp.[3] min., °F | Air Temp.[3] max., °F | Slab Temp. Diff.[3] min., °F | Slab Temp. Diff.[3] max., °F | Zero Gradient Time[4] |
|---|---|---|---|---|---|---|---|---|---|---|---|---|
| Iowa US 169 | 1 2208+50 | 10 | 16-Aug-90 | 2 | 11:30-15:00 | 1600 | 3.00 | 81.8 | 86.9 | 1.7 | 7.8 | 10:30 |
| | | | 17-Aug-90 | 3 | 08:00-14:00 | 1820 | 3.10 | 74.1 | 92.2 | -0.9 | 12.5 | 8:30 |
| | 2 2208+25 | 10 | 16-Aug-90 | 7 | 11:30-15:00 | 2130 | 3.20 | 81.8 | 86.9 | 1.7 | 7.8 | 10:30 |
| | | | 17-Aug-90 | 8 | 08:00-14:00 | 2000 | 3.20 | 74.1 | 92.2 | -0.9 | 12.5 | 8:30 |
| Utah I-15 | 1 2471+50 | 10 | 27-Aug-90 | 3 | 13:30-15:00 | 3370 | 3.10 | 84.5 | 85.3 | 6.6 | 9.2 | 11:00 |
| | | | 30-Aug-90 | 6 | 09:00-16:00 | 4110 | 3.40 | 72.9 | 91.2 | -1.2 | 3.3 | 11:00 |
| | 2 2463+20 | 10 | 27-Aug-90 | 4 | 11:00-15:00 | 2990 | 2.90 | 79.4 | 85.3 | -0.2 | 9.2 | 11:00 |
| | | | 30-Aug-90 | 7 | 07:30-14:00 | 3560 | 3.15 | 71.8 | 86.0 | -2.2 | 3.1 | 11:00 |
| | 3 2455+50 | 10.5 | 27-Aug-90 | 5 | 11:30-15:30 | 3700 | 3.25 | 81.0 | 87.0 | 0.8 | 9.5 | 11:00 |
| | | | 30-Aug-90 | 8 | 8:00-14:30 | 4150 | 3.40 | 71.8 | 86.0 | -1.6 | 3.1 | 11:00 |
| | 4 2862+30 | 10 | 23-Aug-90 | 365 | 07:00-15:00 | 7500 | 4.60 | 52.1 | 82.5 | -11.6 | 8.0 | 11:00 |

NOTES:
[1] Estimated from average pulse velocity at 1-, 2-, and 3-ft surface transducer offset distances from edge.
[2] Estimated from pulse velocity compressive strength.
[3] Temperature during load testing.
[4] Top minus bottom slab temperature differential during load testing.

1000 psi = 6.9 MPa
10 in = 25 cm
°C = 5/9 (°F-32)
1 ft = 0.305 m

**Table 65. Iowa load test response summary.**

| Load Case[1] | Load Type[2] | Wheel Path, in[3] | Slab Location | Slab 1 at 2 Days | | Slab 1 at 3 Days | | Slab 2 at 7 Days | | Slab 2 at 8 Days | |
|---|---|---|---|---|---|---|---|---|---|---|---|
| | | | | Average Strain[4] | Average Stress[5] | Average Strain[4] | Average Stress[5] | Average Strain[4] | Average Stress[5] | Average Strain[4] | Average Stress[5] |
| 1 | Creep | 2 | Slab Edge at Midlength | 39 | 117 | 35 | 109 | 26 | 84 | 27 | 86 |
| 2 | Creep | 18 | Slab Midlength | 30 | 91 | 30 | 92 | 22 | 70 | 22 | 71 |
| 3 | Creep | 18 | Slab Edge at Midlength | 23 | 69 | 23 | 71 | 16 | 51 | 16 | 52 |
| 4 | Creep | 30 | Slab Midlength | 27 | 81 | 26 | 79 | 19 | 61 | 18 | 56 |
| 5 | Creep | 72 | Slab Interior | 22 | 65 | 21 | 65 | 17 | 53 | 16 | 52 |
| 6 | Creep | 30 | Transverse Joint | 9 | 26 | 8 | 24 | 8 | 25 | 7 | 21 |
| 7 | Creep | 72 | Transverse Joint | 11 | 34 | 15 | 46 | 11 | 34 | 10 | 32 |
| 8 | Static | 2 | Slab Edge at Midlength | 48 | 143 | 49 | 152 | 39 | 124 | 36 | 114 |
| 9 | Static | 2 | Edge 1 ft from Load | 38 | 115 | 43 | 134 | 25 | 80 | 25 | 78 |
| 10 | Static | 2 | Edge 2 ft from Load | 24 | 72 | 26 | 80 | 14 | 46 | 14 | 44 |

NOTES:

[1]See figures 3 through 12 in appendix E for wheel and strain locations.
[2]Creep load of 2 mi/h (3.2 km/h).
[3]Distance from free edge to tire edge.
[4]Measured strain in millionths under 20.1-kip (9120-kg) single-axle load.
[5]Modulus of elasticity determined from pulse velocity testing.
(Ec = 3.0, 3.1, 3.2, and 3.2 million psi at 2, 3, 7, and 8 days, respectively)

1000 psi = 6.9 MPa
10 in = 25 cm

**Table 66. Utah load test response summary.**

| Load Case [1] | Load Type [2] | Wheel Path, in [3] | Slab Location | Slab 1 at 3 Days | | Slab 2 at 4 Days | | Slab 3 at 5 Days | | Slab 1 at 6 Days | |
|---|---|---|---|---|---|---|---|---|---|---|---|
| | | | | Average Strain [4] | Average Stress [5] | Average Strain [4] | Average Stress [5] | Average Strain [4] | Average Stress [5] | Average Strain [4] | Average Stress [5] |
| 1 | Creep | 2 | Slab Edge at Midlength | 5 | 16 | 8 | 23 | 8 | 26 | 6 | 20 |
| 2 | Creep | 18 | Slab Midlength | 7 | 22 | 10 | 29 | 7 | 23 | 4 | 14 |
| 3 | Creep | 18 | Slab Edge at Midlength | 3 | 9 | 4 | 12 | 4 | 13 | 3 | 10 |
| 4 | Creep | 2 | Unloaded Shoulder | - | - | - | - | 6 | 20 | - | - |
| 5 | Creep | 2 | Free Shoulder Edge | 15 | 47 | - | - | 11 | 36 | 23 | 78 |
| 6 | Creep | 2 | Free Edge 1 ft from Mid. | - | - | - | - | 14 | 46 | - | - |
| 7 | Creep | 2 | Free Edge 2 ft from Mid. | - | - | - | - | 19 | 62 | - | - |
| 8 | Creep | 30 | Slab Midlength | - | - | 9 | 26 | - | - | - | - |
| 9 | Creep | 72 | Slab Interior | - | - | 8 | 23 | - | - | - | - |
| 10 | Creep | 30 | Transverse Joint | 5 | 16 | 5 | 15 | - | - | 6 | 20 |
| 11 | Creep | 72 | Transverse Joint | - | - | 7 | 20 | - | - | - | - |

NOTES:

[1]See figures 13 through 34 in appendix E for wheel and strain locations.
[2]Creep load of 2 mi/h (3.2 km/h).
[3]Distance from lane - concrete shoulder joint or free edge to tire edge.
[4]Measured strain in millionths under 20.0-kip (9080-kg) single-axle load.
[5]Modulus of elasticity determined from pulse velocity testing.
(Ec = 3.10, 2.90, 3.25, and 3.40 million psi at 3, 4, 5, and 6 days, respectively)

1000 psi = 6.9 MPa
10 in = 25 cm

234

**Table 66. Utah load test response summary (continued).**

| Load Case[1] | Load Type[2] | Wheel Path, in[3] | Slab Location | Slab 1 at 3 Days | | Slab 2 at 4 Days | | Slab 3 at 5 Days | | Slab 1 at 6 Days | |
|---|---|---|---|---|---|---|---|---|---|---|---|
| | | | | Average Strain[4] | Average Stress[5] | Average Strain[4] | Average Stress[5] | Average Strain[4] | Average Stress[5] | Average Strain[4] | Average Stress[5] |
| 12 | Static | 2 | Slab Edge at Midlength | - | - | 12 | 35 | 11 | 36 | 9 | 31 |
| 13 | Static | 2 | Edge 1 ft from Load | - | - | 6 | 17 | - | - | - | - |
| 14 | Static | 2 | Edge 2 ft from Load | - | - | 3 | 9 | - | - | - | - |
| 15 | Static | 2 | Unloaded Shoulder | - | - | 7 | 20 | 7 | 23 | - | - |
| 16 | Static | 2 | Free Shoulder Edge | 20 | 62 | - | - | 21 | 68 | 38 | 129 |
| 17 | Static | 2 | Free Edge 1 ft from Load | - | - | - | - | 11 | 36 | - | - |
| 18 | Static | 2 | Free Edge 2 ft from Load | - | - | - | - | 6 | 20 | - | - |
| 19 | Static | 30 | Loaded Transverse Joint | 6 | 19 | 6 | 17 | - | - | 7 | 24 |
| 20 | Static | 30 | Unloaded Transverse Joint | 5 | 16 | 3 | 9 | - | - | 3 | 10 |
| 21 | Static | 72 | Loaded Transverse Joint | - | - | - | - | - | - | - | - |
| 22 | Static | 72 | Unloaded Transverse Joint | - | - | - | - | - | - | - | - |

NOTES:

[1]See figures 13 through 34 in appendix E for wheel and strain locations.
[2]Creep load of 2 mi/h (3.2 km/h).
[3]Distance from lane - concrete shoulder joint or free edge to tire edge.
[4]Measured strain in millionths under 20.0-kip (9080-kg) single-axle load.
[5]Modulus of elasticity determined from pulse velocity testing.
(Ec = 3.10, 2.90, 3.25, and 3.40 million psi at 3, 4, 5, and 6 days, respectively)

1000 psi = 6.9 MPa
10 in = 25 cm

235

**Table 66. Utah load test response summary (continued).**

| Load Case[1] | Load Type[2] | Wheel Path, in[3] | Slab Location | Slab 2 at 7 Days | | Slab 3 at 8 Days | | Slab 4 at 1 Year | |
|---|---|---|---|---|---|---|---|---|---|
| | | | | Average Strain[4] | Average Stress[5] | Average Strain[4] | Average Stress[5] | Average Strain[4] | Average Stress[5] |
| 12 | Static | 2 | Slab Edge at Midlength | 10 | 32 | 9 | 31 | 16 | 74 |
| 13 | Static | 2 | Edge 1 ft from Load | 7 | 22 | - | - | 8 | 37 |
| 14 | Static | 2 | Edge 2 ft from Load | 4 | 13 | - | - | 4 | 18 |
| 15 | Static | 2 | Unloaded Shoulder | 7 | 22 | 5 | 17 | 7 | 32 |
| 16 | Static | 2 | Free Shoulder Edge | - | - | 22 | 74 | - | - |
| 17 | Static | 2 | Free Edge 1 ft from Load | - | - | 13 | 45 | - | - |
| 18 | Static | 2 | Free Edge 2 ft from Load | - | - | 7 | 23 | - | - |
| 19 | Static | 30 | Loaded Transverse Joint | 7 | 22 | - | - | 13 | 60 |
| 20 | Static | 30 | Unloaded Transverse Joint | 2 | 6 | - | - | 5 | 23 |
| 21 | Static | 72 | Loaded Transverse Joint | - | - | - | - | 4 | 18 |
| 22 | Static | 72 | Unloaded Transverse Joint | - | - | - | - | 3 | 14 |

NOTES:

[1] See figures 13 through 34 in appendix E for wheel and strain locations.
[2] Creep load of 2 mi/h (3.2 km/h).
[3] Distance from lane - concrete shoulder joint or free edge to tire edge.
[4] Measured strain in millionths under 20.0-kip (9080-kg) single-axle load.
[5] Modulus of elasticity determined from pulse velocity testing.
(Ec = 3.15, 3.40, and 4.60 million psi at 7, 8, and 365 days, respectively)

1000 psi = 6.9 MPa
10 in = 25 cm

**Table 66. Utah load test response summary (continued).**

| Load Case[1] | Load Type[2] | Wheel Path, in[3] | Slab Location | Slab 2 at 7 Days | | Slab 3 at 8 Days | | Slab 4 at 1 Year | |
|---|---|---|---|---|---|---|---|---|---|
| | | | | Average Strain[4] | Average Stress[5] | Average Strain[4] | Average Stress[5] | Average Strain[4] | Average Stress[5] |
| 1 | Creep | 2 | Slab Edge at Midlength | 7 | 22 | 8 | 26 | 13 | 60 |
| 2 | Creep | 18 | Slab Midlength | 6 | 19 | 8 | 28 | 10 | 46 |
| 3 | Creep | 18 | Slab Edge at Midlength | 5 | 16 | 5 | 15 | 5 | 23 |
| 4 | Creep | 2 | Unloaded Shoulder | 6 | 19 | 5 | 18 | - | - |
| 5 | Creep | 2 | Free Shoulder Edge | - | - | 14 | 48 | - | - |
| 6 | Creep | 2 | Free Edge 1 ft from Mid. | - | - | 16 | 55 | - | - |
| 7 | Creep | 2 | Free Edge 2 ft from Mid. | - | - | 16 | 55 | - | - |
| 8 | Creep | 30 | Slab Midlength | 8 | 25 | - | - | 8 | 37 |
| 9 | Creep | 72 | Slab Interior | 8 | 25 | - | - | 9 | 41 |
| 10 | Creep | 30 | Transverse Joint | 6 | 19 | - | - | 12 | 55 |
| 11 | Creep | 72 | Transverse Joint | 6 | 19 | - | - | 6 | 28 |

NOTES:

[1]See figures 13 through 34 in appendix E for wheel and strain locations.
[2]Creep load of 2 mi/h (3.2 km/h).
[3]Distance from lane - concrete shoulder joint or free edge to tire edge.
[4]Measured strain in millionths under 20.0-kip (9080-kg) single-axle load.
[5]Modulus of elasticity determined from pulse velocity testing.
(Ec = 3.15, 3.40, and 4.60 million psi at 7, 8, and 365 days, respectively)

1000 psi = 6.9 MPa
10 in = 25 cm

For Iowa creep loads, slab stresses, summarized in table 65 at all testing ages (2, 3, 7, and 8 days) decreased as wheel load position distance increased from the free slab edge inward. Interior slab stresses ranged from about 55 to 66 percent of stresses measured at free edge. Slab stresses at doweled transverse joints were less than at slab interior. Average stress difference between the 2 joint location stresses and interior stress was 29 psi (200 kPa).

Stresses at a transverse joint in Iowa (load case 7) 72 in (1.8 m) inward from pavement free edge were greater by factors ranging from 1.3 to 1.9, than stresses at the transverse joint 30 in (76 cm) inward from pavement free edge (load case 6). The fact that stresses at 72 in (1.8 m) inward from free edge at transverse joints were greater than those 30 in (76 cm) inward from the free edge can be attributed to the fact that the strain gauge at 72 in (1.8 m) was located midway between dowels positioned at 68 and 78 in (1.7 and 2 m) inward from edge. At 30 in (76 cm) inward from edge, the strain gauge and load were positioned immediately above the dowel located 30 in (76 cm) inward from slab edge. A second factor can be that stresses for locations inward from slab corners along a joint generally reach a maximum near midlength between corners.

For the Iowa pavements, average stresses greater than 100 psi (689 kPa) were obtained for slabs up to 3 days old for edge creep load (load case 1) conditions. For static load conditions, stresses greater than 100 psi (689 kPa) were measured for edge load positions (load case 8) on slabs at 2, 3, 7, and 8 days. Stresses were significantly greater for the 2- and 3-day-old slabs than for the 7- and 8-day-old slabs.

For the Utah pavement slabs stresses were relatively low. Only at three load positions were slab stresses greater than 60 psi (414 kPa) for slabs tested at 3, 4, 5, 6, 7, and 8 days and one slab about 1 year old. The stress of 60 psi (414 kPa) was arbitrarily selected since most measured stresses ranged from 10 to 50 psi (69 to 345 kPa) and greater than 60 psi (414 kPa). Creep load tests were made for 11 conditions as listed in table 66. The greater than 60-psi (414-kPa) stresses for creep loads occurred for the following:

- Slab 3 at 5 days: Free shoulder edge 2 ft (61 cm) from midslab -
  62 psi (427 kPa).
- Slab 1 at 6 days: Free shoulder edge - 78 psi (538 kPa).
- Slab 4 at 1 year: Slab edge at midlength - 60 psi (414 kPa).

For static load applications, 6 tests produced pavement stresses greater than 60 psi (414 kPa). These occurred for the following conditions:

- Slab 1 at 3 days: Free shoulder edge - 62 psi (427 kPa).
- Slab 3 at 5 days: Free shoulder edge - 68 psi (469 kPa).
- Slab 1 at 6 days: Free shoulder edge - 129 psi (889 kPa).
- Slab 3 at 8 days: Free shoulder edge - 74 psi (511 kPa).
- Slab 4 at 1 year: Slab edge at midlength - 74 psi (511 kPa).
- Slab 4 at 1 year: Transverse joint - 60 psi (414 kPa).

The use of 10-ft (3.1-m) tied concrete shoulders reduced the free shoulder edge stresses an average of 53 and 60 percent for creep and static loads, respectively. On average for both moving and static loads the edge stress at the slab-shoulder joint was 44 percent of the free edge stress. Low slab stresses for Utah pavement, can be attributed to partial or full bond of slab to the lean concrete base.

No significant decrease in stresses was generally noted as the load moved inward from the shoulder joint by 18 and 72 in (46 and 183 cm). Only for slab 4 at 1 year was a significant decrease in stress measured when the load was moved away from the shoulder joint. Stresses decreased from 60 to 46 psi (414 to 317 kPa) as the load moved 18 in (46 cm) inward from the shoulder. The relatively low shoulder-pavement joint edge stress (compared to other interior type loads) is probably due to a high degree of stress transfer. On average the shoulder stress transfer (unloaded shoulder to loaded slab edge strain) averaged 75 and 58 percent for creep and static loads respectively. The stress transfer calculated from very low strain magnitudes should only be considered as a qualitative indicator of good load transfer and thus may explain the relatively low ledge strains.

The creep load strains were less than the static load cases. On average the dynamic to static ratio was 75, 63, and 86 percent for stresses at the shoulder-slab joint, free shoulder edge and transverse joint (30 in, 76 cm inward from edge), respectively.

## VERIFICATION PROCESS

The ILLI-SLAB program was used to calculate stresses for several of the different loading conditions. The actual, field-measured stresses (from the measured strains) were then compared to the ILLI-SLAB predicted stresses to determine the reasonableness of the results. To facilitate the comparison and to provide an objective basis for the comparisons, a statistical procedure known as the paired t-test was utilized to determine if the ILLI-SLAB predicted stresses are statistically from the same population as the actual, field-measured stresses; that is, if the ILLI-SLAB program is able to adequately predict the field-measured stresses.

The SASTM statistical software was used to perform the paired t-test analysis .[54] The paired t-test assumes the following methodology:

- For every field measured stress and corresponding ILLI-SLAB predicted stress, the difference between the two values is computed.

- The mean of all of the differences is calculated by adding all of the differences and dividing by the number of observations.

- The null hypothesis is then tested. The null hypothesis assumes that the mean difference of the measured and predicted values is zero, or, in other words, that the sample of predicted stresses comes from the same population as the field-measured stresses. The calculated t-statistic (t-calc) is compared to a tabulated t-statistic (t-table) corresponding to a specified confidence level. The 90-percent confidence level was used in this evaluation. If t-calc is greater than t-table, then the null hypothesis is rejected and it can be inferred with 90-percent confidence that the predicted stresses are not from the same population as the sample of field-measured stresses. If t-calc is less than t-table, then the null hypothesis is not rejected and it can not be inferred with 90-percent confidence that the predicted stresses are from different populations.

239

## Analysis of Iowa Field Data

The newly-placed concrete pavement monitored in Iowa was a 10-in (25-cm) doweled JPCP constructed over an aggregate base course. Transverse joints were perpendicular, spaced at 14.2-ft (4.3-m) intervals, with 1.25-in (3-cm) diameter dowel bars on 12-in (30-cm) centers. At the time of the field testing, no outer shoulder had yet been placed.

The pavement was loaded by a 20,100-lb (9130-kg) single-axle with dual wheels, each wheel with an imprint of 95 in$^2$ (613 cm$^2$). This produced a contact pressure of 52.9 psi (365 kPa). Ten different load cases investigated, all of which were also evaluated using ILLI-SLAB:

- Load case 1. Wheel load placed at mid-slab at a distance of 2 in (5 cm) from the slab edge and moved at creep speed. The longitudinal strain at the edge of the slab was measured as shown in figure 3 of appendix E.

- Load case 2. Wheel load placed at mid-slab at a distance of 18 in (46 cm) from the slab edge and moved at creep speed. The longitudinal strain at the edge of the wheel imprint was measured as shown in figure 4 of appendix E.

- Load case 3. Wheel load placed at mid-slab at a distance of 18 in (46 cm) from the slab edge and moved at creep speed. The longitudinal strain at the edge of the slab was measured as shown in figure 5 of appendix E.

- Load case 4. Wheel load placed at mid-slab at a distance of 30 in (76 cm) from the slab edge and moved at creep speed. The longitudinal strain at the edge of the wheel imprint was measured as shown in figure 6 of appendix E.

- Load case 5. Wheel load placed at mid-slab at a distance of 72 in (1.8 m) from the slab edge and moved at creep speed. The longitudinal strain at the edge of the wheel imprint was measured as shown in figure 7 of appendix E.

- Load case 6. Wheel load placed at the transverse joint at a distance of 30 in (76 cm) from the slab edge and moved at creep speed. The transverse stress at the corner of the wheel imprint was measured as shown in figure 8 of appendix E.

- Load case 7. Wheel load placed at the transverse joint at a distance of 72 in (1.8 m) from the slab edge and moved at creep speed. The transverse stress at the corner of the wheel imprint was measured as shown in figure 9 of appendix E.

- Load case 8. Wheel load placed at mid-slab at a distance of 2 in (5 cm) from the slab edge and the static longitudinal strain recorded at the edge of the wheel imprint as shown in figure 10 of appendix E.

- Load case 9. Wheel load placed at mid-slab at a distance of 2 in (5 cm) from the slab edge and the static longitudinal strain recorded at a distance of 12 in (30 cm) from the load at the slab edge as shown in figure 11 of appendix E.

240

- Load Case 10. Wheel load placed at mid-slab at a distance of 2 in (5 cm) from the slab edge and the static longitudinal strain recorded at a distance of 24 in (61 cm) from the load at the slab edge as shown in figure 12 of appendix E.

The loading was done on slabs at ages of 2, 3, 7, and 8 days. Elastic modulus values were determined at each age using pulse velocity testing.

Some of the load cases involved a dynamic loading condition, in which the wheel was moving at creep speed. Since ILLI-SLAB computes only static loading stresses, the resulting stresses in Iowa were adjusted to simulate dynamic loading conditions. From the field data, the creep stress was an average of 74 percent of the static load stress. This factor was applied to the ILLI-SLAB stresses to achieve the dynamic loading conditions.

Finite element meshes were generated for each of the different loading conditions, adhering to guidelines provided in reference 42. Input variables used in the ILLI-SLAB evaluation of the Iowa pavements are shown in table 67. The k-value used in the analysis was assumed to be 250 lb/in$^3$ (68 MPa/m). Although no deflection testing was conducted to verify this value, the Iowa DOT reported that is a typical for pavements of this type.

A summary of the actual and predicted stresses is presented in table 59 of appendix E. Actual stresses were computed by multiplying the modulus of elasticity by the average strain measured during the load test day. The creep loads were adjusted using the creep to static load adjustment factor. A scattergram of predicted versus actual values is shown in figure 107. This figure shows a great deal of scatter about the line of equality. Table 59 of appendix E indicates that the best agreement between the actual and predicted stresses occurs at the interior and edge loading situations. Less agreement was obtained for the transverse joint loading condition.

The mean difference is 5.250 for the 40 pairs of observations. The calculated t-value (t-calc) is 1.391. For a 90 percent confidence level with 40 observations, the tabulated t-value (t-table) is 1.685. Since t-calc is less than t-table, the null hypothesis is not rejected at the 90-percent confidence level and it can not be inferred that the field-measured stresses and the ILLI-SLAB predicted stresses come from different populations.


## Analysis of Utah Field Data

The newly placed concrete pavement in Utah consisted of a 10-in (25-cm) nondoweled JPCP constructed over a 4-in (10-cm) lean concrete base (LCB) and a 4-in (25-cm) granular subbase. Transverse joints were skewed and spaced at 15-, 11-, 10- and 14-ft (4.6-, 3.4-, 3.1-, and 4.3-m) intervals. The 10-ft (3.1-m) wide outer shoulder was placed mono-lithically with the traffic lanes.

The pavement was loaded by a 20,000-lb (9080-kg) single-axle with dual wheels, each wheel having an imprint of 108 in$^2$ (697 cm$^2$). This produced a contact pressure of 46.3 psi (319 kPa). Although 22 different load cases were investigated, only the free edge loading condition (on the outer concrete shoulder) was evaluated using ILLI-SLAB. This was done because the free edge loading condition is the most critical in terms of fatigue cracking development and because of the favorable results obtained from the evaluation of the Iowa loading conditions.

241

**Table 67. Summary of input variables used in ILLI-SLAB evaluation of Iowa data.**

| Pavement Type | Jointed Plain Concrete Pavement | |
|---|---|---|
| Pavement Surface Layer Properties | Thickness, in<br>Poisson's Ratio<br>Elastic Modulus, million psi<br><br><br><br><br>Temperature Gradient | 10<br>0.15<br>3.0 @ 2 days<br>3.1 @ 3 days<br>3.2 @ 7 days<br>3.2 @ 8 days<br>none |
| Subgrade Properties | Model<br>k-value, lb/in$^3$ | Winkler<br>250 |
| Pavement Joint Data | Joint Spacing, ft<br>Lane Width, ft<br>Joint Width, in<br>Dowel Diameter, in<br>Dowel Spacing, in<br>Modulus of Dowel Support, lb/in$^3$<br>Dowel Modulus of Elasticity, psi<br>Dowel Poisson's Ratio<br>Dowel Concrete Interaction, lb/in<br>(Using Friberg's Analysis) | 14.2<br>12<br>0.125<br>1.25<br>12<br>1,500,000<br>29,000,000<br>0.3<br>1,490,000 |
| Wheel Loading | Type of Axle<br>Weight of Axle, lb<br>Tire Imprint, in$^2$<br>Contact Pressure, psi | Single, Dual Wheel<br>20,100<br>95<br>52.9 |

10 in = 25 cm
12 ft = 3.7 m
95 in$^2$ = 613 cm
20,100 lb = 9120 kg
1 million psi = 6900 MPa
250 lb/in$^3$ = 68 MPa/m
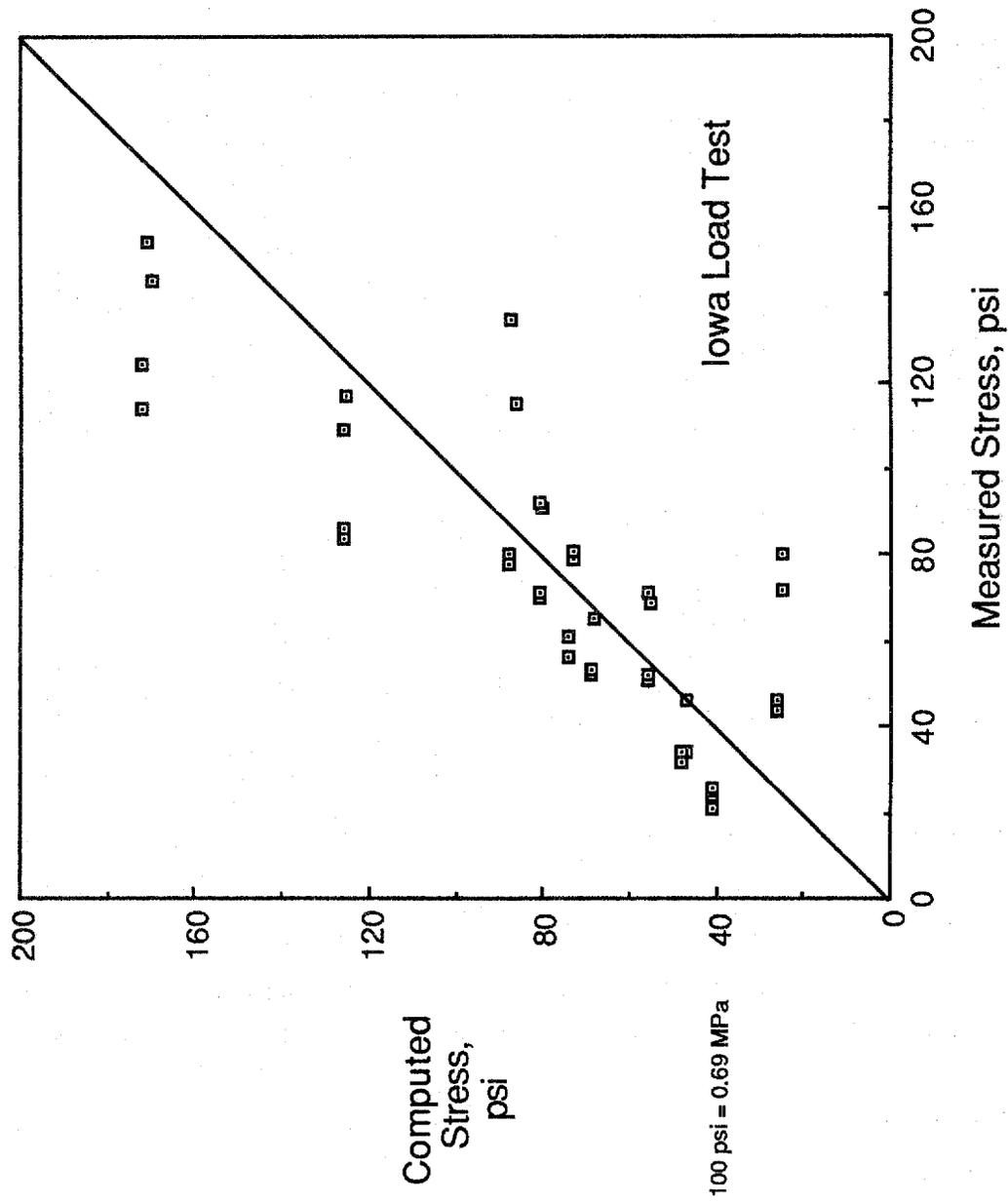1.5 million lb/in = 26,800 kg/mm

242

Figure 107. Predicted vs. actual stresses for Iowa loadings.

The Utah load cases evaluated by ILLI-SLAB include the following:

- Load case 5. Wheel load placed at mid-slab on the outer shoulder at a distance of 2 in (5 cm) from the slab edge and moved at creep speed. The longitudinal strain at the edge of the slab was measured as shown in figure 17 of appendix E.

- Load case 6. Wheel load placed 1 ft from mid-slab on the outer shoulder at a distance of 2 in (5cm) from the slab edge and moved at creep speed. The longitudinal strain at the edge of the slab was measured as shown in figure 18 of appendix E.

- Load case 7. Wheel load placed 2 ft (61 cm) from mid-slab on the outer shoulder at a distance of 2 in (5 cm) from the slab edge and moved at creep speed. The longitudinal strain at the edge of the slab was measured as shown in figure 19 of appendix E.

- Load case 16. Wheel load placed at mid-slab on the outer shoulder at a distance of 2 in (5 cm) from the slab edge. The static longitudinal strain at the edge of the slab was measured as shown in figure 28 of appendix E.

- Load case 17. Wheel load placed 1 ft (30 cm) from mid-slab on the outer should at a distance of 2 in (5 cm) from the slab edge. The static longitudinal strain at the edge of the slab was measured as shown in figure 29 of appendix E.

- Load case 18. Wheel load placed 2 ft (61 cm) from mid-slab on the outer shoulder at a distance of 2 in (5 cm) from the slab edge. The static longitudinal strain at the edge of the slab was measured as shown in figure 30 of appendix E.

The free edge loading condition was only conducted on slabs of ages 3, 5, 6, and 8 days. Elastic modulus values were determined for each age using pulse velocity testing.

As with the Iowa testing, some of the load cases involved a dynamic loading condition, in which the wheel was moving at creep speed. The resulting ILLI-SLAB stresses were adjusted for dynamic loading conditions. From the Utah field data, the creep stress at the free edge was an average of 63 percent of the static load stress. This factor was applied to all of the static ILLI-SLAB free edge stresses for the dynamic loading conditions.

Finite element meshes were again developed for each of the different loading conditions. Input variables for the ILLI-SLAB evaluation of the Utah pavements are shown in table 68. Because of the low magnitude of the stresses collected in the field, complete bonding was assumed between the slab and the underlying LCB. A subgrade k-value of 300 lb/in$^3$ (81 MPa/m) was assumed because of the presence of the 4-in (10-cm) aggregate subbase and an underlying granular subgrade. It should be noted, however, that this value could vary.

A summary of the actual and predicted stresses is presented in table 60 of appendix E. The creep loads were adjusted using the creep to static load adjustment factor. A scattergram of predicted versus measured values is shown in figure 108. The magnitude of the field stresses are quite low, probably indicating that the underlying LCB is bonded to the concrete slab.

**Table 68. Summary of input variables used in ILLI-SLAB evaluation of Utah data.**

| Pavement Type | Jointed Plain Concrete Pavement | |
|---|---|---|
| Pavement Surface Properties | Thickness, in<br>Poisson's Ratio<br>Elastic Modulus, million psi<br><br><br><br>Temperature Gradient | 10<br>0.15<br>3.10 @ 3 days<br>3.25@ 5 days<br>3.40 @ 6 days<br>3.40 @ 8 days<br>none |
| Base Properties | Type<br>Thickness, in<br>Elastic Modulus, million psi<br>Poisson's Ratio<br>State of Bonding | Lean Concrete<br>4<br>2<br>0.2<br>Complete |
| Subgrade Properties | Model<br>k-value, lb/in$^3$ | Winkler<br>300 |
| Pavement Joint Data | Joint Spacing, ft<br>Lane Width, ft<br>Joint Width, in<br>Dowels | 15<br>12<br>0.125<br>None |
| Wheel Loading | Type of Axle<br>Weight of Axle, lb<br>Tire Imprint, in$^2$<br>Contact Pressure, psi | Single, Dual Wheel<br>20,000<br>108<br>46.3 |

10 in = 25 cm
12 ft = 3.7 m
108 in = 697 cm
20,000 lb = 9080 kg
1 million psi = 6900 MPa
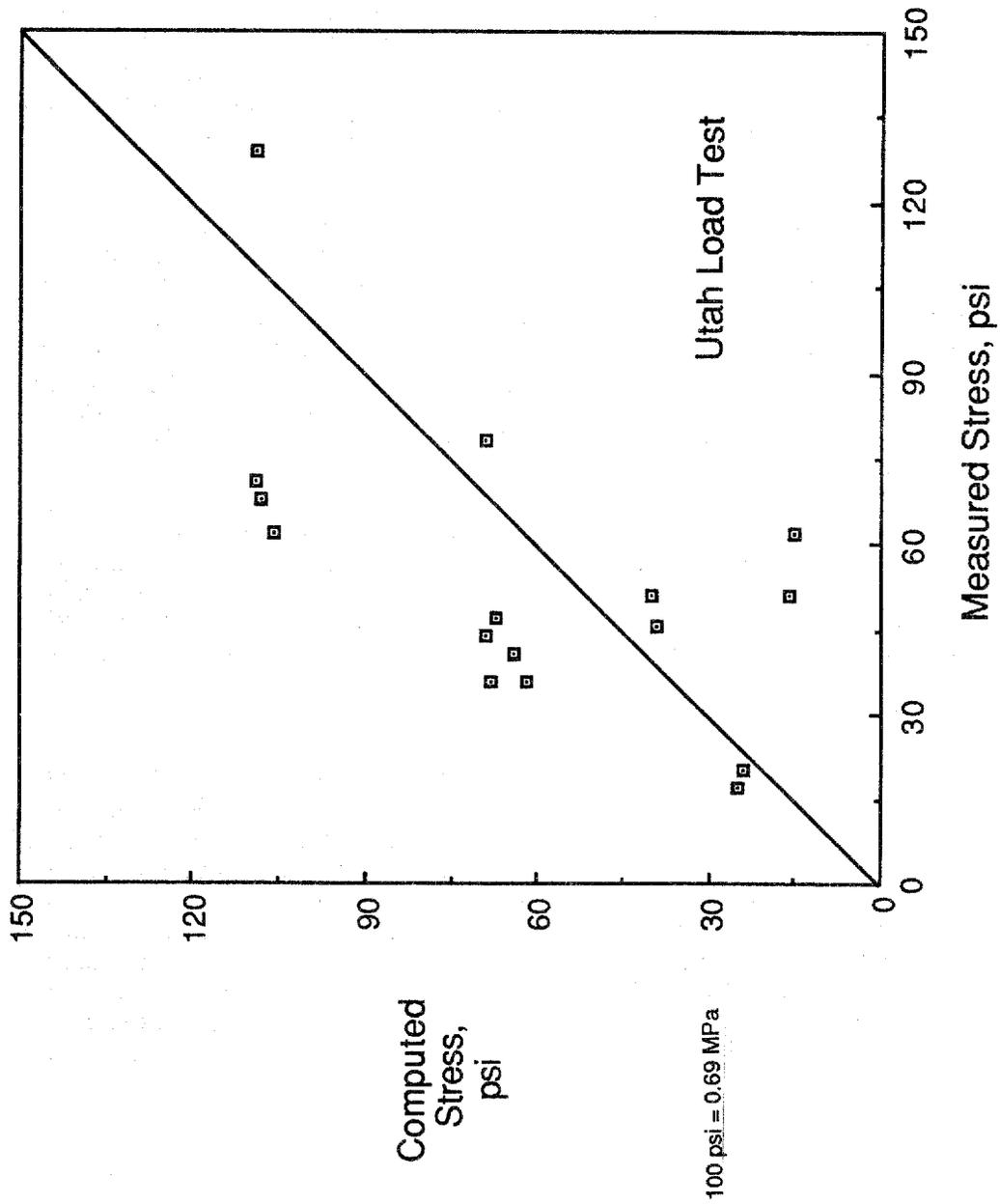300 lb/in$^3$ = 81 MPa/m

245

Figure 108. Predicted vs. actual stresses for Utah loadings.

The mean difference is 8.250 for the 16 pairs of observations. The calculated t-value (t-calc) is 1.207. For a 90-percent confidence level with 16 observations, the tabulated t-value (t-table) is 1.753. Since t-calc is less than t-table, the null hypothesis is not rejected at the 90-percent confidence level and it can not be inferred that the field-measured stresses and the ILLI-SLAB predicted stresses come from different populations.

## CONCLUSIONS

The data obtained for the Iowa and Utah early loading (2 through 8 days) test slabs indicate that pavement stresses at free pavement edges are critical in terms of thickness design or limiting loading ahead of substantial concrete flexural strengths. For the Iowa pavements, slab interior stress (strains) were measured to be less than those of transverse doweled joints. For the Utah slabs, no significant differences of stresses were determined for slab interior versus transverse undoweled skewed joint loading positions.

The highest stress for creep speed loading for Utah and Iowa slabs was 117 psi (807 kPa) for a 20,100-lb (9130-kg) rear axle load in Iowa. For a flexural concrete strength of 250 psi (1.7 MPa) the allowable number of 20,000-lb (9080-kg) single-axle loads using equation 23 is 198,500. When flexural strengths increase to 300 and 350 psi (2.1 and 2.4 MPa) the allowable number increases to 3.9 and 85.7 million loads, respectively. For an anticipated 1000 construction load applications the fatigue damage is 0.5, 0.03, and 0.001 percent for flexural strengths of 250, 300, and 350 psi (1.7, 2.1, and 2.4 MPa), respectively. This conclusion is based on the Iowa and Utah test data and should not be applied to other projects where different axle loads, traffic, subbase support, concrete mixes, and thermal histories exist.

A comparison between actual, field-measured stresses and the stresses generated by the ILLI-SLAB finite element computer program was conducted for various loading conditions. The results of the statistical analyses indicate that for the selected loading conditions and at the 90-percent confidence level, the field-measured stresses and the ILLI-SLAB predicted stresses come from the same population. This indicates that the ILLI-SLAB program is sufficiently able to predict the actual stresses occurring due to early loading of new pavements.

Although the ILLI-SLAB program has been demonstrated to reasonably predict slab stresses, it is still observed that there are some cases where significant differences exist between the actual stresses and the predicted stresses. One possible source of this could be the development of thermal gradients in the slab that could cause some variation in the measured stresses. Strain data measured throughout the day indicated that no consistent or significant changes in load induced strain occurred. Average measured strain for each test day was used to calculate stresses. Although thermal effects were not considered in the evaluation, ILLI-SLAB has the capability to consider it in an analysis. Other sources of variation could be the testing error associated with each of the measurements and the uncertainty over certain input values required in the ILLI-SLAB program (e.g., k-value).

# CHAPTER 8. GUIDANCE RECOMMENDATIONS FOR TIMING OF CONTROL JOINT SAWCUTTING

Guidelines for pavement sawcutting operations are prepared to aid designers, contractors, and owners in the decision making process concerning timing of installing contraction (control) and warping joints in highway pavements. The decision-making process is concerned with 2 limits for the joint sawcutting window of opportunity:

- The near limit, that is the earliest time after pavement placement joint sawcutting can be done without unacceptable concrete sawcut edge ravelling.

- The far limit, that is the time when sawing should be completed in order to avert uncontrolled transverse and longitudinal cracking in pavements.

## NEAR SAWING LIMIT FOR GOOD OR ACCEPTABLE JOINTS

The near limit for the joint sawcutting window of opportunity is the soonest sawcuts should be made if unacceptable concrete joint edge ravelling is to be avoided. Acceptable joints are defined as those that are planned to have sealant reservoir widening after initial sawcuts whereas good joints are defined as those that were judged not to have excessive ravelling when no sawcut widening is to be done. Criteria for good (rating 4) or acceptable (rating 3) and/or unacceptable (rating 2) joint edges were determined from sawcut ratings based on visual evaluations performed by a team of experienced highway engineers. Rating data and correlations of ratings for individual sawcuts with a cumulative measure of spalling incidence per sawcut length were determined as described in Chapter 4. Investigation of Earliest Joint Sawcutting.

### Decision Factors

Influencing factors for decisions on the near sawing limit are concrete strength gain and the criteria as to what constitutes a good or acceptable joint. The quantification of joint edge ravelling was described in chapter 4. In summary, an acceptable joint sawcut produces 0.84 in$^2$ (541 mm$^2$) of ravelling per 24 ft (7.3 m) and a good joint has 0.12 in$^2$ (80 mm$^2$) of ravelling per 24 ft (7.3 m). Concrete mortar matrix strength needed to permit sawcutting to produce an acceptable joint edge can be measured by concrete compressive strength. For early age concrete at less than 24 h tested as part of the work described in chapter 3, failure planes due to compressive strength testing were observed to pass through the concrete mortar matrix and around all concrete coarse aggregates. Results from ratings and companion strength tests as reported in chapter 4, table 46 indicate that sawcuts with a "good" rating can be installed in newly placed pavement slabs when the following concrete compressive strengths are attained with a cement content of 650 lb/yd$^3$ (386 kg/m$^3$):

- 530 psi (3.7 MPa) for concrete made with crushed soft coarse aggregate
- 1010 psi (7.0 MPa) for concrete made with crushed hard coarse aggregate
- 690 psi (4.8 MPa) for concrete made with rounded hard coarse aggregate
- 310 psi (2.1 MPa) for concrete made with rounded soft coarse aggregate

Compressive strength requirements for other concrete mixes to produce sawcuts with good or acceptable ratings are listed in table 46 of chapter 4. The "round soft" coarse

aggregate type was not part of the slab sawing study. Effects of this aggregate type should be further investigated since the dummy variables for aggregate hardness and geometry only account for qualitative not quantitative effects on minimum compressive strength.

The range of cement of 500-to 650-lb/yd$^3$ (297-to 386-kg/m$^3$) concrete covers the amounts of cement specified by most State DOT's. For amounts of cement falling between 500 and 650 lb/yd$^3$ (297 and 386 kg/m$^3$), required compressive strength can be interpolated by direct proportions of cement amount and required strength as listed in table 47.

## Sawcutting Suitability Criteria

To facilitate the decision-making process for determining the near limit for saw-cutting, surrogate tests to compressive strength determinations were selected. Choice of nondestructive test (NDT) methods to monitor insitu concrete pavement compressive strength includes Pulse Velocity (PV) and Maturity Determination (MD) monitoring. Either, as described in chapters 3 and 4, can be correlated well with compressive strength. The Clegg Impact Hammer method is also an alternative. The correlation between compressive strength and impact values was generally poorer than the other 2 NDT methods. The variability in estimation of compressive strength was relatively higher and limitations of the Clegg Impact Hammer should be considered.

Based on results from tests presented in chapter 3, the minimum PV and MD values corresponding to the compressive strengths obtained concurrent with making acceptable sawcuts were calculated and summarized in table 69. As previously discussed, these relationships were developed from the laboratory database generated in this study. The maturity relations and possibly the pulse velocity relationships will change with aggregate source, cement type, cement source, admixture types, and paste volumes.

The minimum pulse velocity maturity values corresponding to the above required compressive strength for near limit window of opportunity sawing were calculated using equations listed in the bottom line of tables 27 through 29 of chapter 3.

The correlations of compressive strength, pulse velocity, and/or concrete maturity should be reaffirmed on a regular basis for project-specific concrete mix designs. For example, use of a different cement source, although the same cement type was used, can significantly alter maturity correlations.

For a specific highway pavement project the site-specific coarse concrete aggregate is matched to the closest corresponding CS, CH, or RH coarse aggregate of this investigation and the corresponding strength requirement listed in table 46. The sequence of events leading to the setting the near limit sawing is shown in figure 109. Either PV or MD test methods can be used for determining insitu concrete strength. The PV method, because it does not require local specific installations of thermocouples, is more flexible in application.

From laboratory tests made in association with concrete mix design tests, site-specific PV versus compressive strength, or MD versus compressive strength correlations are established. These values can be used as criteria for timing near limit sawcutting. Observations of surface joint ravelling during initial concrete placement days for each project should become basis for adjusting near limits for sawcutting.

**Table 69. Nondestructive testing maturity and pulse velocity values for acceptable sawcuts.**

| Aggregate Geometry | Aggregate Hardness | Cement Content, lb/yd $^3$ | Compressive Strength, [1] psi | Pulse Velocity, [2] ft/s | Arrhenius Maturity, [2] hours | Nurse - Saul Maturity, [2] °F-h |
|---|---|---|---|---|---|---|
| Crushed | Soft | 500 | 730 | 11,101 | 18.4 | 530 |
|  |  | 650 | 530 | 10,376 | 14.5 | 440 |
| Crushed | Hard | 500 | 1270 | 12,353 | 33.8 | 817 |
|  |  | 650 | 1010 | 11,835 | 25.1 | 667 |
| Rounded | Soft [3] | 500 | 470 | 10,105 | 13.5 | 414 |
|  |  | 650 | 310 | 9,163 | 10.8 | 343 |
| Rounded | Hard | 500 | 920 | 11,624 | 22.7 | 621 |
|  |  | 650 | 690 | 10,973 | 17.6 | 512 |

NOTES: [1] Minimum compressive strengths for "good" sawcut listed in table 46.

[2] Based on laboratory data general early age relationships listed on the bottom line of tables 27, 28, and 29. Maturity relationships can significantly change with cement type and source (equivalent age at 68°F and datum temperature of 32 °F).
Pulse velocity compressive strength relationships may also change with cement type and source.

[3] Estimated "rounded soft" aggregate type required strength from qualitative dummy variable. regression analysis. Aggregate type not investigated in sawing study.

500 lb/yd $^3$ = 297 kg/m $^3$ , 650 lb/yd $^3$ = 386 kg/m $^3$
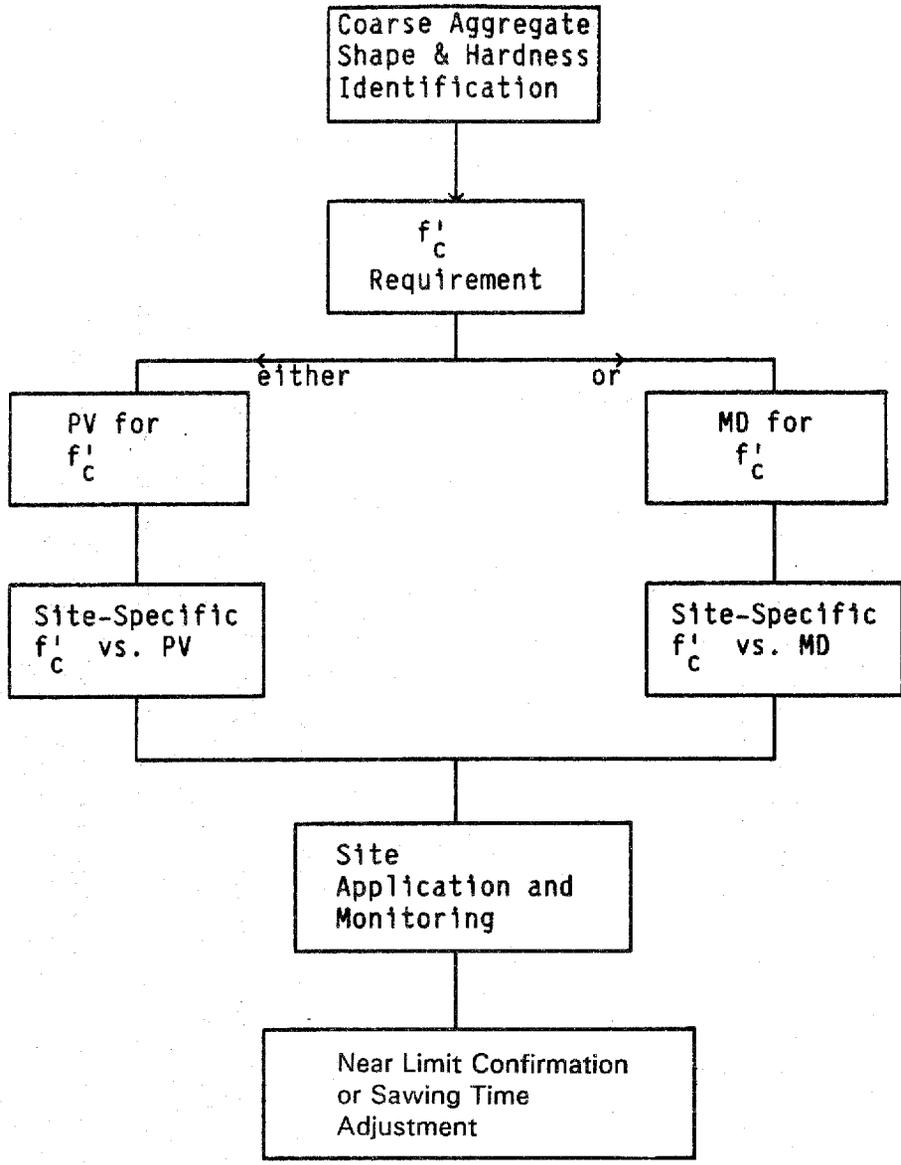100 psi = 0.69 MPa, 1000 ft/s = 305 m/s
°C = 5/9 (°F-32)

Figure 109.  Near limit decision process.

# FAR SAWCUTTING LIMITS TO AVOID UNCONTROLLED CRACKING

To avoid uncontrolled transverse and longitudinal pavement cracking, joints sawcuts should be installed ahead of occurrence of restraint pavement stresses that are in excess of pavement strength. Results of studies on causes of cracking in early age concrete beams and experimental pavements reported in chapter 2 indicate that cracking in early age concrete beams under full axial and bending restraints and in test pavements occurred when top surface concrete experienced 15 °F (8 °C) or higher amounts of cooling from maximum concrete top surface temperatures. Equations presented in chapter 2 indicate that significant pavement slab restraint stresses can occur when cooling occurs from top surface, as indeed occurs in first afternoons and evenings following paving construction or during rainshowers following warm days with solar radiation.

Early age concrete pavements, within the first 24 hours after paving, are very sensitive to the buildup of restraint stresses due to cooling from top surface downward. The drying potential, in modern paving practice, is avoided by applications of curing compound immediately following surface texturing. Surface texturing, in most instances consisting of transverse tining, is installed ahead of appreciable surface hardening. Thus, it is done within a short time of concrete placement, that is before any significant surface drying. The application of curing compound also mitigates potentials of surface moisture evaporation cooling effects. In the absence of curing applications, evaporation from pavement surface could add to the cooling due to ambient effects in afternoons and evenings following concrete paving. Top pavement surface cooling attributable to rain is in many instances avoided by construction planning. Pavements are generally not constructed when precipitation is anticipated. However, in some areas of the continental US rainshowers occur frequently in the early afternoons. In these areas, paving operations should be planned so that concrete placed ahead of anticipated rainshowers can be sawcut before significant surface cooling.

## Factors Influencing Far Sawcutting Limits

Factors influencing far sawcutting limits include the restraint stress increases associated with pavement cooling from top surfaces and the increases of concrete slab strength as early concrete aging occurs. Fortunately, insitu concrete strength gain is relatively rapid on days with large magnitudes of concrete temperature increases attributable to ambient and hydration effects. Very often, ambient events associated with rapid strength gains are followed by relatively large temperature decreases due to rapid cooling. Conversely, when temperature rises of concrete slabs are limited by relatively cool ambient conditions subsequent slab cooling effects are mitigated. Rapid strength gains permit not only early near limit of the window of opportunity sawcutting, but also provides the tensile strength capacity needed to counterbalance the buildup of pavement restraint stresses due to cooling.

Pavement axial and bending (curling) restraint stresses can be calculated using equations 1 in figure 2 and 4 in figure 3. For considerations of far limits of the sawcutting window of opportunity, the joint sawcutting to avert uncontrolled cracking should be done before the concrete tensile strength is exceeded by the sum of axial and bending restraint stresses. A balance of split tensile concrete strength versus axial and bending restraint stresses is, as previously shown in equation 17 of chapter 5 and repeated here for convenience:

$$ST = \sigma_f + \sigma_c \dots\dots\dots\dots\dots\dots\dots\dots\dots\dots\dots\dots\dots\dots (17)$$

Equations 1 and 4 are substituted in equation (17)

$$ST = (wh) \, \mu \, x \, /h + CE\alpha\Delta T/2 \dots \dots \dots \dots \dots \dots \dots \dots (26)$$

where:

[notation are as in chapter 2 (and as a reminder x = 1/2 pavement width or length)].

For example, for rapid cooling at about 10 hours after placing a 38-ft (11.6-m) wide and 10-in (25-cm) thick pavement placed full width over a lean concrete base (LCB) with subgrade friction ($\mu$) value of 10, the required tensile strength to avert cracking is about 260 psi (1.8 MPa) when E is about $1.6 \times 10^6$ psi (6900 MPa) and slab top to bottom temperature difference is 15 °F (8 °C). The split tensile strength can be determined on pavements with maturity or pulse velocity measurements. Split tensile strength may be directly estimated from correlations with NDT or indirectly from NDT estimated compressive strength. Split tensile strength relationships with compressive strength will need to be established if compressive strength is monitored with NDT. From laboratory tests with 100 °F (38 °C) curing, that is similar to a summer day with solar radiation, the 10-hour split tensile strength was about 250 psi (1.7 MPa) for mixes made with a cement content of 650 lb/yd³ (386 kg/m³). An adequate factor of safety should be used to avert uncontrolled cracking. For example, for the same conditions with sawing done before temperature differences are greater than 5 °F (3 °C), the pavement restraint stress would be reduced to 219 psi (1.5 MPa). This relatively small stress reduction due to the substantial reduction of temperature difference is ascribed to the fact that the axial friction factor related restraint stress, as seen in equation 1, has no temperature independent component.

Results from tests to determine coefficients of thermal expansion and contraction on concretes used for this investigation, were reported in chapter 3. Table 31 showed that values ranging from 4.9 to 5.7 millionths in/in/°F (8.8 to 10.3 millionths mm/mm°C) were measured for contraction due to temperature cooling from about 120 to 50 °F (49 to 10 °C). For calculations shown in this study, a coefficient of contraction of 5 millionths in/in°F (9 mm/mm°C) was used.

## Indicator Test Criteria for Far Limit Sawcutting

Using relationships determined in chapter 3 as part of the laboratory early age (4 to 24 hours) tests, split tensile and modulus of elasticity can be related to compressive strength by the following expressions:

$$ST = 5.94 \, (f_c')^{1/2} - 36.1 \text{ (from line 9 table 22 of chapter 3)} \dots \dots \dots \dots (27)$$

$$E = 61000 \, (f_c')^{1/2} \text{ (from chapter 3)} \dots \dots \dots \dots \dots \dots \dots (11)$$

The above relationships of compressive strength with respect to split tensile strength and modulus of elasticity were established for a range of concrete mixes under controlled laboratory conditions. Equation 26 was transposed to set temperature difference between slab top and bottom to be the dependent variable. Calculations were made to determine magnitudes of temperature differences that can be tolerated before uncontrolled cracking occurs in pavements for a range of compressive strength (that is, split tensile strength) properties and associated moduli of elasticity. Calculations were made for 38- and 24-ft (11.6- and 7.3-m) paving width highways, and for coefficient of subgrade friction magnitudes of 2, 5, and 10. The plotted calculation results shown in figure 110 indicate that

pavement width or distance from pavement edge or end (frictional restraint) has a significant impact on the magnitude of temperature difference between slab top and bottom at incipient uncontrolled cracking, that is the temperature difference when concrete pavement tensile strength balances restraint stresses.

As noted before when components of equation 26 are examined, the coefficient of subgrade friction has a significant impact on magnitudes of temperature differences when pavement concrete tensile strength balances restraint tensile stresses. The plotted calculation results also indicate that as concrete pavement strength increases, temperature differences that impact on balancing tensile strength with restraint tensile stress increase. Thus, if cooling is delayed, benefits of concrete strength gain from early cement reaction are accrued and are available to balance concrete restraint stress.

From the point of view of averting uncontrolled cracking and widening the saw-cutting window of opportunity, paving should start in very early morning hours (or even at night) and should be completed by about 10:00 to 11:00 a.m. to minimize top and bottom slab temperature differentials and to maximize concrete strength gains ahead of developing tensile restraint stresses.

Results plotted in figure 110 can be used to estimate the far limit window of opportunity sawcutting time in terms of insitu concrete pavement strength properties when sawing should be completed. For example, measurements by pulse velocity or maturity can indicate that insitu concrete pavement strength is equivalent to 1000 psi (6.9 MPa). Entering horizontally at 1000 psi (6.9 MPa), the curve intercept is at 22 °F (12 °C) for a 38-ft (11.6-m) wide pavement on a granular subbase with estimated subgrade friction value of 2. Using a factor of safety of 2 with respect to temperature, sawing thus should have been completed before a 10 °F (6 °C) temperature drop occurs. When pavements adhere to subbases, higher effective friction factors to first movement are encountered. For example, a pavement over an LCB treated with a medium cure asphalt application may have an effective subgrade friction factor of 5. For the 1000-psi (6.9-MPa) strength and a 38-ft (11.6-m) paving width the curve intercept is at 11 °F (6 °C). For a factor of safety of 2 sawcutting should be completed before a 5 °F (3 °C) temperature difference occurs.

Pulse velocity or maturity to concrete strength predictions should be checked as part of project mix design to assure that good correlations with project mix-specific compressive strength are used.

It should be recognized that the targeting of temperature differences between slab surfaces and bottoms as the time by which sawcutting should be finished, begs the question of how much sawing time is available before the "allowable temperature difference" event occurs. Temperature measurements made on pavements in Utah, for example, as shown in figure 81, chapter 5, showed that a pavement top to bottom temperature change of 15 °F (8 °C) magnitude occurred within a span of less than one hour. The rapid concrete surface cooling was attributed to surface wetting associated with joint sawcutting. Similar rapid surface cooling can occur due to rainshowers. Thus a good rule of thumb may be to start sawcutting as early as possible, that is at the near limit and no later than the time when surface cooling starts.
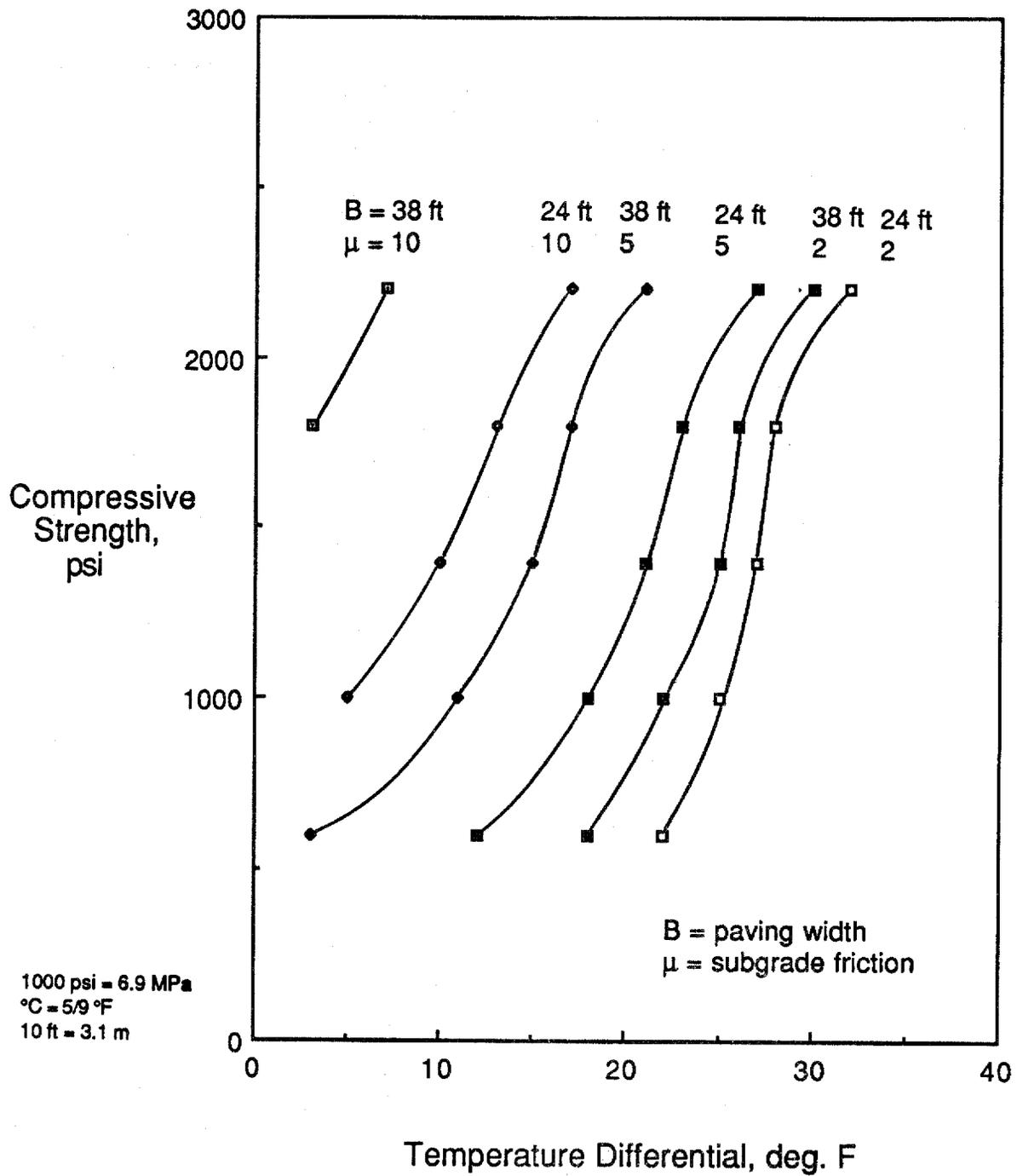
254

Figure 110.   Balance between compressive strength and
tolerable temperature difference.

# CHAPTER 9. GUIDANCE RECOMMENDATIONS FOR EARLY CONCRETE PAVEMENT LOADING

As a means of estimating and restricting the damage done to newly-placed concrete pavements subjected to early loading, general recommendations have been developed. These guidelines are based on the results of chapter 6, which considered the case of a 20,000-lb (9080-kg) single-axle load with 100-psi (0.69-MPa) contact pressure applied at the slab edge, interior, and corner (for dowel bearing stresses). The fatigue damage caused by a 14,500-lb (100-MPa) spansaw was also evaluated. Other load types, load magnitudes, and contact pressures could easily be evaluated using the procedure outlined in chapter 6. It is important for each agency to evaluate the damage caused by the specific types of construction vehicles that may load their concrete pavement at an early age.

The amount of fatigue damage to be consumed by early construction loading is a critical issue that must be evaluated by the responsible agency. This value is largely influenced by the design traffic loadings and the design life (in years) of the pavement, and is discussed in a subsequent section.

The flow chart in figure 111 depicts the recommended procedure for determining the time that the pavement can be subjected to early loading. The details of the specific steps were thoroughly described in chapter 6, and hence, only some of the more critical aspects will be discussed herein.

## INFLUENCING FACTORS

Critical factors influencing the potential load amount of damage done to a concrete pavement are listed below:

- Pavement design characteristics (thickness, foundation support, load transfer).

- Concrete strength at the time of anticipated early loading.

- Rate of concrete strength gain.

- Type of early loading construction vehicle (gross weight, axle weight, axle type, contact pressures).

- Position of the early loadings (i.e., edge, interior, corner).

- Number of repetitions of early loading vehicles.

With the exception of the second and thrid items, all of the factors are known or can be reasonably estimated. Therefore, it is critical that there is a means to estimate the insitu strength of the concrete slab at any time.

Because compressive strength is the most commonly performed strength measurement and was correlated with elastic modulus, the early loading evaluation utilized compressive strength as the primary indicator of concrete strength. As discussed in chapter 6, many different methods are available for estimating the concrete compressive strength, but it is highly desirable that compressive strength represent the insitu properties of the concrete slab. While casting of cylinders at the time of placement for later testing at selected time
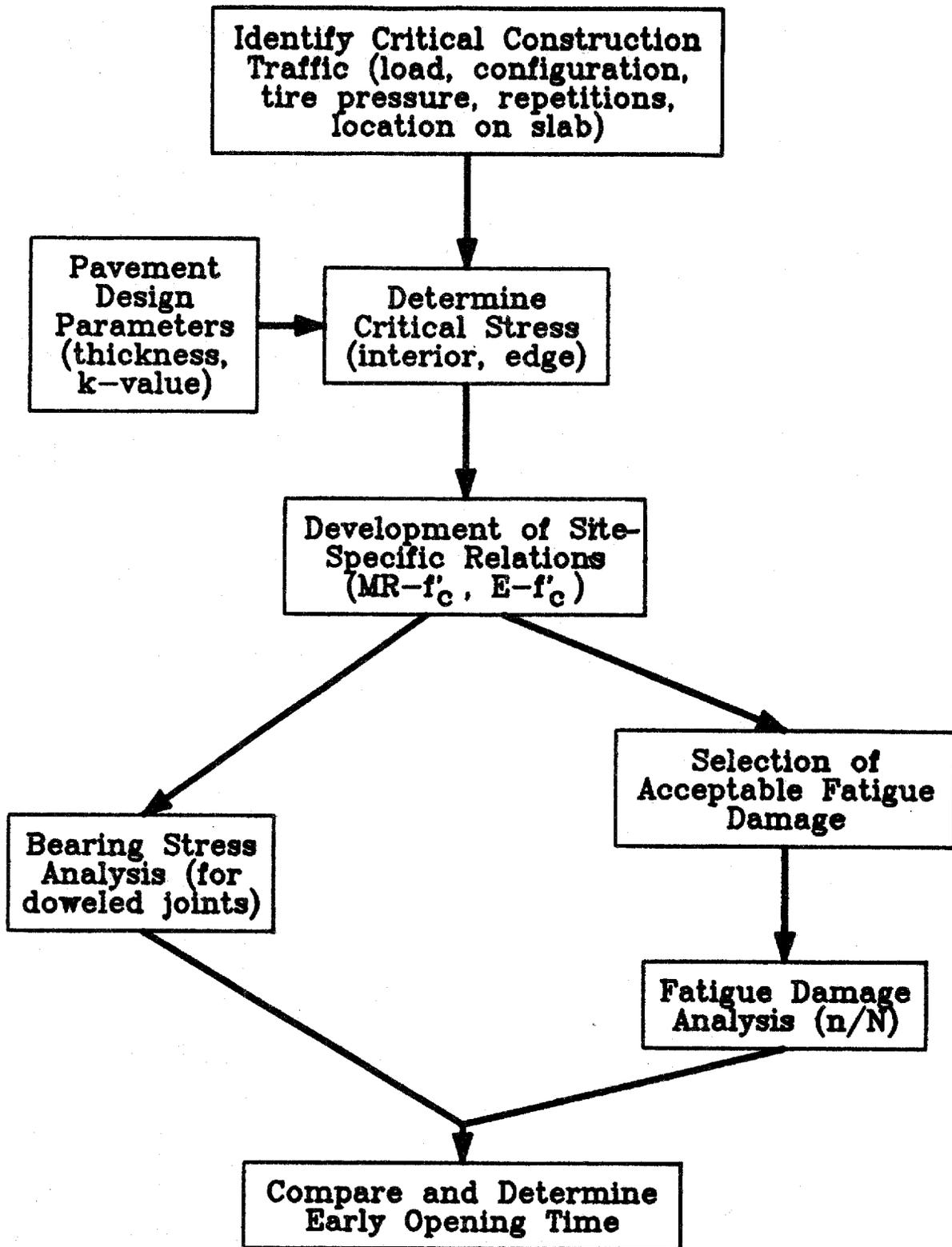
Figure 111. Early loading decision process.

intervals is the most common, this procedure may underestimate the actual strength of the inplace slabs, unless the cylinders are maintained at the same temperature and humidity as the slab.

Other methods which are available include the maturity and pulse velocity methods. The pulse velocity method measures the velocity of a sound wave passing through a slab and uses the wave velocity to approximate the strength. The maturity method incorporates both time and curing temperature effects. Maturity is then used to approximate strength. Both methods can be correlated so that the measured values can be used to estimate the insitu compressive strength of the concrete. This process is described in more detail in chapters 2 through 4.

The concrete modulus of rupture is also required for the fatigue damage analysis, and, therefore, a relationship is needed between the compressive strength and the modulus of rupture. A general relationship was presented in chapter 3, but it was recommended that a series of laboratory tests be conducted to determine the best relationship for each job mix formula that is used. Any changes in cement source or type, aggregate source, gradation or water content could alter the relationship.

## ACCEPTABLE DAMAGE FROM EARLY LOADING

A critical issue in the assessment of early loading fatigue damage is determining how much damage due to early loading is acceptable. The impact of defining this acceptable value is clear, as the consumption of a large percentage of the concrete pavement's fatigue life at an early age could produce failure of the pavement long before it has achieved its design traffic loadings.

The decision on the acceptable amount of early pavement loading is ultimately up to the responsible agency, but, as discussed in chapter 6, it will depend upon the performance period and the design traffic loading of the particular pavement. For example, consider a pavement designed for the following conditions:

Design Life: 20 years

Design Traffic: 20,000,000 ESAL applications (assume 6 percent, or 1,200,000 million, are edge load applications)

If early edge loading consumes 5 percent of the life, then approximately 60,000 edge load ESAL's (2,200,000*0.05) will be consumed. This represents about 1 year of life (1,200,000/20), or, in other words, the design life will be reduced to 19 years. If this reduction in life is acceptable to the responsible agency, then the amount of early loading that causes 5 percent damage is admissible. In most cases, a reduction in life of 1 year is probably unacceptable, particularly when all of the unknowns in actual traffic loadings and in traffic projections are considered. Life reductions on the order of 3 to 6 months are probably more in line with what most agencies would accept; given this criteria, the acceptable damage due to early loading for the above example would be 1.25 to 2.5 percent. For most cases, a value of 2 percent is probably a reasonable average. However, while these values are probably appropriate for most situations, they should be carefully evaluated by each agency for their specific conditions.

# RESULTS FROM EARLY LOADING EVALUATION

The fatigue damage evaluation conducted in chapter 6 considered a 20,000-lb (9080-kg) single-axle load placed at various locations for 8-, 10-, and 12-in (20, 25, and 30-cm) slabs. Also considered was the fatigue damage caused by a typical spansaw placed at an interior location.

Tables 70 and 71 have been developed based on the results of chapter 6 and assuming a maximum of 2 percent fatigue damage due to early loading. Table 70 is for the edge loading condition and table 71 is for the interior and transverse joint loading condition. These tables provide a ready reference for estimating the number of loadings to which a slab of a given strength may be subjected before exceeding the 2 percent fatigue damage limit.

For example, table 70 shows that a 10-in slab (25 cm) with a compressive strength of 260 psi (1.8 MPa) and a k-value of 300 lb/in$^3$ (81 MPa/m) can sustain only 14 edge applications of a 20,000-lb (9080-kg) single-axle before it reaches 2 percent fatigue damage. However, if the loading of the slab is delayed until the concrete has achieved a compressive strength of 1041 psi (7.2 MPa), the slab can now sustain approximately 227 edge applications.

An examination of tables 70 and 71 indicates that the edge loading condition is much more critical than the interior loading condition. In fact, even for the lowest compressive strength 260 psi (1.8 MPa), only the 8-in (20-cm) slab has a low number (less than 500) of allowable loadings to control fatigue damage. Thus, if early load applications can be kept away from the slab edges, then the pavement may be loaded much earlier for the same percentage of damage. Since the transverse joint stresses were similar to these for the interior loading condition, table 71 is applicable to the transverse joint loading condition (for both doweled and nondoweled joints). However, in the case of doweled joints, the bearing stresses exerted by the dowel on the concrete must be evaluated.

Table 72 provides a summary of the bearing stresses for a doweled joint under a 10,000-lb (4540-kg) wheel load placed at the slab corner. For the situation where the bearing stress exceeds the compressive strength of the slab, crushing of the concrete may occur. This crushing will serve to increase the size of the dowel socket and create looseness of the dowel, which ultimately may lead to premature and excessive levels of transverse joint faulting. Thus, a doweled slab should not be loaded until the compressive strength of the slab is larger than the bearing stress that would be developed under the anticipated traffic.

In comparing table 72 with table 70, it is seen that, for doweled joints, early loading may often be controlled by the bearing stresses and not by the fatigue damage from edge loading. For example, an 8-in (20-cm) slab with a k-value of 300 lb/in$^3$ (81 MPa/m) and a compressive strength of 1041 psi (7.2 MPa) could sustain 29 edge load applications before reaching the 2-percent fatigue damage. However, the maximum dowel bearing stress for the same slab with 1.00-in (25-mm) dowels is 3610 psi (25 MPa), indicating that crushing of the concrete around the dowel bars may occur. This will create looseness of the dowels in their sockets and could lead to accelerated development of joint faulting. For the above example, the slab probably should not be loaded until the concrete has reached a compressive strength of 4162 psi (28.7 MPa) because of bearing stress considerations. This corresponds to the 8-in (20-cm) slab being able to sustain about 448 early edge loading applications 2-percent consumption.

**Table 70. Number of 20-kip (9080-kg) edge load applications for 2-percent fatigue damage.**

| Slab Thickness, in | k-value, lb/in³ | Number of 20-kip (9080 kg) Edge Load Applications for 2 Percent Fatigue Damage | | | | |
|---|---|---|---|---|---|---|
| | | Slab Compressive Strength, psi | | | | |
| | | 260 | 1041 | 2341 | 4162 | 6504 |
| 8 | 100 | 1 | 3 | 20 | 125 | 849 |
| | 300 | 2 | 9 | 78 | 448 | 5765 |
| | 500 | 3 | 17 | 170 | 1689 | 10,000+ |
| 10 | 100 | 4 | 52 | 911 | 10,000+ | 10,000+ |
| | 300 | 14 | 227 | 5726 | 10,000+ | 10,000+ |
| | 500 | 27 | 528 | 10,000+ | 10,000+ | 10,000+ |
| 12 | 100 | 34 | 1673 | 10,000+ | 10,000+ | 10,000+ |
| | 300 | 194 | 10,000+ | 10,000+ | 10,000+ | 10,000+ |
| | 500 | 440 | 10,000+ | 10,000+ | 10,000+ | 10,000+ |

20,000 lb = 9080 kg
10 in = 25 cm
1000 psi = 6.9 MPa
100 lb/in³ = 27.1 MPa/m³

260

## Table 71. Number of 20-kip (9080-kg) interior load applications for 2-percent fatigue damage.

| Slab Thickness, in | k-value, lb/in³ | Number of 20-kip (9080-kg) Interior Load Applications for 2-Percent Fatigue Damage | | | | |
|---|---|---|---|---|---|---|
| | | Slab Compressive Strength, psi | | | | |
| | | 260 | 1041 | 2341 | 4162 | 6504 |
| 8 | 100 | 21 | 602 | 10,000+ | 10,000+ | 10,000+ |
| | 300 | 103 | 6907 | 10,000+ | 10,000+ | 10,000+ |
| | 500 | 230 | 10,000+ | 10,000+ | 10,000+ | 10,000+ |
| 10 | 100 | 662 | 10,000+ | 10,000+ | 10,000+ | 10,000+ |
| | 300 | 7597 | 10,000+ | 10,000+ | 10,000+ | 10,000+ |
| | 500 | 10,000+ | 10,000+ | 10,000+ | 10,000+ | 10,000+ |
| 12 | 100 | 10,000+ | 10,000+ | 10,000+ | 10,000+ | 10,000+ |
| | 300 | 10,000+ | 10,000+ | 10,000+ | 10,000+ | 10,000+ |
| | 500 | 10,000+ | 10,000+ | 10,000+ | 10,000+ | 10,000+ |

20,000 lb = 9080 kg
10 in = 25 cm
1000 psi = 6.9 MPa
100 lb/in³ = 27.1 MPa/m³

**Table 72. Maximum dowel bearing stresses for 10,000-lb (4540-kg) wheel load.**

| Slab Thickness, in | k-value, lb/in$^3$ | Maximum Bearing Stress, psi Compressive Strength, psi [1] | | | | |
|---|---|---|---|---|---|---|
| | | 260 | 1041 | 2341 | 4162 | 6504 |
| 8 | 100 | 2940 | 2990 | 3100 | 3380 | 3550 |
| 1.00 in dowels | 300 | 3510 | 3610 | 3770 | 4130 | 4350 |
| | 500 | 3790 | 3920 | 4100 | 4510 | 4750 |
| 10 | 100 | 1760 | 1780 | 1840 | 2010 | 2110 |
| 1.25 in dowels | 300 | 2130 | 2180 | 2260 | 2470 | 2600 |
| | 500 | 2310 | 2380 | 2470 | 2710 | 2850 |
| 12 | 100 | 1160 | 1170 | 1200 | 1310 | 1370 |
| 1.50 in dowels | 300 | 1410 | 1430 | 1490 | 1620 | 1700 |
| | 500 | 1540 | 1570 | 1630 | 1780 | 1870 |

[1] NOTE: Compressive strength estimated from equation 20, chapter 6.

1 in = 25 mm
100 lb/in$^3$ = 27.1 MPa
1000 psi = 6.9 MPa

262

The dowel bar diameter was observed to be very effective in reducing the magnitude of the dowel bearing stresses. This was illustrated in table 60 for 10-in (25-cm) slabs. The bearing stresses for the slab with 1-in (25-cm) diameter dowels are about twice those for the slab with 1.5-in (38-cm) diameter dowels. Larger diameter dowel bars are believed to be effective in reducing joint faulting, and the data from table 60 suggests that they may also allow for the slab to be subjected to earlier loading than a similar slab with smaller diameter dowel bars.

A summary of the observations that are apparent from the tables and from the early loading evaluation of chapter 6 are provided below:

- The edge loading condition, in which the load is placed at the mid-point of the slab at the edge, was determined to be the most critical. The stresses that develop in the slab at this location are much higher than those that develop at the slab interior or at the transverse joint for the same loading. Greater foundation support reduced the stress that developed in the slab.

- As would be expected, the edge stresses were highest for the thinner 8-in (20-cm) slab than for the thicker slabs. Subsequently, fatigue damage was much less for slab thickness typical of today's construction of 10 and 12 in (25 and 30 cm).

- Interior loading produced virtually no fatigue damage for 10- and 12-in (25- and 30-cm) slabs, even if loaded when the compressive strength was 260 psi (1.8 MPa). Some fatigue damage occurred for the 8-in (20-cm) slabs under an interior loading condition, but generally requires a large number of repetitions (greater than 500) at low compressive strengths of less than 1000 psi (6.9 MPa). This indicates the ability to subject a slab to early loading with very little fatigue damage if the loads stay away from the slab edge.

- Slab stresses that develop for the transverse joint loading contion (both doweled and nondoweled joints) are comparable to those for the interior loading condition. However, for doweled joints, the bearing stresses exerted by the dowel on the concrete is a primary concern.

- For doweled joints, the bearing stresses produced by the dowel on the concrete were determined to often be the controlling factor in considering early loading. Particularly for the slabs with lower compressive strengths, it was observed that the bearing stress often exceeded the compressive strength of the concrete, even though it may have developed sufficient strength to withstand a large number of edge or interior load repetitions. The bearing stresses due to early loading were also observed to be more critical for thinner slabs, which typically use smaller diameter dowel bars. Larger diameter bars were very effective in reducing the magnitude of the dowel bearing stress.

- A fatigue analysis was also conducted on the amount of damage done to a slab by a 14,500-lb (6580-kg) spansaw. The results indicate that no significant fatigue damage was done by the spansaw, provided that the slab had a minimum compressive strength of 260 psi (1.8 MPa).

- The results of the fatigue analysis indicate that tremendous benefits, in terms of far less fatigue damage, can be obtained by delaying as long as possible the early loading in order for the concrete to gain additional strength. For instance, a 10-in (25-cm) slab with a k-value of 300 lb/in$^3$ (81 MPa/m) can withstand 25 times as many edge loads for a 2-percent level of fatigue damage if the slab is allowed to attain a compressive strength of 2341 psi (16.2 MPa) instead of 1041 psi (7.2 MPa). Or, looking at from another way, the same number of early load applications on the slab with the compressive strength of 1041 will cause far less damage than those same applications on the slab with the lower compressive strength.

It is again worth noting that the tables and the observations given above are based on the assumed loads and loading conditions described in chapter 6. The resulting fatigue and bearing stress calculations assumed relationships between compressive strength and modulus of elasticity or modulus of rupture. Different material relationships, axles, axle loads, and contact pressures may produce different results, and an analysis similar to the one described in chapter 6 must be performed.

# REFERENCES

1. P. J. Nussbaum, and E. C. Lokken, "Design and Construction of Concrete Pavements," Proceedings, First International on Concrete Pavement Design, Purdue University, West Lafayette, IN, 1977.

2. R. Sharp, "European Concrete Roads Standards and Practices," Proceedings, First International on Concrete Pavement Design, Purdue University, West Lafayette, IN, 1977.

3. N. J. VanNess, "Summary of State Highway Practices on Rigid Pavement Joints and Their Performance," Memorandum to Regional Federal Highway Administrators, Washington, DC, May 19,1987.

4. H. O. Lamprecht, and A. Vollpracht, "Synoptic Table on Standards and Practices for Concrete Roads in Europe," Proceedings, International Symposium on Concrete Roads, Aachen, West Germany, 1986.

5. Concrete Society, "Joints in Concrete Roads: Aspects of Construction and Performance," Technical Report No. 28, London, November 1985.

6. K. D. Smith, D. G, Peshkin, M. I. Darter, A. L. Mueller, and S. H. Carpenter, "Performance of Jointed Concrete Pavements." Volume I, "Evaluation of Concrete Pavement Performance and Design Features," FHWA-RD-89-136, Federal Highway Administration, Washington, DC, March 1989.

7. C. H. Saraf, and B. F. McCullough, "Controlling Longitudinal Cracking in Concrete Pavements," Transportation Research Record, No. 1043, Washington, DC, 1985.

8. Andres Zachlehner, "Beanspruchong von Betonfahrbahnen Durch Einflusse aus Hydration und Witterung," Technische Universitat, Munchen, Heft 57, 1989. English translation of "Stresses in Young Concrete" is available from FHWA.

9. R. D. Bradbury, "Reinforced Concrete Pavement" Wire Reinforcement Institute, Washington, DC, 1938.

10. J. Eisenmann, "Bemessung von Zementbetondecken" KirschbaumVerlag Bonn-Bad Godesberg, Heft 82, 1970.

11. R. Springenschmid, and Peter Nischer, "Untersuchung uber die Ursache von Querrissen im jungen Beton," Beton und Stahlbeton, September 1973.

12. G. G. Carette and V. M. Malhotra, "In Situ Tests, Variability and Strength Prediction of Concrete at Early Ages," In Situ/Nondestructive Testing of Concrete, ACI Publication SP-82, American Concrete Institute, Detroit, MI, 1984.

13. P.A. Okamoto, B.T. Bock, and P.J. Nussbaum, "Nondestructive Tests for Determining Compressive Strength of Cement Stabilized Soils," presented at the Annual Meeting Transportation Research Board (TRB), Washington, D.C., January 1991.

14. M. Sadegzadeh and R. Kettle, "Indirect and Non-Destructive Methods for Assessing Abrasion Resistance of Concrete," Magazine of Concrete Research, Vol. 38, No. 137, London, England, December 1986.

15. R. H. Elvery and L. A. M. Ibrahin, "Ultrasonic Assessment of Concrete Strength at Early Ages," Magazine of Concrete Research, Vol 28, No. 97, London, England, December 1976.

16. J. Byfors, "Properties of Concrete at Early Age, Studies on Concrete Technology, Swedish Cement and Concrete Research Institute at the Royal Institute of Technology, Stockholm, Sweden, 1979.

17. V. R. Stirrup, F. J. Vecchio, and H. Caratin, "Pulse Velocity as a Measure of Concrete Compressive Strength," In Situ/Nondestructive Testing of Concrete at Early Ages, ACI Publication SP-82, American Concrete Institute, Detroit, MI 1984.

18. T. J. Parsons and T. R. Naik, "Early Age Concrete Strength Determination by Maturity," Concrete International, Detroit, MI, February 1985.

19. L. M. Khoo, "Pullout Technique - An Additional Tool for In Situ Concrete Strength Determination," In Situ/Nondestructive Testing of Concrete at Early Ages, ACI Publication SP-82, American Concrete Institute, Detroit, MI, 1984.

20. Guo Chengju, "Maturity of Concrete: Method for Predicting Early-Stage Strength," ACI Materials Journal, V. 86, No. 4, Detroit, MI, July-August 1989.

21. "Early Strength Gain and Concrete Maturity," Demonstration Project No. 75, Federal Highway Administration, Demonstration Projects Division, Washington, D.C., December 1988.

22. F. A. Oluokun, E. G. Burdette, and J. H. Deatherage, "Early-Age Concrete Strength Prediction by Maturity - Another Look," ACI Materials Journal, V. 87, No. 6, Detroit, MI, November-December 1990.

23. N. J. Carino, "Maturity Functions for Concrete," Proceedings, RILEM International Conference on Concrete at Early Ages (Paris, 1982), Vol. I, Ecole Nationale des Ponts et Chausses, Paris, France, 1982.

24. N. J. Carino, H. S. Lew, and Charles K. Volz, "Early Age Temperature Effects on Concrete Strength Prediction by the Maturity Methods," ACI Journal, March-April 1983.

25. N. J. Carino, "The Maturity Method," Chapter 5 CRC Handbook on Nondestructive Testing of Concrete, CRC Press, Boca Raton, FL, 1991.

26. C. F. Kee, "Relationship Between Strength and Maturity of Concrete," ACI Journal, Detroit, MI, March 1971.

27. Y. Kasai, "Method of Estimation for Compressive Strength of Concrete at Early Ages," Proceedings, RILEM International Conference on Concrete at Early Ages (Paris, 1982), Vol. I, Ecole Nationale des Ponts et Chausses, Paris, France, 1982.

28. Cold Weather Concreting (ACI 306R-78), American Concrete Institute ACI 306R-78, Detroit, MI, 1989.

29. Instruction manual for James Instruments Model C-4902 and Model C-4901 V-Meter, James Instruments Inc., Chicago, IL.

30. R. Jones, "Testing of Concrete by Ultrasonic - Pulse Technique," Highway Research Record Proceedings, Washington, DC, 1953.

31. H. N. Tomsett, "The Practical Use of Ultrasonic Pulse Velocity Measurements in the Assessment of Concrete Quality, Magazine of Concrete Research, Vol. 32, No. 110, London, England, March 1980.

32. J. Byfors, "Pulse Velocity Measurements for Indication of the Compressive Strength at Early Ages," Proceedings, RILEM International Conference on Concrete at Early Ages (Paris, 1982), Vol. I, Ecole Nationale des Ponts et Chausses, Paris, France, 1982.

33. R. B. J. Casson and P. I. J. Domone, "Ultrasonic Monitoring of the Early Age Properties of Concrete," Proceedings, RILEM International Conference on Concrete at Early Ages (Paris, 1982), Vol. I, Ecole Nationale des Ponts et Chausses, Paris, France, 1982.

34. S. G. Bergstrom and J. Byfors, "Properties of Concrete at Early Ages," Proceedings, RILEM International Conference on Materials and Structures, Rio de Janeiro, October 1979.

35. T. R. Naik and V. M. Malhotra, "The Ultrasonic Pulse Velocity Method," Chapter 7 CRC Handbook on Nondestructive Testing of Concrete, CRC Press, Boca Raton, FL, 1991.

36. Recommended Practice for Evaluation of Strength Test Results of Concrete (ACI 214-77, reapproved 1983), American Concrete Institute, Detroit, MI, 1988.

37. Building Code Requirements for Reinforced Concrete (ACI 318-89) and Commentary (ACI 318R-89), American Concrete Institute, Detroit, MI, 1989.

38. J. H. Emanuel and J. L. Hulsey, "Prediction of the Thermal Coefficient of Expansion of Concrete," ACI Journal, Detroit, MI, April 1977.

39. Tabatabaie, A. M., E. J. Barenberg, and R. E. Smith, "Longitudinal Joint Systems in Slip-Formed Rigid Pavements, Volume II, Analysis of Load Transfer Systems for Concrete Pavements," Report No. FAA-RD-79-4,II, Federal Aviation Administration, Washington, DC, November 1979.

40. A.M. Tabatabaie and E. J. Barenberg, "Structural Analysis of Concrete Pavement Systems," Transportation Engineering Journal, American Society of Civil Engineers, Volume 106, No. TE5, New York, NY, September 1980.

41. M.R. Thompson, A. M. Ioannides, E. J. Barenberg, and J. A. Fischer, "Development of a Stress Dependent Finite Element Slab Model," U.S. Air Force Systems Command, May 1983.

42. A.M. Ioannides, "Analysis of Slabs-on-Grade for a Variety of Loading and Support Conditions," Ph.D. Dissertation, University of Illinois, Urbana, IL, 1984.

43. G.T. Korovesis, "Analysis of Slab-on-Grade Pavement Systems Subjected to Wheel and Temperature Loadings," Ph.D. Dissertation, University of Illinois, Urbana, IL, 1990.

44. M.A. Miner, "Cumulative Damage in Fatigue," Transactions, American Society of Mechanical Engineers, Volume 67, 1945.

45. D.C. Stark, D., report in preparation on relative humidity of concrete, verbal communication, Construction Technology Laboratories, Inc., Skokie, IL, March 1991.

46. D.G. Zollinger and E.J. Barenberg, "Background for Development of Mechanistic Based Design Procedure for Jointed Concrete Pavements," Civil Engineering Studies, Transportation Engineering Series No. 56, Illinois Cooperative Highway Research Program, University of Illinois, Urbana, IL, May 1989.

47. H.M. Westergard, "Analysis of Stresses in Concrete Pavements Due to Variations in Temperature," Proceedings, Sixth Annual Meeting, Highway Research Board, Washington, DC, 1927.

48. M. I. Darter, "Design of Zero-Maintenance Plain Jointed Concrete Pavement, Volume I, Development of Design Procedure," FHWA-RD-77-111, Federal Highway Administration, Washington, DC, June 1977.

49. K. W. Heinrichs, M. J. Liu, M. I. Darter, S. H. Carpenter, and A. M. Ioannides, "Rigid Pavement Analysis and Design," FHWA-RD-88-068, Federal Highway Administration, Washington, DC, June 1989.

50. B.F. Friberg, "Design of Dowels in Transverse Joints of Concrete Pavements," Transactions of the American Society of Civil Engineers, Volume 105, New York, NY, 1940.

51. A.M. Ioannides, Y.H. Lee, and M. I. Darter, "Control of Faulting Through Joint Load Transfer Design," Paper presented at the 69th Annual Meeting of the Transportation Research Board, Washington, DC, January 1990.

52. S.D. Tayabji and B. E. Colley, "Improved Rigid Pavement Joints," FHWA/RD-86/040, Federal Highway Administration, Washington, DC, February 1986.

53. D.D. Davis and M. I. Darter, "Early Opening of PCC Full-Depth Repairs," Paper presented at the 63rd Annual Meeting of the Transportation Research Board, Washington, DC, 1984.

54. Statistical Analysis System (SAS), Version 6.04, SAS Institute Inc., Cary, North Carolina, 1990.